Recognition Agents for DNA and RNA Quadruplex Structures

Hannah Louise Pritchard

A thesis submitted to the University of Birmingham for the degree
of Doctor of Philosophy

School of Chemistry
University of Birmingham
September 2014

UNIVERSITY OF BIRMINGHAM

University of Birmingham Research Archive

e-theses repository

Abstract

The design and synthesis of a new class of G-quadruplex DNA recognition agents are discussed in this thesis along with their binding abilities to both duplex and G-quadruplex forming DNA. A selection of G-quadruplex binders reported in the literature to date have been reviewed and their interactions with the quadruplex DNA structure analysed.

The biisoquinoline ligand used to incorporate into the metal complexes synthesised in this thesis was chosen because of its large aromatic surface area which is ideal for end stacking onto G-quartets. Both the palladium and platinum biisoquinoline complexes bind to quadruplex forming DNA, monitored by UV-vis and circular dichroism. The platinum complex has the most promising DNA binding results showing a selectivity for quadruplex DNA over duplex DNA when examined by gel electrophoresis.

Biisoquinoline complex interactions with RNA G-quadruplexes have been investigated to make comparisons of that with DNA. The palladium complex binds less well to parallel quadruplex conformers suggesting its mode of interaction differs from that of the platinum complex. A toxicity assay against two cancer cell lines showed the platinum and palladium complexes to have IC_{50} values in the nM range.

Modifications to the biisoquinoline structure were also attempted in order increase the specificity of the complex to G-quadruplexes by incorporating components that could interact with the quadruplex loops.

Acknowledgments

Contents

Abbreviations

^{13}C NMR	carbon nuclear magnetic resonance
^{1}H NMR	proton nuclear magnetic resonance
2D-COSY	two dimensional correlation spectroscopy
A	adenine
A2780	ovarian cancer cell line
ATP	adenosine triphosphate
BF_4	tetrafluorborate
br	broad - IR
C	cytosine
CD	circular dichroism
CD_3CN	deuterated acetonitrile
c-myc	oncogene DNA sequence
ct-DNA	calf thymus DNA
d	doublet
dd	doublet of doublets
D_2O	deuterated water
d_6-DMSO	deuterated dimethyl sulfoxide
DC_{50}	concentration required to decrease fluorescence by 50 %
DFT	density functional theory
DMF	dimethylformamide
DNA	deoxyribose nucleic acid
DOSY	diffusion ordered spectroscopy

ds26	self complementary (26 base) duplex forming DNA
EI	electron impact - mass spectrometry
ESI	electrospray ionisation - mass spectrometry
FAM	6-carboxyfluorescein
FID	fluorescent indicator displacement
FRET	förster resonance energy transfer
G	guanine
G4	guanine quartet
h	hour
H_3PO_4	phosphoric acid
HMG	high mobility group
htelo	telomeric DNA sequence
ibiq	3,3-biisoquinoline
IC_{50}	half maximal inhibitory concentration
ICD	induced circular dichroism
ILD	induced linear dichroism
IR	infrared
J	coupling constant - NMR
K	kelvin
K^+	potassium cation
kb	kilobase
KCl	potassium chloride
LD	linear dichroism
LiOH	lithium hydroxide

m	medium - IR
M	molar
m	multiplet - NMR
m/z	mass to charge ratio
mdeg	millidegrees
MeOD	deuterated methanol
min	minute
mM	millimolar
MTT	3-(4,5-dimethylthiazol-2-yl)-2,5-diphenyltetra-zolium bromide
Na^+	sodium cation
NH_4OH	ammonium hydroxide
nm	nanometre
NMR	nuclear magnetic resonance
NOESY	nuclear overhauser effect spectroscopy
os	circular
PAGE	polyacrylamide gel electrophoresis
PF_6	hexafluorophosphate
ppm	parts per million
PQS	putative quadruplex sequences
RNA	ribonucleic acid
s	singlet
s	strong - IR
sc	supercoiled
SPR	surface plasmon resonance

T	thymine
t	triplet
T47D	breast cancer cell line
TAMRA	6-carboxytetramethylrhodamine
THF	tetrahydrofuran
TLC	thin layer chromatography
T_m	melting temperature
TO	thiazole orange
TRAP-LIG	modified telomere repeat amplification protocol
UV	ultraviolet
UV-vis	ultraviolet-visible
vs	very strong - IR
w	weak - IR
δ	chemical shift - NMR
ε	molar absorption coefficient
λ	wavelength
λ_{max}	maximum wavelength
μM	micromolar

Chapter 1: Introduction

This thesis will explore the design and activity of a new class of G-quadruplex DNA recognition agents. To contextualise why such agents are so important, existing structures of DNA and the agents that bind to them first need to be considered.

Part A: DNA Structures, Recognition Sites and Binders

1.1 DNA and its Structure

Deoxyribonucleic acid (DNA) is fundamental to life as it encodes all of our genetic information and is responsible for the function and development of living organisms. Understanding processes that occur when the DNA is *active,* such as replication and gene expression, can help with the diagnosis of diseases such as cancer where the rate of these processes is much higher. Already there is a library of metallo-anticancer agents that have been shown to interact with duplex DNA in order to alter its function, the most famous metallo-drug being cisplatin. The emergence however of more unusual types of DNA as targets has led to the creation of new more specialised complexes that are more specific for one type of DNA over another. The goal therefore is to now create an effective anticancer agent that has a specific DNA structure target and is highly potent to cancerous cells whilst minimising its effect on healthy cells.

1.1.1 Duplex DNA Structure

DNA is composed of three components; a pentose sugar, a phosphate group (which connects the sugars by phosphodiester bonds to form the sugar phosphate backbone) and a

heterocyclic base which can be either guanine (G), thymine (T), cytosine (C) or adenine (A).[1] Specific base pairings between adenine to thymine and cytosine to guanine arise due to hydrogen bonding between the two bases, *Fig. 1.1*. These interactions are more commonly known as Watson Crick base pairings and were first elucidated in 1953.[2] The two scientists, Watson and Crick, discovered the double helical B-form of DNA where one strand runs anti-parallel to the other.[1][2] Grooves of different magnitudes in the DNA (major or minor) are created because of the spatial arrangement of the base pairs.[3][4]
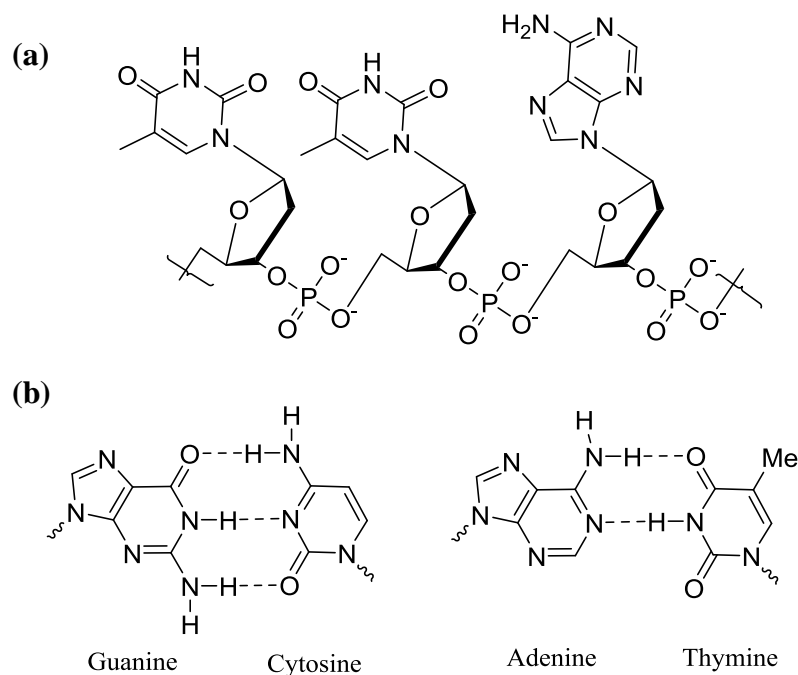
Figure 1.1 **a.** The structure of the DNA sugar phosphate backbone with the base sequence TTA, **b.** Base pairs that link the two strands of DNA and the hydrogen bonds that hold them together.

There are three common types of duplex DNA; B, A and Z (*Fig. 1.2*), differing in direction of winding and number of bases in one helical turn. B-DNA exists as a right handed helical structure and is the most common form of helicate in biological systems.[3] A-DNA is also right handed however forms a shorter and fatter type of helix that is seen in DNA-

RNA hybrids and dehydrated DNA duplexes.[4] Z-DNA is left handed and is also seen in biological systems.[3][5]
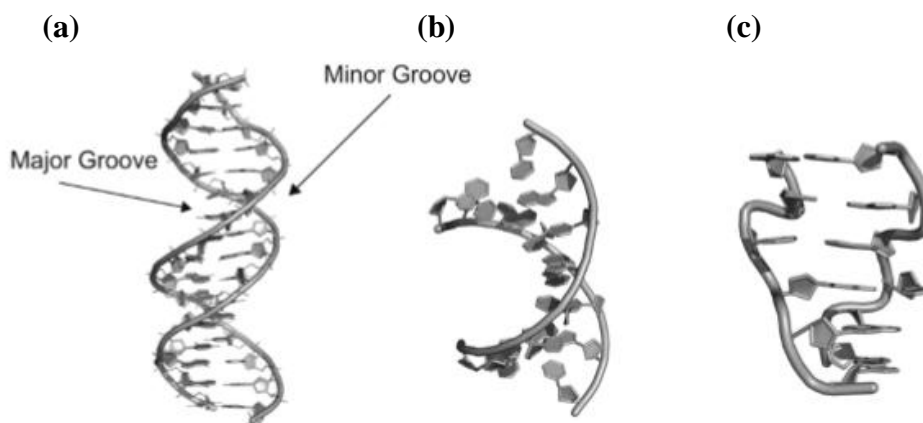
Figure. 1.2 **a.** B-DNA right handed helicate, **b**. A-DNA shorter and fatter right handed helicate, **c.** Z-DNA left handed helicate. [Reproduced from Ref [6]]

1.1.2 Other Types of DNA Structures

DNA is also seen in a variety of other structures other than the duplex form when processes such as replication, transcription and recombination are occurring.[7][8] The structures that emerge during these active processes may prove to be more effective targets for anticancer drugs as it is the loss of control in these processes (over expression of proteins or enzymes) which account for the proliferation of cancer.[9][10]

1.1.2.1 Replication Forks

Replication will see the formation of a Y shaped junction as the duplex DNA strands uncoil and separate in order for transcription to start. The separated parent strands act as a template against which the DNA polymerase can match complementary nucleotides (synthesizes new strand in a 5' to 3' direction) in order to create a copy of the DNA. The branch point created consists of four bases which creates a cavity that has the potential to

be targeted by specific synthetic agents that can bind to and halt the replication processes.[11]

1.1.2.2 Three Way Junctions

Three way junctions are formed from the convergence of duplex DNA strands that meet to produce a Y shaped structure (*Fig. 1.3*) creating a hydrophobic cavity at the centre.[12][13] The formation of the three way junction has been linked to diseases such as Huntington's when found in genetically unstable genomic DNA which can accommodate looped out triplet-repeat expansions.[12][14] Sinden *et al* reported fourteen genetic neurodegenerative diseases in which the expansion of mutated DNA triplet repeat tracts occur.[14] In such diseases three way junctions are likely to emerge from mis-paired hairpins introducing considerable kinks or bends into the DNA.[14]
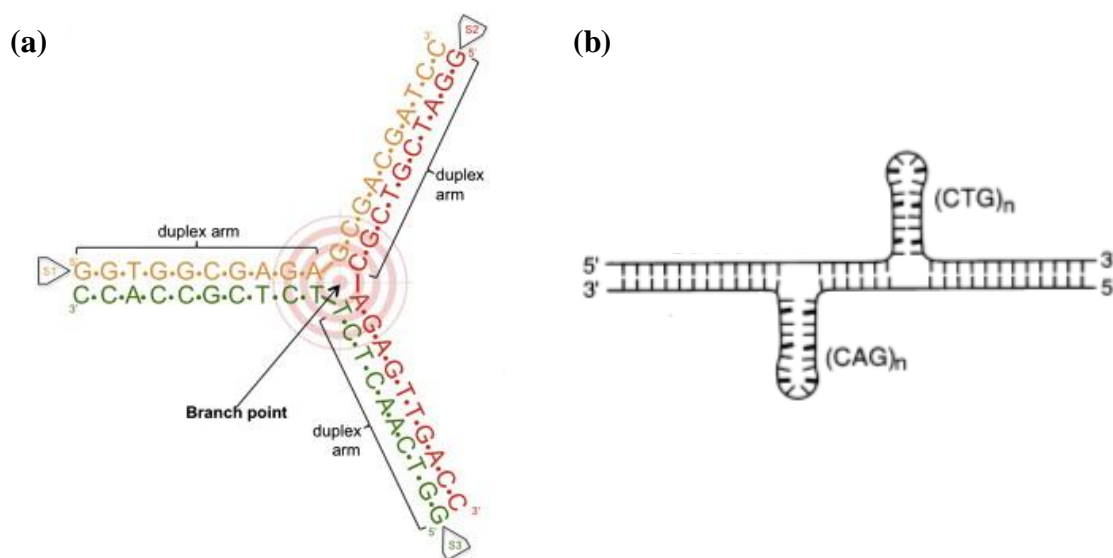
Figure 1.3 **a.** Representation of a three-way junction showing its formation from three separate strands; S1 (yellow), S2 (red) and S3 (green) [Reproduced from Ref [13]], **b**. Slipped strand structure formed within repeated DNA sequences from a misalignment of complementary duplex strands resulting in the formation of loops. [Reproduced from Ref [14]]

1.1.2.3 Holliday Junctions

Holliday junctions, also known as four-way junctions, are the result of homologous recombination which occurs during the repair of collapsed replication forks.[3][15] This mechanism of recombination was proposed by Holliday in 1964 and involves an X-shaped structure, formed from two duplexes which have come together and exchanged genetic material with four duplex arms that emerge from its convergence point (*Fig 1.4*).[16]
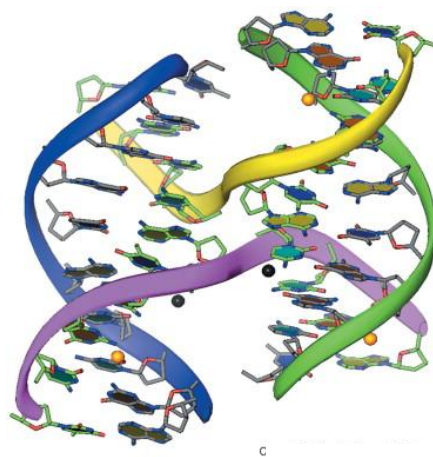
Figure 1.4 Crystal Structure of a Holliday junction showing the central branch point with four duplexes emerging from it. [Reproduced from Ref [17]]

1.1.2.4 G-Quadruplexes and the i-motif

Interactions available to a guanine base, other than Watson-Crick base pairing, arise from the heteroatoms N7 and O6 along its Hoogsteen face (*Fig. 1.5*). The hydrogen bonds formed along this face with other guanine bases allow the formation of 3D DNA structures called G-quadruplexes.[18] A G-quadruplex is composed of layers of G-quartets (first reported by Gellert *et al*)[19] where each quartet is formed from four guanine molecules assembled into a planar structure. The guanine bases interact through hydrogen bonds involving the Watson-Crick edge of one guanine and the Hoogsteen edge of its neighbour as shown in *Fig. 1.5*.[20][21] The quartet is stabilised further by the electrostatic interactions between the oxygen atoms from the guanines and the metal ion (Na^+ or K^+) at the

centre.[18]   The ability of the alkali metal ions to stabilise the quadruplex is dependent on the amount of energy released when electrostatic bonds are formed with the inside oxygen atoms of the guanine bases and the energy required to desolvate the cation.[22] The π surface of a G-quartet is about twice as large as a Watson-Crick base pair, therefore burying hydrophobic groups increases the stability of the structure as it forms a G quadruplex.[18]   The biological relevance of G-quadruplexes, further structural analysis, types of binders (organic and metal based) and experimental monitoring will be discussed in subchapters **1.3**, **1.4**, **1.5**, **1.6**, **1.7** and **1.8** respectively.
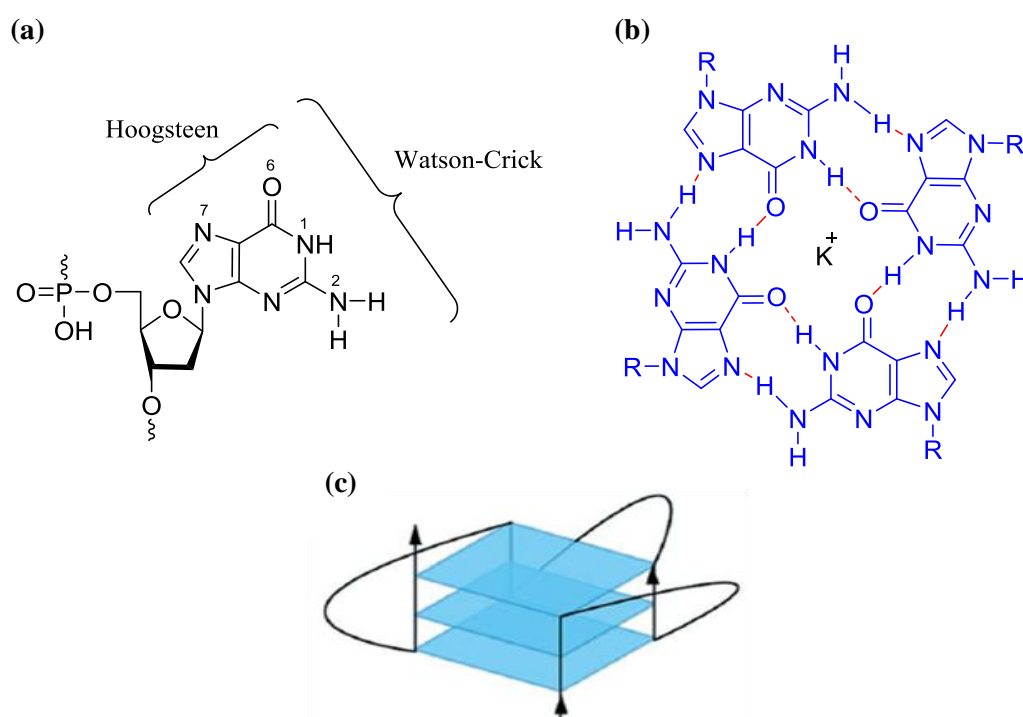
Fig. 1.5 **a.** Guanine base showing the two bonding faces that interact in a G-quartet, **b**. Structure of a G-quartet made up of four guanine moieties showing the position of the hydrogen bonds and the electrostatically stabilising cation, **c**. Parallel G-quadruplex structure of a guanine rich strand of DNA. [Reproduced from Ref [23]]

i-Motif

The i-motif is another type of tetraplex this time formed from a cytosine rich sequence of DNA.[24]   The cytosine rich sequence, under slightly acidic conditions, can form two

parallel duplexes where the cytosine bases can interact with each other through hydrogen bonds and also intercalate between each other in an antiparallel fashion, see *Fig. 1.6*.[24][25] Where there is a G-rich duplex section of DNA that has the potential to refold into a G-quadruplex there will also be a C-rich section of DNA that has the potential to fold into the i-motif. Attention has been drawn to the i-motif as it may also be present in transcription, replication and negative supercoiling where G-quadruplexes are usually found.[24] The thermal stability of the i-motif however is much less than that of the G-quadruplex therefore more attention has been focused on the G-rich sequences than the C-rich ones. [25][26]
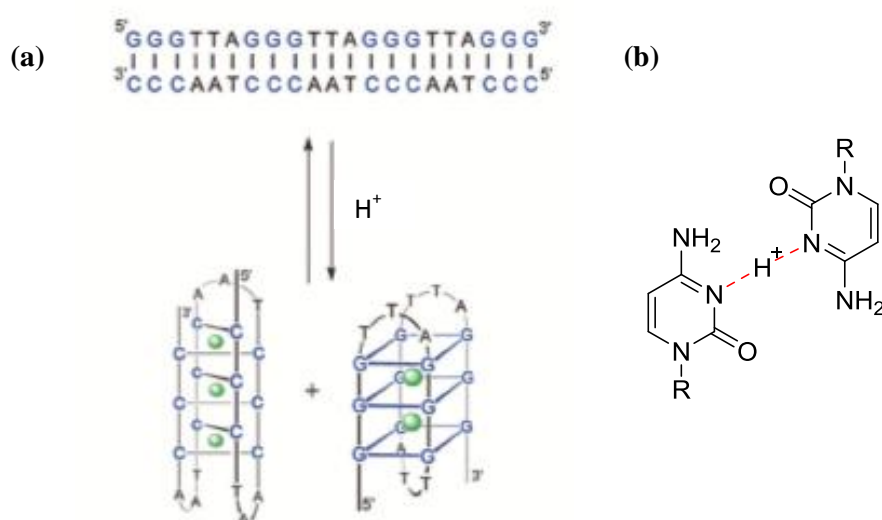
Figure 1.6 **a**. DNA duplex made up of a guanine rich strand and its complementary cytosine rich strand (top), during biological processes conditions arise that enable secondary structures to form i-motifs (left) and G-quadruplexes (right) [Reproduced from Ref [24]], **b**. Hemiprotonated C-C[+] base pair.

1.1.2.5 Mismatches and Bulges

Bulges in DNA are usually formed as a consequence of DNA mismatches.[27] Single base errors (*Fig. 1.7*) are normally corrected by a mismatch repair pathway.[27] However, when

left uncorrected the mismatches can be replicated creating a mutated form of the DNA.[27]

The mutation rate, and therefore the onset of cancer, is elevated when the mismatch repair

pathway breaks down.[27]

Figure 1.7 Examples of DNA hairpins and a duplex containing single base bulges.
[Reproduced from Ref [28]]

1.2 Anticancer Drugs and Their Mode of Action

The structure of biologically relevant B-DNA has five different molecular recognition sites

available for potential binding events which are the major groove, the minor groove,

intercalation between base pairs, the sugar phosphate backbone and covalent or metallo

interactions directly with the bases.[3] The mode of action of an anticancer drug is dictated,

to a certain degree, by its molecular structure and will be aimed at a specific recognition

site. This becomes more apparent when searching for a binder that is specific to secondary

DNA structures.[29]

1.2.1 Cisplatin and Other Coordinative Binders

Cisplatin, cis-[Pt(NH$_3$)$_2$(Cl)$_2$], (*Fig. 1.8*) is one of the most recognisable anticancer agents

as its ability to cause cell death by direct DNA base binding is unsurpassed.[30]   The

effectiveness of the drug lies in its ability to hinder the replication process, to which cancer cells devote much of their energy.[30]
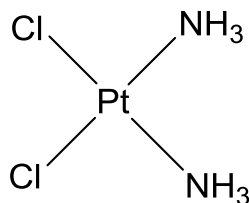
Figure 1.8 Chemical structure of cisplatin.

Once administered by injection into the bloodstream it is able to access cells across the cell membrane by passive diffusion or possibly by active transport.[30] The complex is then able to hydrolyse due to the lower chloride concentration in the cell (high concentration of chloride ions in plasma prevents the drug hydrolysing before it has entered the cell) allowing it to coordinatively bind to DNA through the interaction of two adjacent guanine bases (through N7) from the same strand.[31] This process leaves a $\{Pt(NH_3)_2\}$ unit on the DNA and causes the DNA to kink (*Fig. 1.9*).[31] The kinked DNA is recognised by a high mobility group protein (HMG) which binds to the kinked DNA and prevents it from being repaired.[30][32]
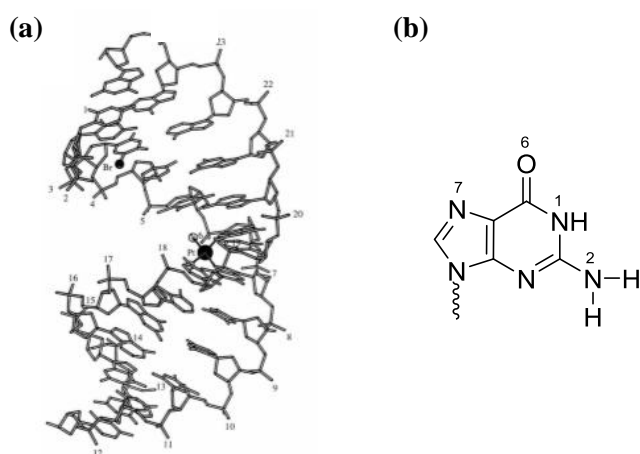
Figure 1.9 **a**. Kinking of DNA after the binding of cisplatin through N7 of two adjacent guanine bases, brominated oligo used to follow the kinking process. [Reproduced from Ref [31]] **b**. Structure of guanine showing the location of N7.

Despite its medical success, its use can lead to 'cisplatin resistant' cancers and prevents its re-administration. The drug also causes many side effects due to its unspecificity and the platinum's favoured binding to sulfur residues on amino acids rather than the DNA.[32] Other platinum binders include carboplatin and oxaliplatin which have been developed from the cisplatin model in that they also have two cis-amine groups and two leaving groups (*Fig. 1.10*).[32]
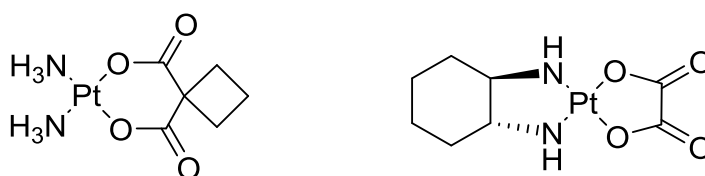
Figure 1.10 Structure of carboplatin (left) and oxaliplatin (right).[32]

Carboplatin shows lower toxicity levels than cisplatin due to its less labile leaving group making it a good choice of drug when the patients are too ill to cope with the toxic effects of cisplatin.[30] Despite this, it is not effective against cisplatin resistant tumours because it leaves the same $\{Pt(NH_3)_2\}$ unit on the DNA.[31] Oxaliplatin has been found to be more effective than cisplatin against breast cancer, melanoma and colorectal cancer due to its bidentate diaminocyclohexane ligand which causes different DNA adducts to be formed.[32] Some side effects associated with cisplatin are also eliminated with oxaliplatin and it has the capability to treat some cisplatin resistant tumours.[33]

Other transition metals that can be used in anticancer agents have also been investigated, two of which are shown in *Fig. 1.11*.[34][35] Ruthenium(II) is particularly useful as it possesses similar ligand exchange kinetics to platinum(II) and mass spectrometry

experiments have shown that guanine is the preferred binding partner for both metals when forming adducts.[36][37] Two ruthenium based complexes that show anticancer activity are indazolium trans-[tetrachloridobis(1H-indazole)ruthenate(III)] (KP1019) and imidazolium trans-[tetrachlorido(1H-imidazole)(S-dimethylsulfoxide)ruthenate(III)] (NAMI-A).[34][35]
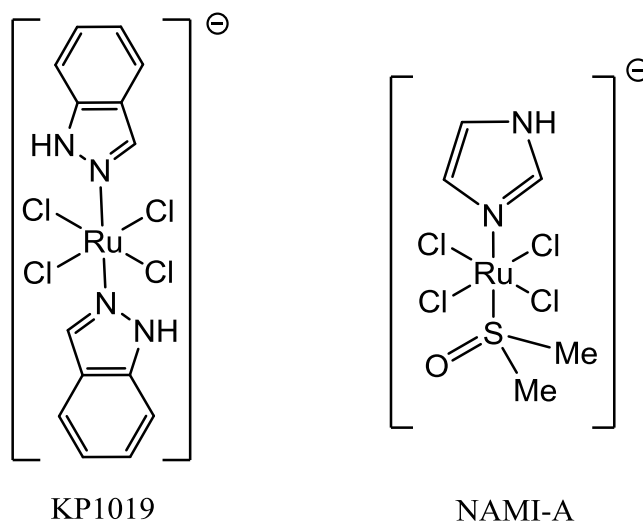
KP1019   NAMI-A

Figure 1.11 Two ruthenium complexes, KP1019 and NAMI-A, that demonstrate anticancer activity.[34][35]

KP1019 has anticancer activity against primary tumours and works by causing programmed cell death by a mitochondrial pathway[34] while NAMI-A is inactive against primary tumours but displays anti-metastatic properties.[35] It has been postulated that protein binding may play a part in their overall activity as the ruthenium complex DNA adduct formation occurs more slowly than with cisplatin.[37][38][39]

Iridium is another transition metal that has demonstrated anticancer activity through the formation of guanine adducts[40]. A collection of novel half-sandwich organometallic iridium(III) cyclopentadienyl complexes have been synthesised (an example is shown in *Fig. 1.12*) that are potent cytotoxic and cytostatic agents showing submicromolar

activity.[41] The complexes are able to bind to the DNA bases directly through N7 in guanine and intercalate between the bases also.[40] Despite this class of complexes being monofunctional (only one chloride ligand to hydrolyse) they can disrupt the replication process when iridium(III) binds to the DNA.[41]
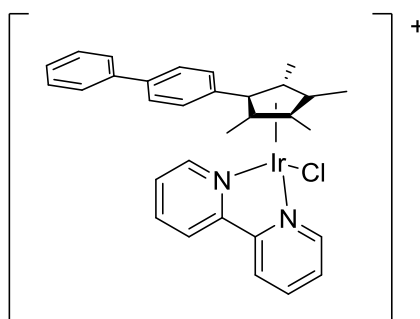
Figure 1.12 Iridium(III) cyclopentadienyl complex that shows submicromolar activity in the human ovarian cancer cell line.[41]

1.2.2 Intercalators

Intercalation, initially proposed by Lerner in the 1960s[42], involves the non-covalent binding of a planar aromatic π system that is able to insert in between stacked base pairs of a DNA double helix from either the major or minor groove.[3] Heterocyclic aromatic systems possess large hydrophobic surfaces that can be efficiently buried within the DNA structure.[43] The electrostatics of the system, induced through the binding of a metal cation to the heterocyclic aromatic group, can further promote this form of binding.[3] When intercalation occurs it disrupts the normal DNA structure causing it to unwind (the degree of which is determined by the intercalator), stiffen and lengthen.[44] Changes such as this to the DNA can result in the disruption of replication and transcription.[44]

Anthracycline antibiotics are planar aromatic compounds that can intercalate into DNA and in doing so act as anticancer agents.[45] The drug doxorubicin (which is classified as an anthracycline antibiotic) is a particularly good anticancer agent and acts by inhibiting topoisomerases causing the disruption of replication that leads to cell death.[45][46] It shows a preference for intercalation between the bases guanine and cytosine and also interacts with the bases in the minor groove through its amino sugar (*Fig. 1.13*).[46]

(a)

(b)
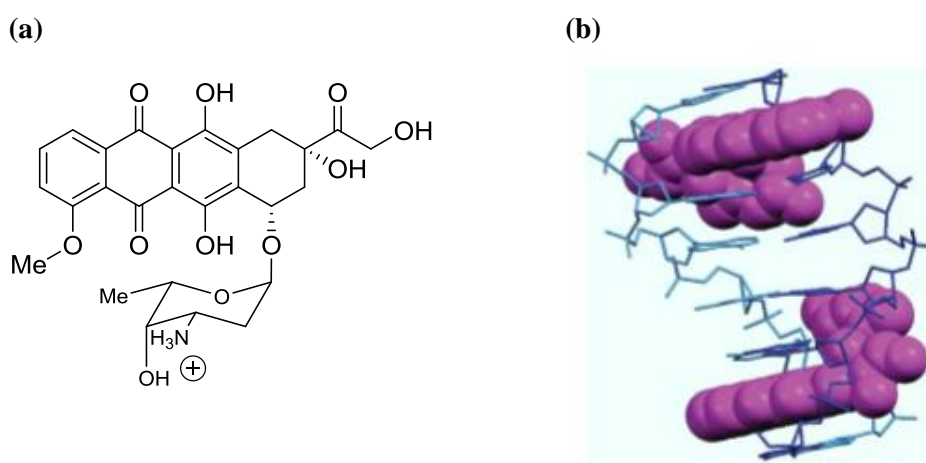
Figure 1.13 **a**. The structure of doxorubicin, **b**. Intercalation of two doxorubicin drugs between the base pairs of DNA. [Reproduced from Ref [3]]

Metallo intercalators are another sub-group of binders that can encompass more easily the positive charge required to provide favourable electrostatic interactions and therefore a higher binding affinity with the DNA.[47] The metal also creates new geometries for binding, compared with the organic compounds, providing new and more specific ways that the metal complex can be specially adapted to target the DNA.[47]

The types of ligand that are used as duplex DNA intercalators include phen, phi and dppz shown in *Fig. 1.14* as part of rhodium and ruthenium complexes.[44] Incorporating metals

such as ruthenium can be particularly useful due to the luminescent properties of ruthenium(II) providing diagnostic value. Rhodium(III) complexes have the added benefit of performing DNA cleavage by undergoing photoinduced oxidation.[3]
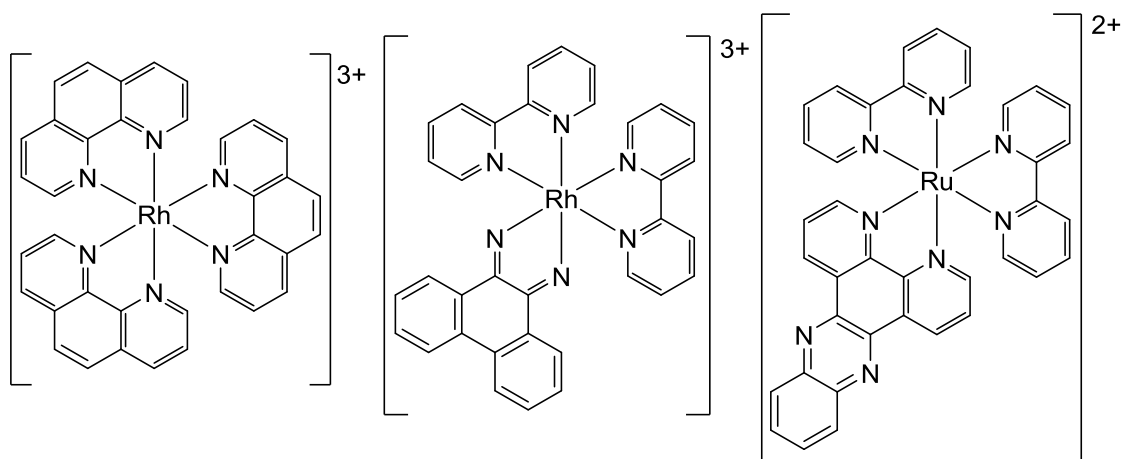
Figure. 1.14 Types of heterocylic ligands that can be used to intercalate between bases in duplex DNA: [Rh(phen)$_3$]$^{3+}$ (left), [Rh(bpy)$_2$phi]$^{3+}$ (middle), [Ru(bpy)$_2$dppz]$^{2+}$ (right).[44]

One of the first studies investigating the intercalation of metal complexes with DNA was conducted by Lippard *et al* in the 1970s and involved the intercalation of platinum terpyridine complexes (*Fig. 1.15*) into calf thymus DNA (ct-DNA).[47][48] The aromatic hydrophobic group on the complex can be effectively buried in the DNA resulting in a strong binding interaction between the DNA and the complex.[43]
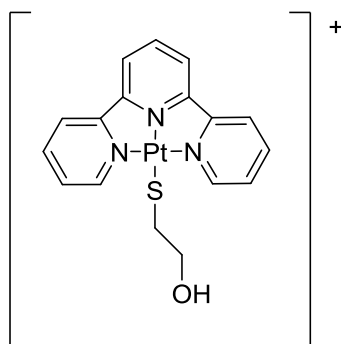
Figure 1.15 Platinum(II) terpyridine DNA intercalating complex reported by Lippard.[48]

1.2.3 Major and Minor Groove Binders

Major Groove

The major groove of the DNA double helix (*Fig.1.16*) is able to interact with both proteins and oligonucleotides.[3] It has a width of 11.6 Å and depth of 8.5 Å providing easy access for bulky molecules.[49] Hydrogen bond donor and acceptor interactions are important for DNA-protein recognition as they allow the DNA bases and amino acids to interact with a degree of specificity.[50] Hydrophobic contacts and other water mediated hydrogen bonds also influence the binding between the DNA and proteins.[51]
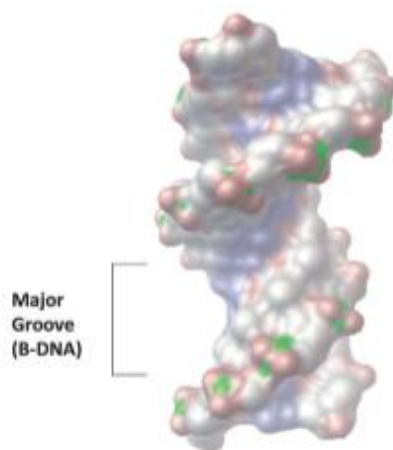
Figure 1.16 Major groove of B-DNA. [Reproduced from Ref [50]]

The most frequently used secondary structure of protein for major groove DNA recognition is the α-helix.[51] An example of a protein structure with an α-helical binding domain is a zinc finger which is able to make sequence specific contacts with the DNA bases, often matching one finger motif with four or more bases.[51] Other structures with an α-helical binding domain include leucine zipper proteins and helix-loop-helix motifs.[51]

Oligonucleotides can bind to DNA within the major groove to generate triple-helical nucleic acids stabilised by hydrogen bonds (Hoogsteen or reverse Hoogsteen) between the outer groups on the purine strand of the duplex DNA and the bases from the new strand.[52] The new strand can be added in either a parallel or anti-parallel fashion, the parallel form being the most stable where guanine-cytosine pairs are recognised by a protonated cytosine (C^+.GC) and adenine-thymine pairs are recognised by thymine (T.AT), (*Fig.1.17*).[52]
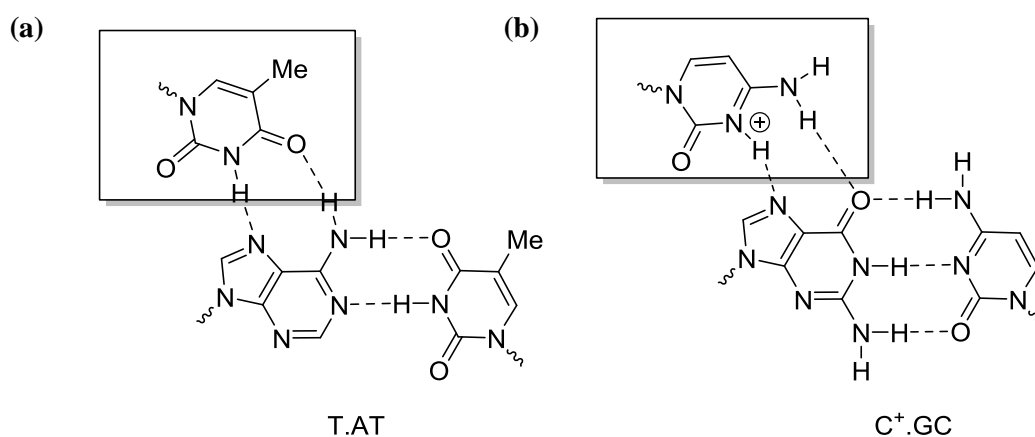
Figure 1.17 Chemical structure of the base triplets formed when a parallel triplex motif is formed. **a**. AT base pair from duplex bound to thymine from new third strand, **b**. GC base pair from duplex bound to protonated cytosine from new third strand.[52]

The formation of triplexes are linked to gene expression therefore the development of oligonucleotides for use in gene therapeutics is important.[53] DNA oligonucleotides however are not the best candidates as they suffer from biological degradation, difficult synthesis, poor cellular uptake and lack of solubility.[53] Peptide nucleic acid (*Fig. 1.18 - a*) is an alternative type of structure that can be used to substitute a DNA oligonucleotide in a triplex, although cell uptake is a problem.[54] Despite it replacing the sugar phosphate backbone with a sequence of (2-aminoethyl) glycine units it is able to mimic the base pairing interactions with a strand of complementary DNA creating triplexes that are thermally stable with a high degree of specificity.[53][54] However, it preferentially forms

(PNA)$_2$(DNA) over (PNA)(DNA)$_2$ triplexes.[3] LNA (locked nucleic acid) is another nucleic acid analogue which is composed of conformational restricted sugar groups.[55] When bound to DNA it is responsible for the A conformation of the heteroduplex due to its ribofuranose sugars which become locked in a 3'-endo conformation (additional bridging exists between 2O and 4C on the ribose, *Fig. 1.18 - b*). The structure has a very high affinity for both RNA and DNA.[55]

(a)   **(b)**
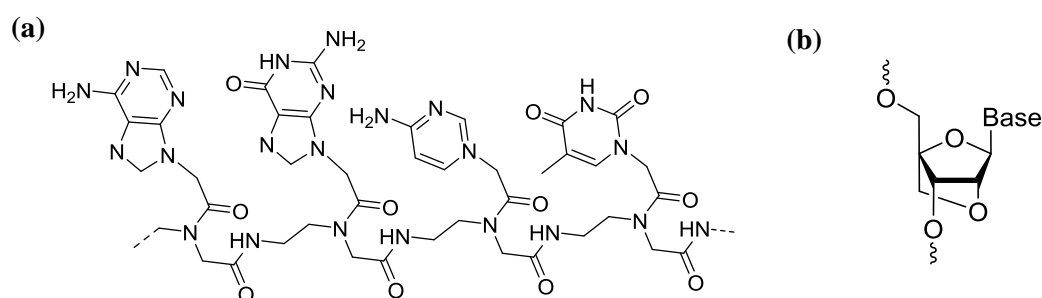
Figure. 1.18 a. The structure of peptide nucleic acid (PNA)[54], b. LNA monomer with bridge between 2O and C4 atoms of the ribose.[55]

The major groove has also been shown to interact favourably with a selection of natural and synthetic products (*Fig. 1.19*) including pluramycins, aflatoxins (both natural) and ditercalinium (synthetic).[50] However research into major groove binding is less studied for synthetic agents due to the availability of the smaller minor groove that is a better fit for smaller synthetic agents.[50]
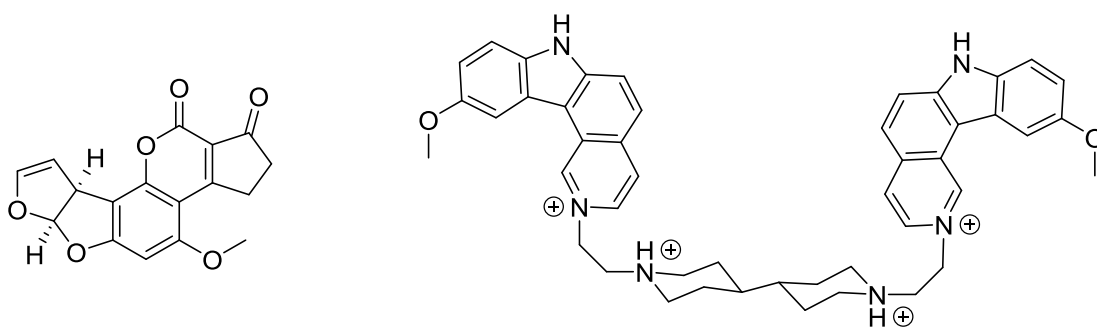
Figure 1.19 The structures of two major groove binders; aflatoxin B$_1$ (left) and ditercalinium (right).[50]

Minor Groove

The minor groove is more narrow and so better suited to small organic synthetic agents.[49] Minor groove binders frequently consist of an aromatic structure that is concave in shape (in order to match the convex shape of the groove) and can form hydrogen bonds with the bases and has amine groups capable of protonation under physiological conditions to form favourable interactions with the sugar phosphate backbone.[49]

Distamycin A fulfils the brief of minor groove binder with its three pyrrole rings connected by amide bonds and an amidino side chain that interacts electrostatically with the DNA (*Fig. 1.20*).[56] The amidino group helps the compound bind to the groove by interacting with the tightly packed phosphate groups in the backbone, thereby acting as an anchor.[49] It is able to hold the compound in place through electrostatic interactions while the rest of the compound sits in the groove interacting with the A and T rich DNA bases.[49]
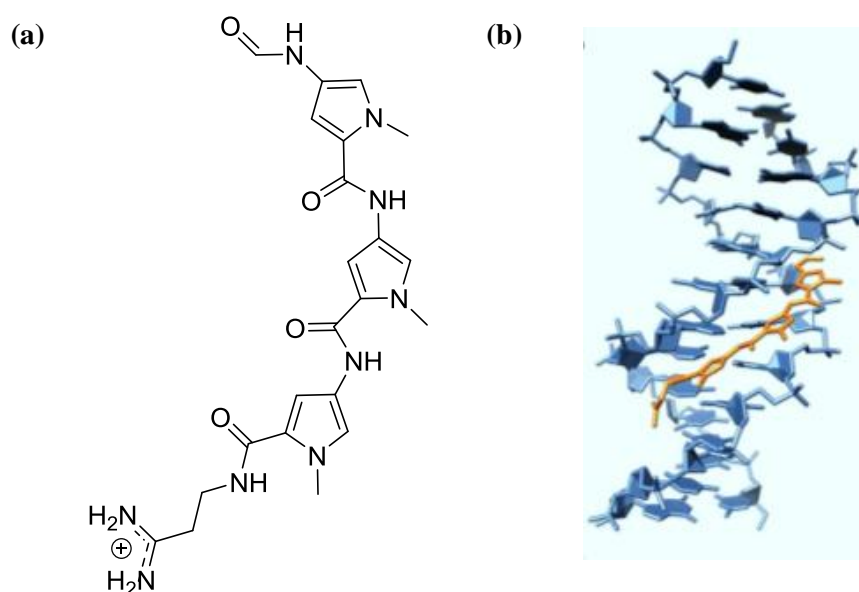
Figure 1.20 **a**. The structure of Distamycin A, **b**. X-ray structure of B-DNA with the binding mode of distamycin A in the minor groove. [Reproduced from Ref [54]]

18

The cytotoxic activity of distamycin is limited as it lacks a permanent anchor to the minor groove. Alkylating agents can be attached to the N-terminus of the structure producing benzoyl N-mustard and substituted acetamide type compounds.[57] The compound shown in *Fig. 1.21*, a tetrapyrrole which possesses a α-bromoacryloyl alkylating group, is approximately 1000 times more cytotoxic than distamycin demonstrating the effectiveness of incorporating additional alkylating agents.[56]
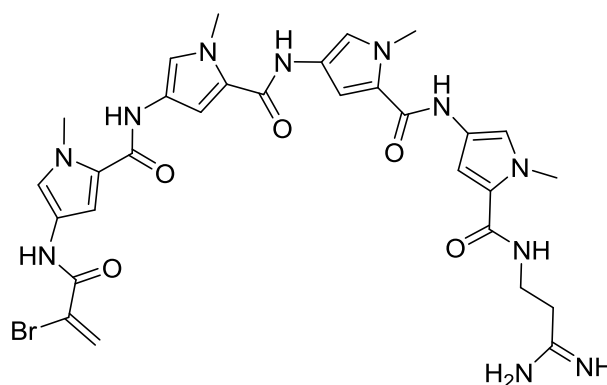
Figure 1.21 Modified distamycin compound with an additional pyrrole group and an α-bromoacryloyl alkylating group[58]

Tallimustine (*Fig. 1.22*) is a derivative of distamycin that displays a higher activity than the parent compound in a broad range of antitumor activities.[49][59] As well as having the essential distamycin framework it also contains a benzyl nitrogen mustard for alkylating functionality.[49] This was chosen because it is less likely to react with biological nucleophiles such as thiols.[49][56] The increased cytotoxic behaviour stems from the ability of the drug to locate in the minor groove while the benzyl nitrogen mustard, after producing aziridium, alkylates the DNA at different positions.[49]
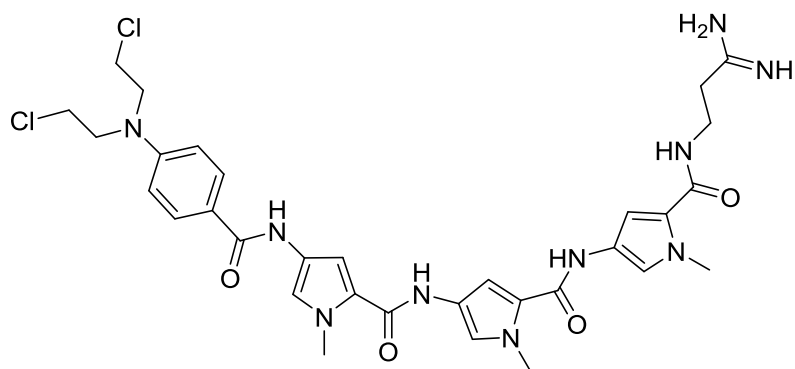
Figure 1.22 The structure of tallimustine.[49]

Another binder of the minor groove is Hoechst 33258 (*Fig. 1.23*) which is a synthetic compound that is particularly interesting due to fact it becomes strongly fluorescent when it binds to DNA.[60] The Hoechst dye selectively binds to A-T rich sequences with a binding site of four or five A-T base pairs stabilised by the burial of hydrophobic groups as the minor groove is largely hydrophobic.[43] The hydrogen bonds occur between the amine protons in the compound and the oxygen and nitrogen atoms from the thymine and adenine bases.[61] This fluorescent agent can be used in live cells.[56]
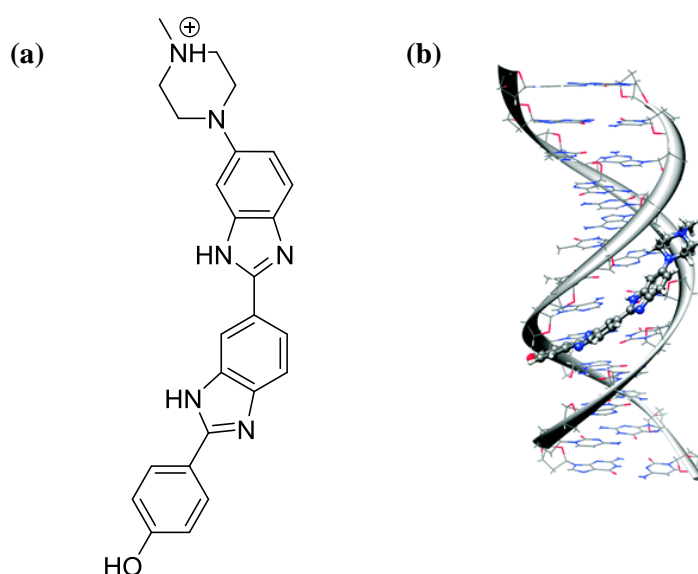
Figure 1.23 **a**. The chemical structure of Hoechst 33258, **b**. The structure of a segment of duplex DNA with Hoechst 33258 bound in the minor groove. [Reproduced from Ref [60]]

1.2.4 Sugar Phosphate Backbone Binders

A degree of backbone binding is exhibited in most of the non-covalent binders discussed so far, as most of the binders carry positive charges. The binders are electrostatically attracted to the negatively charged sugar phosphate backbone, helping to anchor them in place. A novel phosphate backbone binder has been reported by Farrell and co-workers which acts as a 'phosphate clamp' (*Fig 1.24*).[62]
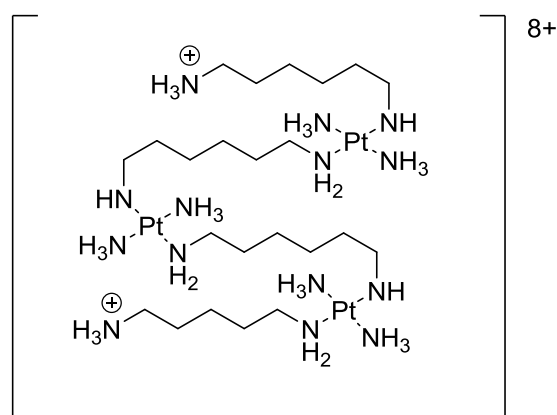
Figure 1.24 The chemical structure of 'phosphate clamp' [{trans -Pt-$(NH_3)_2(NH_2(CH_2)_6(NH_3^+)\}_2$-μ-{ trans -Pt$(NH_3)_2(NH_2(CH_2)6NH_2)_2$}].

In the complex, shown in *Fig 1.24,* the three platinum(II) groups are connected by flexible hydrophobic spacers that allow the phosphorus binding platinum to be matched up with the phosphate groups of the DNA backbone.[62] The Pt(II) amine and ammine units will then coordinate through hydrogen bonds to the phosphate oxygen atoms to form bidentate interactions (*Fig 1.25*).[54] The lack of any potential covalent interactions or aromatic heterocyclic regions allows it to be specific only for backbone binding.[62]
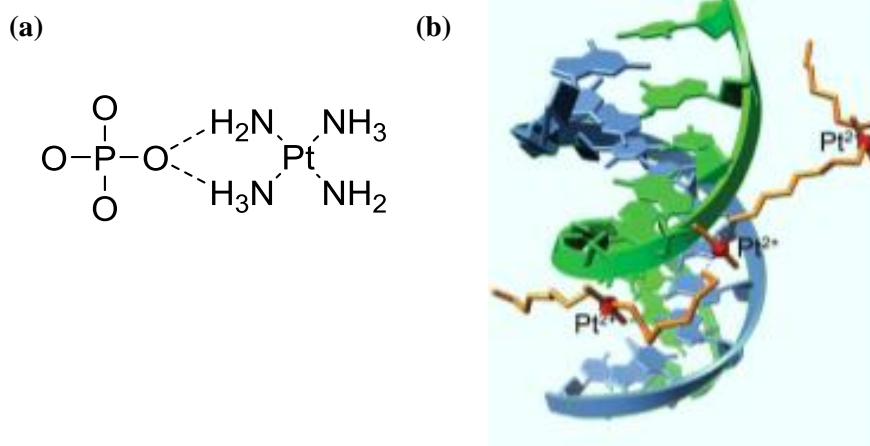
Figure 1.25 **a**. The hydrogen binding interactions which occur between the platinum ligands and the phosphate backbone groups, **b**. Structure of the platinum(II) complex binding to DNA. [Reproduced from Ref [54]]

1.2.5 Anticancer Agents that Target Other DNA Structures

Three-Way Junction Binder

Potential binders for three way junctions require a good size fit for the internal cavity of the structure in order to stall the replication process in cancerous cells; providing selectivity for this structure over the more common duplex form.[54]   Hannon and co-workers have shown how supramolecular divalent iron triple helicates can bind in the cavity of the three way junction (*Fig. 1.26*).[11] The three fold symmetry of the three-way junction matches with that of the iron supramolecular helicate allowing efficient burial of hydrophobic surfaces at the branch point.[63] The non-covalent interactions are stabilised further by the cationic nature of the complex and the anionic nature of the DNA.[63]

The cylinder has also been shown to bind to DNA dimers which are another type of Y shaped junction where at the branch point there are four bases instead of six.[11] The complex may bind in a similar way to both types of Y shaped junctions however three way

junction binding does not alter the DNA structure whereas dimer binding has more of an effect on the dimers shape and flexibility.[11]
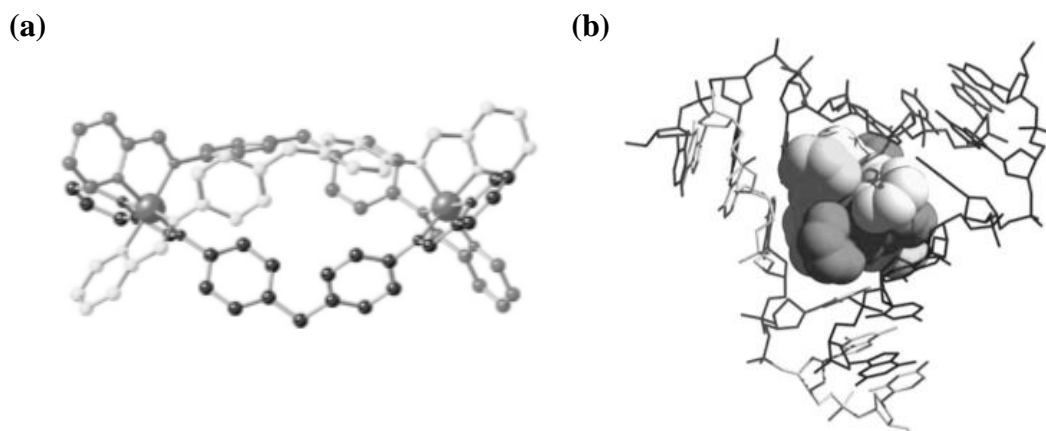
Figure 1.26 **a**. The structure of the cylinder $[Fe_2L_3]^{4+}$, **b**. Diagram based on X-ray crystallographic results of the iron supramolecular cylinder binding in a three way junction. [Reproduced from Ref [11]]

Holliday Junction Binder

Holliday junction binders in the literature employ a bis-intercalator design binding to two DNA sites that are close together in a cooperative manner.[64] The compound bis-acridine has been successful at binding to the four way junction, shown in *Fig 1.27*.[15] The acridine units interact favourably with the DNA bases through the efficient burial of hydrophobic surfaces.[15][43] The hydrophobic side chains reside in the minor grooves of the junction and the charge on the protonated molecule stabilises the structure through electrostatic interactions.[15]
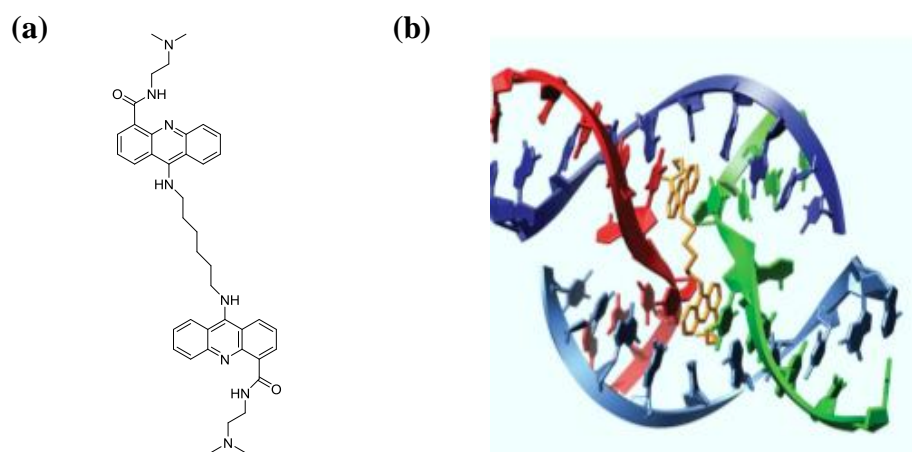
Figure 1.27 **a**. The structure of a bis-acridine compound, **b**. Diagram based on X-ray crystallographic results of bis-acridine binding to the four way junction. [Reproduced from Ref [54]]

DNA Mismatch and Bulge Binders

The bulges created, due to DNA mismatches, are able to accommodate the binding of larger aromatic structures as they do not have the same Watson-Crick pairing interactions that normal duplex DNA has. As a result, metallo-complexes with larger aromatic groups have been synthesised that have the potential to be selective for mismatches over duplex DNA as they would be too big to fit between the bases in a normal double helical structure.[65]

Complexes based on chrysi ligands have been synthesised by Barton and used for mismatch DNA targeting.[27] Their octahedral bulky rhodium complexes, an example of which can be seen in *Fig 1.28*, preferentially bind to the DNA at sites where there is a thermodynamically destabilised mismatch.[27] $[Rh(bpy)_2chrysi]^{3+}$ has been found to bind specifically to 80% of mismatches, with binding constants of 10^6 M^{-1}, through the insertion of the chrysi ligand into the duplex DNA at the mismatched site from the side of the minor

groove.[27] This in turn causes the mismatched bases to be pushed out of the DNA stack allowing the chrysi ligand to fully interact with the base pairs.[27]
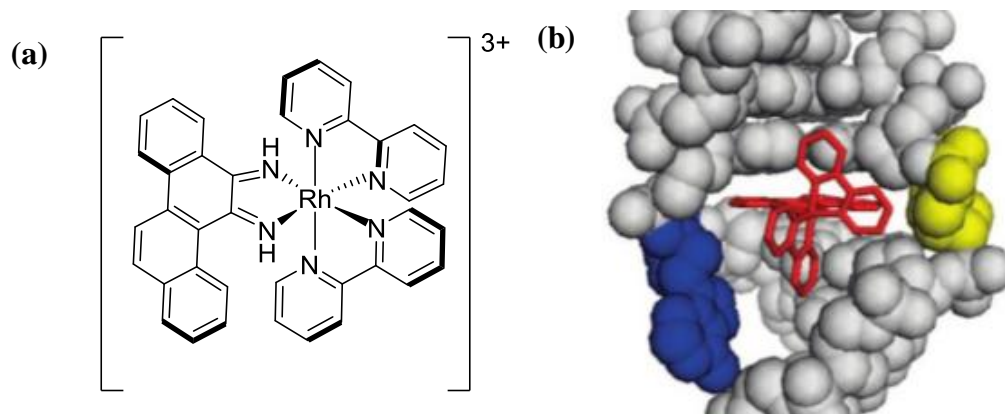
Figure 1.28 **a**. Structure of the bulge binder [Rh(bpy)$_2$chrysi]$^{3+}$ synthesised by Barton, **b**. Crystal structure of the Rhodium complex (red) bound to a CA mismatch (A - blue, C - yellow). [Reproduced from Ref [27]]

Part B: Structure, Chemistry and Function of G-Quadruplexes

The presence of G-quadruplexes in the human genome has sparked great interest in the study of quadruplex formation, function and targeting. Their formation is linked to active DNA processes and therefore they offer a way of selectively targeting DNA instead of targeting the duplex structure which can be described as DNA in 'sleep mode'. The rest of the introduction will give a detailed review on the structure of G-quadruplexes, where and why they form and examples of binders and experimental techniques that are being used to study them.

1.3 G-Quadruplex Conformations: Loops and Metal Ions

The introduction to G-quadruplexes covered in **1.1.2.4** only touches the surface on the types of structure a G-quadruplex can form. G-quadruplexes can be formed from a number of strands of either one, two (dimeric) or 4 (tetrameric) strands (*Fig 1.29*) (intramolecularly or intermolecularly) and arranged in either a parallel or antiparallel fashion.[23]
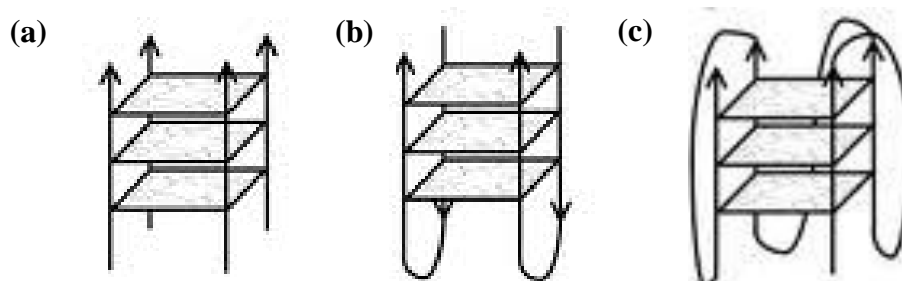
Fig. 1.29 Three types of G-quadruplex: **a**. Parallel tetrameric (four strands), **b**. Antiparallel dimeric (two strands), **c**. Parallel, intramoleculary folded single strand. [Reproduced from Ref [66]]

The overall conformation of the quadruplex stems from the arrangement of the strand(s) and in the process produces loops that further differentiate one type of quadruplex from another providing extensive structural diversity.[66] *Fig. 1.30* shows a selection of intramolecular G-quadruplex structures that can be formed from a guanine rich DNA sequence found in telomeric regions.[23] For each conformation the loop positions differ because of strand stoichiometry, strand polarities, glycosidic torsion angles and location of loops that link the guanine strands.[23][66]
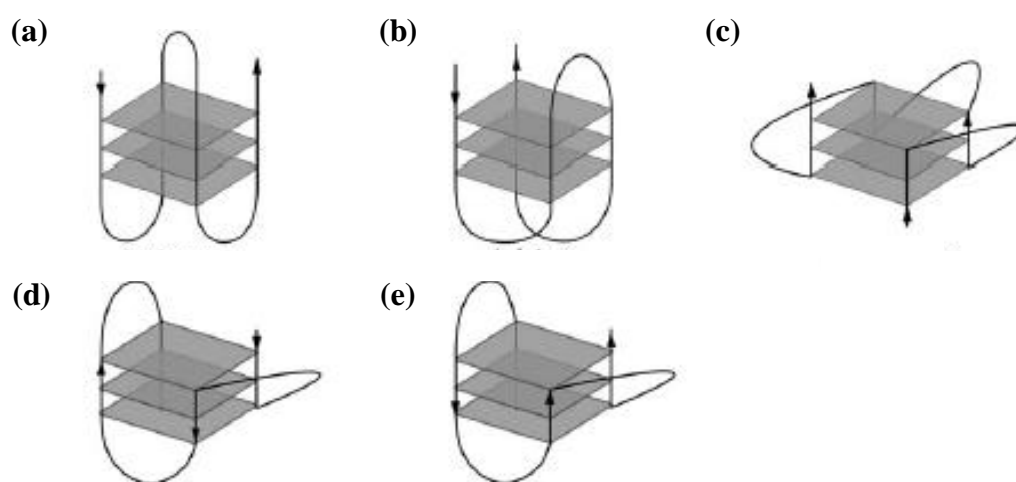
Figure 1.30 Five conformational analogues of one G-rich telomeric DNA sequence. **a.** Basket type (antiparallel), **b**. Chair type (antiparallel), **c**. Propeller type (parallel), **d.** Mixed type (antiparallel hybrid), **e**. Mixed type (antiparallel hybrid). [Reproduced from Ref [23]]

There are three main types of loops that are formed which influence the overall topology of the quadruplex. Propeller type loops are formed from adjacently linked parallel strands where the loop is required to link the bottom G-tetrad with the top G-tetrad in a medium groove[67] (*Fig 1.30 - c*). Parallel complexes have all of their guanine glycosidic angles in an anti-conformation.[68][69] Lateral loops are found in antiparallel structures (where at least

one of the four strands is antiparallel to the others) and join adjacent G-strands forming either narrow grooves (syn-anti) or wide grooves (anti-syn) (*Fig 1.30 - **d** and **e***). [66][68][70] Diagonal loops are also found in antiparallel structures and join opposite G strands; the direction of adjacent strands must alternate between parallel and antiparallel (*Fig 1.30 - **a** and **b***).[66] Antiparallel quadruplexes possess both syn and anti-guanine conformations.[66][71] The two types of conformations are shown in *Fig 1.31*, where interconversion occurs by rotation about the glycosidic bond.[18]

syn
$0^{o} < X < 90^{o}$
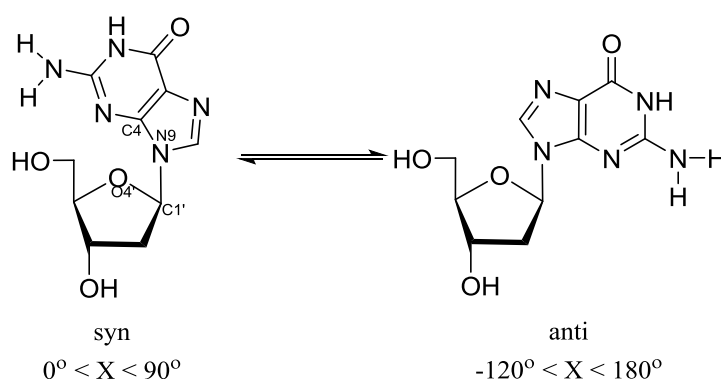
anti
$-120^{o} < X < 180^{o}$

Figure 1.31 The interconversion between the syn and anti conformations of guanine (both C2'-endo) which occurs by rotation around the glycosidic bond X (angle O4'-C1', N9-C4).[18]

Another important factor in the formation of a G-quadruplex is the type of cation present. In the G-quadruplex structure the cations are located in the central cavity, along the helical axis and form interactions with the carbonyl oxygen of the guanine bases (*Fig 1.32*).[72]
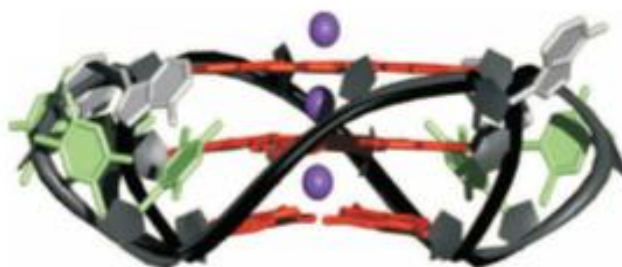
Figure 1.32. Side view of a G-quadruplex structure showing the potassium ions in the central cavity between the G-quartet planes produced by single crystal X-ray diffraction analysis. [Reproduced from Ref [72]]

The exact location of the cations depends on the size of the ion. Na^+ has been observed in the plane of the G-tetrad in some structures and between two G-tetrads in others[18] while K^+ ions are always found equidistant between each tetrad plane giving the K^+ ion a distorted square antiprism coordination geometry.[71][72] The type of cation present has been found to influence the conformation of quadruplex formed as in telomeric G-rich DNA Na^+ stabilised quadruplexes are antiparallel conformers whereas K^+ stabilised quadruplexes are antiparallel hybrids (showing both antiparallel and parallel characteristics).[73] The position of the cation may also affect the planarity of the top G4 tetrad. The cation is optimally positioned between the O6 atoms of the guanine bases in order to interact electrostatically which may result in the tetrad becoming slightly twisted.[22]

Potassium ions are known to be much more abundant than sodium ions in intracellular environments and therefore it is believed that the K^+ stabilised quadruplexes are more biologically relevant.[72][74] This can be rationalised by the best size fit along the helical axis (*Fig 1.33*), evidence for which has been provided by Wu *et al,* where a NMR solid state experiment was conducted using a guanosine 50-monophosphate composed guanine tetrad.[75] The result showed that the affinity of monovalent cations for the G-quadruplex cavity follows this order $K^+ > NH_4^+ > Rb^+ > Na^+ > Cs^+ > Li^+$.[75]
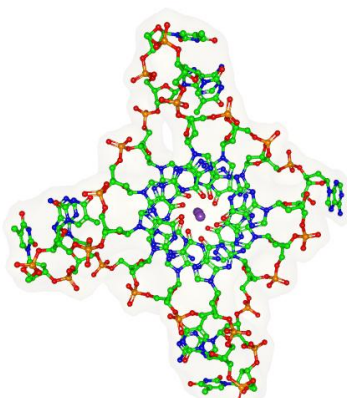
Figure 1.33. Arial view of G-quadruplex structure showing the central channel of potassium ions. (PDB 1KF1)[76]

In some parts of the human genome there are guanine rich sequences present in double stranded DNA.[18] In order for intramolecular G-quadruplexes to form in this region the stability of the duplex DNA needs to be compromised (Watson-Crick base paring made less favourable). The stability of the single stranded structure (quadruplex) must also be encouraged.[18] When exposed to additional factors from within the cell, the equilibrium can be shifted from the double stranded structure towards quadruplex formation.[18] These additional factors can include; duplex supercoiling, molecular crowding and the presence of specific complexes or proteins that can interact with the quadruplexes.[18]

1.4 Biological G-Quadruplexes and their Function

G-Quadruplexes are an emerging target for anticancer complex development and are presently attracting the attention of many research groups trying to find the best specific binder. In order to target such a structure, the rationale for G-quadruplex formation and the conditions under which this occurs need to be examined. G-quadruplex structures have been found throughout the human genome in telomeric regions, oncogene promoter regions, immunoglobulin switch regions and areas where mutation is high (see subchapter 1.4.2).[23]

The number of putative quadruplex sequences (PQS) that exist in the genome has been studied by Huppert and Balasubramanian.[77] Together they developed the 'folding rule' with the formula $d(G_{3+}N_{1-7}G_{3+}N_{1-7}G_{3+}N_{1-7}G_{3+})$ which is used in a computer generated quadparser algorithm.[77] The results after the analysis of the whole human genome with the quadparser algorithm found 376,000 PQS that may be capable of forming G-quadruplexes.[77] Telomeres, consisting of a simple repeat sequence, were found to account for around 20,000 of the PQS found.[77] This indicates that there is likely to be many more quadruplexes found in other areas such as oncogene promoter regions.[77]

1.4.1 Telomeric DNA

Chromosome ends are protected by a single stranded DNA sequence (telomere) that holds no genetic information, unlike the rest of the chromosomal DNA.[78] Telomeres are necessary due to the nature of the replication process because after every successive cycle the DNA is shortened.[79] They also prevent the ends from being recognised as broken DNA and being 'stuck together' by specific repairing proteins.[79]

When DNA unwinds in order to replicate, one strand becomes the leading strand and the other the lagging strand. This occurs because DNA polymerase III (an enzyme that builds the new strand in humans) synthesises in the $5' \rightarrow 3'$ direction which is the same direction that the DNA is being unwound.[80] Therefore the strand being created in the direction of unwinding is the leading strand and the strand running in the opposite direction has to be synthesised in fragments (Okazaki fragments) hence called the lagging strand (*Fig 1.34*).[80] The shortening occurs due to the RNA primers that are required to initiate the new strand synthesis as they provide the 3'-hydroxyl group to attach the next DNA

fragment. Once strand formation is complete the RNA primers are removed and replaced by DNA however any RNA primer at the 5' end of the new daughter strands cannot be replaced as there are no hydroxyl groups to attach the DNA to.[80]
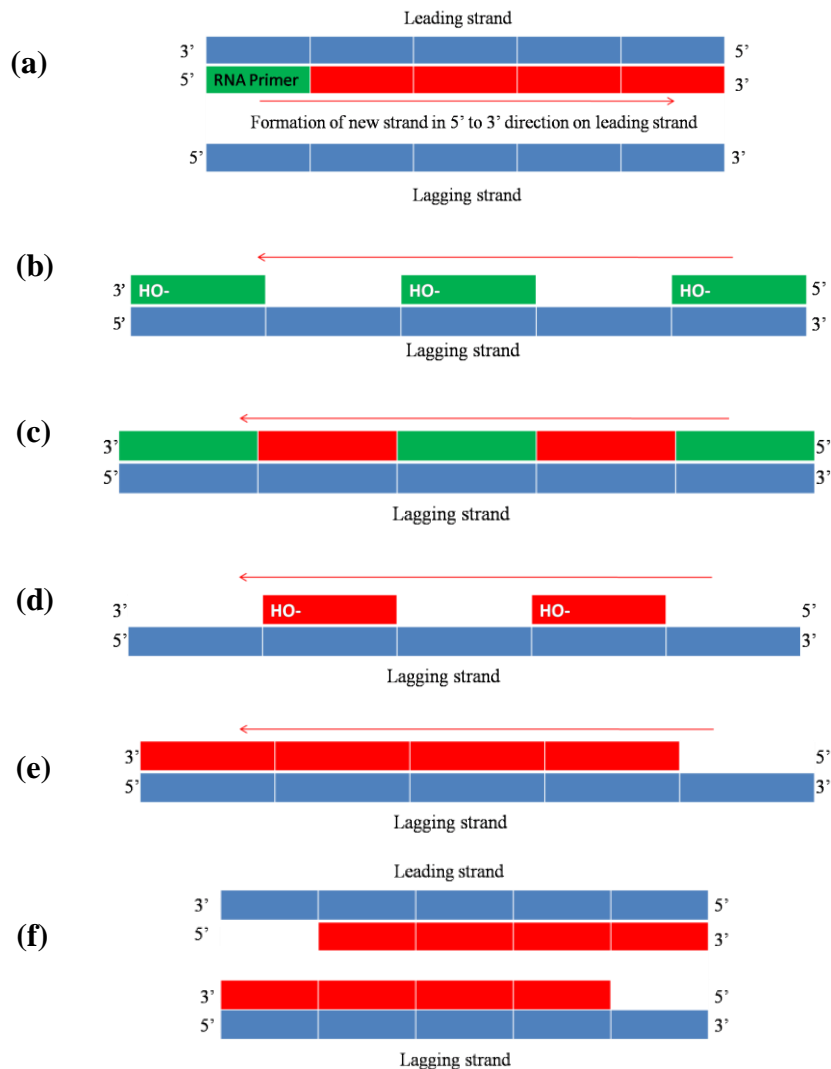
Figure 1.34. Process of telomere shortening during replication. **a**. Growing strand elongated in 5' to 3' direction in both strands; RNA primer required to start strand as it provides a 3'-OH group. Leading strand forms quicker than lagging strand as DNA polymerase works in the same direction as the double helix is being unwound. **b.** New strand formation has to be done in pieces in lagging strand as DNA polymerase works in opposite direction; it begins with the creation of RNA primers, **c**. Short segments of DNA are synthesised between primers, **d**. The RNA primers are then removed, **e**. And replaced with DNA, **f**. Replication results in two new daughter strands shorter than the parent strands. This is because DNA cannot be replicated at the 5' ends where the first RNA primer was added as there is no 3'-OH group to build from.

They are therefore essential for a normal healthy lifespan as they allow our genetic information to be repeatedly copied until the telomeres reach a critical length which then causes the cell to undergo apoptosis.[81]

Human telomeric DNA is made up of a repeat base sequence, **5'-TTAGGG-3'**, which varies in length between 5 and 10 kilobases.[81][82] The guanine rich nature of this segment of DNA means it is able to fold into the intramoleculary stable G-quadruplex structure and has been proven to do so under cellular conditions.[83] The formation of G-quadruplexes is particularly useful in this area as it is believed that their formation inhibits the action of the enzyme telomerase which acts to extend the length of the telomere by adding on TTA-GGG repeats to the ends of the DNA.[84]

Telomerase is essential for the lifespan of frequently replicated cells such as white blood cells and embryonic stem cells. However, in tumour cells it becomes over-expressed and indeed it is up regulated in 85-90% of cancers.[84] This normally occurs when a mutated form of DNA has reached a critical length and instead of undergoing apoptosis telomerase is introduced and the system continues to replicate indefinitely (*Fig 1.35*).[85]

Somatic cell
chromosome   Many divisions   Cell apoptosis
No telomerase present

Cancer cell   Many divisions   Immortality
Telomerase present
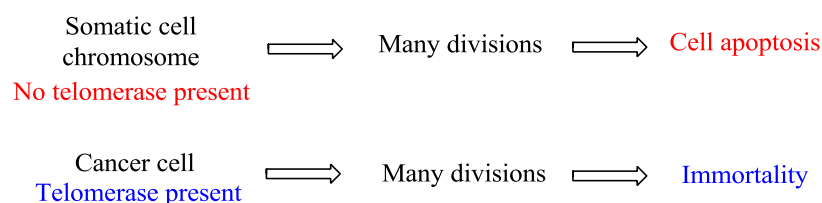
Figure 1.35. Summary of telomerase presence and its consequence.

1.4.2 Oncogene Promoter Regions

Other areas of DNA that possess G-quadruplex motifs can be found in oncogene promoter regions.[23] This region of DNA can be found upstream of a gene (5' end) and is the control point for regulated transcription.[86] Specific DNA sequences can be recognised by specific proteins leading to the activation of RNA polymerase and the creation of RNA from the coding part of the gene.[86]

Mutated genes that have the potential to cause cancer are called oncogenes. Their transformation leads to the abnormal regulation of cellular processes which can result in the loss of control of growth signals, the disruption of anti-growth signals, avoidance of apoptosis, continuous angiogenesis, unlimited replication abilities and metastasis.[86] Stable G-quadruplexes are able to form in oncogene promoter regions and as a consequence they can be linked to the genes altered expression when associated with critical proteins (*Fig 1.36*).[86]
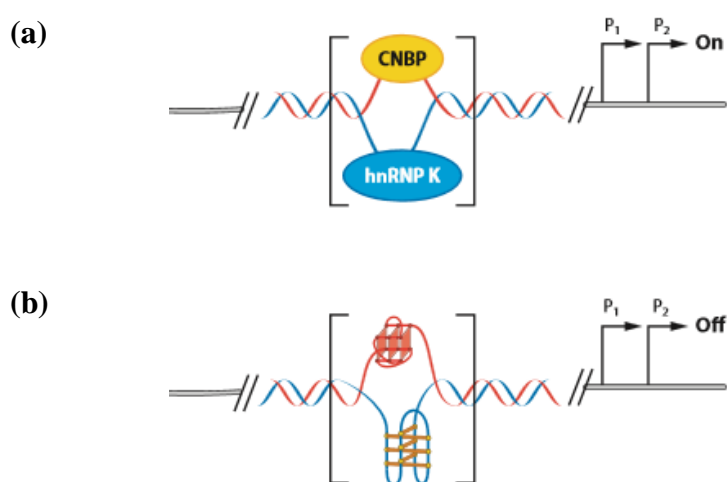
Figure 1.36. **a**. The binding of proteins CNBP (zinc finger protein 9) and hnRNP K (heterogeneous nuclear ribonucleoprotein K) to a promoter region causing transcription to be turned on, **b**. When the G-quadruplex and also i-motif are able to form in the G-rich sequences the protein can no longer bind and transcription is turned off. [Reproduced from Ref [87]]

The structural diversity of G-quadruplex structures due to differing loop lengths, loop bases and folding patterns in the different oncogene gene promoter regions, potentially allows selective targeting to be accomplished.[88] Examples of specific oncogene promoter regions where G-quadruplex formation is beneficial to their regulation are shown in *Table 1.1*.

Promoter Region	Effect of Transformation (Deregulation)	Quadruplex Effect
c-myc, c-kit and KRAS	Loss of control of growth signals	The formation and stabilisation of G-quadruplexes in these areas causes gene silencing, therefore preventing the activation of a specific process such as uncontrolled cell growth.[86]
pRb	Disruption of anti-growth signals	If an oncogenic protein binds to this DNA region it can stop the tumour repressor protein from being transcribed which would normally prevent excessive cell growth.[88] G-quadruplexes formed in this region help to prevent the binding of oncogenic proteins preventing insensitivity to tumour growth.[88]
Bcl-2	Avoidance of apoptosis	Up regulation can play a role in the resistance of conventional cancer treatments and deregulation of cell death.[89] G-quadruplex formation upstream of the P1 promoter can help prevent Bcl-2 transcription.[89]

hTERT	Uncontrolled replication	Stabilization of G-quadruplexes formed in this area leads to the inhibition of gene expression.[86] This directly inhibits telomerase expression instead of preventing actual telomerase binding to the telomeres.[86]
PDGF-A	Metastasis	This gene plays and essential role in cellular growth, proliferation, differentiation and development which when over expressed causes tumour growth.[90] DNA G-quadruplexes formed in this region of the human gene promoter have also been found to inhibit transcriptional activity.[90]

Table 1.1 Examples of oncogene DNA regions where G-quadruplexes are able to form due to their guanine rich compositions and the transformations that occur due to deregulation of the oncogene.

The formation of quadruplexes which turn on and off transcription factors can be better understood when considering the well studied oncogene c-myc.[87] C-myc expression has been linked to several cancers including breast, cervix, colon, small cell lung cancers, glioblastomas, osteosarcomas and myeloid leukemias.[87][91] As a proto-oncogene it has a crucial role in the regulation of cellular processes controlling cell growth, cell cycle progression and apoptosis.[92] Strict regulation of c-myc transcription is essential for the role it plays in biological processes.[92] Deregulation can occur when there are alterations in upstream promoter region signalling pathways which in turn leads to an increase in transcription.[92]

The c-myc promoter region DNA is able to exist in alternate forms to the normal double helical B-DNA structure.[93] The transition from B-DNA to single stranded DNA and other non-B-DNA forms such as G-quadruplexes and the i-motif can only occur when accompanied by localised unwinding or melting of the double helix.[93] Negative supercoiling stress (under winding, *Fig 1.37*) facilitates this unwinding (melting) process which is naturally formed behind the RNA polymerase complex during gene transcription. [93][94]
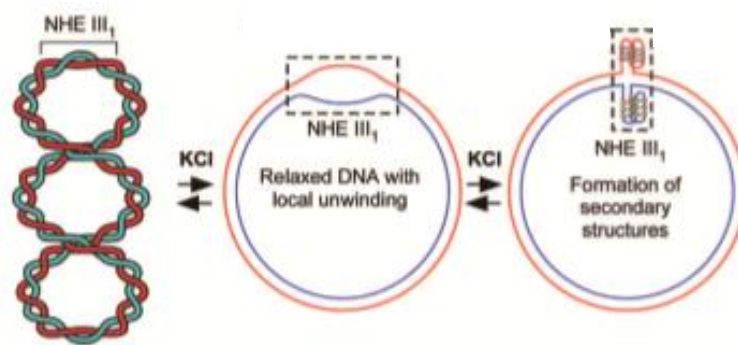
Figure 1.37. The unwinding of supercoiled DNA demonstrated with a Del4 wild type plasmid with NHE III$_1$ element showing the difference between the supercoiled and partially relaxed forms that occur during negative superhelical stress. [Reproduced from Ref [93]]

The area of most interest in the c-myc promoter region is the nuclease hypersensitive element III$_1$ region (NHE III$_1$) as it is here where the G-quadruplexes have the ability to form.[87] The slow equilibrium between duplex B-DNA, single stranded DNA and tetra stranded DNA is essential for controlling the binding of proteins in this area as up to 90% of c-myc transcription has been shown to be regulated by this part of the gene.[87][93]

1.5 Proteins that Bind G-Quadruplexes

In the oncogene cases put forward so far (in the Subchapter 1.4.2) the formation of the G-quadruplex structure prevents the binding of proteins, which require a single stranded binding site, and in doing so are able to alter transcription. There are however proteins that favour G-quadruplex binding over other types of DNA conformations.[95]

Interactions with some proteins help to stabilise the G-quadruplex structure and are reported to play a role in transcription and the control of cellular cycles.[95] RecA is one such repair protein that catalyses DNA strand exchange reactions between homologous double stranded DNA and single stranded DNA (homologous recombination).[96] The RecA protein is able to bind to single stranded DNA forming a nucleoprotein and it is this ATP dependent process that maintains genomic stability in both prokaryotic and eukaryotic cells.[96] More than 50% of the total genomic DNA is made up of repeat DNA sequences many of which form the majority of non-B DNA type structures.[96] Research into RecA-DNA interactions has been primarily focused on single stranded DNA that is able to form duplexes; understanding the interactions that evolve between proteins and non-B DNA forming sequences could be more biologically important.[96]

Further research has found that a labelled human telomeric sequence can preferentially bind to a RecA protein in the presence of K^+ ions in its G-quadruplex state over its single stranded from *(Fig. 1.38)*.[96] The nucleoprotein structure formed between the RecA protein and the single stranded telomeric sequence (in the absence of K^+ ions) will dissociate in the

presence of K^+ ions with the single stranded sequence folding into its G-quadruplex structure before again forming a nucleoprotein structure with the RecA protein.[96]
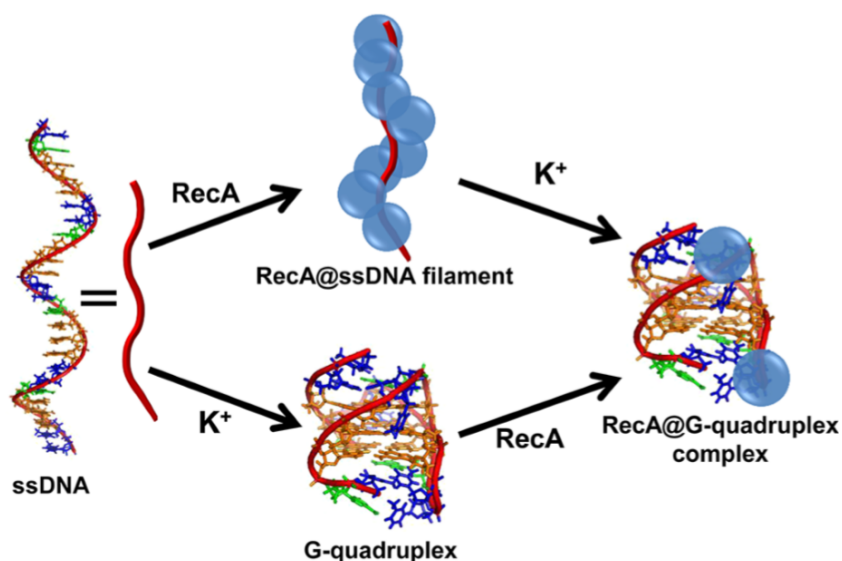
Figure 1.38. Escherichia coli RecA protein and dye-labelled human telomeric sequence (Cy5-5′- TAGGG-(TTAGGG)$_3$-TT-3′-Cy3) binding preferences with and without the presence of K^+ ions. [Reproduced from Ref [96]]

Another G-rich sequence of interest (5'-GGTTGGTGTGGTTGG-3') that folds into an antiparallel G-quadruplex structure, TBA (thrombin binding aptamer), is of particular interest as it is known to bind specifically to the protein thrombin (a coagulation protease) inhibiting it (*Fig. 1.39*).[97]   Under molecular crowding conditions in a cell mimicking environment (reflects osmotic pressure which changes in live cells where altering water activity can affect biomolecule hydration); binding experiments were conducted to examine the thermodynamics of TBA-thrombin interaction.[97] The investigation revealed that both the binding affinity of the TBA-thrombin interaction and the G-quadruplex stability decrease when conducted in molecular crowding conditions.[95] This leads to the assumption that water is required for G-quadruplex-protein binding.[95]
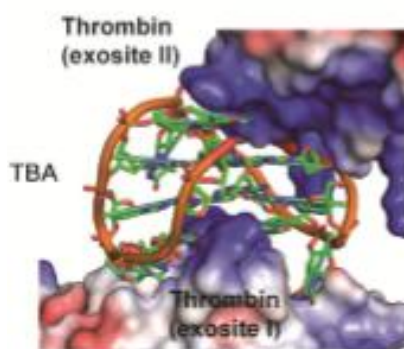
Figure 1.39. Structure showing the interaction between G-quadruplex (TBA) and thrombin. Binding occurs through two TT loops and one TGT loop of the quadruplex. [Reproduced from Ref [95]]

This type of binding system can be exploited in order to provide a sensor for thrombin at low detection limits.[98] Hemin is an iron-containing porphyrin (*Fig 1.40*) which has been found to bind to TBA in an end stacking mode interacting through electrostatics and hydrophobic interactions, resulting in a complex with horseradish peroxidase type activity.[98] The complex formed between the DNA and hemin is known as a DNAzyme and has been used for the detection of metal ions, small molecules, DNA and proteins.[99]
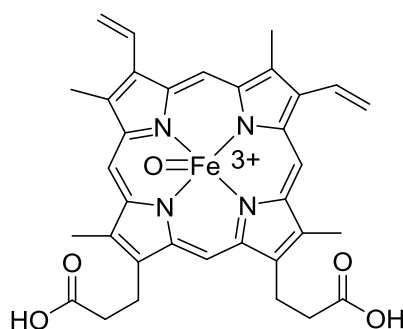
Figure 1.40. Structure of hemin, chloro(protoporphyrinato)iron(III). [98]

The TBA-hemin system is particularly useful as it is able to catalyse the H_2O_2 mediated oxidation of potential fluorophores.[99] In the presence of thrombin the activity of the TBA-hemin system is further increased giving rise to a strong fluorescent emission

signal.[99] Advantages of fluorescence detection include low reagent concentrations as the method is highly sensitive, simple experiment set up and quick result turnaround.[99] This system therefore is very attractive in the generation of biological sensors.[99] The potential fluorophore of interest is that of thiamine which is itself non-fluorescent however after oxidation with H_2O_2 it transforms to the strongly fluorescent compound thiochrome (*Fig 1.41*).[98][99]

Using this method of fluorescence detection for thrombin, concentrations as low as 1 pM can be recorded creating a highly sensitive thrombin aptasensor.[99] This type of interaction can also be exploited in nano device protein sensors.[95][96]
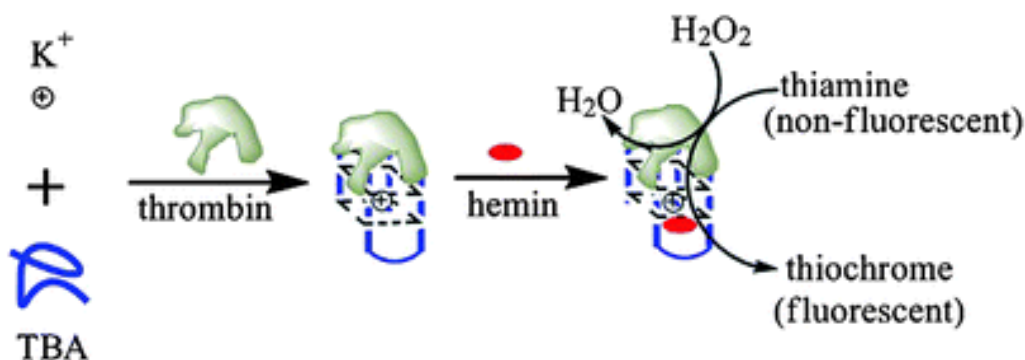
Figure 1.41. The production of fluorescent thiochrome through the hydrogen peroxide mediated oxidation step initiated by the formation of TBA-hemin complex and thrombin. This results in the fluorescent detection of thrombin. [Reproduced from Ref [99]]

1.6 G-Quadruplex Binders: Organic Compounds

There are many ligands that have been reported to bind to G-quadruplexes; the appearance of which came after a selection of organic amido-anthraquinone derivatives were found to inhibit telomerase through quadruplex formation.[100] The basic requirements for G-

quadruplex binding include a planar heteroaromatic system which interacts by stacking with the G-quartets and terminal basic groups for favourable interactions with the DNA loop sugar phosphate backbone.[20]

1.6.1 BRACO-19

BRACO-19 is a 3,6,9-trisubstituted acridine compound (*Fig 1.42*) that interrupts telomerase function, hence showing promising tumour inhibition.[101] When assessing its binding affinity to different types of DNA using surface plasmon resonance (SPR) studies it was found to bind to G-quadruplexes 40 times more strongly than duplexes.[102] When exposed to human uterus carcinoma cells in a non cytotoxic concentration the telomeres were found to have shortened from 2.7 to 2.3 kb after 15 days.[101] The same effect has been seen in breast cancer cells with a 17% decrease in telomere length after 39 days, reducing telomere length from 6 kb to 5 kb.[101] The crystal structure of the complex with a telomeric sequence of DNA revealed a parallel topology with the complex end stacked between two quadruplexes (*Fig 1.42*).[100]
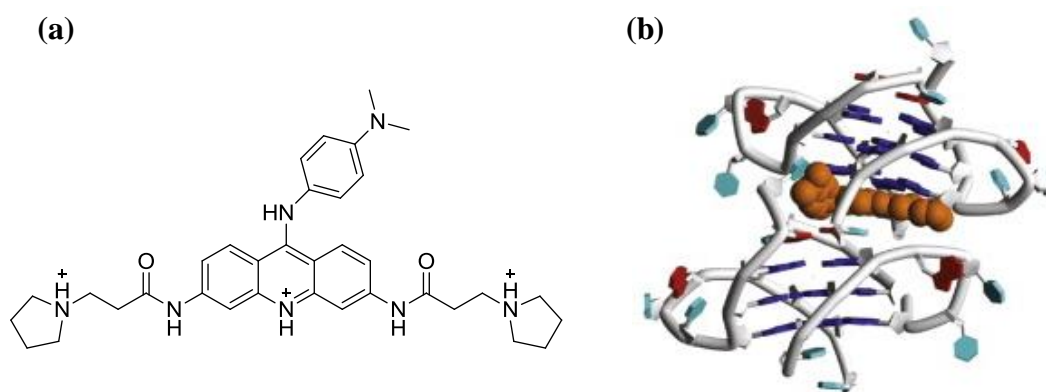
Figure 1.42 **a**. Organic compound, BRACO-19, **b**. Crystal structure of two parallel G-quadruplexes with BRACO-19 stacked in-between. [Reproduced from Ref [100]]

TTA loop conformations in these types of structures allow the formation of pockets in which the complexes side groups can reside.[100] The crystal structure obtained for this system is also heavily hydrated thereby demonstrating how important water molecules are in the attraction between the two components.[100] No direct electrostatic interactions can be formed between the positively charged ligand substituents and the negatively charged DNA backbone.[100] Acridine ligands, in general, show anticancer activity because of their ability to interact with nucleic acids.[101] This can be achieved by intercalation between DNA base pairs and dissociating the catalytic subunit of telomerase (hTERT) from its capping function or by stabilisation of quadruplex formation preventing telomerase action.[101][103][104] BRACO-19 is in the latter category and due to its significant anticancer activity it is now being adapted to incorporate a monomethine cyanine dye which will enable the system to act as a pH-sensitive, fluorescent and colorimetric G-quadruplex binder.[103]

1.6.2 TMPyP4

Porphyrins have large aromatic surfaces and four meso positions that can be substituted to functionalise the complexes for specific binding making them ideal G-quadruplex binders.[105] TMPyP4 is a tetra-N-methyl-pyridyl porphyrin (*Fig. 1.43*) that is able to bind to G-quadruplexes and consequently probe the quadruplex structure due to its high positive charge.[100][105]

Investigations have primarily taken place with c-myc quadruplexes and they have been shown to repress c-myc transcription.[106] The ligand-DNA interaction is believed to stem

from the N-methyl pyridyl rings of the ligand which are close (3.5 Å) to the terminal G-quartet for effective stacking interactions.[100]
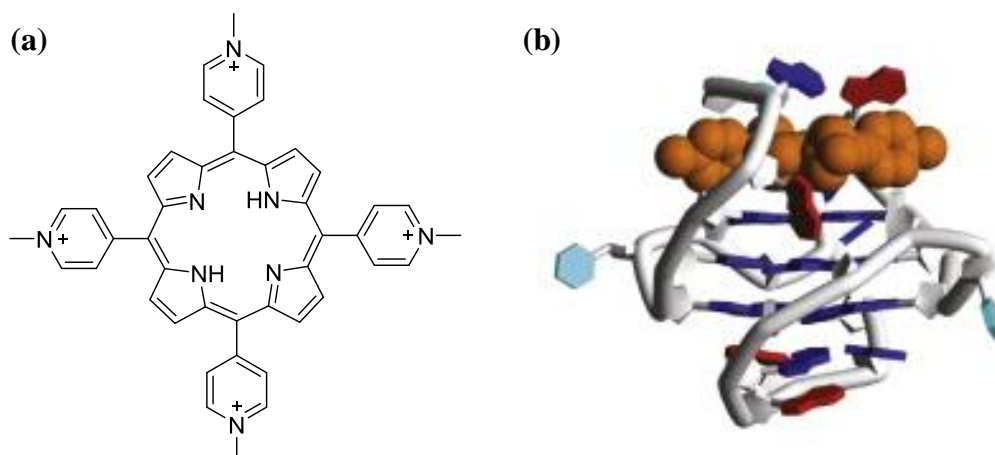
Figure 1.43 **a**. Cationic porphyrin TMPyP4, **b**. Structure of a parallel G-quadruplex binding to TmPyP4. [Reproduced from Ref [100]]

A problem with this ligand arises because it isn't very selective for G-quadruplex DNA over duplex DNA.[107] Alterations to the porphyrin complex design are being achieved by incorporating cationic substituent's at the meso positions and metal ions in the central cavity in order to provide better selectivity.[107]

1.6.3 TQMP

A porphyrin derivative which has been shown to bind to G-quadruplexes inhibiting telomerase is the phenol quaternary ammonium porphyrin, TQMP (5,10,15,20-tetra[4-hydroxy-3-(tri-methylammonium)methyl-phenyl]porphyrin, *Fig. 1.44*).[108] A SPR study has shown that it binds to G-quadruplexes 35 times more strongly than to DNA duplexes.[108] The complex is believed to be a cross linking agent which could cross link G-quadruplexes that form in the telomeric region through an o-quinone methide intermediate when photoactivated.[108] The enhanced selectivity of TQMP for quadruplexes over duplexes reported, when compared with TMPyP4, may be because it

has more flexible appendages and additional hydroxyl groups which can participate in further potentially stabilising hydrogen bonding.[108]
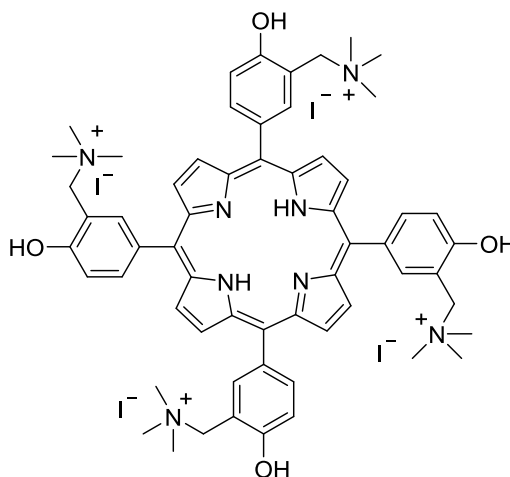
Figure 1.44 Structure of phenol quaternary ammonium porphyrin, TQMP.

1.6.4 Telomestatin

Telomestatin is a natural product that has been isolated from the micro-organism Streptomyces anulatus 3533-SV4.[109] Its structure consists of eight heterocyclic rings including a thiazoline, two methyloxazoles and five oxazoles all joined together in a macrocycle (*Fig. 1.45*).[110] The naturally occurring compound is one of the tightest known binders to G-quadruplexes.[66] It is able to bind to the basket structure of a G-quadruplex found in the telomeric region, TTAGGG repeats, of DNA.[110] The anti-parallel quadruplex that it stabilises prevents the binding of telomerase to the ends of the DNA thereby preventing the extension of telomeres allowing the cell to eventually succumb to apoptosis.[110]
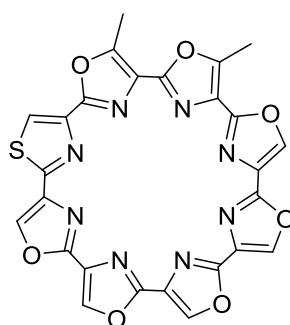
Figure 1.45 Structure of Telomestatin.

The macrocycle is reported to have an EC_{50} (concentration for half maximum effect) of 0.9 - 1.2 µM inducing the apoptosis of various cancer cells.[66][109] An important advantage of this drug is its 70-fold selectivity for intramolecular G-quadruplex DNA structures over that of duplex DNA.[111] This can be attributed to its circular shape and its ability to coordinate a monovalent cation such as K^+.[112] When telomestatin stacks on top of a G-quartet the K^+ cation is likely to reside between the two units.[112] The molecule is also too large to intercalate in between the duplex base pairs. *Fig. 1.46* shows the results of the density functional theory calculations used to optimise the telomestatin - cation - G-quartet geometries.[112]
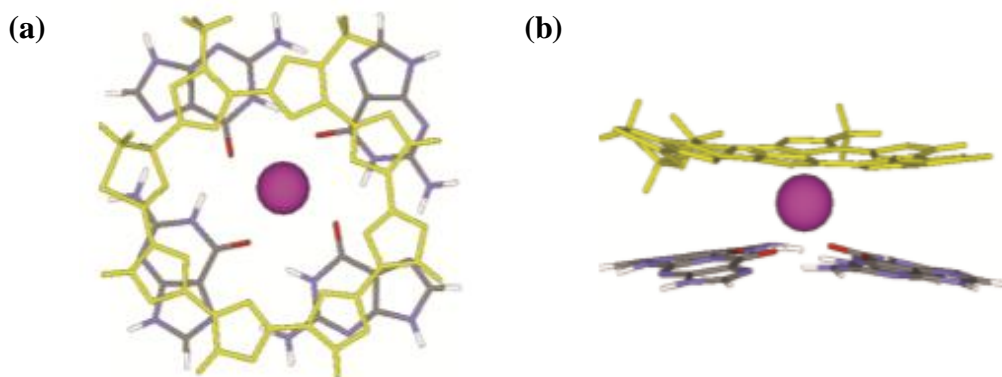
Figure 1.46 **a**. Overlaid structure of telomestatin (yellow) over a G-quartet (blue) with a potassium ion in the central cavity, **b.** The location of the potassium ion sits directly between the two layers (telomestatin and G-quartet) mimicking the position of the cation between two G-quartet layers. [Reproduced from Ref [112] both generated by DFT analysis using B3LYP and 6-31G(d,p)].

1.7 Using Metal Complexes to Target G-Quadruplexes

The incorporation of a metal into the structure of a potential G-quadruplex binder has a number of advantages which include:

- ***Providing a structural centre:*** The electronic configuration of the metal is able to dictate and organise the geometry of the ligands surrounding it, Pt^{2+} for example is a d^8 metal and

therefore forms square planar structures. Using the metal as a template allows for a relatively straight forward synthesis procedure which can generate a small collection of related complexes.[112] Ligands can be modified whilst retaining the geometry around the metal centre or the metal can be changed giving rise to a change in geometry and/or new optical properties.[113]

- ***Increasing the strength of stacking interactions:*** The positively charged metal is able to withdraw electron density from the π system of which it is coordinated leading to stronger interactions between the electron poor system and the G-quartets.[113] The metal is also able to electrostatically stabilise the system by imitating the potassium and sodium cations that usually sit in between the G-quartet layers of the G-quadruplex structure.[113]

- ***Provides cationic charge:*** This is very important for DNA binding due to the negatively charged DNA backbone.

- ***Allows direct interaction with nucleic acids:*** Through coordinate bonding.

- ***Detection:*** Complexes can be examined using fluorescence, redox or UV-vis techniques.[113]

1.7.1 Terpyridine Based Metal Complexes

Terpyridine (2,2':6',2''-terpyridine, tpy) is a tridentate ligand which, because of its triple chelation binding mode and its planar surface, is used extensively in coordination chemistry (*Fig 1.47*).[114] Metals such as Cu(II), Pt(II), Zn(II) and Ru(III) can easily be accommodated by the ligand allowing a whole host of different metal complexes (with differing geometries) to be synthesised with ease.[114] Tolyl-terpyridine ligand (4-(4-methylphenyl)-2,2':6',2''-terpyridine) is another terpyridine derivative which also has extensive co-ordination chemistry.[114]
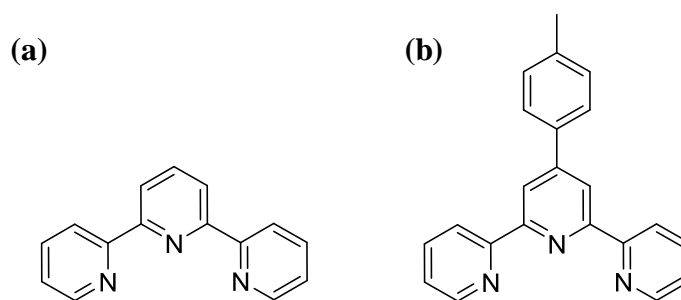
Figure1.47 **a.** Terpyridine structure (tpy), **b**. Tolyl-Terpyridine structure (ttpy).[114]

The ability of terpyridine type metal complexes to act as G-quadruplexes binders has been reported by Teulade-Fichou *et al*.[114] The [Cu-ttpy][(NO$_3$)$_2$] complex was found to be the most promising candidate as it showed a strong affinity and selectivity for quadruplex DNA over duplex DNA (22 times more selective by fluorescent indicator displacement (FID) analysis).[114] This can be rationalised by considering its pseudo-square pyramidal structure (*Fig 1.48*).[114] The complex is able to; utilise its planar aromatic face to stabilise the G-quadruplex through hydrophobic interactions, centralise the position of the Cu^{2+} ion to mimic the naturally occurring cations that stabilise the quadruplex structure, prevent intercalation with duplex DNA and induce electrostatic interactions as a result of the highly polarised metal-ligand bonds.[114]
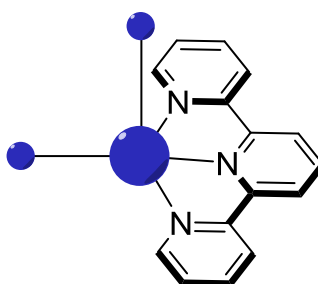
Figure 1.48 Square pyramidal copper(II) terpyridine structure.[114]

The effect of palladium based terpyridine complexes to stabilise G-quadruplexes have been investigated as a comparison to platinum.[115] Platinum(II) and palladium(II) are both soft Lewis acids, have square planar geometries and show similar trends when binding to nitrogen containing chelates.[115] Their difference arises from ligand exchange kinetics where the rate of hydrolysis, for instance, is much faster for palladium than it is for platinum (105 times faster).[115] The kinetic instability of palladium-DNA complexes has prohibited the use of palladium in DNA binding drugs.[115] The ability however to change the properties of the metal through the type of heterocylic ligands bound to it has seen an increase in the number of palladium complexes being synthesised for DNA targeting.[115] Both [Pd(ttpy)] and [Pd(tMebip)] (ttpy = tolyl-terpyridine, tMebip = 2,2'-(4-p-tolylpyridine-2,6-diyl)-bis-(1-methyl-1H-benzo[d]imidazole)) complexes (*Fig 1.49*) have been found to bind more quickly to G-quadruplexes (in less than 1 hour) and display better inhibition of cancer cell growth than their platinum analogues.[115] They are believed to bind coordinatively to the base thymine (through N3) in the quadruplex loops of the DNA sequence (TGGGGT)$_4$ after hydrolysis, rather than in an end stacking mode to the terminal G-quartet.[115]
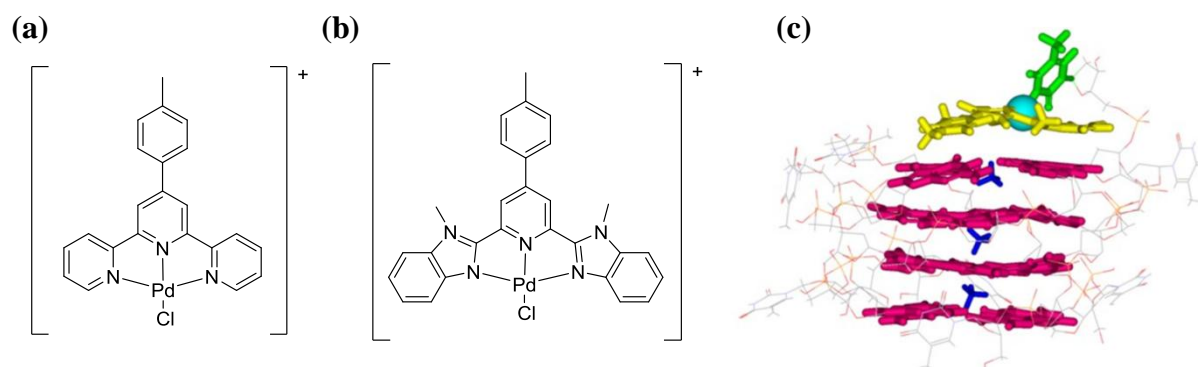
Figure 1.49 Structures of **a**. [Pd(ttpy)Cl]$^+$, **b**. [Pd(tMebip)]$^+$, c. Molecular model showing the Pd-tMebip complex and its proposed interaction with the quadruplex sequence (TGGGGT)$_4$ through thymine. [115]

There are also other substituted terpyridine ligands which have incorporated cyclic amine side chains in order to provide extra interactions with the DNA (*Fig 1.50*).[113] The protonated amines can interact with the loops and grooves of the DNA whilst providing increased water solubility for the aromatic complex.[113] Increasing the bulkiness of the complexes through addition of the side groups can also enhance the selectivity for quadruplex DNA over duplex DNA.[113]
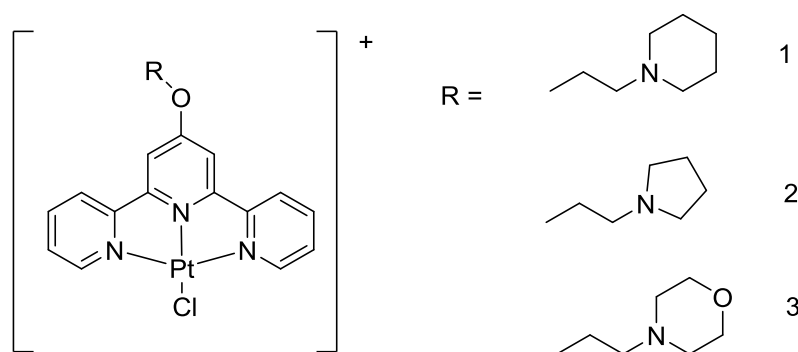
Figure 1.50 Platinum(II) terpyridine functionalised with amine containing ligands that were found to bind well to quadruplex DNA.[113]

Di-metal terpyridine complexes (with Cu^{2+}, Pt^{2+} and Zn^{2+}) have been explored by Vilar *et al* (*Fig. 1.51*).[20] They are designed to interact with the G-quartet through the stacking of the terpyridine analogues and also the DNA phosphate backbone through the interaction of the metal dipicolylamine moiety by electrostatics or direct coordination (depending on the metal).[20] Binding experiments were conducted with the ligands alone as well as with those that were in complexes with the metals.[20] While the di-copper and di-platinum complexes (*Fig 1.51*) were able to form strong interactions with the quadruplex DNA with binding constants as high as 10^6 M^{-1} and 100 fold selectivity over duplex DNA, the ligands alone were not able to display comparable activity.[20] This led to the conclusion that

metals are essential for the binding affinities seen between the aromatic polydentate ligands and the quadruplex DNA.[20]
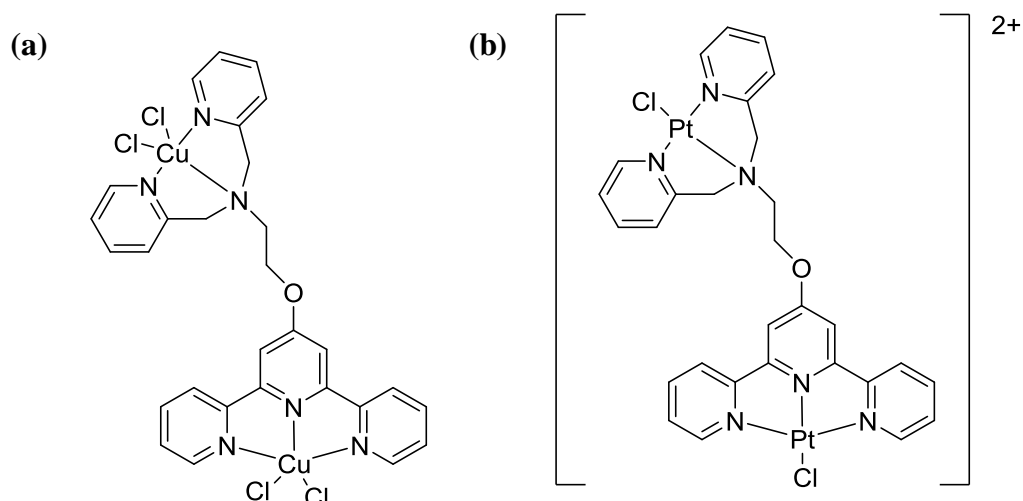
Figure 1.51 Structures of **a**. Di-metallic copper(II) complex, **b**. Di-metallic platinum(II) complex.[20]

1.7.2 Phenanthroline Containing Metal Complexes

Phenanthroline is another aromatic ligand that can provide a metal complex with the required efficient hydrophobic interactions in order to bind well to G-quadruplexes.[116] The ligand can be easily modified to create protonatable side groups which allow further interactions with DNA loops and grooves.[116] Phenanthroline derivatives have also attracted attention because of their pharmacological effects in many drugs.[116] The following two phenanthroline examples show a degree of quadruplex DNA binding.

a. [Pt(phen)$_2$][PF$_6$]$_2$ has been examined for its binding affinity towards a human telomeric DNA sequence and despite its simple design (*Fig 1.52*) it was able to show effective binding through stacking to the end face of the G-tetrad.[117] It was even found to change the quadruplex conformation from parallel to antiparallel by being able to stabilise one

form over another due to the position of the loops.[117] The reason for its success is partially ascribed to its close size match to a G-quartet itself being 10.4 Å (length) which is very close to that of a G quartet at 10.8 Å.[117]

b. Neidle and co-workers have developed a square planar phenanthroline based platinum complex that shows a high degree of G-quadruplex stabilisation and telomerase inhibition with a 40 fold selectivity for quadruplex DNA over duplex DNA.[118] The phenanthroline system is modified with a cyclic amine or pyridine side arm that can interact with the loops of the quadruplex achieving efficient binding while the phenanthroline moiety stacks on top of the G-tetrad.[118] The metal plays an essential part in electrostatics and mimicking the naturally present cations (*Fig. 1.52*).[118]
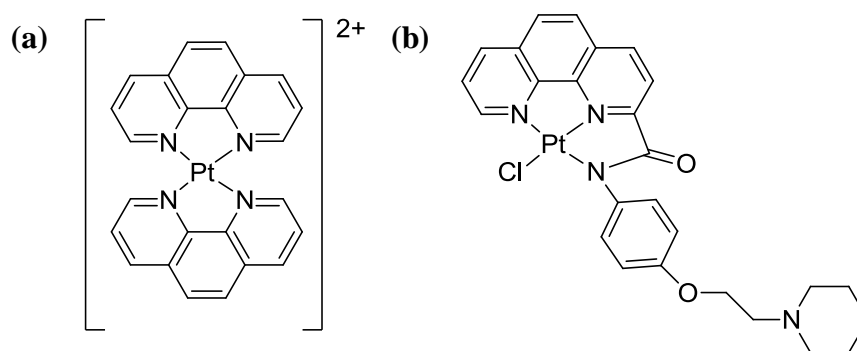
Figure 1.52 Structures of **a.** [Pt(Phen)$_2$]$^{2+}$ [117], **b.** Pt^{2+} mono-substituted phenanthroline.[118]

1.7.3 Platinum Phenanthroimidazole Complexes

Sleiman and co-workers have synthesised a platinum complex with an extended phenanthroimidazole ligand that increases the stacking surface area (*Fig. 1.53*).[119] Binding studies were conducted with both intermolecular G-quadruplex forming DNA (d(T$_4$G$_4$T$_4$)$_4$) and duplex DNA where the binding constant calculated for the quadruplex

DNA was found to be about two orders of magnitude larger than to duplex DNA, 10^7 versus 10^5 M^{-1} (binding constant established from UV-vis spectroscopy).[119] The high binding affinity for the complex to the G-quadruplex was likely to have arisen due to the size of the surface area of the phenanthroimidazole complex.[119] Using molecular modelling the complex was shown to form many favourable stacking interactions with the bases of the terminal G-quartet along with additional stabilising hydrogen bonds between the ethylenediamine ligands and the sugar phosphate backbone (*Fig. 1.53*).[119]
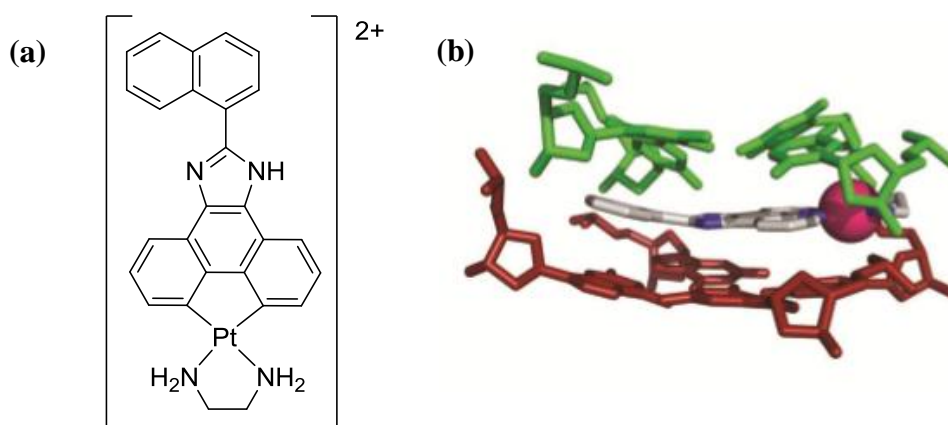
Figure 1.53 **a.** Structure of naphthylphenanthroimidazole ethylenediamine platinum(II), **b**. Molecular modelling prediction of complex-intermolecular quadruplex binding showing the end G-quartet (brown), thymine bases (green) and the platinum complex (grey). [Reproduced from Ref [119]]

1.7.4 Salphen Based Metal Complexes

Vilar and co-workers have reported the binding of nickel(II) and copper(II) salphen metal complexes to human telomeric DNA.[120] The X-ray crystal structures of these systems show the metal complexes binding to the quadruplex DNA through an end stacking mode with the metal ion located almost in line with the other potassium ions in the central cavity (*Fig. 1.54*).[120] Both complexes show antiproliferative effects in a selection of cancer cell lines and telomerase inhibition in a modified telomere repeat amplification protocol

(TRAP-LIG) assay (see page 61).[120] Despite their similar structures the nickel complex shows better quadruplex binding than the copper analogue which can be rationalised when considering their X-ray crystal structures.[120] The nickel(II) and copper(II) complexes both have butterfly (bent) like conformations and when they are bound to the quadruplex this bent formation is significantly reduced (*Fig. 1.54*).[120] Despite this reduction the copper(II) complex displays a significant degree of bent character therefore cannot stack on top of the G-quartet as efficiently as the flatter nickel(II) complex; leading to the difference in binding abilities.[120] The nickel(II) complex is especially promising as it shows around a 1400 fold selectivity for telomeric quadruplex DNA over duplex DNA when examining their binding constants by UV-Vis spectroscopy.[120]
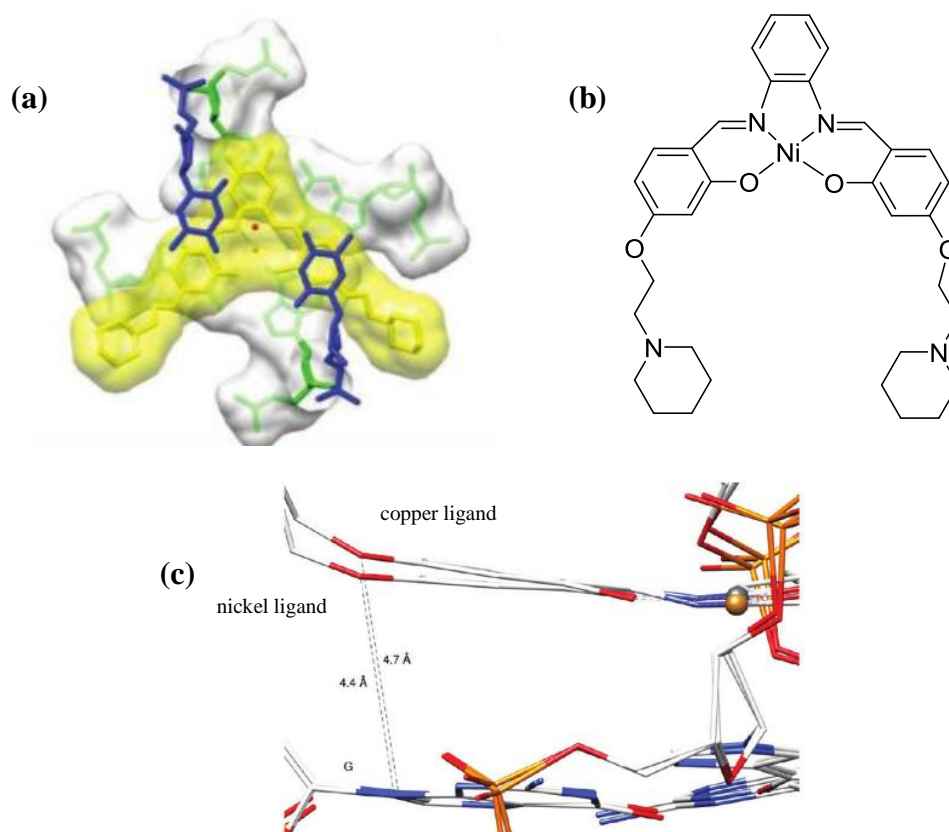
Figure 1.54 **a**. Structure of the Ni(II) salphen complex binding to a G-quartet, showing the near overlap of the central cavity potassium ion and the Ni(II) ion [Reproduced from Ref [120]], **b**. Structure of Ni(II) salphen complex, **c**. Difference in planarity between nickel and copper complexes. [Reproduced from Ref [120]]

1.7.5 Platinum Supramolecular squares

Supramolecular squares are an attractive molecular design for targeting G-quadruplexes as they can be constructed by supramolecular self assembly which is appealing as complexes can be created in a single step, often in good yields also.[121] The platinum supramolecular square shown in *Fig 1.55* is an efficient G-quadruplex binder and telomerase inhibitor.[121] The reason for which is because of the high positive charge of the complex (8+), the arrangement of the four bipyridyl ligands and the hydrogen bonding interactions between the phosphates of the DNA backbone and the ethylenediamine ligands.[121] The aromatic rings of each of the 4,4-bipyridyl ligands add to the overall binding affinity by being able to interact with the guanine bases in a distorted T-shape geometry.[121]
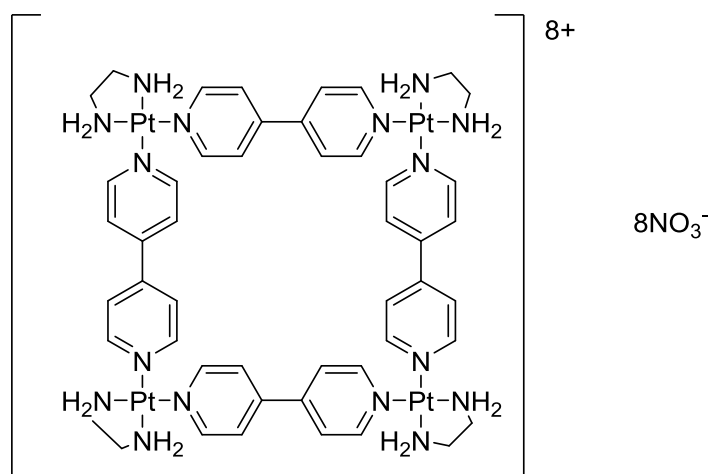
Figure 1.55 Structure of the supramolecular platinum square.[121]

1.7.6 Nickel Supramolecular Helicate

The nickel supramolecular helicate (*Fig. 1.56*) is based on the design of the metallo supramolecular helicates synthesised by Hannon *et al* with the formula $[M_2L_3]^{4+}$.[11] Work conducted by Qu *et al* suggests that the P enantiomer of the nickel supramolecular helicate

is able to selectively stabilise quadruplexes formed in the telomeric region of DNA.[122] The complex was found to be 20 times more selective for G-quadruplexes over duplexes using UV melting experiments in a sodium rich buffer.[122] Qu reports that the helicate has a hydrophobic surface which is similar in size to the G-quartet.[122] The complex is able to bind by externally stacking to the end of the G-quadruplex by interacting with the two lateral loops.[122] Circular dichroism studies on the complex have shown that it is able to convert an antiparallel quadruplex conformer into a hybrid conformer when conducted in a Na^+ rich buffer.[122]

(a)

$[Ni_2L_3]^{4+}$

L

(b)
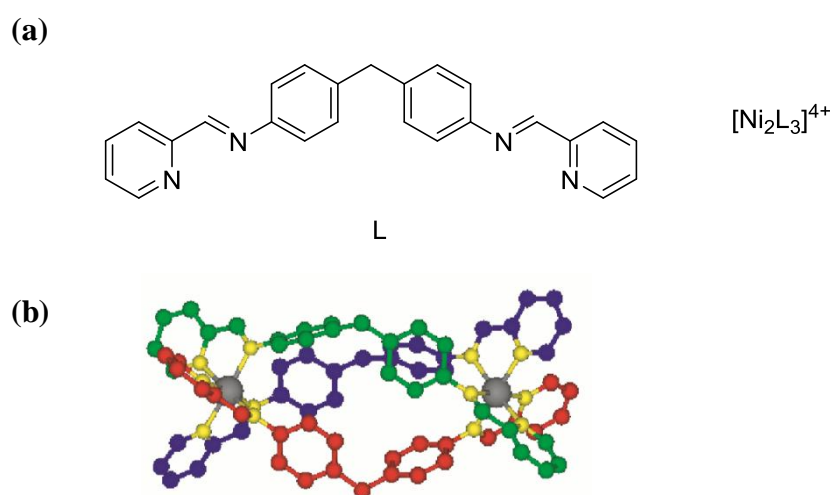
Figure 1.56 **a**. Structure of the nickel supramolecular helicate, **b**. crystal structure of the nickel helicate. [Reproduced from Ref [122]]

1.7.7 Substituted Salicylaldehyde Dibenzyl Semicarbazones

Copper(II) salicylaldehyde semicarbazone complexes have recently been investigated for their use as G-quadruplex binders after they were found to be very cytotoxic against a number of cancer cell lines.[123] In human leukaemia cells the complex is able to induce apoptosis and cause the down regulation of proteins that are used in processes such as translation, protein folding and transcription.[123] The binding strength of the complex, shown in *Fig. 1.57*, to telomeric quadruplex DNA is more than 200 times stronger than to

duplex DNA.[123] The binding constant obtained between the complex to the quadruplex DNA (10^5 M^{-1}) can be attributed to the positive charge it carries which leads to favourable electrostatic interactions between itself and the electron rich guanine bases.[123] The square planar structure of the complex with its π surface area allows it to stack onto the end of a G-quartet.[123] Circular dichroism studies found that the complex doesn't alter the structure of telomeric quadruplexes in the presence of K$^+$ or help template their formation in cation free buffer.[123] They are however able to recognise and bind to pre-formed quadruplexes which may affect the stability of the quadruplex.[123] The complex is also selective for one type of quadruplex over another as it is 22 times more selective for telomeric quadruplexes over c-myc quadruplexes.[123]
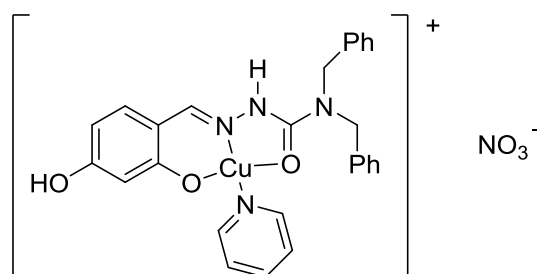
Figure 1.57 Structure of a copper(II) salicylaldehyde semicarbazone complex.

1.7.8 Pentacationic Manganese(III) Porphyrin

A manganese(II) porphyrin (*Fig. 1.58*) has been synthesised that encompasses an aromatic centre and four cationic side arms, both favourable attributes for an effective G-quadruplex binder.[29] The complex does in fact bind very well to quadruplexes and shows a selectivity for telomeric quadruplex DNA over duplex DNA by 4 orders of magnitude when measured by SPR (10^8 versus 10^4 M^{-1}).[29] The poor binding affinity of the complex to duplex DNA may be due to the size of the bulky cationic arms with prevents the two species from being very close in space.[29] On the other hand the strong binding affinity of

the complex for quadruplex DNA is likely to have arisen from the stacking of the aromatic core over the end G-quartet and interactions between the cationic arms and the loops of the quadruplex DNA.[29]
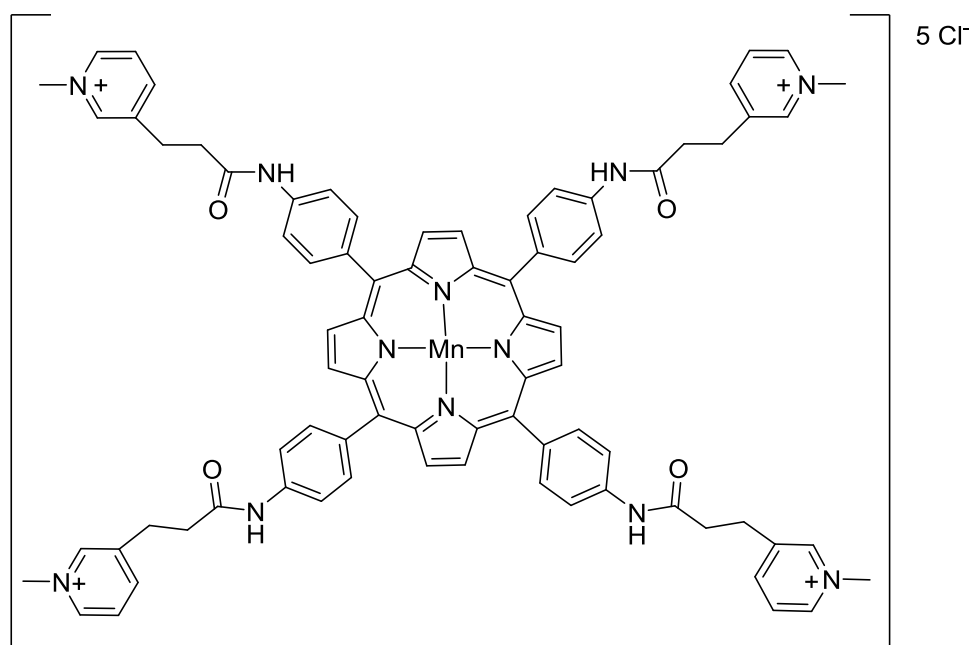
Figure 1.58 Structure of a pentacationic manganese(III) porphyrin.

1.8 Experimental Monitoring of Quadruplex formation

There are a multitude of techniques to study the formation of quadruplexes, a few of which, and the thesis sections they can be found in, are shown in *Table 1.2* below:

CD spectroscopy	Specific CD spectra related to the topology of the quadruplex. Able to differentiate between parallel and antiparallel G-quadruplex structures.	*Chapter 3.2*

Fluorescent intercalator displacement (FID) assay	Thiazole orange binds to DNA and is displaced if the complex binding affinity for DNA is higher. Specificity of drug for one type of DNA over another can be analysed.	*Chapter 3.4*
UV-Vis binding studies	Shifts in MLCT bands during titrations indicate binding of DNA to complex. Possible to calculate binding constants from UV-vis titration data.	*Chapter 3.5*
Proton NMR	Imino protons of quadruplex DNA can be examined and compared with and without the presence of the complex. Changes in symmetry of DNA or complex protons can indicate binding.	*Chapter 3.6*
FRET melting assay	Labelled DNA strands that have the potential to fold into G-quadruplex structures can be analysed. FRET only occurs when the ends of DNA are close in space, allows stability to be assessed.	*Chapter 3.8*

Table 1.2 Techniques used to study G-quadruplex formation and topology and the chapter of this thesis they are explained in detail.

Paving the way for the experimental monitoring of G-quadruplex structures in biological systems is Shankar Balasubramanian who after conducting a genome-wide study showed pyridostatin (*Fig. 1.59*), a quadruplex stabilising small molecule, was able to induce DNA damage in areas of the genome rich in G-quadruplex motifs.[83] The DNA damage may be caused by pyridostatin binding to quadruplexes during transcription and replication, preventing the corresponding gene expression.[124] This can eventually lead to DNA breakage brought about the activation of a DNA damage response.[24]
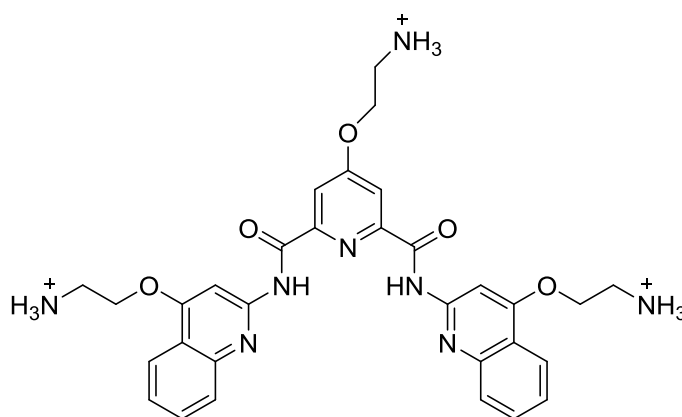
Figure 1.59 Structure of the pyridostatin.

Further research conducted by Balasubramanian *et al* features a structure-specific antibody which is able to quantitatively visualise G-quadruplexes in human cells.[83] The technique is particularly useful as it employs the single chain antibody clone (BG4), selected from over 10^{10} other antibodies due to its high affinity for G-quadruplexes.[83] It is then treated with another antibody to amplify the fluorescence signal before adding a tertiary fluorochrome labelled antibody.[83] Following the treatment of isolated chromosomes with the BG4 antibody it was found that the antibody localised at the chromosomal ends as well

as other locations within the DNA (oncogene promoter regions are a likely source).[83]

(*Fig 1.60*)

Figure 1.60 Two metaphase chromosomes isolated from cervical cancer cells. Immunofluorescence of the BG4 antibody (seen in red) occurs both in telomeric and non-telomeric regions of DNA. [Reproduced from Ref [83]]

Other techniques which help probe G-quadruplex and potential binder interactions include TRAP and scratch wound healing assays.[124][125]   In the TRAP (telomere repeat amplification protocol) assay the ability of the quadruplex binder to inhibit telomerase in vitro is determined.[125] A non-telomeric sequence of DNA is able to be extended by telomerase with telomeric repeats and then amplified by PCR producing a ladder of results depending on the length of telomere produced by the telomerase.[126] If a complex induces or stabilises a G-quadruplex structure the telomerase is inhibited therefore the PCR results would show a reduction in telomere length with the introduction of the complex.[126] The example TRAP assay results shown in *Fig 1.61* have been produced by two ruthenium complexes [Ru(bpy)$_2$(ptpn)]$^{2+}$ (complex 1) and [Ru(phen)$_2$(ptpn)]$^{2+}$ (complex 2) (also in *Fig 1.61*) where addition of higher concentrations of the complexes reduced the amount of telomere bands seen at higher base pair (bp) numbers.[126]
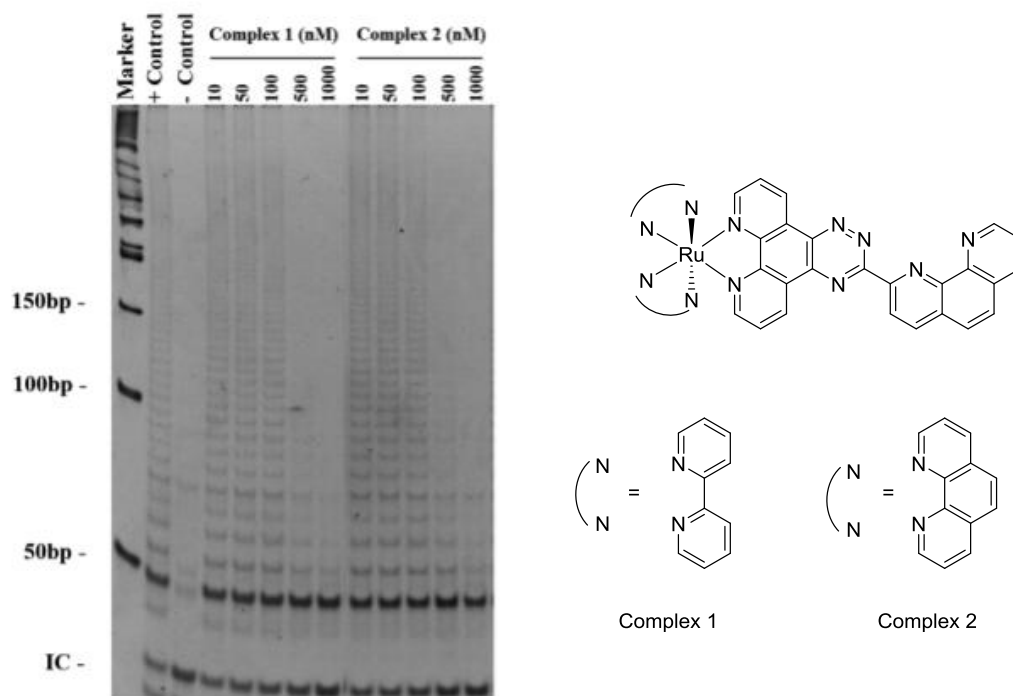
Figure 1.61 The results of a telomerase inhibition assay where the effect of the complexes on telomere length in the presence of telomerase was compared with telomerase + DNA (+ Control) and the DNA alone (- Control). IC is the internal control primer (left) [Reproduced from Ref [125]], Ruthenium complexes used in this study (right).

Scratch assays have been used to show how the mobility of cells are hindered by the addition of a DNA binding complex.[127] In the assay cells are grown on a surface in a single monolayer before making a wound (scratch) on the monolayer.[127] Pictures are then taken at regular intervals to capture the migration of cells around the wound, in principle mimicking cell migration during wound healing in vivo.[127]

The proto-oncogene SRC produces a non-receptor protein that phosphorylates specific tyrosine residues in other proteins playing an essential role in cell motility and invasion.[124] As with other oncogenes the protein can be over expressed leading to cancer.[124] The promoter region of the SRC gene is a G-quadruplex rich area where the ability of pyridostatin (which is a selective G-quadruplex binder) was investigated to see if

it would have an effect on the mobility of a breast cancer cell line by inhibiting the production of the SRC protein.[124] The scratch assay results showed that after creating a wound across the cell plate the cells were unable to migrate back into it (*Fig 1.62*).[124] This was a good indication that the mobility was being inhibited due to the binding of the pyridostatin and preventing the activation of the SRC gene; although not the sole explanation as the disruption of other cellular processes cannot be disregarded.[124] The same experiments with another DNA binder, doxorubicin, were unable to show the same results as the cells were able to migrate back into the wound despite both complexes being able to induce similar cell damage in cell proliferation tests.[124] Doxorubicin, therefore does not appear to target the SRC gene which infers that it is not able to bind as successfully to quadruplexes as pyridostatin.[124]

(a) Untreated (0 h)   **(b) Untreated (48 h)**

(c) Pyridostatin (48 h)   **(d) Doxorubicin (48 h)**
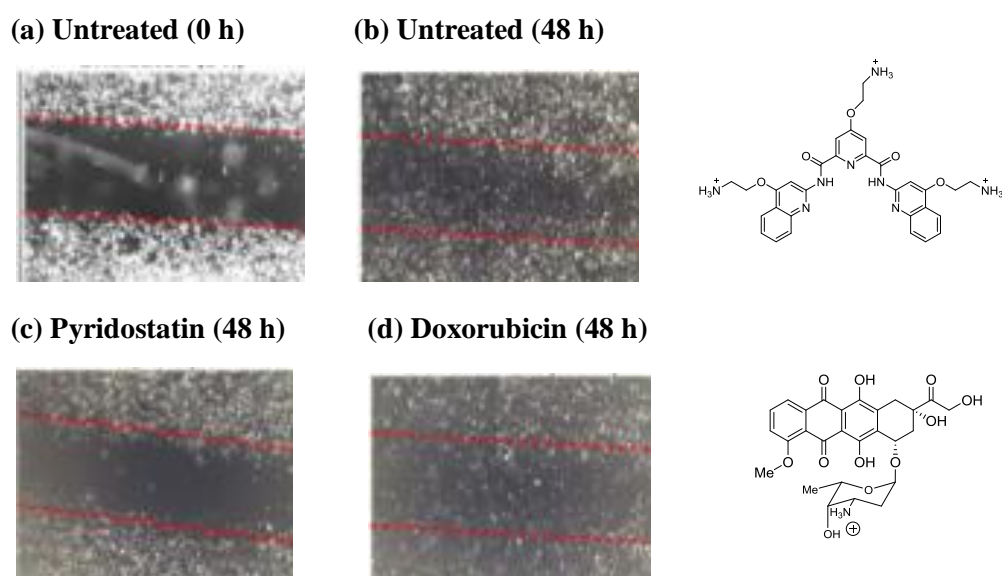
Figure 1.62 Scratch assay conducted with the breast cancer cell line MDA-MB-231. **a**. Untreated wound at the start of the assay, **b**. Untreated wound after 48 h shows the migration of cells back into the wound, **c.** Treatment with pyridostatin (2 μM) shows very little migration back into the wound, **d.** Treatment with doxorubicin (100 nM) still sees the migration of cells back into the wound area. [Reproduced from Ref [124]]

1.9 Summary and Thesis Aims

The function and binding capabilities of selected DNA structures have been reviewed in order to better understand the design of complexes to target them. Structures of interest presented in the literature include the DNA three way junction and DNA bulges. A three way junction has a hydrophobic cavity at its centre that a supramolecular iron cylinder is able to selectively bind to as it is the perfect size match for the cavity.[3] DNA bulges, created by DNA mismatches, can be targeted by large intercalating aromatic systems (such as Bartons $[Rh(bpy)_2chrysi]^{3+}$ complex) that are too bulky to interact with DNA in its normal double helical structure.[27]

G-Quadruplexes may be very important DNA structures to target as they have been linked to processes which control transcription and replication.[113] The complexes reviewed possess aromatic surfaces intended for the interaction with a G-quartet of a quadruplex which is also composed of an aromatic surface. The nickel(II) salphen complex reported by Vilar *et al* has been found to bind to G-quadruplexes formed in the telomeric region selectively over duplex DNA (shows more than 1000 fold activity for quadruplex DNA over duplex DNA).[120] The selectivity of the salphen complex and other complexes reported, such as the series of terpyridine complexes investigated by Teulade-Fichou *et al*, may be due to a combination of factors.[114][120] These include; good overlap of π surfaces, cationic charge imparted by the incorporation of a metal such as platinum, square planar arrangement and additional side arms containing protonatable nitrogen containing groups which can potentially interact with the loops of the quadruplex. Interestingly the nickel(II)

salphen complex had a bent rather than fully planar surface which may reflect the actual surface planarity of a G-quartet which may also be slightly distorted from planarity.[120]

The work of this thesis focuses on the targeting of G-quadruplexes where a simple binder has been designed that has the potential to bind specifically to G-quadruplex forming DNA. The design incorporates biisoquinoline which is able to create a large planar π surface area when coupled with metals such as platinum and palladium (which impart cationic charge) to create a complex that is able to bind by stacking onto the terminal G-quartet of a G-quadruplex structure. It is hoped that by attempting to synthesise a complex that has an excellent size and shape match for a G-quartet, enhanced selectivity will be obtained. The interactions of the complex with both duplex and quadruplex forming DNA will be investigated using; circular dichroism where conformation changes of the quadruplex can be monitored and the presence of induced signals linked to binding modes, fluorescent indicator displacements to determine selectivity using thiazole orange, UV-vis spectroscopy to determine binding constants, NMR spectroscopy to monitor changes in the quadruplex spectrum as complex is added, FRET melting experiments to monitor whether complex binding is able to increase the stability of the complex and gel electrophoresis which can help determine the selectivity when all relevant types of DNA are present. The ability of the binder to interact with RNA quadruplexes will also be investigated along with cytotoxic assays on selected cancer cell lines.

1.10 References

1. J. D. Watson, F. H. C. Crick. *Cold Spring Harb. Symp. Quant. Biol.,* 1953, **18**, 123.

2. J. D. Watson, F. H. C. Crick. *Nature,* 1953, **171**, 737.

3. M. J. Hannon. *Chem. Soc. Rev.,* 2007, **36**, 280.

4. *Nucleic acids in chemistry and biology,* G. M. Blackburn, M. J. Gait, Oxford University Press, New York, 1996.

5. A. Rich, S. Zhang. *Nat. Rev. Genet*., 2003, **4***,* 566.

6. Susana. R. Vitorino, Ph.D. thesis, University of Birmingham, 2011.

7. J. Zlatanova, K. Van Holde. *FASEB J.,* 1998, **12**, 421.

8. P. Gottipati, T. Helleday. *Mutagenesis,* 2009, **24**, 203.

9. M. Micco, G. W. Collie, A. G. Dale, S. A. Ohnmacht, I. Pazitna, M. Gunaratnam, A. P. Reszka, S. Neidle. *J. Med. Chem.,* 2013, **56**, 2959.

10. A. C. G. Hotze, N. J. Hodges, R. E. Hayden, C. Sanchez-Cano, C. Paines, N. Male, M. K. Tse, C. M. Bunce, J. K. Chipman, M. J. Hannon. *Chem. Biol.,* 2008, **15**, 1258.

11. J. Malina, M. J. Hannon, V. Brabec. *Chem. Eur. J.,* 2007, **13**, 3871.

12. S. Muhuri, K. Mimura, D. Miyoshi, N. Sugimoto. *J. Am. Chem. Soc.,* 2009, **131**, 9268.

13. S. Vuong, L. Stefan, P. Lejault, Y. Rousselin, F. Denat, D. Monchaud. *Biochimie*, 2012, **94**, 442.

14. R.R. Sinden, V. N. Potaman, E. A. Oussatcheva, C. E. Pearson, Y. L. Lyubchenko, L. S. Shlyakhtenko. *J. Biosci.,* 2002, **27**, 53-65.

15. A. L. Brogden, N. H. Hopcroft, M. Searcey, C. J. Cardin. *Angew. Chem. Int. Ed.,* 2007, **46**, 3850.

16. P Shing Ho, B. F. Eichman. *Curr. Opin. Struc. Biol.,* 2001, **11**, 302.

17. M. Egli. *Curr. Opin. Chem. Biol.,* 2004, **8**, 580.

18. S. L. B. König, A. C. Evans, J. L. Huppert. *Bio. Mol. Concepts.,* 2010, **1**, 197.

19. M. Gellert, M. N. Lipsett, D. R. Davies. *Proc. Natl. Acad. Sci. USA*, 1962, **48**, 2013.

20. K. Suntharalingam, A. J. P. White, R. Vilar. *Inorg.Chem.,* 2010, **49**, 8371.

21. J. Reed, A. White, S. Neidle, R. Vilar. *Chem. Commun.*, 2007, **42**, 4366.

22. J. Gu, J. Leszczynski. *J. Phys. Chem. A.,* 2002, **106***,* 529.

23. T. Ou, Y. Lu, J. Tan, Z. Huang, K. Wong, L. Gu. *Chem. Med. Chem.*, 2008, **3**, 690.

24. B. R. Vummidi, J. Alzeer, N. W. Luedtke. *Chem. Bio. Chem.*, 2013, **14**, 540

25. H. A. Day, C. Huguin Z. A. E. Waller. *Chem. Commun.,* 2013, **49**, 7696.

26. J. Choi, S. Kim, T. Tachikawa, M. Fujitsuka, T. Majima. *J. Am. Chem. Soc.,* 2011, **133**, 16146.

27. R. J. Ernst, H. Song, J. K. Barton. *J. Am. Chem. Soc.,* 2009, **131**, 2359.

28. I. M. A. del Mundo, M. A. Fountain, J. R. Morrow. *Chem. Commun.,* 2011, **47**, 8566.

29. I. M. Dixon, F. Lopez, A. M. Tejera, J. Estève, M. A. Blasco, G. Pratviel, B. Meunier. *J. Am. Chem. Soc.,* 2007, **129**, 1502.

30. Y. Ho, S. C. F. Au-Yeung, K. K. W. To. *Med. Res. Rev.,* 2003, **23**, 633.

31. P. M. Takahara, A. C. Rosenzweig, C. A. Frederick, S. J. Lippard. *Nature*, 1995, **377**, 649.

32. M. J. Hannon. *Pure Appl. Chem.*, 2007, **79**, 2243.

33. M. Noji, R. Kizu, Y. Takeda, N. Akiyama, I. Yoshizaki, M. Eriguchi, Y. Kidani. *Biomed. Pharmacother.* 2005, **59,** 224.

34. E. Alessio, G. Mestroni, A. Bergamo, G. Sava. *Curr. Top. Med. Chem,.* 2004, **4**, 1525.

35. C. G. Hartinger, S. Zorbas-Selfried, M. A. Jakupee, B. Kynast, H. Zorbas, B. K. Keppler. *J. Inorg. Biochem.,* 2006, **100**, 891.

36. J. Reedijk. *Platinum Metals Rev*., 2008, **52**, 2.

37. M. Groessl, Y. O. Tsybin, C. G. Hartinger, B. K. Keppler. P. J. Dyson. *J. Biol. Inorg. Chem.,* 2010, **15**, 677.

38. I. Khalaila, A. Bergamo, F. Bussy, G. Sava, P. J. Dyson. *Int. J. Oncol.,* 2006, **29**, 261.

39. G. Sava, G. Jaouen, E. A. Hillard, A. Bergamo. *Dalton Trans.,* 2012, **41**, 8226.

40. J. M. Hearn, I. Romero-Canelón, B. Qamar, Z. Liu, I. Hands-Portman, P. J. Sadler. *ACS Chem. Biol.,* 2013, **8**, 1335.

41. Z. Liu, A. Habtemariam, A. M. Pizarro, S. A. Fletcher, A. Kisova, O. Vrana, L. Salassa, P. C. A. Bruijnincx, G. J. Clarkson, V. Brabec, P. J. Sadler. *J. Med. Chem.,* 2011, **54**, 3011.

42. L. S. Lerner. *J. Mol. Biol.,* 1961, **3**, 18.

43. J. Ren, T. C. Jenkins, J. B. Chaires. *Biochemistry*, 2000, **39**, 8439.

44. H. Liu, P. J. Sadler. *Acc. Chem. Res.,* 2011, **44**, 349.

45. A. Mukherjee, R. Lavery, B. Bagchi, J. T. Hynes. *J. Am. Chem. Soc.,* 2008, **130**, 9747.

46. C. A. Frederick, L. D. Williams, G. Ughetto, G. A. van der Mare1, J. H. van Boom, A. Rich, A. H. J. Wang. *Biochemistry,* 1990, **29**, 2538.

47. K. J. Davis, J. A. Carrall, B. Lai, J. R. Aldrich-Wright, S. F. Ralph, C. T. Dillon. *Dalton Trans.,* 2012, **41**, 9417.

48. K. W. Jennette, S. J. Lippard, G. A. Vassiliades, W. R. Baueri. *Proc. Nat. Acad. Sci. USA,* 1974, **71**, 3839.

49. G. S. Khan, A. Shah, Z. Rehman, D. Barker. *J. Photochem. Photobiol., B,* 2012, **115**, 105.

50. P. Hamilton, D. Arya. *Nat. Prod. Rep.,* 2012, **29**, 134.

51. R. Rohs, X. Jin, S. M. West, R. Joshi, B. Honig, R. S. Mann. *Annu. Rev. Biochem.,* 2010, **79**, 233.

52. K. R. Fox, T. Brown. *Biochem. Soc. Trans.,* 2011, **39**, 629.

53. P. Wittung, P. Nielsen, B. Nordèn. *J. Am. Chem. Soc.,* 1996, **118**, 7049.

54. D. R. Boer, A. Canals, M. Coll. *Dalton Trans.,* 2009, 399.

55. C. Briones, M. Moreno. *Anal. Bioanal. Chem.,* 2012, **402**, 3071.

56. P. G. Baraldi, A. Bovero, F. Fruttarolo, D. Preti, M. A. Tabrizi, M. G. Pavani, R. Romagnoli. *Med. Res. Rev.,* 2004, **24**, 475.

57. M. Lee, A. L. Rhodes, M. D. Wyatt, M. D'Incalci, S. Forrow, J. A. Hartley. *J. Med. Chem.,* 1993, **36**, 863.

58. R. Romagnoli, P. G. Baraldi, O. Cruz-Lopez, C. Lopez Cara, M. D. Carrion, J. Balzarini, E. Hamel, G. Basso, R. Bortolozzi, G. Viola. *Bioorg. Med. Chem. Lett.,* 2010, **20**, 2733.

59. C. Bailly, J. B. Chaires. *Bioconjugate Chem.,* 1998, **9**, 513.

60. H. Wanga, C. A. Laughton. *Phys. Chem. Chem. Phys.,* 2009, **11**, 10722.

61. P. E. Pjura, K. Grzeskowiak, R. E. Dickerson. *J. Mol. Biol.,* 1987, **197**, 257.

62. S. Komeda, T. Moulaei, K. Kruger Woods, M. Chikuma, N. P. Farrell, L. Dean Williams. *J. Am. Chem. Soc.,* 2006, **128**, 16092.

63. A. Oleksi, A. G. Blanco, R. Boer, I. Usón, J. Aymam, A. Rodger, M. J. Hannon, M. Coll. *Angew. Chem. Int. Ed.,* 2006, **45**, 1227

64. M. Tanada, S. Tsujita, S. Sasaki. *J. Org. Chem.,* 2006, **71**, 125.

65. H. Song, J. T. Kaiser, J. K. Barton. *Nat. Chem.,* 2012, **4**, 615.

66. J. L. Huppert. *Chem. Soc. Rev.,* 2008, **37**, 1375.

67. A. Risitano, K. R. Fox. *Nucleic Acids Res.,* 2004, **32**, 2598.

68. M. Webba da Silva, M. Trajkovski, Y. Sannohe, N. Ma'ani Hessari, H. Sugiyama, J. Plavec. *Angew. Chem. Int. Ed.,* 2009, **48**, 9167.

69. A. Phan, D. J. Patel. *J. Am. Chem. Soc.,* 2003, **125**, 15021.

70. A. Kettani, S. Bouaziz, A. Gorin, H. Zhao, R. A. Jones, D. J. Patel. *J. Mol. Biol.,* 1998, **282**, 619.

71. S. Burge, G. Parkinson, P. Hazel, A. Todd, S. Neidle. *Nucleic Acids Res.*, 2006, **34**, 4502.

72. J. Müller. *Metallomics,* 2010, **2**, 318.

73. R. Gray, J. Chaires. *Biophys. Chem.,* 2011, **151**, 205.

74. A. Ambrus, D. Chen, J. Dai, R. A. Jones, D. Yang. *Biochemistry.,* 2005, **44**, 2048.

75. A. Wong, G. Wu. *J. Am. Chem. Soc.,* 2003, **125**, 13895.

76. G. N. Parkinson, M. P. H. Lee, S. Neidle. *Nature*, 2002, **417**, 876.

77. J. L. Huppert, S. Balasubramanian. *Nucleic Acids Res.,* 2005, 33, 2908.

78. C. B. Harley, A. Bruce Futcher, C. W. Greider. *Nature,* 1990, **345**, 458.

79. J. Thilagavathi, S. Venkatesh, R. Dada. *Andrologia*, 2013, **45**, 289.

80. *An Introduction to Genetic Analysis. 7th edition,* A. J. F. Griffiths, J. H. Miller, D. T. Suzuki. W. H. Freeman, New York, 2000.

81. T. Finkel, M. Serrano. M. A. Blasco. *Nature,* 2007, **16**, 448.

82. J. Reed, A. J. P. White, S. Neidle, R. Vilar. *Dalton Trans,* 2009, 2558.

83. G. Biffi, D. Tannahill, J. McCafferty, S. Balasubramanian. *Nature,* 2013, **5**, 182.

84. J. R. Williamson. *Proc. Natl. Acad. Sci. USA*, 1993, **90**, 3124.

85. C. Lobetti-Bodoni, E. Bernocco, E. Genuardi, M. Boccadoro, M. Ladetto. *Hematol. Oncol.,* 2010, **29**, 157.

86. T. A. Brooks, S. Kendrick, L. Hurley. *FEBS J.,* 2010, **277**, 3459

87. V. González, L. H. Hurley. *Annu. Rev. Pharmacol. Toxicol.,* 2010, **50**, 111.

88. Y. Mikami-Terao, M. Akiyama, Y. Yuza, T. Yanagisawa, O. Yamada, T. Kawano, M. Agawa, H. Ida, H. Yamada. *Exp. Eye Res.,* 2009, **89**, 200.

89. V. H. Le, N. Nagesh, E. A. Lewis. *PLOS ONE,* 2013, **8**, 1.

90. Y. Chen, P. Agrawal, R. V. Brown, E. Hatzakis, L. Hurley, D. Yang. *J. Am. Chem. Soc.,* 2012, **134**, 13220.

91. J. A. Nilsson, J. L. Cleveland. *Oncogene,* 2003, **22**, 9007.

92. S. Nasi, R. Ciarapica, R. Jucker, J. Rosati, L. Soucek. *FEBS Lett.,* 2001, **490**, 153.

93. D. Sun, L. H. Hurley. *J. Med. Chem.,* 2009, **52**, 2863.

94. L. F. Liu, J. C. Wang. *Proc. Nati. Acad. Sci. USA,* 1987, **84**, 7024.

95. S. Nagatoishi, N. Isono, K. Tsumoto, N. Sugimoto. *Chem. Bio. Chem.,* 2011, **12**, 1822.

96. A. Tanaka, J. Choi, S. K. Kim, T. Majima. *J. Phys. Chem. B.,* 2013, **117**, 6711.

97. J. Seo, E.S. Hong, H. Yoon, S. K. Shin. *Int. J. Mass. Spectrom.,* 2012, **330**, 262.

98. E. Golub, R. Freeman, I. Willner. *Angew. Chem. Int. Ed.,* 2011, **50**, 11710.

99. Y. Zhang, B. Li, Y. Jin. *Analyst,* 2011, **136**, 3268.

100. S. Neidle. *Curr. Opin. Struct. Biol.,* 2009, **19**, 239.

101. A. M. Burger, F. Dai, C. M. Schultes, A. P. Reszka, M. J. Moore, J. A. Double, S. Neidle. *Cancer Res*., 2005, **65**, 1489.

102. M. Read, R. J. Harrison, B. Romagnoli, F. A. Tanious, S. H. Gowan, A. P. Reszka, L.R. Kellands, S. Neidle. *Proc. Natl. Acad. Sci. USA,* 2001, **98**, 4844.

103. C. Percivalle, T. Mahmood, S. Ladame. *Med. Chem. Commun.,* 2013, **4**, 211.

104. J. Debray, W. Zeghida, M. Jourdan, D. Monchaud, M. Dheu-Andries, P. Dumy, M. Teulade-Fichou, M. Demeunynck. *Org. Biomol. Chem.,* 2009, **7**, 5219.

105.   P. Zhao, J. Lu, F. Hong, B. Ou, F. Zhang, L. Ma, H. Guo. *Spectrochim. Acta, Part A,* 2013, **108**, 1.

106.   H. T. Le, M. Clarke Miller, R. Buscaglia, W. L. Dean, P. A. Holt, J. B. Chaires, J. O. Trent. *Org. Biomol. Chem.,* 2012, **10**, 9393.

107.   C. Romera, O. Bombarde, R. Bonnet, D. Gomez, P. Dumy, P. Calsou, J. Gwan, J. Lin, E. Defrancq, G. Pratvie. *Biochimie,* 2011, **93**, 1310.

108.   P. Wang, L.Ren, H. He, F. Liang,X. Zhou, Z. Tan. *Chem. Bio. Chem.,* 2006, **7**, 1155.

109.   T. Miyazaki, Y. Pan, K. Joshi, D. Purohit, B. Hu, H. Demir, S. Mazumder, S. Okabe, T. Yamori, M. Viapiano, K. Shin-ya, H. Seimiya, I. Nakano. *Clin. Cancer Res.,* 2012, **18**, 1268.

110.   T. Doi, K. Shibata, M. Yoshida, M. Takagi, M. Tera, K. Nagasawa, K. Shin-ya, T. Takahashi. *Org. Biomol. Chem.,* 2011, **9**, 387.

111.   H. Tahara, K. Shin-ya, H. Seimiya, H. Yamada, T. Tsuruo, T. Ide. *Oncogene,* 2006, **25**, 1955.

112.   F. Rosu, V. Gabelica, N. Smargiasso, G. Mazzucchelli, K. Shin-Ya, E. De Pauw. *J. Nucleic Acids,* 2010, **121259**, 1.

113.   S. N. Georgiades, N. H. Abd Karim, K, Suntharalingam, R. Vilar. *Angew. Chem. Int. Ed.,* 2010, **49**, 4020.

114.   H. Bertrand, D. Monchaud, A. De Cian, R. Guillot, J. Mergny, M. Teulade-Fichou. *Org. Biomol. Chem.,* 2007, **5**, 2555.

115.   E. Largy, F. Hamon, F. Rosu, V. Gabelica, E. De Pauw, A. Guédin, J. Mergny, M. Teulade-Fichou. *Chem. Eur. J.,* 2011, **17**, 13274.

116.   L. Wang, Y. Wen, J. Liu, J. Zhou, C. Lib, C. Wei. *Org. Biomol. Chem.,* 2011, **9**, 2648.

117.   J. Wang, X. Zheng, Q. Xia, Z. Mao, L. Jia, K. Wang. *Dalton Trans.,* 2010, **39**, 7214.

118.   J. E. Reed, S. Neidle, R. Vilar. *Chem. Commun.,* 2007, **42**, 4366.

119.   R. Kieltyka, J. Fakhoury, N. Moitessier, H. F. Sleiman. *Chem. Eur. J.*, 2008, **14**, 1145.

120.   N. H. Campbell, N. H. Abd Karim, G. N. Parkinson, M. Gunaratnam, V. Petrucci, A. K. Todd, R. Vilar, S. Neidle. *J. Med. Chem.*, 2012, **55**, 209.

121.   R. Kieltyka, P. Englebienne, J. Fakhoury, C. Autexier, N. Moitessier, H. F. Sleiman, *J. Am. Chem. Soc.,* 2008, **130**, 10040.

122.   H. Yu, X. Wang, M. Fu, J. Ren, X. Qu. *Nucleic Acids Res.,* 2008, **36**, 5695.

123.   S. M. Haidad Ali, Y. K. Yan, P. P. F. Lee, K. Z. Xiang Khong, M. Alam Sk, K. Hwa Lim, B. Klejevskaja, R. Vilar. *Dalton Trans.,* 2014, **43**, 1449.

124.   R. Rodriguez, K. M. Miller, J. V. Forment, C. R. Bradshaw, M. Nikan, S. Britton, T. Oelschlaegel, B. Xhemalce, S. Balasubramanian, S. P. Jackson. *Nat. Chem. Biol.,* 2012, **8**, 301.

125.   X. Chen, J, Wu, Y. Lai, R. Zhao, H. Chao, L. Ji. *Dalton Trans.,* 2013, **42**, 4386.

126.   J. Fajkus. *Clin. Chim. Acta,* 2006, **371**, 25.

127.   J. C. Yarrow**,** Z. E. Perlman**,** N. J. Westwood, T. J. Mitchison. *BMC Biotechnol.,* 2004, **4,** 1.

Chapter 2: Design, Synthesis and Characterisation of 3,3-Biisoquinoline

Metal Complexes

2.1 Introduction

The majority of research into G-quadruplex binders involves the synthesis of organic compounds such as porphyrins and acridine based structures. Despite showing good G4 binding abilities their synthesis is often not simple and they don't all show very good selectivity.[1] Introducing metals into complexes used to target G-quadruplexes can help improve binding in many ways as it helps strengthen electrostatic interactions, mimics cations already present in the quadruplex structure and enables the relatively easy synthesis of multiple complexes where the metal imparts structural deviations between each complex. Terpyridine, salphen and phenanthroline metal complexes show a good affinity for G-quadruplexes however are not designed to maximise G-quartet coverage therefore stacking opportunities are missed.[1][2][3] As discussed with the three way junction binder, the iron supramolecular helicate, an excellent size match is essential for efficient binding between a complex and a specific DNA structure. It is therefore pertinent to explore whether a G-quadruplex binder that can be created with an excellent size match for end stacking will have the most efficient binding affinity.

This chapter focuses on the methodology explored whilst finding a suitable ligand to use in metal complexes which undergo efficient G-quadruplex binding. The synthesis of biisoquinoline, the ligand of choice, and the biisoquinoline complexes of the platinum,

palladium, rhenium and rhodium analogues will be discussed explaining the design and methodology behind each complex.

2.2 Molecular Design of G-Quadruplex End Stacking Biisoquinoline Complexes

The isoquinoline structure is found in many medicinal products.[4] An example of this is berberine which is a natural alkaloid and is able to bind to telomeric parallel quadruplexes in a 2:1 fashion (*Fig. 2.1*).[4] When examined by FRET melting experiments with quadruplex forming DNA, berberine derivatives were found to increase the melting temperature of the DNA by up to 25 °C with binding constants calculated at 10^6 M^{-1}.[5] When the same FRET melting experiments were repeated with excess duplex present in the solution (50 times more duplex than quadruplex DNA) the melting temperature was similar to the quadruplex DNA only solution. This indicates that the compound prefers to bind to G-quadruplex forming DNA over duplex DNA. This is because if the compound that was bound to the quadruplex favoured binding to the duplex DNA instead the melting temperature would decrease as the quadruplex is no longer stabilised by compound.[5]

Berberine and its interaction with G-quadruplexes has been investigated by X-ray crystallography where it was found to stack side by side onto a G-quartet at the 3'-end and 5'-end of the quadruplex (*Fig. 2.1*).[4] Interestingly at the 3'-end of the intramolecular quadruplex the G-quartet is bent with an angle of 13.9° with the two sets of guanine pairs arranged in a coplanar way (slightly funnel shaped).[4] The two berberine compounds

which bind to the 3'-end are also bent having an angle of 19.7° in order to efficiently stack

onto the also bent G-tetrad.[4]

(a) **(b)**
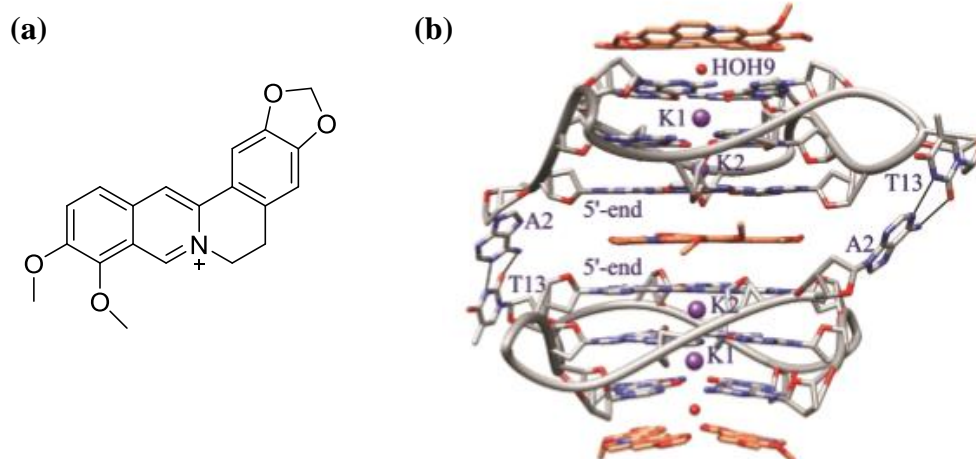
Figure 2.1 **a.** Structure of berberine , **b.** Crystal structure of the Ber/h-Tel23 adduct showing the binding of two berberine molecules to both the 3'-end and 5'-end of a G-quadruplex. [Reproduced from Ref [4]]

When isoquinoline is coupled with itself to form biisoquinoline and then complexed with

platinum it creates a square planar complex that has the potential to be an excellent size

match for a G-quartet (*Fig. 2.2*).[6] The complex also benefits from a large aromatic

surface for efficient stacking and a metal cation to enhance electrostatic interactions, hence

the investigation of this complex and its derivatives.

(a) **(b)**
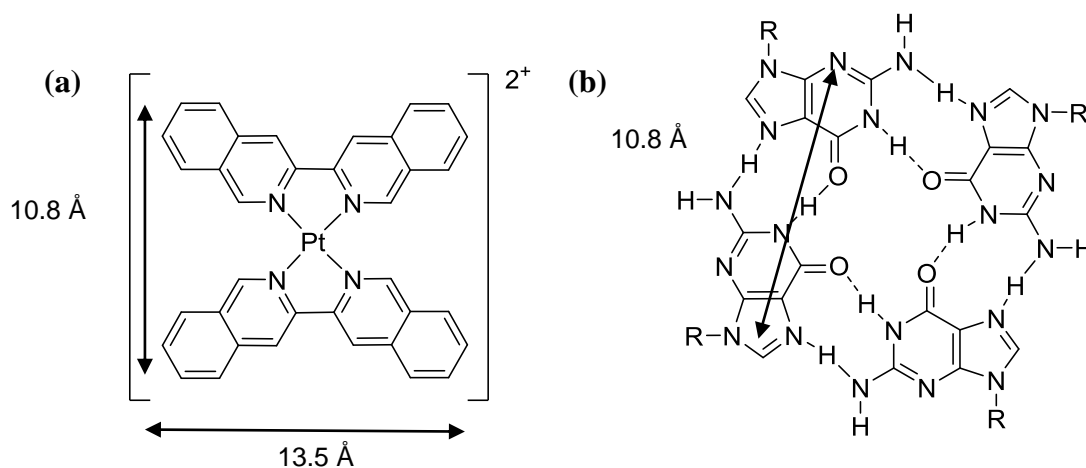
Figure 2.2 **a.** Structure and size of [Pt(ibiq)]$^{2+}$, **b.** Structure and size of G-quartet.[6][7]

2.2.1 Isoquinoline Building-Blocks

The isoquinoline building-block (3-chloroisoquinoline), required to make biisoquinoline, can be synthesised in three steps starting from the readily available and inexpensive homophthalic acid (*Scheme 2.1*).[8]
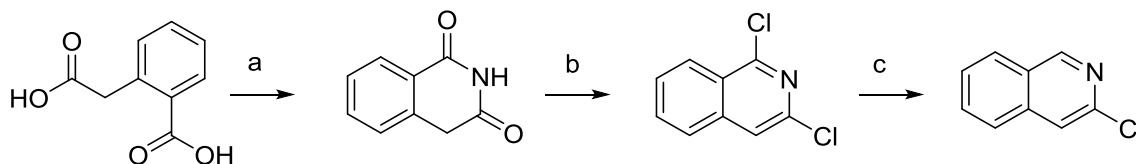
Scheme 2.1 Synthesis of 3-chloroisoquinoline under the following conditions: **a** NH_4OH, 1,2-dichlorobenzene, 200ºC; **b** $PhP(O)Cl_2$, 160ºC; **c** Sn^0, HOAc/HCl, 60ºC.

Step a: The first step of the reaction involves the formation of an ammonium carboxylate salt. Carboxylic acids do not undergo the same nucleophilic substitution reactions that occur with acid chlorides and esters (unless a dehydrating agent is used such as dicyclohexylcarbodimide - DCC).[9] Instead the strong base, NH_4OH , will undergo an acid-base reaction with the carboxylic acid (*Scheme 2.2*).[9] In the second step the intermediate is converted to an amide, when heated to 200 °C, by dehydration (*Scheme 2.2*).[9] The amide generated can then react in the same way (however this time intramoleculary) with the other carboxylic acid moiety.
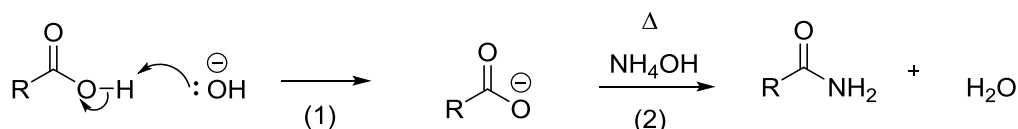
Scheme 2.2 Two step formation of amide between carboxylic acid and ammonia. (1) acid-base reaction, (2) dehydration of intermediate.

Step b: This is followed by a chlorodehydroxylation step with phenylphosphonic dichloride. The chloride ions are able to partake in nucleophilic addition reactions involving the carbonyl groups (*Scheme 2.3*). The hydrolysis products from the reaction include phenylphosphonic acid and its salts which are water soluble therefore easy to isolate from the chlorodehydroxylation product.[10]
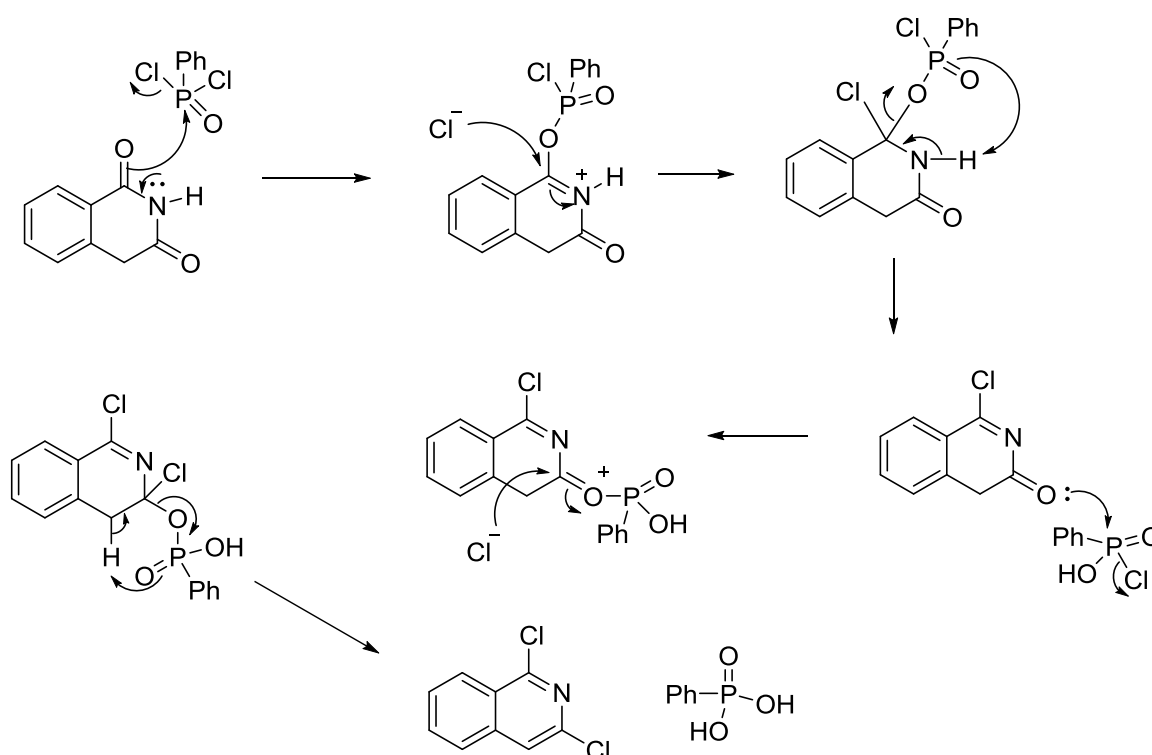
Scheme 2.3 Reaction scheme showing the mechanism of chlorodehydroxylation using phenylphosphonic dichloride.

Step c: The third step from *Scheme 2.1* involves the removal of the 1-chloro substituent using tin powder in a reaction mixture with hydrochloric acid. The tin is able to regioselectively reduce 1,3-dichloroisoquinoline which can be rationalised when considering the aromaticity of the compound when the charge is delocalised.[11] Structure **a** in *Fig. 2.3* is important because this is the only delocalised form that doesn't disrupt the

78

aromaticity of the benzene ring.[11] This leaves C1 as the most electron deficient therefore

the position of attack for nucleophiles. C3 is also a possibility for nucleophilic attack but

to achieve this charged state aromaticity of the benzene ring has to be interrupted (structure

b).
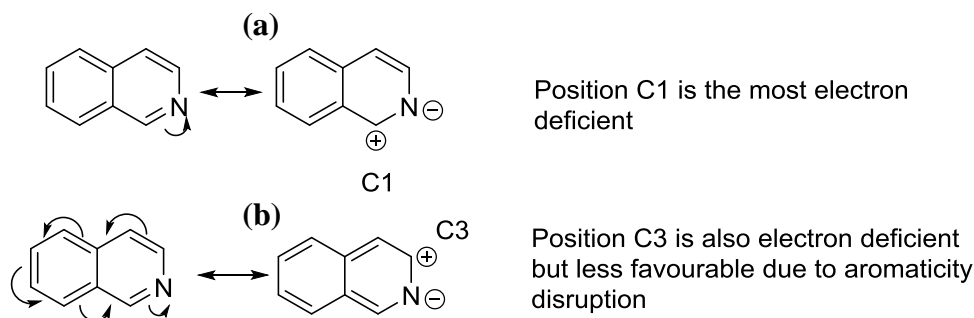
Figure 2.3 Charged structures of isoquinoline rationalising likely places of nucleophilic attack.

2.2.2 Metal Catalysed Homocoupling

The 3-chloroisoquinoline building-block can then be used in a homocoupling reaction

which sees the evolution of 3,3-biisoquinoline. There are a plethora of methods available

in the literature that can be used for such coupling reactions. Three different metals are

described and how they are used to catalyse the homocoupling of aryl halides.

Copper

Ullmann-type coupling is a copper catalysed condensation reaction which enables the

formation of important carbon-carbon or carbon-heteroatom bonds in organic synthesis.[12]

Despite its past success in generating synthetic targets, its use is restricted due to the harsh

reaction conditions required to conduct the condensation reactions; often needing polar

solvents with high boiling points such as dimethylformamide or nitrobenzene (230°C).[12]

The reaction is also less favourable because it requires stoichiometric amounts of copper reagents, has only a limited range of substrates and is low yielding.[12]

The proposed reaction scheme for the Ullmann reaction would involve the oxidative addition of 3-chloroisoquinoline to the copper and the removal of the coupled product by reductive elimination, shown below in *Scheme 2.4*.[13]

$$ArX \xrightarrow{Cu^{(0)}} ArCu^{(II)} X \quad \text{oxidative addition}$$

$$ArCu^{(II)} X \xrightarrow{Cu^{(0)}} Cu^{(I)}Ar \ + \ Cu^{(I)}X$$

$$Cu^{(I)}Ar \xrightarrow{ArX} (Ar)_2Cu^{(III)}X \quad \text{oxidative addition}$$

$$(Ar)_2Cu^{(III)}X \longrightarrow Ar\text{-}Ar \ + \ Cu^{(I)}X \quad \text{reductive elimination}$$
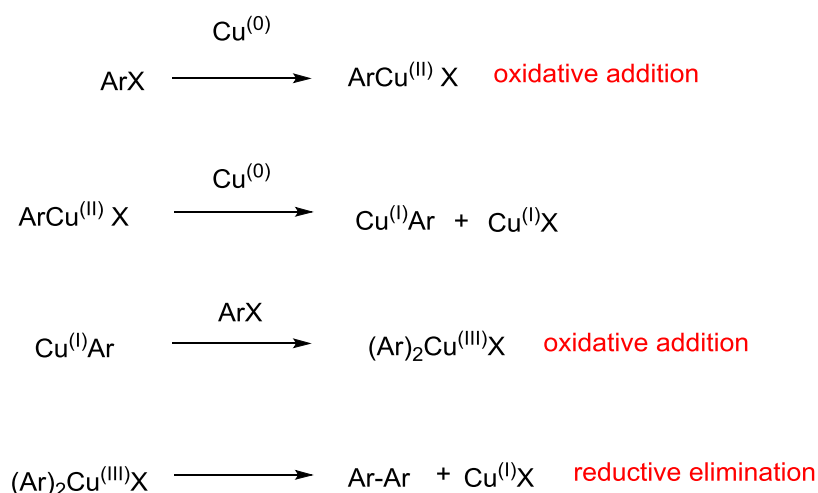
Scheme 2.4 Proposed Ullmann reaction scheme for the formation of biaryls.[12][13]

Palladium

Palladium can also potentially be used in the homocoupling of isoquinolines in Ullmann type reactions.[14] One particular synthesis of interest in the literature describes the synthesis of homocoupled aryl halides using the palladium complex $Pd(OAc)_2$ in the presence of homogenous reductant, hydroquinone.[14] The synthesis is attractive because it operates under relatively mild conditions (basic, 50°C) and can be used to successfully couple electron rich and electron deficient aromatic bromides and iodides.[14] Chlorides couple less successfully and generally produce low yields (in some instances no reaction occurs).[14]

The suggested mechanism for this catalytic cycle is shown in *Fig. 2.4* where under basic conditions the Pd species is able to eliminate benzoquinone generating an anionic aryl palladium species.[14] A halogenated aryl group (Ar-I) can then react with the palladium species with the loss of I⁻ to produce the biarylpalladium species.[14] Reductive elimination will then see the reformation of the Pd^0L_2 catalyst and the coupled biaryl product.[14]
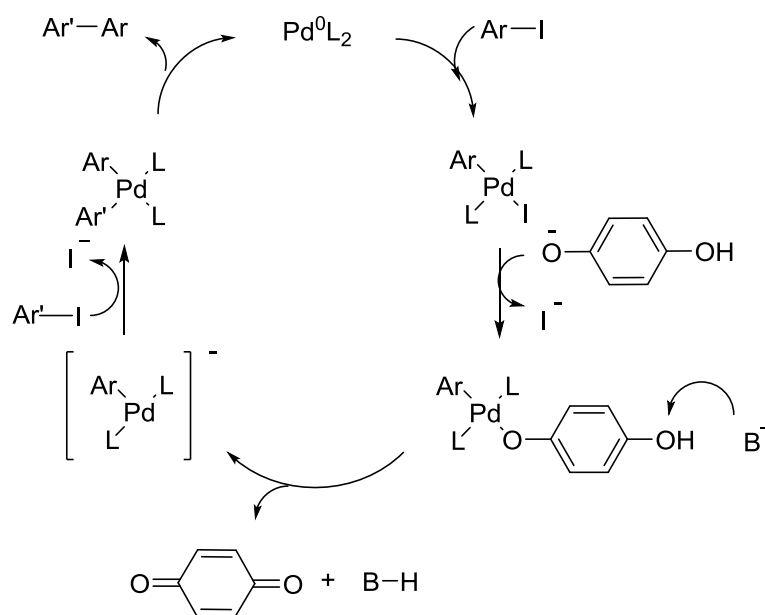
Figure 2.4 Catalytic cycle of aryl homocoupling using palladium in an Ullmann type reaction with the addition of hydroquinone.[14]

Despite the success of palladium cross coupling reactions the palladium complexes required can be expensive.[15] This is because they are required in equimolar quantities to the starting material in some reactions whilst in others, despite using a catalytic amount, the palladium cannot be used repeatedly.[15][16]

Nickel

Using a nickel catalysed reaction in the homocoupling of aryl halides is an attractive alternative as only mild conditions are required for it to proceed, other functional side

groups such as ketones and aldehydes do not interfere in the coupling of the halides and nickel catalysts are relatively cheap and readily available when compared to their palladium analogues.[17] The reaction also produces the product in a relatively good yield and is dependent on the choice of nickel complex, solvents and additional reagents such as triphenyphosphine, iodide or bromide.[18]

The preparation of the reactive nickel(0) reagent occurs in situ (Ni^0 is air sensitive) from a mixture of nickel(II) hexahydrate, triphenylphosphine and zinc in DMF.[18] During this setup the reduction of Ni^{II} to Ni^0 occurs through the activated zinc.[18] The solution turns from blue/green to deep red/brown indicating the formation of the active reagent.[18] At this point the aryl halide can be added which, as it forms the biaryl product, transforms the solution back to its initial Ni^{II} colour blue/green.[18] The bidentate ligand is then easily removed with a weak solution of ammonia.

The proposed reaction scheme for the nickel catalysed reaction is shown in *Scheme 2.5* where the first step is the oxidative addition of the aryl halide to $Ni^{(0)}$.[19] This is followed by its metathesis to a diarylnickel(II) complex and corresponding nickel halide.[19] In the third step reductive elimination produces the desired biaryl and the initial $Ni^{(0)}$ species.[19]

$$ArX + Ni^{(0)} \longrightarrow ArNi^{(II)}XL_2$$

$$2ArNi^{(II)}XL_2 \longrightarrow Ar_2Ni^{(II)}L_2 + Ni^{(II)}X_2L_2$$

$$Ar_2Ni^{(II)}L_2 \longrightarrow Ar\text{-}Ar + Ni^{(0)}$$
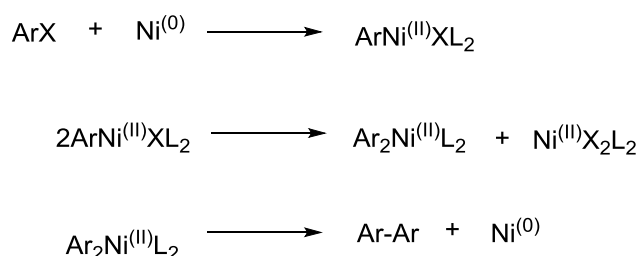
Scheme 2.5 Proposed nickel mediated biaryl formation reaction.[19]

This type of synthesis has also been used in order to produce 2,2':6',2"6",2"'-quarterpyridine (*Fig. 2.5*) which chelates strongly to the nickel therefore has to be precipitated out in its complex form before using potassium cyanide to remove the metal, liberating the ligand. [18][20]
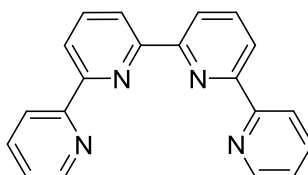
Figure 2.5 Structure of 2,2':6',2"6",2"'- quarterpyridine synthesised in a nickel homocoupling reaction.

Nickel was chosen as the catalyst of choice for the homocoupling of 3-chloroisoquinoline because of its advantages in availability, feasibility and expense. The reaction scheme, *Scheme 2.6,* shows the formation of the homocoupled product, 3,3-biisoquinoline, using the nickel template.
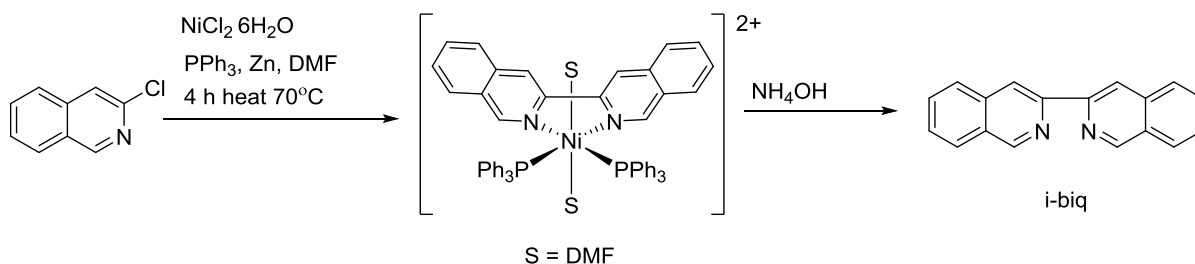
Scheme 2.6 Synthesis of 3,3-biisoquinoline using a nickel based homocoupling reaction.

Following synthesis, 3,3-biisoquinoline will be complexed with platinum and then palladium in a square planar geometry to compare how each metal alters the complexes ability to interact with DNA. The octahedral structure of a rhenium complex with one

biiosoquinoline ligand will be also be synthesised in order to compare how geometry affects DNA binding and finally a rhodium analogue will be explored in order to explore how the lower charge of Rh[(I)] (also Re[(I)]) will effect DNA binding.

2.3 3,3-Biisoquinoline Synthesis and Characterisation

2.3.1 *Isoquinoline-1,3-dione (1)*

Homophthalic acid was used as the starting material in the production of the required building block 3-chloroisoquinoline according to a literature procedure.[8][21] The first step in this synthesis was to convert the acid into isoquinoline-1,3-dione. (*Scheme 2.7*) Homophthalic acid was dissolved in excess ammonium hydroxide which was then removed in *vacuo* leaving the ammonium carboxylate salt. The salt was suspended in 1,2-dichlorobenzene and heated to 200°C to allow the dehydration of the product to form the amide. The product obtained was sufficiently pure to continue to the next stage of the reaction in an 88 % yield.
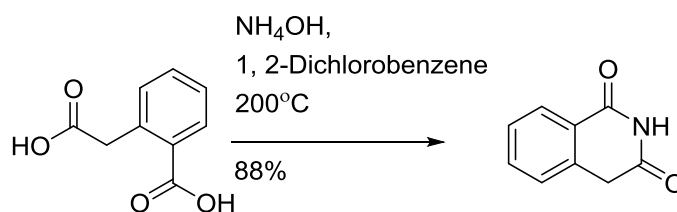
Scheme 2.7 Synthesis of isoquinoline 1,3-dione.

Electron ionisation mass spectrometry data produced a molecular ion peak consistent with the product formation. The ^{1}H-NMR spectrum (*Fig. 2.6*) was assigned with the use of 2D COSY (see *Appendix 1.1* for COSY, NOESY and mass spectrometry data). In order to

characterise fully the spectrum NOESY was also acquired to differentiate between protons H_2 and H_5 (as only H_2 would exhibit the long range coupling with H_1).
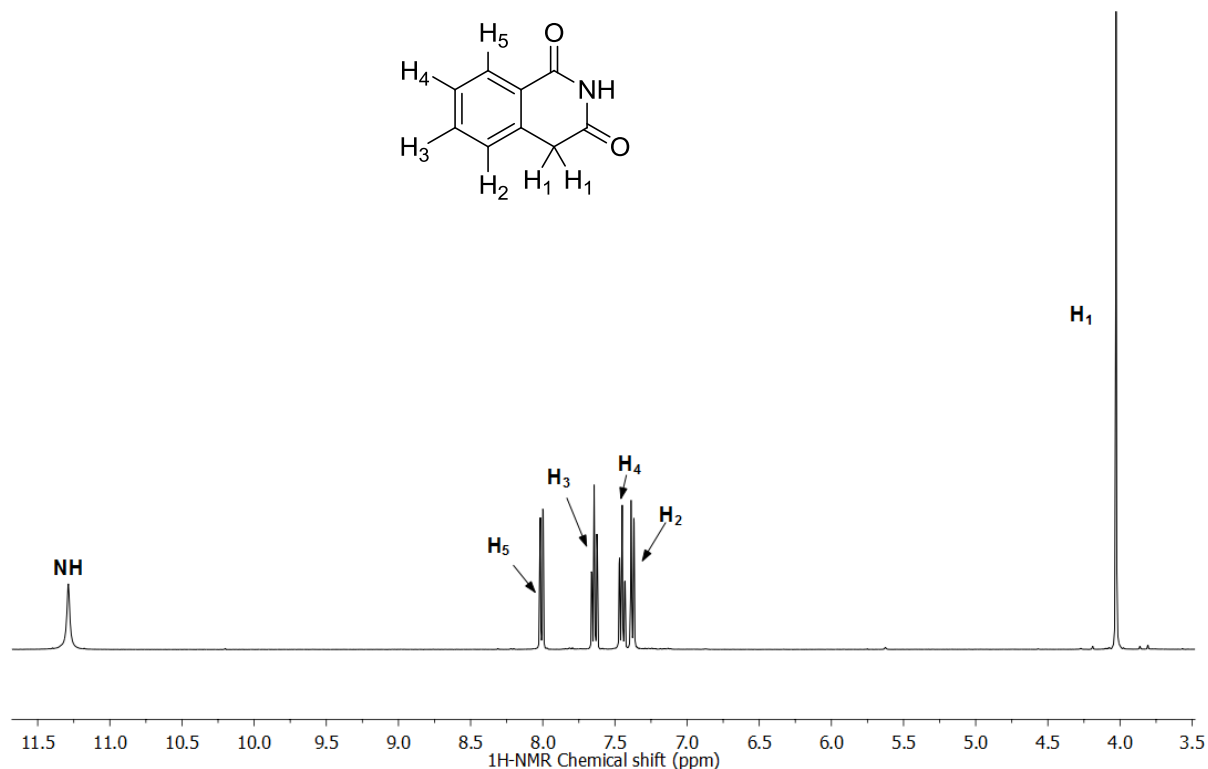
Figure 2.6 ^{1}H-NMR spectrum (300 MHz, d_6-DMSO, 298 K) of isoquinoline 1,3-dione.

2.3.2 1,3-Dichloroisoquinoline (2)

The second stage of the building block synthesis involved the chlorodehydroxylation of **1** (isoquinoline 1,3-dione) using phenylphosphonic dichloride carried out according to a literature procedure[8] (*Scheme 2.8*). Following this reaction, after a three hour reflux, the solution was treated with both THF and water. The unwanted hydrolysis products are water soluble therefore were easily removed during the extraction process. The extracted product was purified using column chromatography to give a final yield of 59 %.
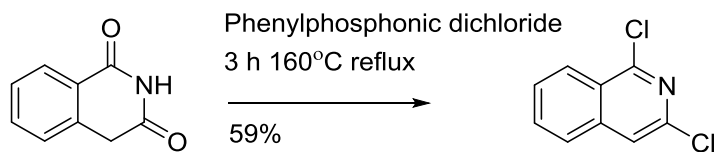
Scheme 2.8 Synthesis of 1,3-dichloroisoquinoline.

The molecular ion peak corresponding to $[H + (C_9H_5Cl_2N)]^+$ was found when analysing the compound by electron ionisation mass spectrometry and elemental analysis confirms the composition. The ^{1}H-NMR spectrum was fully assigned (*Fig. 2.7*), with the help of 2D COSY spectra (*Appendix 1.2*), and shows the emergence of a fully aromatic system with all protons within the range 7.88 - 8.38 ppm and the disappearence of sp^3 and NH protons.
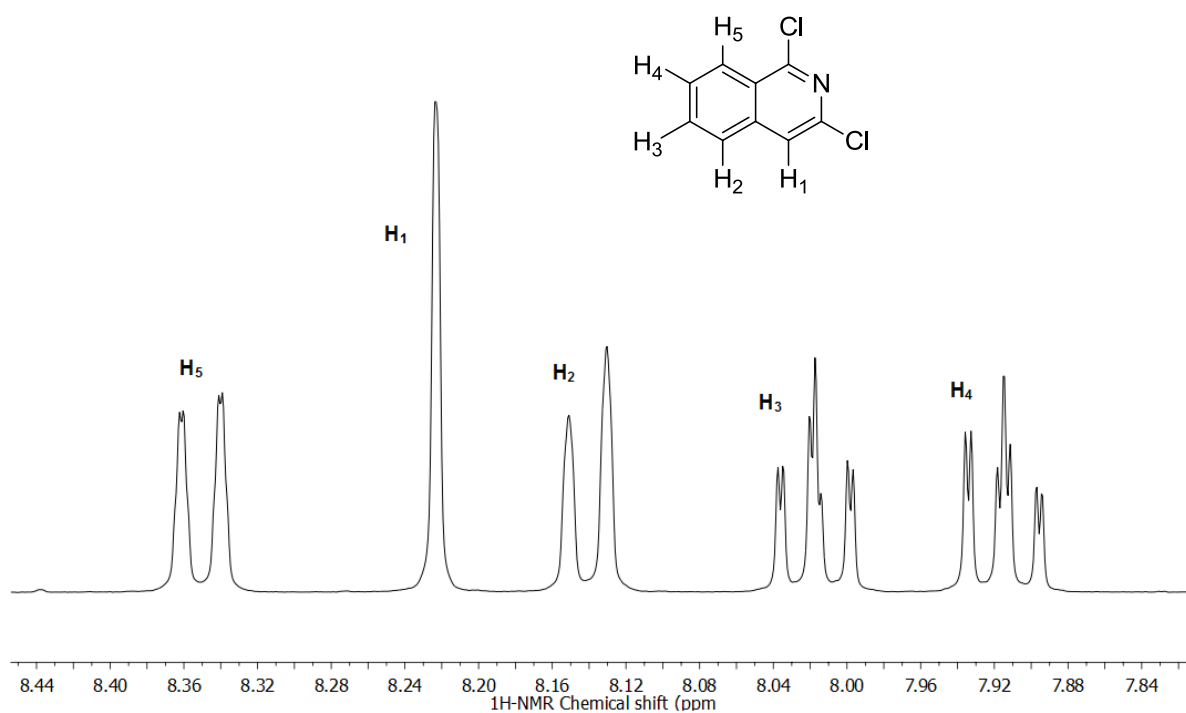
Figure 2.7 ^{1}H-NMR spectrum (300 MHz, d$_6$-DMSO, 298 K) of 1,3-dichloroisoquinoline.

2.3.2 3-Chloroisoquinoline (3)

In the final transformation from 1,3-dichloroisoquinoline to 3-chloroisoquinoline (*Scheme 2.9*), tin was used to selectively remove the chloride through nucleophilic attack at the chloride position nearest H_5 (position most prone to nucleophilic attack due to resonance stabilisation - see 2.2.1). At the end of the reaction the tin(II) chloride generated was neutralised using ammonium hydroxide causing the precipitation of SnO or $SnO.H_2O$.[22]

Following the reaction and work up a waxy orange product was produced which was purified using column chromatography on silica before using in the coupling reaction. The yield of compound **3** at the end of the reaction was 10 %. The lack of product may have been due to its difficult isolation at the end of the reaction from the Sn precipitates. When followed by TLC the full conversion of the dichloro compound to the monochloro was achieved before ending the experiment (Rf values in CH_2Cl_2, compound **2**: 0.8, compound **3**: 0.5).
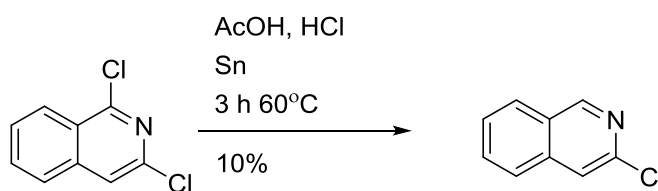
Scheme 2.9 Synthesis of 3-chloroisoquinoline.

Mass analysis using electron ionisation produced a molecular ion peak that corresponded with the product. The ^{1}H-NMR spectrum (*Fig. 2.8*) shows a new proton environment, formed from the selective removal a one chloride group, slightly further downfield to the other aromatic protons as it is adjacent to the more electronegative nitrogen. Full

identification of each of the proton peaks was achieved from the analysis of a 2D COSY spectrum. (*Appendix 1.3*)
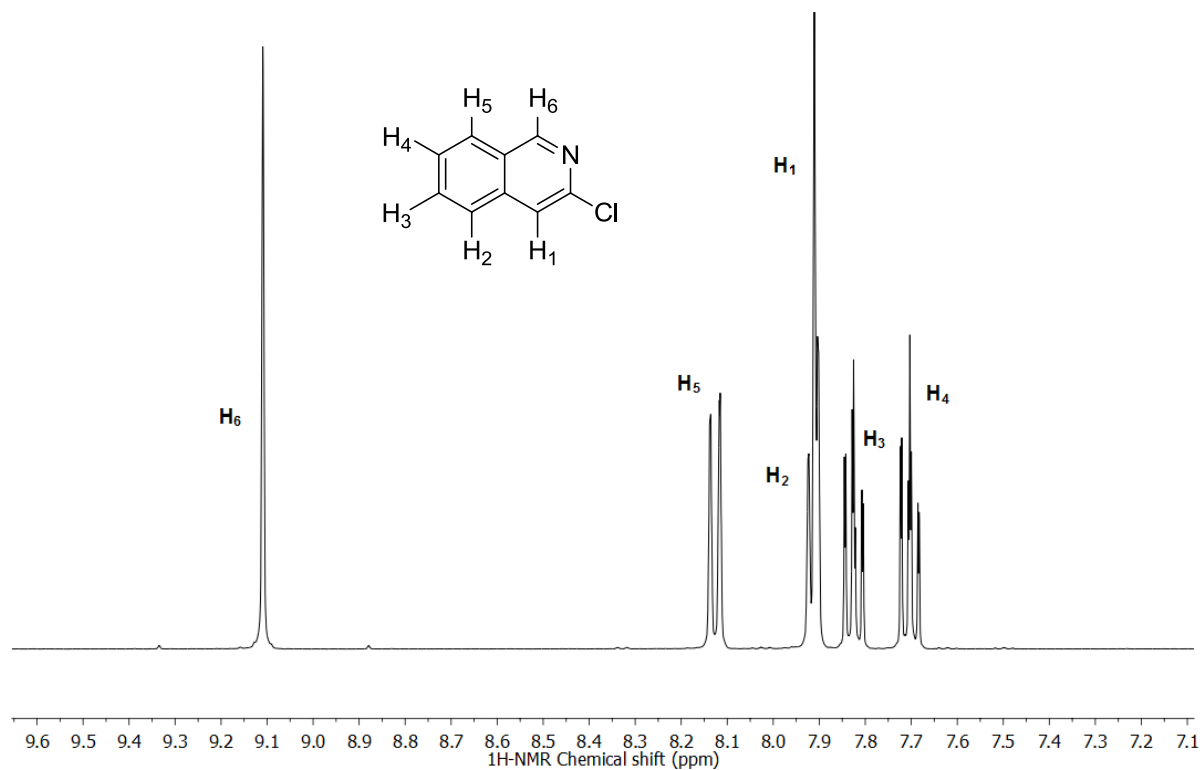
Figure 2.8 ^{1}H-NMR spectrum (300 MHz, MeOD, 298 K) of 3-chloroisoquinoline.

2.3.4 3,3-Biisoquinoline (ibiq) (4)

The nickel homocoupling reaction described in Subchapter 2.2.2 was used to couple two 3-chloroisoquinoline units together to create the required bidentate ligand to complex with the desired metal. *(Scheme 2.10)*
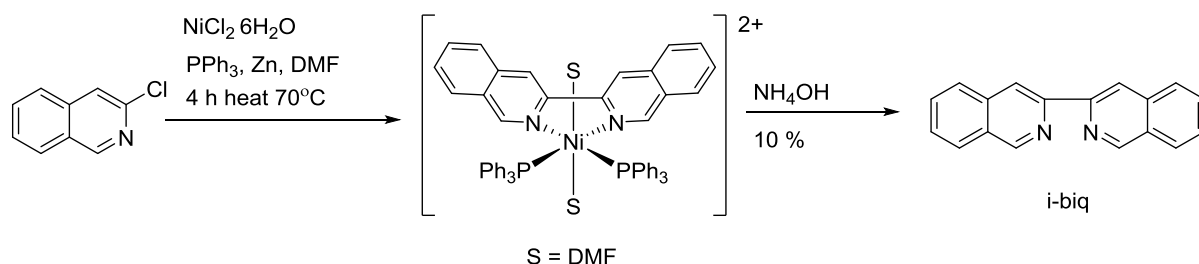
Scheme 2.10 Synthesis of 3,3-biisoquinoline.

88

Before starting the reaction the zinc acting as the reducing agent was activated by washing with dilute HCl, water, ethanol, acetone and diethyl ether before drying under vacuum.[23] Once thoroughly dry it was used to reduce the Ni(II) complex in situ, in a solution containing DMF and triphenylphosphine under argon, to Ni(0). Only once the solution had turned from green to brick red could the 3-chloroisoquinoline be added to the reaction mixture to start the coupling process. The reaction mixture was heated to 70°C for 4 hours and was kept air free for the duration. After the 4 hours the reaction was allowed to cool before pouring into a 7% solution of ammonium hydroxide. The aim of this was to dissociate any newly formed bidentate ligand from the nickel into solution to be extracted whilst substituting it with NH_3 ligands. The blue aqueous solution formed as a result of this nickel complex formation could be seen in the water layer after extraction had taken place.

The biisoquinoline product isolated was heavily contaminated with the side product triphenylphosphine oxide (from triphenylphosphine oxidation) and excess DMF which were removed following extensive washing with water to remove the DMF and multiple column chromatography silica columns in diethyl ether to remove the triphenylphosphine oxide. The yield from this reaction was 10% and despite it being very low the nickel reaction using $NiCl_2.6H_2O$ was the only synthesis procedure that yielded the coupled product. Biaryl synthesis using bis-triphenylphosphine palladium chloride and another using $NiBr_2(PPh_3)_2$ yielded no product.[19][24] The main problem with the homocoupling reactions is the relative unreactivity of the heteroaryl chlorides when compared with their bromide and iodide counterparts.[25] This is due to the aryl (Ar) C-Cl bond strength (Ar-Cl = 96 kcal mol^{-1}, Ar-Br = 81 kcal mol^{-1} and Ar-I = 65 kcal mol^{-1}), which makes it harder for

the chloride to bind to the nickel centre during the oxidative addition step.[25] They are however the most attainable aryl halides as they are inexpensive and widely available.[25]

The electron ionisation mass spectrometry analysis identified the molecular ion peak. The ^{1}H-NMR spectrum shown in *Fig. 2.9* in MeOD shows the new position of H_1 further downfield after the coupling process when compared to its position in 3-chloroisoquinoline due to the larger area of aromaticity. Both 2D COSY and NOESY were used to accurately assign all protons in the system *(Appendix 1.4)* thus confirming synthesis of the desired product.
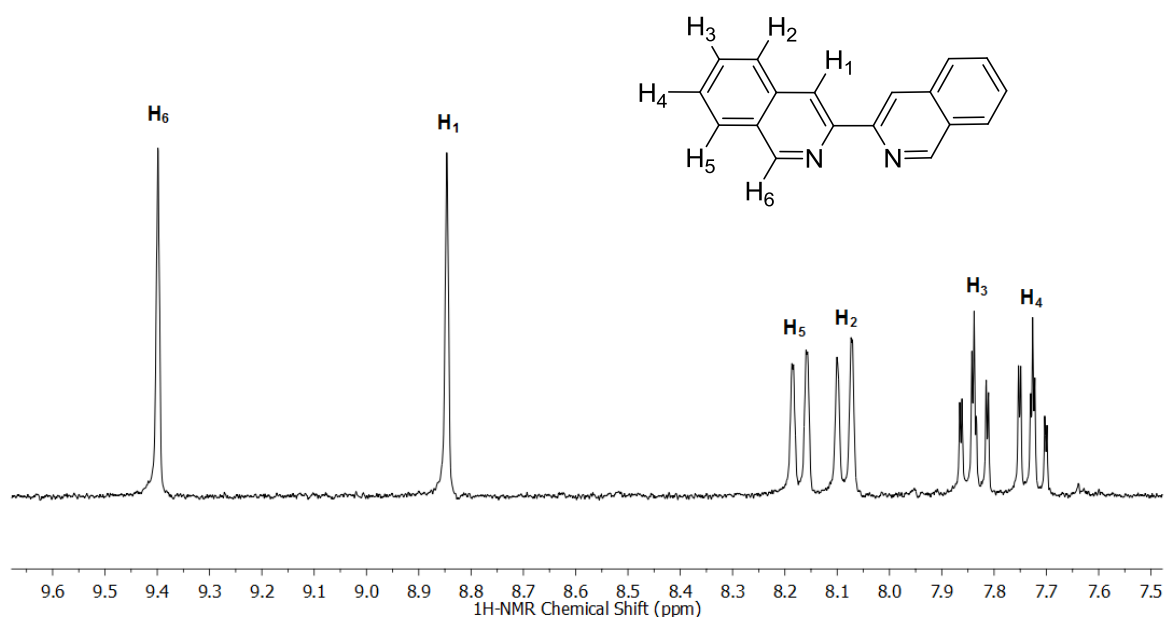
Fig 2.9 ^{1}H-NMR spectrum (300 MHz, MeOD, 298 K) of 3,3-biisoquinoline.

2.4 Synthesis and Characterisation of Palladium, Platinum, Rhenium and Rhodium Biisoquinoline Complexes

2.4.1 [Pd(ibiq)$_2$][BF$_4$]$_2$ (5)

The starting material used for the palladium complex was tetrakis(acetonitrile) palladium(II) tetrafluoroborate which was simply reacted with the newly formed 3,3-biisoquinoline ligand in a 2:1 ratio by stirring overnight in acetonitrile (*Scheme 2.11*). The product of the reaction was then washed with methanol and diethyl ether to remove the starting materials leaving pure [Pd(ibiq)$_2$][BF$_4$]$_2$ in a 50% yield which was soluble in both acetonitrile and dimethyl sulfoxide.
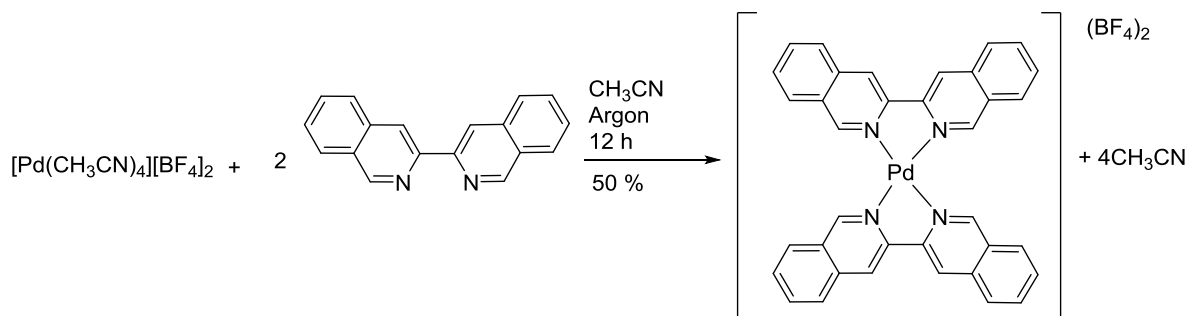
Scheme 2.11 Synthesis of [Pd(ibiq)$_2$][BF$_4$]$_2$.

The mass spectrum produced using electrospray ionisation showed peaks at 653 and 309 m/z corresponding to the species [Pd(C$_{18}$H$_{12}$N$_2$)$_2$Cl]$^+$ and [Pd(C$_{18}$H$_{12}$N$_2$)$_2$]$^{2+}$ respectively (*Appendix 1.5*). ^{1}H-NMR spectroscopy showed the presence of the proton peaks seen in the 3,3-biisoquinoline spectrum (*Fig. 2.10*) and to confirm the synthesis of the compound

complexed to the palladium both the ligand and palladium product were run in CD_3CN to compare the positions of the proton peaks H_1 and H_6.
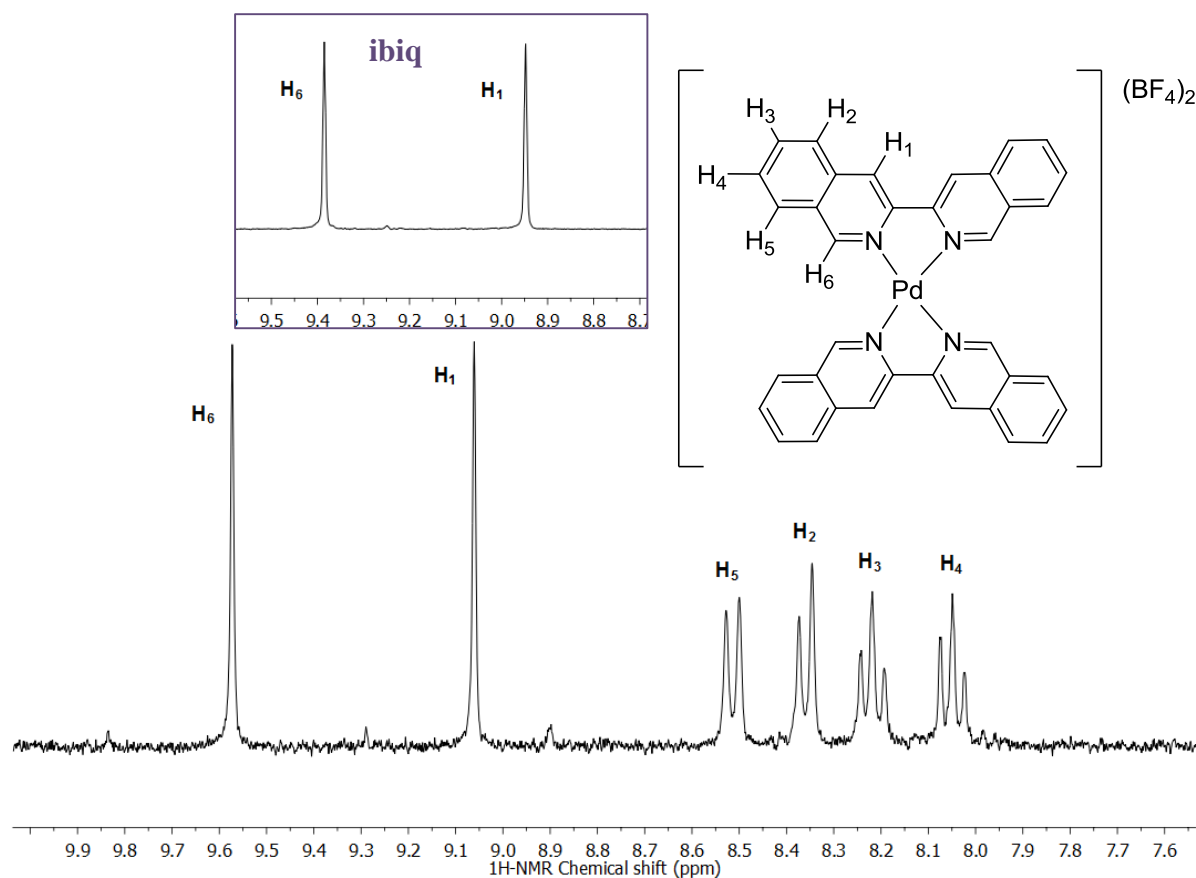
Figure 2.10 ^{1}H-NMR spectrum (300 MHz, CD_3CN , 298 K) of [Pd(ibiq)$_2$][BF$_4$]$_2$ and comparison with 3,3-biisoquinoline (ibiq) in the same solvent.

There is a shift further downfield for the protons in the ligand bound to the palladium as the palladium withdraws electron density from the aromatic system. This will increase the stacking ability of the complex for electron rich aromatic rings helping to form stronger interactions with other aromatic surfaces.

The crystal structure of the palladium biisoquinoline complex was probed by single crystal X-ray diffraction *(results provided by Dr Louise Male, University of Birmingham)*. The results revealed a bowed structure similar to the literature structure seen for the platinum

analogue of the complex (*Fig. 2.11*).[6] The similarity of the two complexes implies that they will have similar stacking interactions with the DNA. A slipped stack structure is formed by the palladium complex in the crystal with overlaid biisoquinoline units (*Fig. 2.12*). This has been reported for the platinum complex in the literature.[6]

(a)　　　　　　　　　　　　　　　　　　**(b)**
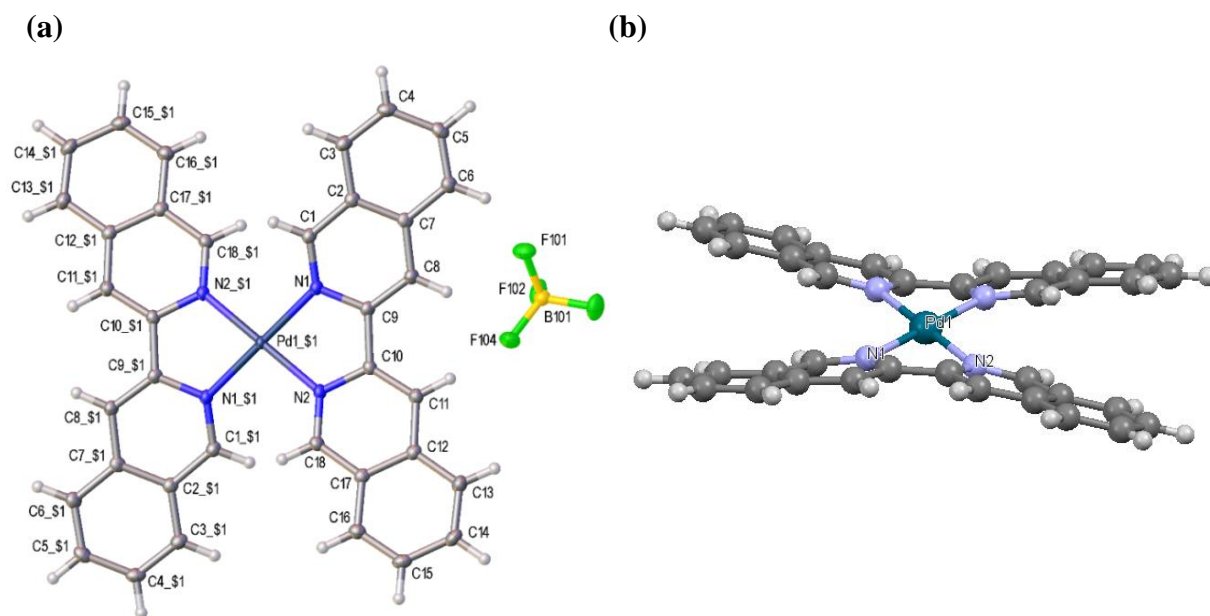
Fig 2.11 **a**. The structure of Pd(ibiq)$_2$ with ellipsoids drawn at the 50 % probability level. Benzene solvent has been omitted for clarity. The Pd complex is located on inversion centre such that only half the molecule is crystallographically unique. Symmetry transformation used to generate equivalent atoms: $1: 1-x, -y, 1-z. **b**. Side view showing the bowed conformation of the complex.

Examination of the selected bond lengths in *Table 2.1* shows there is a slight difference in the N-Pd bond lengths from the nitrogen atoms in the same biisoquinoline unit (0.003 Å). This difference is greater than the platinum complex (0.001 Å) indicating that the palladium complex may be slightly more distorted from planarity.[6][26][27] To investigate any distortion from planarity further the angles between the two opposing isoquinolyl groups were considered. For a truly planar surface this would be 0° however it is known that both systems are bowed therefore the extent of this angle will be linked with the degree of distortion. The angle between the isoquinolyl groups in the platinum complex is

93

26° whereas in the palladium complex it is 24° (angles between planes, see page 99, *Fig. 2.16* for further images).[6] Despite this each isoquinolyl group within each ligand is almost planar for both complexes.
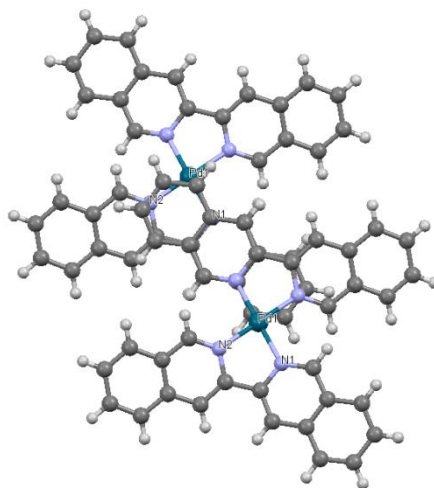
Fig 2.12 Slipped stack structure of $[Pd(ibiq)_2]^{2+}$.

Metal	Pd-N1(ibiq)	Pd-N2(ibiq)	N1-Pd-N2	N1-Pd-N2'
Pd	2.033(13)	2.036(14)	79.6(6)	100.4(6)

Table 2.1 Selected bond lengths (Å) and bond angles (deg) from the crystal structure of $[Pd(ibiq)_2][BF_4]_2$.

2.4.2 $[Pt(ibiq)Cl_2]$ (6)

The synthesis of $[Pt(ibiq)Cl_2]$ was similar to the synthesis of $[Pt(bpy)Cl_2]$ where one equivalent of bipyridine was heated under reflux in water with platinum tetrachloroplatinate and a small amount of HCl for 1.5 hours (*Scheme 2.12*).[28] Achieving the same type of complex with biisoquinoline instead of bipyridine required the use of a 50:50 mixture of water and acetonitrile as an alternative to 100% water to aid the

dissolution of the biisoquinoline ligand, as reported in the literature.[6] Once the reaction starts the product is quickly formed as a yellow solid that starts to precipitate out of the solution. The presence of HCl in the reaction is particularly important as a concentrated solution will favour the formation of the red version of the complex whereas when less is used the yellow version of the complex is synthesised.[28] The complexes both exhibit the same chemical structure and differ only in the arrangement of molecules within the crystal.[28] The formation of the yellow form was optimised in the experiment as its production was more reliable than the red form which often reverted back to the yellow form in solvents such as chloroform and dichloromethane.[28] It was also important not to leave the reaction for longer periods of time as it led to the formation of the doubly substituted platinum complex $[Pt(ibiq)_2]^{2+}$.
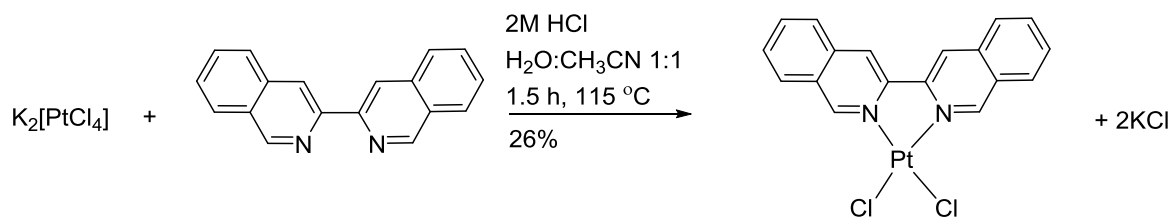
Scheme 2.12 Synthesis of [Pt(ibiq)Cl$_2$].

Once synthesised, the yellow filamentous needles were washed with chloroform, acetonitrile, methanol and diethyl ether producing the final product in a 26% yield. Disappointingly the complex was only sparingly soluble in dimethyl sulfoxide and insoluble in all other solvents which hindered its use in the binding experiments.

Electrospray ionisation mass spectrometry was able to confirm the synthesis of the platinum complex by the observation of a m/z peak at 545 corresponding to $[Na(Pt(C_{18}H_{12}N_2)_2Cl_2)]^+$ (*Appendix 1.6*). The proton NMR (*Fig. 2.13*) showed a pattern of peaks similar to the biisoquinoline ligand alone however this time they were shifted much further downfield, particularly H_6. The dramatic shift of proton H_6 arises because it points directly in the field of the chloride ligand. This downfield shift is well known in other metal polypyridyl complexes such as $[Ru(tpy)(HL)Cl][PF_6]$ where HL is 6-phenyl-2,2'-bipyridine.[29] The quality of the spectrum is poor due to the poor solubility of complex.
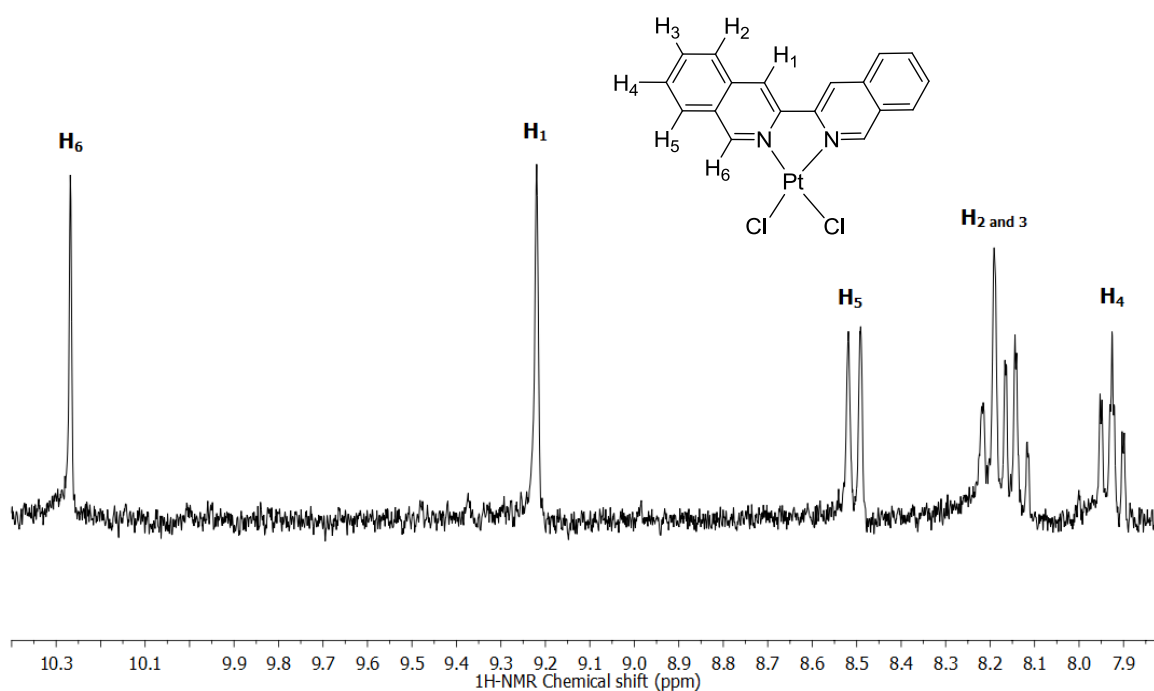
Fig 2.13 ^{1}H-NMR spectrum (300 MHz, d_6-DMSO, 298 K) of [Pt(ibiq)Cl$_2$].

2.4.3 *[Pt(ibiq)$_2$][PF$_6$]$_2$ (7)*

The synthesis of [Pt(ibiq)$_2$][PF$_6$]$_2$ was also carried out simply by heating under reflux potassium tetrachloroplatinate and 3,3-biisoquinoline in a 50:50 mixture of acetonitrile and water overnight (*Scheme 2.13*). After 12 h the hot solution was filtered to remove any [Pt(ibiq)Cl$_2$] that may have formed during the reaction and unreacted ligand. The product

was precipitated out by treating the refluxed solution with a methanolic solution of NH$_4$PF$_6$. When NaBF$_4$ was used instead the resulting product was poorly soluble in both CH$_3$CN and DMSO therefore only the PF$_6$ counter ion was used. Careful washing with methanol and diethyl ether resulted in the pure product being obtained in a 27% yield.
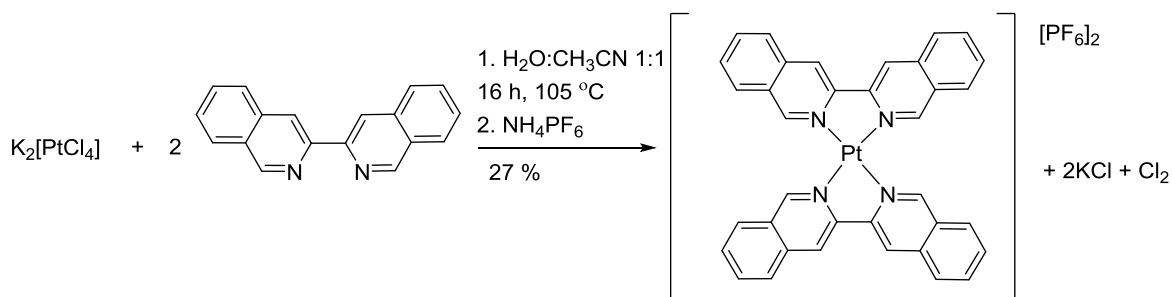
Scheme 2.13 Synthesis of [Pt(ibiq)$_2$][PF$_6$]$_2$.

Mass analysis using ESI gave molecular ion peaks at 353 and 742 m/z corresponding to [Pt(C$_{18}$H$_{12}$N$_2$)$_2$]$^{2+}$ and [Cl(Pt(C$_{18}$H$_{12}$N$_2$)$_2$)]$^+$ respectively (*Appendix 1.7*). The ^{1}H-NMR spectrum (*Fig. 2.14*) showed only the biisoquinoline peak symmetry but with slight shifts in ppm allowing the differentiation of the platinum complex from the unbound ligand.
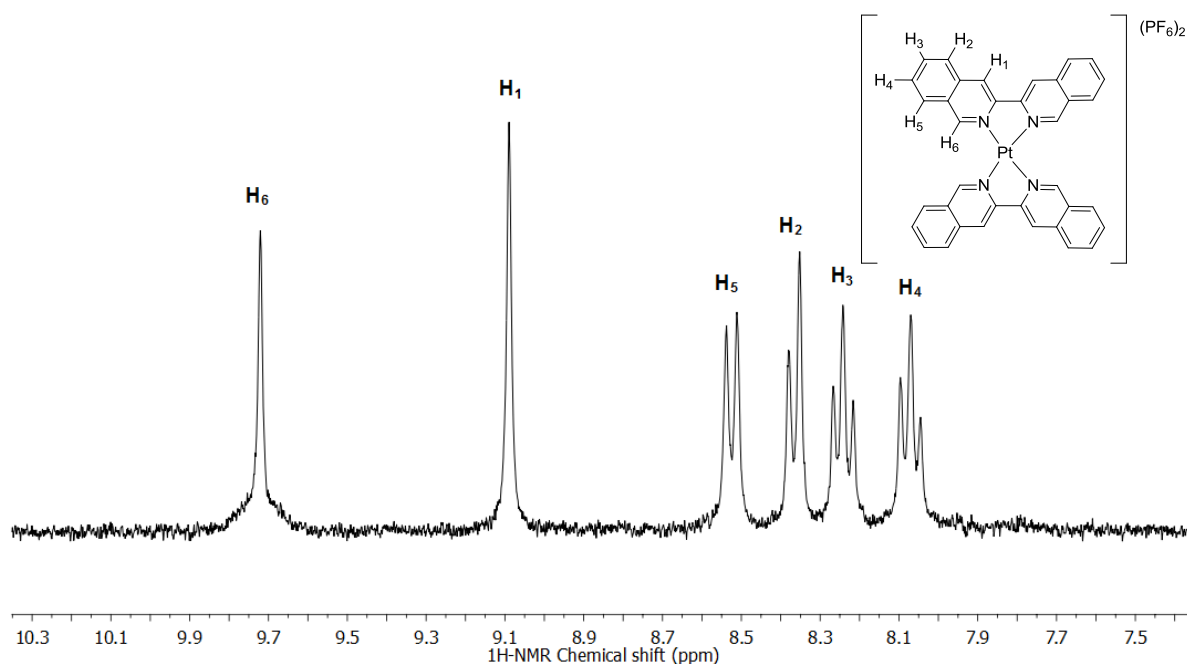
Figure 2.14 ^{1}H-NMR spectrum (300 MHz, CD$_3$CN, 298 K) of [Pt(ibiq)$_2$][PF$_6$]$_2$.

97

Unfortunately, during these experiments only small crystals of $[Pt(ibiq)_2][PF_6]_2$ were produced that could not be used in further single crystal x-ray diffraction studies. [6] The complex is known to exist in a bowed conformation in a similar way that bipyridine platinum complexes exist.[6][30] The figure below, reported in the literature, (*Fig. 2.15*) shows the crystal structure and also the side on view showing its bowed nature.[6] Selected bond lengths and angles are also displayed in *Table 2.2*.
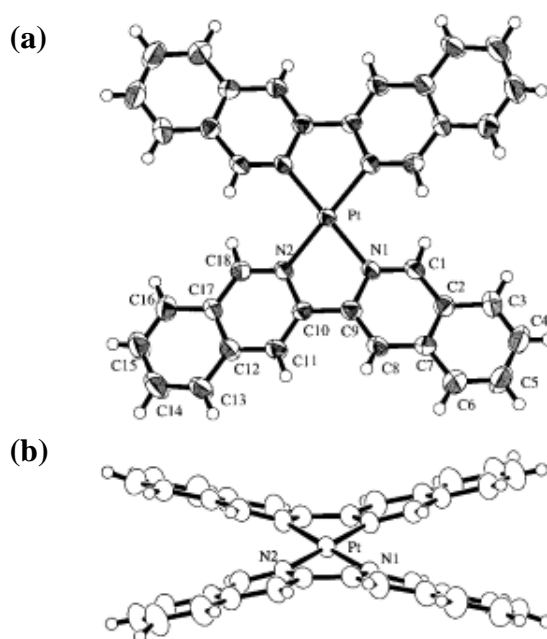
Figure 2.15 ORTEP drawings of $[Pt(ibiq)_2][PF_6]_2$ showing the (**a**) top and (**b**) side view of the crystal. Thermal ellipsoids are depicted at the 50% probability level. [Reproduced from Ref [6]]

Metal	Pt-N1(ibiq)	Pt-N2(ibiq)	N1-Pt-N2	N1-Pt-N2'
Pt	2.012(4)	2.011(4)	79.4(2)	100.6(2)

Table 2.2 Selected bond lengths (Å) and bond angles (deg) from the crystal structure of $[Pt(ibiq)_2][PF_6]_2$.[6]

The palladium and platinum structures when overlaid show very little difference in planarity or size, both have a bowed structure (*Fig. 2.16*).
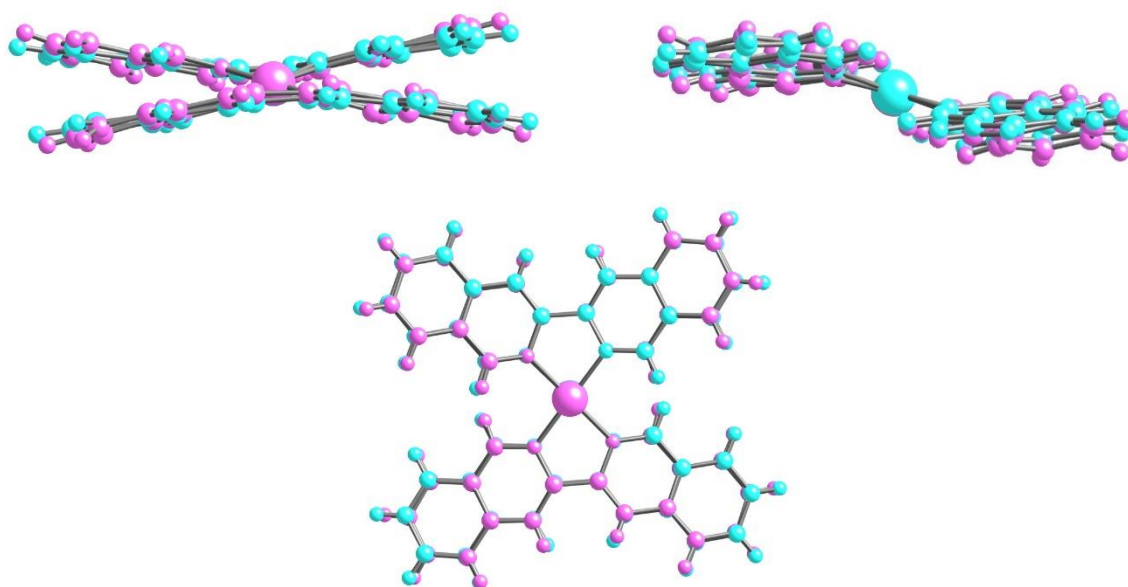
Figure 2.16 Superimposed crystal structures of [Pt(ibiq)$_2$][PF$_6$]$_2$ (pink) and [Pd(ibiq)$_2$][BF$_4$]$_2$ (blue).

2.4.4 [Re(CO)$_3$(ibiq)(Py)][CF$_3$SO$_3$] (8)

Pentacarbonylchlororhenium(I) was used as the starting point for incorporation of the biisoquinoline ligand into an octahedral arrangement. The reaction was carried out in three parts (*Scheme 2.14*) involving first the addition of the bidentate ligand replacing two of the carbonyl groups. The next part involved exchanging the chloride group for acetonitrile using silver trifluoromethanesulfonate which was done to facilitate the exchange of that ligand in the next step of the reaction. Acetonitrile ligands are displaced more easily by other σ-donor ligands making them in general more labile for ligand substitution reactions.[31] In the final step of the reaction the actonitrile group was displaced by pyridine to give the product in a 50% yield.
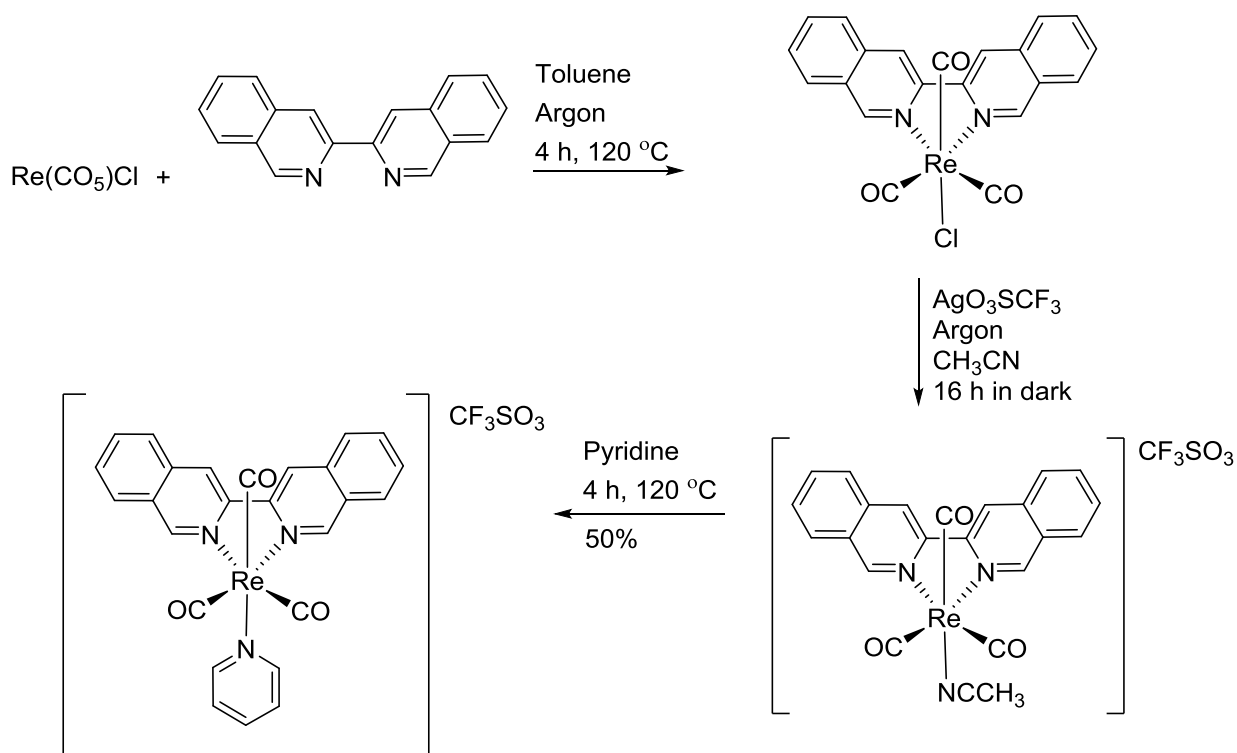
Scheme 2.14 Synthesis of [Re(CO)$_3$(ibiq)(Py)][CF$_3$SO$_3$].

The mass spectrum of the final product conducted using electrospray ionisation showed a peak at a m/z of 606 corresponding with the molecular ion [Re(C$_{12}$H$_{18}$N$_2$)(CO)$_3$(C$_5$H$_5$N)]$^+$. The H-NMR spectrum (*Fig. 2.17*) accounts for all of the protons in the 3,3-biisoquinoline unit and the pyridine group in the correct integrations and was assigned fully with the use of 2D COSY and NOESY spectra (*Appendix 1.8*). The downfield shift of proton H$_6$ when bound to the rhenium is consistent with other rhenium complexes in the literature.[32] In the complex fac-[(4,4'-bpy)Re^I(CO)$_3$(dppz)]$^+$, proton H$_6$ of the dppz ligand shifts 5 ppm downfield when compared to the free ligand and in another complex containing phenanthroline a 6 ppm shift downfield can be seen.[32][33]
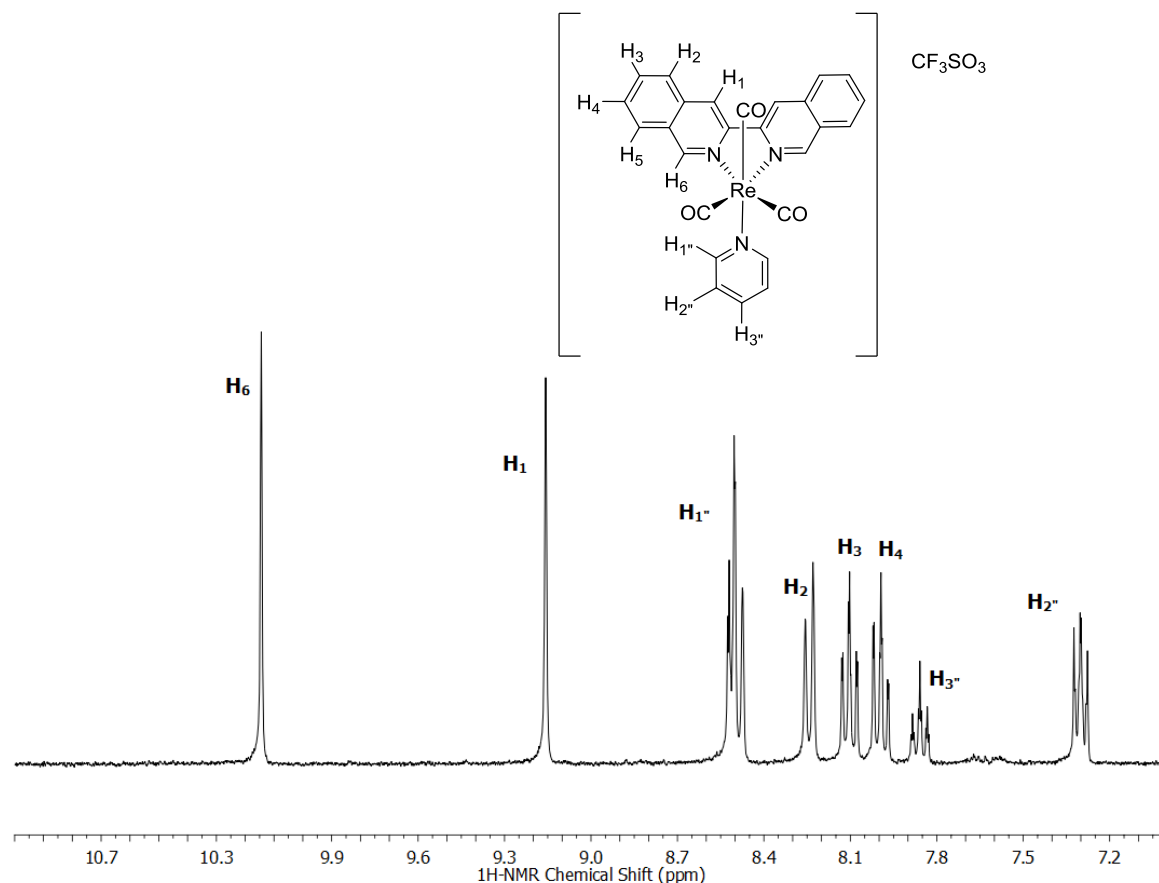
Figure 2.17 ^{1}H-NMR spectrum (300 MHz, MeOD, 298 K) of [Re(CO)$_3$(ibiq)(Py)][CF$_3$SO$_3$].

Crystals of the rhenium complex were obtained through slow diffusion of benzene into a solution of the complex in methanol. The single crystal x-ray structure determined confirms the structure of the rhenium complex (*Fig. 2.18*).

The rhenium metal centre sits in an octahedral arrangement which is six-coordinate. The two biisoquinoline Re-N bonds are similar lengths 2.162 and 2.169 Å (shows similar values to bipyridine in the literature[34]) whereas the Re-N bond originating from the pyridine ligand is slightly larger at 2.208 Å indicating the bidentate ligand is slightly more strongly bound than the monodentate ligand. The N1-C9 and N2-C10 bond lengths are the same length at 1.386 Å and the torsion angle between the two isoquinolyl unts is 9.6°

101

indicating that a small amount of twisting is occurring therefore the biisoquinoline unit is slightly distorted from planarity. The three carbonyl Re-C bonds are all similar lengths 1.917 - 1.929 Å. A table of selected bond lengths and angles for the complex is shown in *Table 2.3*.

Metal	Re-N$_{(ibiq)}$	Re-N$_{(pyr)}$	N$_{(ibiq)}$-Re-N$_{(ibiq)}$	N1-C9-C10	N2-C10-C9
Re	2.162(2)	2.208(2)	75.85(8)	115.3(2)	115.2(2)
	2.169(2)				

Table 2.3 Selected bond lengths (Å) and bond angles (deg) from the crystal structure of [Re(CO)$_3$(ibiq)(Py)][CF$_3$SO$_3$].
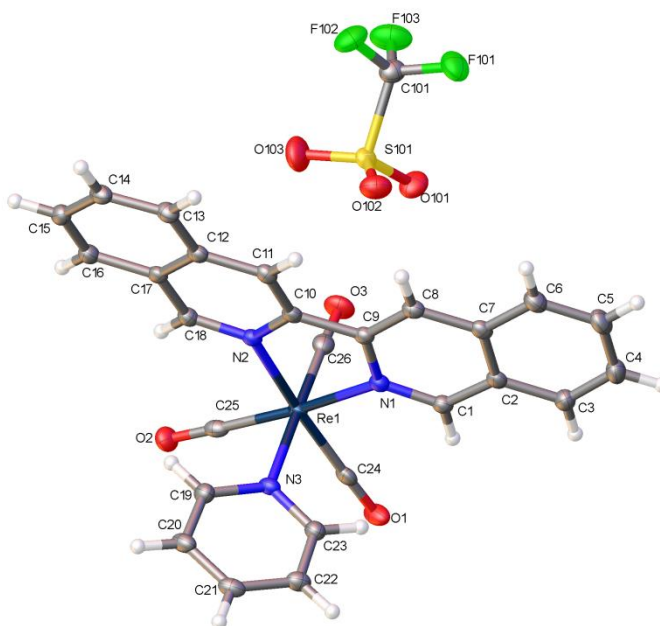
Figure 2.18 The structure of [Re(CO)$_3$(ibiq)(Py)][CF$_3$SO$_3$] with ellipsoids drawn at the 50 % probability level. Benzene solvent has been omitted for clarity.

2.4.5 [Rh(COD)(ibiq)]Cl₂ (9)

A cyclooctadiene rhodium chloride dimer was used as the starting material where the chloride ligand was exchanged for 3,3-biisoquinoline.[35] The reaction required very little preparation or reaction time producing the singly substituted complex, [Rh(COD)(ibiq)][PF₆] in a 72% yield, after only 15 minutes vigorous stirring with potassium hexafluorophosphate in dichloromethane at room temperature (*Scheme 2.15*). Reactions carried out at higher temperatures, with longer time scales and with different stoichiometries did not produce the doubly substituted complex. The rhodium hexaflourophosphate salt produced in the reaction was later converted to its chloride form using Dowex which made the complex water soluble.
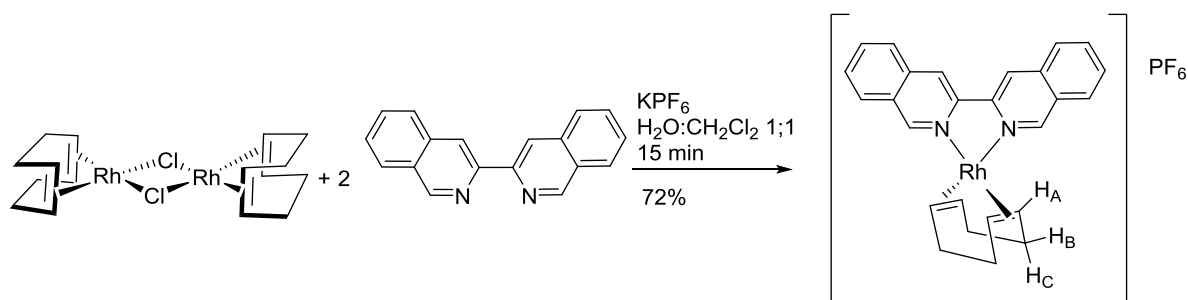
Scheme 2.15 Synthesis of [Rh(COD)(ibiq)][PF₆].

The molecular ion peak corresponding to $[Rh(C_{12}H_{18}N_2)(C_8H_{12})]^+$ was observed at a m/z of 467 following electrospray ionisation mass spectrometry (*Appendix 1.9*). The ¹H-NMR spectrum (*Fig. 2.19*) shows the presence of both the COD and biisoquinoline groups with the latter when compared with the ligand alone and also with the other metal complexes, being seen further upfield (less charge on metal centre therefore less electron withdrawing).
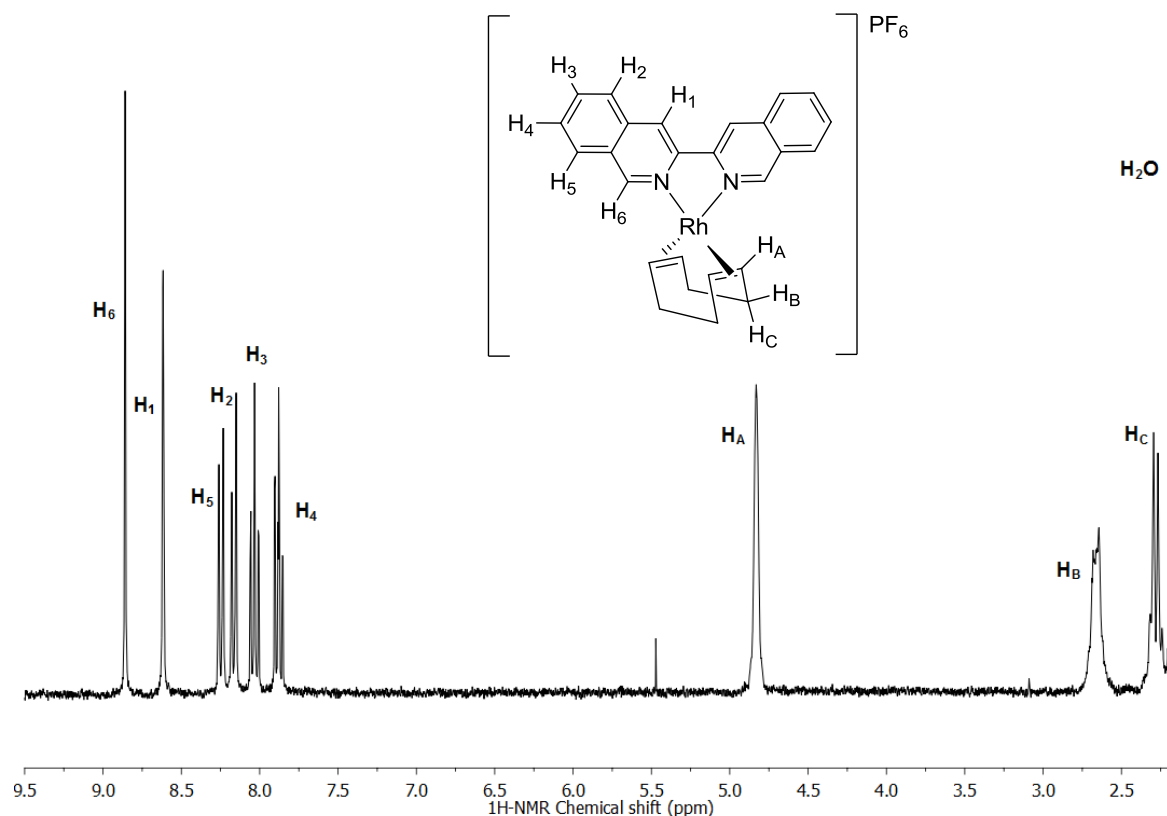
Figure 2.19 ^{1}H-NMR spectrum (300 MHz, CD$_3$CN, 298 K) of [Rh(COD)(ibiq)][PF$_6$].

2.5 UV-Visible Absorbance Characteristics - *Complexes 4 - 9*

The absorbance spectrum of 3,3-biisoquinoline (**4**) shows very strong π-π* ligand transitions in the UV region at 250 nm with further lower energy peaks at 304 and 324 nm which may be due to n-π* transitions from the lone pairs on the nitrogen atoms. This strong π-π* transition is seen in all of the other complexes **5-9** between 251-263 nm. In the rhenium complex, **8**, UV transitions can be seen as low as 217 nm attributed to π-π* transitions from the pyridine ligand.

104

Ligands with a higher degree of delocalisation such as biisoquinoline have a smaller energy gap between their bonding and anti-bonding orbital's causing absorptions to be seen at longer wavelengths; less energy is required to excite an electron. Pyridine has less of an aromatic surface for delocalisation to occur across, therefore exhibits higher energy transitions.[36]

Further charge transfer bands are seen between 370 - 452 nm in the metal containing complexes. As these bands do not appear in the biisoquinoline only absorbance spectrum, it is likely that they are due to interactions between the metal centre and the ligands, especially for complexes **5** and **7** where there are no other ligands apart from biisoquinoline present. The bands seen at 370 nm and 382 nm for $[Pd(ibiq)_2]^{2+}$ and $[Pt(ibiq)_2]^{2+}$ respectively may originate from MLCT transitions because the metal centre for each is in a relatively low oxidation state and the biisoquinoline ligand has low lying π^* orbitals.

MLCT bands have been observed in similar complexes containing bipyridine ligands, such as $[Ru(bpy)_3]^{2+}$.[37] The UV-vis spectrum for the ruthenium bipyridine complex shows absorbance peaks at both 452 nm and 243 nm which originate from MLCT transitions.[37] The most intense peak, seen at 286 nm, is the result of ligand centred π-π^* transitions.[37][38] The platinum bipyridine complex $[Pt(bpy)(dppm)]^{2+}$ also exhibits MLCT transitions, which can be found at 334 nm and 320 nm.[39]

The extinction coefficient for each of the transitions and the wavelengths they occur at can be seen *Table 2.4* for all synthesised complexes.

Complex	UV-Vis Transitions / λ_{max}(nm) (ε_{max}/dm^3 mol^{-1} cm^{-1})
4[a]	250 (30,100), 304 (60,600), 324 (17,600)
5[b]	251 (95,600), 305 (31,600), 328 (27,500), 370 (16,400)
6[c]	263 (39,300), 308 (29,700), 360 (11,200), 380 (15,300)
7[b]	262 (72,400), 335 (19,300), 382 (13,000)
8[a]	217 (43,500), 256 (46,300), 303 (33,300), 354 (11,900), 374 (13,800)
9[d]	219 (33,400), 260 (37,400), 315 (22,000), 364 (8,400), 452 (1,100)

Table 2.4 UV-vis transitions and extinction coefficients occurring in complexes 4-9 under the following conditions, **a**. MeOH, **b**. 15% DMSO:85% H_2O, **c**. DMSO, **d**. H_2O.

2.6 Conclusions

The molecular design proposed fulfils the necessities for a G-quadruplex binder in that the palladium and platinum complexes have a planar aromatic surface for stacking and efficient burial of hydrophobic surfaces and a metal centre providing electrostatic interactions by withdrawing electron density from the aromatic ligands, mimicking the monovalent cation that usually sits in the central channel of the quadruplex structure.

After considering the possible synthetic routes for the homocoupling of 3-chloroisoquinoline, the catalytic cycle involving nickel was chosen not only because of the availability and price of the nickel complex, but also the feasibility of the reaction (relatively mild conditions).

The synthesis of the ligand 3,3-biisoquinoline and the palladium, platinum, rhenium and rhodium complexes incorporating this ligand have been described. Despite the relatively

low yields of the products, enough of each was attained to carry out the necessary characterisations and subsequent binding experiments discussed in the next chapter.

The anions for the palladium and platinum complexes differ because of differences in solubility. This may have an effect on the binding and cell studies however both anions are non-coordinating and if they were to interact it would most likely be through fluorine which both anions contain.

In Chapter 3 the ability, of the complexes synthesised, to bind different structures of DNA will be assessed using fluorescent indicator displacements, circular dichroism, linear dichroism, UV-vis titrations, H-NMR, gel electrophoresis and FRET melting.

2.7 Experimental

General Methods

All characterisation techniques took place within the University of Birmingham. NMR spectra were recorded in $CDCl_3$, CD_3CN, CD_3OD and d_6-DMSO. 1D ^1H NMR and COSY spectra were recorded on Bruker AV(III)300 and AV(III)400 instruments operating at 300 MHz and 400 MHz respectively. ^{13}C NMR and HSQC spectra were recorded on a Bruker AV(III)400 instrument operating at 100 MHz (see appendix for spectra). Electrospray ionisation was performed on a Waters LCT Time of Flight Spectrometer, electron impact mass spectrometry on a VG ZabSpec mass spectrometer and elemental analysis on a CE Instrument EA1110. A Varian Cary 5000 UV-Vis spectrometer was used to obtain UV-Vis spectra for the complexes and infrared spectra were recorded on a Perkin

Elmer Spectrum 100 FT-IR spectrometer. The single crystal X-ray structures were obtained by Dr Louise Male (University of Birmingham crystallographer) and carried out on an Agilent SuperNovadiffractometer using an Atlas detector. The data collections were driven and processed and absorption corrections were applied using CrysAlisPro.[40]

The compounds and solvents used were obtained from Fisher, Sigma Aldrich, Scientific Laboratory Supplies and Acros organics. All the solvents were of a standard grade and were used without further purification. Silica gel was used for the chromatographic separation of products using columns run under gravity.

Isoquinoline-1,3-dione (1) [8][21]

Molecular weight = 160.15 gmol^{-1}

Molecular Formula = $C_9H_7O_2N$
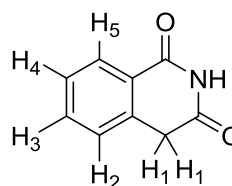
Homophthalic acid (15.0 g, 0.08 mol) was dissolved in concentrated (28 %) NH_4OH (100 ml) and then was evaporated to dryness under *vacuo*. This part of the procedure was repeated with additional NH_4OH (50 ml). 1, 2-dichlorobenzene (70 ml) was added to the resulting orange residue and heated with stirring at 200°C for 2 h without a condenser making sure the residue dissolved. The concentrated mixture was allowed to cool to room temperature, diluted with methanol (300 ml), and allowed to stand overnight. The precipitate was collected by filtration, washed with methanol, and dried under reduced pressure to leave tan shards. 11.28 g, 88% yield.

^{1}H NMR (300 MHz, d_6-DMSO): δ 11.29 (s, 1H, NH), 8.01 (d, 1H, J = 6.0, H_5), 7.64 (t, 1H, J = 6.0, H_3), 7.45 (t, 1H, J = 6, H_4), 7.38 (d, 1H, J = 6.0, H_2), 4.03 (s, 2H, H_1).

^{13}C NMR (100 MHz, d_6-DMSO): δ 170.9, 165.3, 136.6, 133.4, 127.8, 127.4, 127.1, 124.9, 35.9.

Elemental analysis. Calculated for $C_9H_7O_2N$; C, 67.1; N, 8.7; H, 4.4. Found: C, 67.1; N, 8.5; H, 4.1.

Mass analysis (EI, +ve): m/z = 161 $[H(C_9H_7O_2N)]^+$.

IR (Solid): ν = 3163 (m), 3061 (m), 2885 (m), 1673 (vs), 1608 (s), 1583 (w), 1462 (m), 1336 (w), 1367 (m), 1282 (s), 1136 (m), 1031 (w), 926 (w), 877 (m), 736 (s) cm^{-1}.

1,3-Dichloroisoquinoline (2) [8]

Molecular weight = 198.05 gmol^{-1}

Molecular Formula = $C_9H_5Cl_2N$
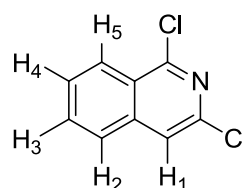
Phenylphosphonic dichloride (19.0 ml, 0.13mol) was added to (**1**) isoquinoline-1,3-dione (8.86 g, 0.06 mol) and heated under reflux (160 °C) for 3 hours. The reaction was left to cool to room temperature and then left to stand overnight. The brownish yellow solid formed was collected by filtration, and re-dissolved in tetrahydrofuran (250 ml), treated with water (70 ml), and then the solution was concentrated under *vacuo* to remove the tetrahydrofuran. The aqueous material remaining was neutralized with concentrated NH$_4$OH (28 %) before being extracted with ethyl acetate (3 × 150ml). The ethyl acetate phases were combined, washed with water, brine, dried over Na$_2$SO$_4$ and reduced under *vacuo* to form a yellow

powdery solid. This was then purified by column chromatography (silica gel, CH_2Cl_2, Rf 0.8) to give an off white solid, 6.46g, 59% yield.

^{1}H NMR (300 MHz, d_6-DMSO): δ 8.36 (d, 1H, J = 8.7, H_5), 8.24 (s, 1H, H_1), 8.15 (d, 1H, J = 8.4, H_2), 8.03 (t, 1H, J = 8.1, H_3), 7.92 (t, 1H, J = 8.4, H_4).

^{13}C NMR (100 MHz, d_6-DMSO): δ203.7, 145.4, 132.1, 128.7, 126.6, 126.3, 119.8, 100.4, 60.8.

Elemental analysis: Calculated for $C_9H_7Cl_2N$; C, 54.6; N, 7.1; H, 2.5. Found: C, 55.1; N, 7.1; H, 2.3.

Mass analysis (EI, +ve): m/z = 199 $[H(C_9H_5Cl_2N)]^+$.

IR (Solid): ν = 3082 (w), 3060 (w), 1616 (m), 1575 (m), 1552 (m), 1486 (m), 1395 (w), 1295 (s), 1252 (s), 1151 (w), 1094 (s), 982 (s), 839 (s), 755 (m), 745 (s), 706 (s) cm^{-1}.

3-Chloroisoquinoline (3) [8]

Molecular weight = 163.61 gmol^{-1}

Molecular Formula = C_9H_6ClN
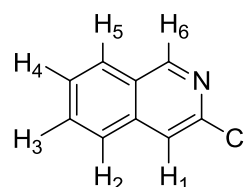
1,3-Dichloroisoquinoline (**2**) (7.68 g, 0.04 mol from multiple batches) was suspended in glacial acetic acid (42.1 ml) and concentrated HCl (14.9 ml). It was then treated with tin powder (13.9 g, 0.12 mol) and stirred and heated at reflux (55°C) for 3 hours. The mixture was cooled to room temperature and the precipitated tin salts were removed by filtration through celite. The filtrate was basified to pH 9 with concentrated NH_4OH and then extracted with ethyl acetate (5 × 150 ml). The organic extracts were combined, washed

with saturated $NaHCO_3$ solution, dried over Na_2SO_4, and concentrated in *vacuo*. The waxy yellow residue produced was purified by column chromatography (silica gel, CH_2Cl_2, Rf 0.5) to give a pale yellow solid, 0.63 g, 10 % yield.

^{1}H NMR (300 MHz, MeOD): δ 9.12 (s, 1H, H_6), 8.14 (d, 1H, J = 8.4, H_5), 7.92 (d, 1H, J = 8.4, H_2), 7.92 (s, 1H, H_1), 7.83 (t, 1H, J = 8.1, H_3), 7.71 (t, 1H, J = 8.4, H_4).

^{13}C NMR (100 MHz, MeOD): δ 153.8 (C_{H6}), 133.0 (C_{H3}), 129.2 (C_{H4}), 129.0 (C_{H5}), 127.0 (C_{H2}), 121.5 (C_{H1}).

Mass analysis (EI, +ve): m/z = 163 $[C_9H_6ClN]^+$.

IR (Solid): ν = 3075 (w), 3052 (w), 1626 (m), 1584 (w), 1572 (m), 1485 (m), 1426 (m), 1390 (w), 1334 (m), 1273 (m), 1197 (w), 1138 (w), 1064 (s), 1011 (w), 944 (s), 884 (vs), 855 (s), 738 (vs) cm^{-1}.

3,3-Biisoquinoline (4)

Molecular weight = 256.30 gmol^{-1}

Molecular Formula = $C_{18}H_{12}N_2$
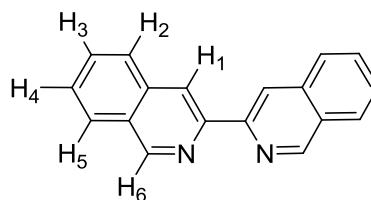
Operating under an argon atmosphere $[NiCl_2.6H_2O]$ (278 mg, 1.17mmol), PPh_3 (1.23 g, 4.68 mmol) and zinc dust washed with dilute HCl, H_2O, EtOH and Et_2O (82 mg, 1.24 mmol) were added to a schlenk tube. DMF (13 ml) was then added by syringe into the sealed vessel. The brick red solution that formed was left to stir at 70°C for an hour before adding a degassed solution of 3-chloroisoquinoline, **3**, (0.19 g, 1.17 mmol) in DMF (6.5 ml). The mixture was then left to heat at 70°C for 4 h. After heating, the mixture was

allowed to cool to room temperature before pouring onto a 7 % ammonium hydroxide solution (19 ml) – a small amount of concentrated (28 %) ammonium hydroxide was added to ensure all the ligand had been removed from the metal. The product was then extracted in dichloromethane and diethyl ether (2:1, 3 x 65 ml) before removing the solvent from the organic layer in *vacuo*. The yellow-orange oil that remained was diluted with dichloromethane (40 ml) and washed with water (4 x 13 ml) and brine (26 ml) before drying over $MgSO_4$ and reducing in *vacuo* to an off white solid. This was purified by column chromatography (silica gel, CH_2Cl_2 to remove un-reacted compound **3** Rf 0.5, followed by ethyl acetate to elute the coupled product Rf 0.2) to give a pale yellow solid. This was followed by another column to remove any traces of triphenylphosphine oxide (silica gel, diethyl ether) which again left a pale yellow solid, 0.059 g, 10 % yield.

^{1}H NMR (300 MHz, MeOD): δ 9.40 (s, 2H, H_6), 8.85 (s, 2H, H_1), 8.17 (d, 2H, J = 8.1, H_5), 8.09 (d, 2H, J = 8.1, H_2), 7.84 (t, 2H, J = 6.9, H_3), 7.73 (t, 2H, J = 6.9, H_4).

Mass analysis (EI, +ve): m/z = 256 $[C_{12}H_{18}N_2]^+$.

IR (Solid): ν = 3048 (w), 2973 (w), 1620 (m), 1575 (m), 1553 (m), 1487 (m), 1433 (m), 1387 (w), 1338 (w), 1295 (m), 1253 (m), 1190 (m), 1140 (w), 1026 (w), 983 (m), 940 (m), 872 (m), 818 (w), 775 (m), 745 (s), 706 (m) cm^{-1}.

UV-Vis (MeOH) λ_{max} [nm] (ε_{max}/dm^3 mol^{-1} cm^{-1}): 213 (30200), 250 (60600), 304 (23200), 324 (17600), 351 (3100).

[Pd(i-biq)₂](BF₄)₂ (5)

Molecular weight = 792.63 gmol^{-1}

Molecular Formula = PdC$_{36}$H$_{24}$N$_4$B$_2$F$_8$
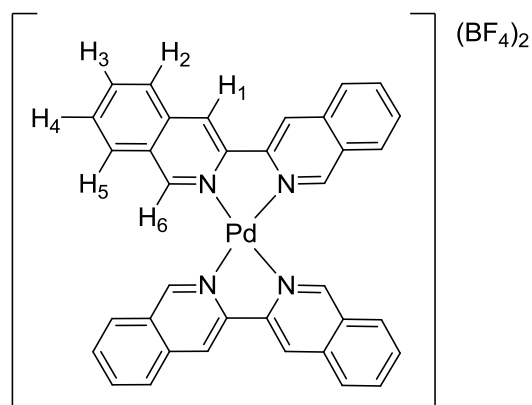
A solution of 3,3-biisoquinoline, **4**, (9.5 mg, 0.037 mmol) in acetonitrile (6 ml) was added to a schlenk tube and placed under an argon atmosphere. Tetrakis(acetonitrile)palladium(II) tetrafluoroborate (8.5 mg, 0.019 mmol) was then added to the mixture and left to stir overnight. The solution was then filtered and the filtrate reduced in *vacuo* to a yellow solid. This was then washed with chloroform (5 ml), methanol (5 ml) and diethyl ether (5 ml) and left to dry under vacuum. 7.6 mg, 50 % yield.

^{1}H NMR (300 MHz, CD$_3$CN): δ 9.30 (s, 4H, H$_6$), 8.79 (s, 4H, H$_1$), 8.23 (d, 4H, J = 8.1, H$_5$), 8.08 (d, 4H, J = 8.1, H$_2$), 7.93 (t, 4H, J = 7.2, H$_3$), 7.77 (t, 4H, J = 7.5, H$_4$).

^{1}H NMR (300 MHz, DMSO): δ 9.97 (s, 4H, H$_6$), 9.40 (s, 4H, H$_1$), 8.64 (d, 4H, J = 8.1, H$_5$), 8.35 (d, 4H, J = 8.1, H$_2$), 8.25 (t, 4H, J = 6.9, H$_3$), 8.06 (t, 4H, J = 7.5, H$_4$).

^{13}C NMR (100 MHz, DMSO): δ158.6 (C$_{H6}$), 135.5 (C$_{H3}$), 130.7 (C$_{H4}$), 130.3 (C$_{H5}$), 127.5 (C$_{H2}$), 121.1 (C$_{H1}$).

Mass analysis (ESI, +ve): m/z = 309 [Pd(C$_{12}$H$_{18}$N$_2$)$_2$]$^{2+}$, 637 [F + (Pd(C$_{12}$H$_{18}$N$_2$)$_2$)]$^+$.

IR (Solid): ν =3612 (vw), 3058 (w), 1631 (m), 1602 (w), 1495 (m), 1441 (w), 1392 (m), 1355 (w), 1328 (w), 1289 (w), 1210 (w), 1013 (vs), 972 (s), 905 (s), 751 (s) cm^{-1}.

UV-Vis (15 % DMSO : 85 % H$_2$O) λ$_{max}$ [nm] (ε$_{max}$/dm^3 mol^{-1} cm^{-1}): 251 (95600), 305 (31600), 328 (27500), 370 (16400).

113

[Pt(i-biq)Cl$_2$ (6) [6]

Molecular weight = 521.00 gmol^{-1}

Molecular Formula = PtC$_{18}$H$_{12}$N$_2$Cl$_2$
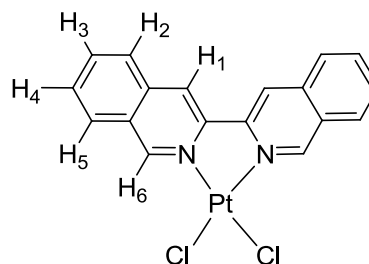
Potassium tetrachloroplatinate (13.0 mg, 0.03 mmol) was dissolved in water (2.2 ml) before adding 2 M HCl (0.1 ml) and then a suspension of 3,3-biisoquinoline (8.0 mg, 0.03 mmol) in acetonitrile (2.2 ml). The mixture was heated under reflux for 1.5 h during which time a yellow solid precipitated. The solution was left to cool to room temperature before filtering, washing with acetonitrile and then drying under vacuum. 4.0 mg, 26 % yield.

^{1}H NMR (300 MHz, d$_6$-DMSO): δ 10.26 (s, 2H, H$_6$), 9.21 (s, 2H, H$_1$), 8.50 (d, 2H, J = 8.4, H$_5$), 8.15 (m, 4H, H$_{2 \text{ and } 3}$), 7.91 (t, 2H, J = 8.1, H$_4$).

Mass analysis (ESI, +ve): m/z = 545 [Na(Pt(C$_{18}$H$_{12}$N$_2$)Cl$_2$)]$^+$

IR (Solid): ν = 3092 (w), 3054 (w), 3027 (w), 1629 (w), 1602 (w), 1496 (m), 1438 (w), 1389 (m), 1355 (m), 1290 (w), 1150 (w), 1048 (m), 1018 (m), 961 (m), 904 (m), 884 (m), 743 (s) cm^{-1}.

UV-Vis (DMSO) λ$_{max}$ [nm] (ε$_{max}$/dm^3 mol^{-1} cm^{-1}): 263 (39300), 308 (29700), 360 (11200), 380 (15300).

114

[Pt(i-biq)₂][PF₆]₂ (7) [6]

Molecular weight = 997.09 gmol^{-1}

Molecular Formula = PtC$_{36}$H$_{24}$N$_4$P$_2$F$_{12}$
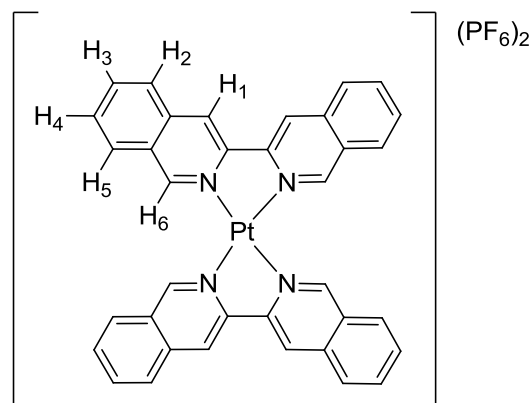
Potassium tetrachloroplatinate (4.5 mg, 0.01mmol) was dissolved in water (5 ml) before adding a suspension of 3,3-biisoquinoline (5.5 mg, 0.02 mmol) in acetonitrile (5 ml). The mixture was heated under reflux overnight producing a yellow solution. The solution was hot filtered before adding a methanolic solution of NH$_4$PF$_6$. An off white solid precipitated immediately which was collected, washed with chloroform, methanol and diethyl ether before leaving to dry under vacuum. 2.7 mg, 27 % yield.

^{1}H NMR (300 MHz, CD$_3$CN): δ 9.68 (s, 4H, H$_6$), 9.05 (s, 4H, H$_1$), 8.48 (d, 4H, J = 8.1, H$_5$), 8.33 (d, 4H, J = 8.4, H$_2$), 8.20 (t, 4H, J = 7.5, H$_3$), 8.03 (t, 4H, J = 8.1, H$_4$).

Mass analysis (ESI, +ve): m/z = 353 [Pt(C$_{18}$H$_{12}$N$_2$)$_2$]$^{2+}$, 742 [Cl + (Pt(C$_{18}$H$_{12}$N$_2$)$_2$)]$^+$.

IR (Solid): ν = 3649 (vw), 3069 (w), 1622 (m), 1575 (w), 1552 (w), 1488 (m), 1392 (m), 1357 (w), 1294 (m), 1253 (w), 1210 (w), 1155 (w), 1013 (vs), 909 (s), 983 (s), 924 (m), 755 (s) cm^{-1}.

UV-Vis (15 % DMSO : 85 % H$_2$O) λ$_{max}$ [nm] (ε$_{max}$/dm^3 mol^{-1} cm^{-1}): 262 (72400), 335 (19300), 382 (13000).

[Re(i-biq)(CO)₃Py][CF₃SO₃] (8)

Molecular weight = 757.73 gmol^{-1}

Molecular Formula = $C_{27}H_{17}N_3ReO_6F_3S$
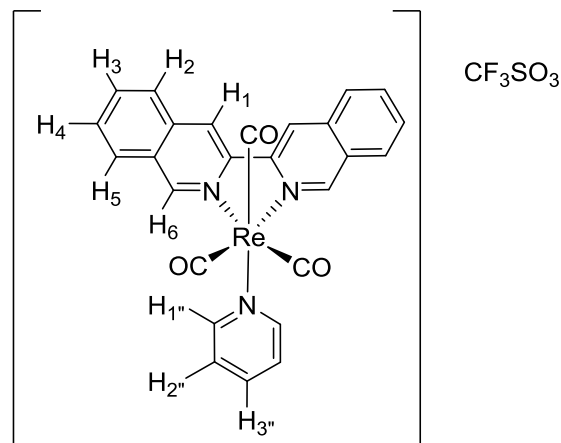
Part 1

3,3-biisoquinoline (**4**) (8.0 mg, 0.031 mmol) and pentacarbonylchlororhenium(I) (5.4 mg, 0.015 mmol) were put under an argon atmosphere before being suspended in toluene (5 ml). The solution was heated at 120°C for 4 hours and then left to cool to room temperature before filtering and collecting the yellow solid formed.

Part 2

[Re(i-biq)(CO)₃Cl] (from **part 1**) (11.0 mg, 0.019 mmol) and AgO₃SCF₃ (5.0 mg, 0.019 mmol) were put under an argon atmosphere before dissolving in CH₃CN (15 ml). The reaction mixture was left to reflux in the dark for 16 h before cooling to room temperature. The solution was then filtered and the filtrate reduced in *vacuo* to leave a yellow residue which was then directly used in the next step of the reaction.

Part 3

The residue of [Re(i-biq)(CO)₃CH₃CN][CF₃SO₃] from **part 2** was heated under reflux in pyridine (4 ml) for 4 h. The yellow oil produced after reducing the solution in *vacuo* was precipitated out using diethyl ether. A beige solid was collected. 6.6 mg, 50 % yield.

^{1}H NMR (300 MHz, MeOD):δ 10.12 (s, 2H, H$_6$), 9.14 (s, 2H, H$_1$), 8.50-8.45 (m, 4H, H$_{5, 1", 5"}$), 8.21 (d, 2H, J = 8.1, H$_2$), 8.08 (t, 2H, J = 6.9, H$_3$), 7.97 (t, 2H, J = 6.9, H$_4$), 7.84 (t, 1H, J = 7.8, H$_{3"}$), 7.28 (t, 2H, J = 6.3, H$_{2", 4"}$).

^{13}C NMR (100 MHz, MeOD): δ 158.8 (C$_{H6}$), 153.3 (C$_{H5 \text{ or } H1"/5"}$), 141.1 (C$_{H3"}$), 135.8 (C$_{H3}$), 132.0 (C$_{H4}$), 130.0 (C$_{H5 \text{ or } H1"/5"}$), 129.0 (C$_{H2}$), 127.9 (C$_{H3"}$), 122.8 (C$_{H1}$).

Mass analysis (ESI, +ve): m/z = 606 [Re(C$_{12}$H$_{18}$N$_2$)(CO)$_3$(C$_5$H$_5$N)]$^+$

IR (Solid): ν = 3068 (w), 2022 (s), 1898 (vs), 1628 (m), 1602 (m), 1488 (m), 1446 (m), 1391 (m), 1358 (w), 1272 (m), 1256 (s), 1218 (m), 1139 (m), 1067 (m), 1028 (s), 902 (m), 750 (s) cm^{-1}.

UV-Vis (MeOH) λ$_{max}$ [nm] (ε$_{max}$/dm^3 mol^{-1} cm^{-1}): 217 (43500), 256 (46300), 303 (33300), 354 (11900), 374 (13800).

[Rh(ibiq)(COD)][PF$_6$] (9) (COD = Cycloocta-1,5-diene)

Molecular weight = 671.24 gmol^{-1}

Molecular Formula = C$_{29}$H$_{33}$N$_2$RhPF$_6$
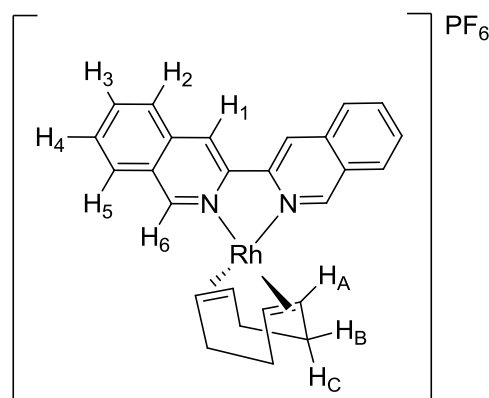
[Rh$_2$Cl$_2$(COD)$_2$] (2.56 mg, 0.005 mmol) in dichloromethane (3 ml) and potassium hexafluorophopshate (2.56 mg) in water (3 ml) were placed in the reaction vessel before adding ibiq (10 mg, 0.04 mmol) and vigorously stirring for 15 min. After this time the orange dichloromethane layer was extracted from the solution and washed with more water

($3\times$ 2 ml). The washed solution was then reduced to ~ 1 ml with nitrogen gas before adding ethanol (0.3 ml) followed by slowly adding another (0.6 ml) of ethanol to fully precipiate out the product. The product was then filtered, washed with diethyl ether and left to air dry to leave an orange powder, 4.8 mg, 72 % yield.

^{1}H NMR (300 MHz, CD$_3$CN): δ 8.83 (s, 2H, H$_6$), 8.58 (s, 2H, H$_1$), 8.21 (d, 2H, J = 8.1, H$_5$), 8.14 (d, 2H, J = 9.0 H$_2$), 8.00 (t, 2H, J = 7.2, H$_3$), 7.85 (t, 2H, J = 6.9, H$_4$), 4.84 - 4.76 (m, 4H, H$_A$), 2.68 - 2.59 (m, 4H, H$_B$), 2.29 - 2.20 (m, 4H, H$_c$)

Mass analysis (ESI, +ve): m/z = 467 [Rh(C$_{12}$H$_{18}$N$_2$)(C$_8$H$_{12}$)]$^+$

IR (Solid): ν = 3647 (w), 3271 (br m), 3011 (m), 2946 (m), 2913 (m), 2881 (m), 2838 (m), 2167 (w), 1976 (w), 1626 (m), 1598 (m), 1494 (m), 1434 (w), 1390 (m), 1352 (m), 1304 (w), 1212 (w), 1078 (w), 1045 (w), 1011 (m), 980 (m), 911 (m), 755 (s) cm^{-1}.

UV-Vis (H$_2$O) λ_{max} [nm] (ε_{max}/dm^3 mol^{-1} cm^{-1}): 219 (33400), 260 (37400), 315 (22000), 364 (8400), 452 (1100).

2.8 References

1. E. Largy, F. Hamon, F. Rosu, V. Gabelica, E. De Pauw, A. Guédin, J. Mergny, M. Teulade-Fichou. *Chem. Eur. J.,* 2011, **17**, 13274.

2. N. H. Campbell, N. H. Abd Karim, G. N. Parkinson, M. Gunaratnam, V. Petrucci, A. K. Todd, R. Vilar, S. Neidle. *J. Med. Chem.*, 2012, **55**, 209.

3. L. Wang, Y. Wen, J. Liu, J. Zhou, C. Lib, C. Wei. *Org. Biomol. Chem.,* 2011, **9**, 2648.

4. C. Bazzicalupi, M. Ferraroni, A. R. Bilia, F. Scheggi, P. Gratteri. *Nucleic Acids Res.,* 2013, **41**, 632.

5. Y. Ma, T. M. Ou, J. H. Tan, J. Q. Hou, S. L. Huang, L. Q. Gu, Z. S. Huang. *Bioorg. Med. Chem. Lett.,* 2009, **19**, 3414.

6. M. Kato, K. Sasano, C. Kosuge, M. Yamazaki, S. Yano, M. Kimura. *Inorg. Chem.,* 1996, **35**, 116.

7. T. Ou, Y. Lu, J. Tan, Z. Huang, K. Wong, L. Gu. *Chem. Med. Chem.*, 2008, **3**, 690.

8. C. H. Lee, E. Bayburt, S. DiDomenico, I. Drizin, A. Gomtsyan, J. Koenig, R. Perner, R. Schmidt, S. Turner, T. Jinkerson, G. Zheng. US Pat., 20050113576A1, 2005.

9. *Organic Chemistry, third edition.* M. Jones Jr, W. W. Norton and Company, Inc, New York, 2005.

10. M. M. Robinson. *J. Am. Chem. Soc.*, 1958, **80**, 5481.

11. *Heterocyclic Compounds - Isoquinolines.* ed. G. Grethe, John Wiley & Sons, Inc, Hoboken, NJ, 1981.

12. F. Monnier, M. Taillefer. *Angew. Chem. Int. Ed.*, 2009, **48**, 6954.

13. E. Sperotto, G. P. M. van Klink, G. van Koten, J. G. de Vries. *Dalton Trans.,* 2010, **39**, 10338.

14. D. Hennings, T. Iwama, V. H. Rawal. *Org. Lett.,* 1999, **1**, 1205.

15. A. V. Aksenov, V. I. Goncharov. *Chem. Heterocycl. Compd.,* 2008, **44**, 1491.

16. J. Hassan, V. Penalva, L. Lavenot, C. Gozzi, M. Lemaire. *Tetrahedron,* 1998, **54**, 13793.

17. X. Tao, W. Zhou, Y. Zhang, C. Dai, D. Shen. M. Huang. *Chin. J. Chem.,* 2006, **24**, 939.

18. Michael J. Hannon, *PhD Thesis,* University of Cambridge, 1993.

19. M. Iyoda, H. Otsuka, K. Sato, N. Nisato, M. Oda. *Bull. Chem. Soc. Jpn.,* 1990, **63**, 80.

20. E. C. Constable, S. M. Elder, J. Healy. *J. Chem. Soc., Dalton Trans.,* 1990, 1669.

21. O. Wolfbeis, I. Trummer, A. Knierzinger. *Liebigs. Ann. Chem.,* 1981, **10**, 811.

22. M. N. Gitlitz, M. K. Moran. *Tin Compounds, Kirk-Othmer Encyclopedia of Chemical Technology.* John Wiley & Sons Inc, 2006.

23. C. R. Smith. *Synlett.,* 2009, **9**, 1522.

24. Y. Yamamoto, A. Yanagi. *Chem. Pharm. Bull.,* 1982, **30**, 2003.

25. J. Hashima, C. O. Kappe. *Adv. Synth. Catal.,* 2007, **349**, 2353.

26. B. Milani, A. Anzilutti, L. Vicentini, A. Sessanta o Santi, E. Zangrando, S. Geremia, G. Mestroni. *Organometallics,* 1997, **16**, 5064.

27. G. Anderegg, H. Wanner. *Inorg. Chim. Acta,* 1986, **113**, 101.

28. G. T. Morgan, F. H. Burstall. *J. Chem. Soc.,* 1934, 965.

29. E. C. Constable, M. J. Hannon. *Inorg. Chim. Acta.,* 1993, **211**, 101

30. A. W. Cordes, B. Durham, P. N. Swepston, W. T. Pennington, S. M. Condren, R. Jensen, J. L. Walsh. *J. Coord., Chem.,* 1982, **11**, 251.

31. T. Hayashida, H. Nagashima. *Organometallics,* 2002, **21**, 3884.

32. G. T. Ruiz, M. P. Juliarena, R. O. Lezna, E. Wolcan, M. R. Feliz, G. Ferraudi. *Dalton Trans.,* 2007, **20**, 2020.

33. K. K.W. Lo, K. H. K. Tsang, N. Zhu. *Organometallics,* 2006, **25**, 3220.

34. J. Guilhem, C. Pascard, J. Lehn, R. Ziessel. *J. Chem. Soc., Dalton. Trans.,* 1989, 1449.

35. R. R. Schrock, J. A. Osborn. *J. Am. Chem. Soc.,* 1971, **93**, 2397.

36. Z. Li, E. Badaeva, A. Ugrinov, S. Kilina, W. Sun. *Inorg. Chem.,* 2013, **52**, 7578.

37. M. B. S. Kirketerp, S. B. Nielsen. *Int. J. Mass Spectrom.,* 2010, **297**, 63.

38. H. Y. Li, L. X. Cheng, J. Xiong, L. C. Kang, Q. L. Xu, Y. C. Zhu, Y. M. Tao, Y. X. Zheng, J. L. Zuo, X. Z. You. *Inorg. Chim. Acta,* 2011, **370**, 398.

39. J. DePriest, G. Y. Zheng, N. Goswami, D. M. Eichhorn, C. Woods, D. P. Rillema. *Inorg. Chem.,* 2000, **39**, 1955.

40. Agilent Technologies, CrysAlisPro, Version 1.171.36.28, 2013.

Chapter 3: DNA Binding Studies

3.1 Introduction

The binding properties of the complexes $[Pd(ibiq)_2][BF_4]_2$, $[Pt(ibiq)_2][PF_6]_2$ and $[Re(CO)_3(py)(ibiq)][CF_3SO_3]$ with both duplex and G-quadruplex type DNA will be explored in this chapter using a variety of spectroscopic techniques. In order for a complex to be a good potential binder for a G-quadruplex it needs to specifically target this structure over the more commonly found duplex form. The square planar complexes have ligands that should be too large to fit between a base pair in a double helical structure; instead they should be the right size and shape to stack on top of a G-quartet.

The binding studies with the complex $[Pt(ibiq)Cl_2]$ were limited due to its poor solubility in DMSO and water, whereas $[Pd(ibiq)_2][BF_4]_2$ and $[Pt(ibiq)_2][PF_6]_2$ experiments required 15 % DMSO solutions, $[Re(CO)_3(py)(ibiq)][CF_3SO_3]$ 15 % methanolic solutions and $[Rh(COD)(ibiq)]Cl_2$ was fully soluble in water. Different solvent systems were used due to the varying solubility of the four compounds; no one solvent could dissolve all of the complexes. Despite the majority of complexes requiring additional solvents to be fully soluble, the final percentage of these solvents in the experimental DNA binding solutions did not exceed 2 %.

3.1.1 Types of DNA Investigated in Binding Studies

Four types of DNA will be used in the binding experiments in order to assess how selective the complexes are for one type of DNA sequence or structure over another. The types of DNA to be used are ct-DNA, htelo quadruplex forming DNA, c-myc quadruplex forming

DNA and ds26 (a self-complimentary duplex forming sequence); each of which will be discussed in detail.

ct-DNA

Calf thymus DNA (ct-DNA) is composed of a varying selection of bases and therefore DNA sequences, consisting of mainly double but also single stranded regions. The concentration of ct-DNA is measured in bases determined by UV spectroscopy as strand concentration cannot be calculated. The ability of the complexes to bind to duplex DNA will be assessed using ct-DNA in stability assessment, circular dichroism, linear dichroism and UV-vis titration experiments.

Htelo DNA

Human telomeric DNA is made up of a repeat base sequence of TTA-GGG which has been identified as a G-quadruplex forming region due to it being guanine rich. Htelo is a 22 base sequence composed of the bases; 5'-**A-GGG-TTA-GGG-TTA-GGG-TTA-GGG**-3', which mimics the DNA sequence found at the telomeric ends.[1] Under the appropriate salt conditions the sequence is able to take the form of either an antiparallel or antiparallel hybrid G-quadruplex structure (*Fig. 3.1*), monitored using circular dichrosim. The ability of the complexes to stabilise, bind or even induce a G-quadruplex structure in this region of DNA can be investigated using circular dichroism, UV-vis titrations, ^{1}H-NMR, FRET melting and fluorescent indicator displacement experiments.
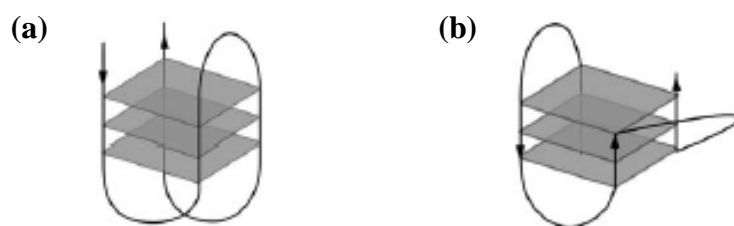
Figure 3.1 **a**. Antiparallel G-quadruplex, **b**. Antiparallel hybrid G-quadruplex. [Reproduced from Ref [1]]

C-myc DNA

Sequences found in oncogene promoter regions of DNA are guanine rich and have the potential to fold into G-quadruplexes.[1] The c-myc sequence is made up of 22 bases taken from part of the oncogene promoter region; 5'-**TGA-GGG-TGG-GTA-GGG-TGG-GTA-A**-3'. Parallel G-quadruplex structures (*Fig. 3.2*) are formed from the c-myc sequence when placed in the same conditions as the htelo DNA sequence. It can therefore be used as a direct comparison with the htelo DNA to look at selectivity and hence binding modes. The loops of the quadruplex differ in each case and may give more clues towards how the complex is interacting with the quadruplex. C-myc DNA will be used in circular dichroism, UV-vis titration and fluorescence indicator experiments.
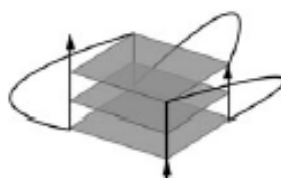
Figure 3.2 Parallel G-quadruplex. [Reproduced from Ref [1]]

ds26

A 26 base self-complimentary sequence used in similar experiments in the literature, 5'-**CAA-TCG-GAT-CGA-ATT-CGA-TCC-GAT-TG**-3', was used as a comparison to the guanine rich quadruplex forming sequences.[2] The number of binding sites for this strand and also the quadruplex DNA has been evaluated with the dye thiazole orange during fluorescent indicator displacement experiments, allowing a direct comparison between the two types of DNA. The duplex forming ds26 sequence is also used as a competitor in the FRET melting and PAGE experiments.

Using the results from the binding experiments and also the crystal structures recorded for complexes **5**, **7** and **8**, the possible modes of binding to each type of DNA will be explored. The influence of cations on DNA structure in solution will also be examined for G-quadruplex forming sequences whose structure can change depending on the type of cation present.

3.1.2 Stability of Complexes 5, 7, 8, 9

Before starting the binding experiments the stability of each of the complexes was assessed using UV-vis spectroscopy to observe the change in absorbance over time (*Fig. 3.3*). The most stable of the complexes would show no difference in their λ_{max} throughout the duration of the experiment. Of the four complexes, when tested alone in solution, $[Re(CO)_3(py)(ibiq)][CF_3SO_3]$ (**8**) was the most stable and showed only a 0.2 % decrease in absorbance intensity over 12 hours. $[Pt(ibiq)_2][PF_6]_2$ (**7**) was the next stable with a loss of intensity of only 8 % over the same duration of time. The palladium (**5**) and rhodium (**9**) complexes both showed much higher losses of absorbance, 16 % and 31 % respectively.

Complex stability was further investigated in the presence of calf thymus DNA (ct-DNA) where the stability of all but one of the complexes improved upon the addition of ct-DNA (*Fig. 3.3*). The palladium complex showed a decrease of 4 % in absorbance compared with the previous 16 %. The same was true for the rhodium complex absorbance which in the presence of the ct-DNA decreased 7 % instead of 31 %. The platinum complex (**7**) was relatively stable in solution alone however the stability did increase when ct-DNA was added from an absorption loss of 8 % to 7 %. The rhenium complex appeared to destabilise upon adding the DNA differing by 4 % which may have been the result of experimental error.

Since the biisoquinoline ligands should be too large to intercalate, the complexes may be binding to the grooves of the DNA through electrostatic interactions provided by the metal centres withdrawing electron density from the aromatic ligand structure. Coordinative binding is another possible binding mode for complexes **5** and **7** as their complex and complex+DNA spectra at 0 h do not match (*Fig. 3.3 - c and d*). The band which is suspected to be attributed to MLCT has been red shifted. The complexes which show the greatest UV-vis stabilisation are more likely to have bound more favourably to the ct-DNA. Once bound it is possible that they are protected from the effects of solvent degradation by the DNA. Complex **8** is already quite stable in solution therefore the presence of DNA changes the stability very little making it harder to determine whether the two species are interacting in solution. It is hoped that the complexes will act in a similar (or better) way in the presence of G-quadruplex forming DNA. Complexes which interact through end stacking with a G-quadruplex may be shielded from the effects of solvent degradation by the quadruplex loops. However, for this study, only ct-DNA was examined

which demonstrates that complexes **5**, **7** and **9** are potentially interacting with duplex DNA because their absorption loss decreases upon the addition of ct-DNA. It is also worth noting that ct-DNA is not solely made up of duplex sequences and therefore may have the ability to fold into quadruplexes and other structures in its single stranded regions. The stability seen in the complexes may arise from binding to other secondary structures rather than duplex type DNA alone.
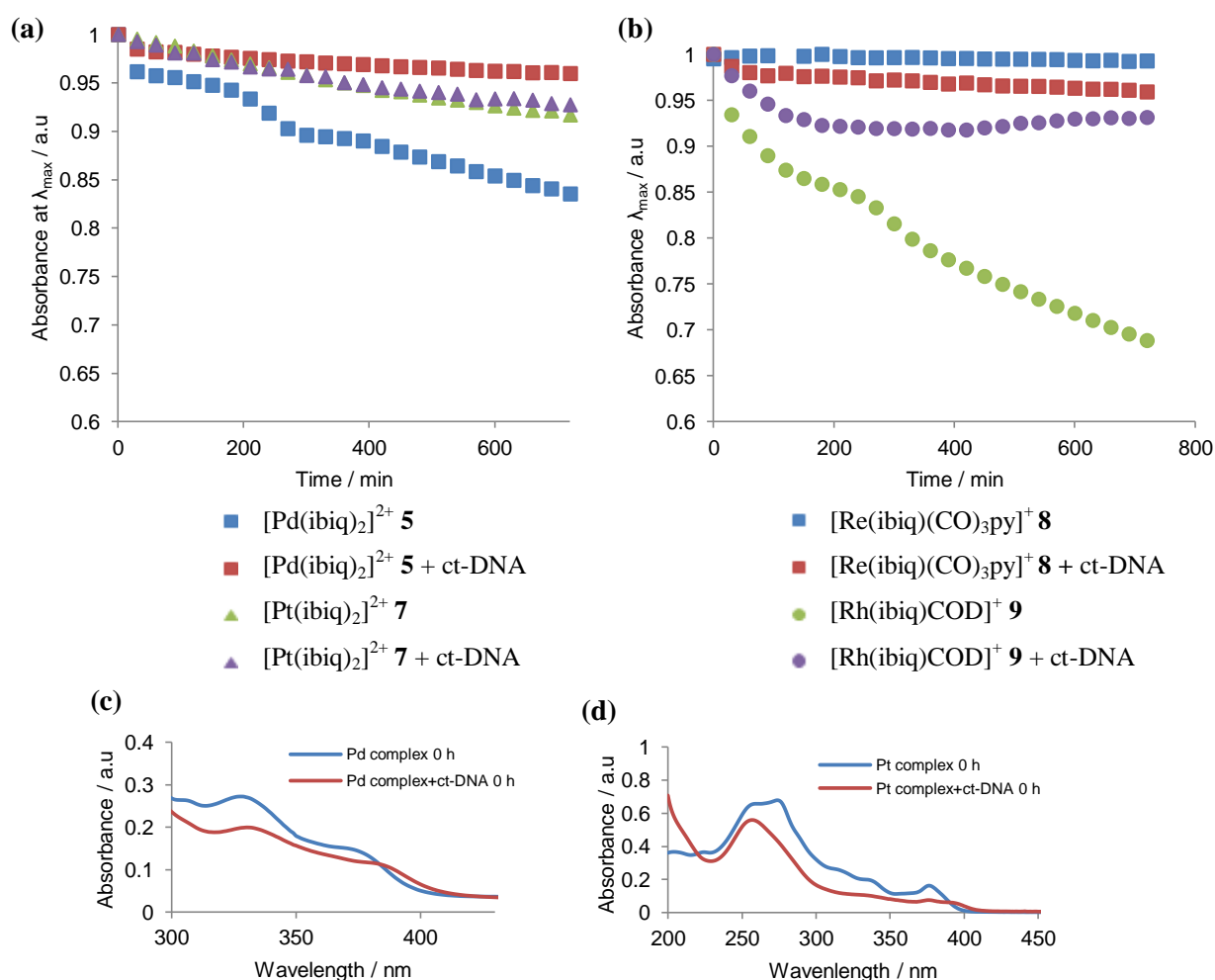
Figure 3.3 **a**. Normalised UV-Vis stability studies of complexes **5** and **7** at room temperature (10 uM, 15 % DMSO: H_2O) and the same complexes in the presence of ct-DNA in a 6:1 ratio DNA:complex (DNA buffer contains 6.7 mM NaCl and 0.33 mM $Na(CH_2)_2AsO_2.3H_2O$, 2.1 % DMSO: H_2O). **b**. Normalised UV-Vis stability studies of complexes **8** and **9** at room temperature (15% $MeOH:H_2O$ and H_2O only respectively) and in the presence of DNA in a 6:1 ratio DNA:complex (DNA buffer contains 6.7 mM NaCl and 0.33 mM $Na(CH_2)_2AsO_2.3H_2O$, 2.1 % MeOH: H_2O and H_2O only respectively) λ_{max} = 329 nm for $[Pd(ibiq)_2][BF_4]_2$, 378 nm for $[Pt(ibiq)_2][PF_6]_2$, 376 nm for $[Re(CO)_3(py)(ibiq)][CF_3SO_3]$ and 312 nm for $[Rh(ibiq)COD][Cl]$, **c**. Comparison of Pd complex and Pd complex+ct-DNA spectra at 0 h, **d**. Comparison of Pt complex and Pt complex+ct-DNA spectra at 0 h.

3.2 Circular Dichroism with complexes 5, 7, 8 and 9

Circular dichroism (CD) is a spectroscopic technique that can be used to probe the conformation of different types of DNA. The observed spectrum obtained from an experiment is generated by measuring the difference in absorbance between left (A_l) and right (A_r) circularly polarised light giving a CD signal expressed in degrees which is known as the ellipticity, θ.[3]

Circularly polarised light arises from superposition of oscillating horizontal and vertical polarised light (both linear).[4] The size of electric field vector remains constant but rotates in the form of a helix about the propagation direction (*Fig. 3.4*).[4] Whether left or right circularly polarised light is produced depends on whether the vector forms a left or right handed helix. The magnitude vector will be perpendicular to the electric field at any point in time and space.[4]
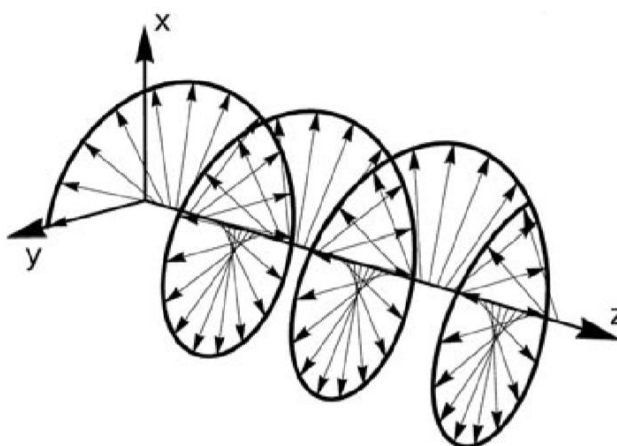
Figure 3.4 Left-circularly polarized light that is propagating in z-direction. The rotating electric field vector is represented by the small arrows. [Reproduced from Ref [5]]

128

Only molecules which are chiral can produce a CD spectrum. Non-chiral molecules can only be seen when they are interacting with the chiral molecule producing induced circular dichroism (ICD). Chiral molecules have non-superimposable mirror images and they do not have a plane of reflection therefore interact differently with left and right circularly polarised light.[4] The extinction coefficients for each type of circularly polarised light will be different and this difference is plotted against wavelength to give a CD spectrum.[4]

The relationship between left and right circularly polarised light is shown in the two equations that follow using the signal expressed in degrees (top) and molar extinction coefficients (bottom):

$$\mathbf{CD = A_l - A_r}\ [\theta]$$

$$\mathbf{\Delta\varepsilon = \varepsilon_l - \varepsilon_r}\ [M^{-1}\,cm^{-1}]$$

Chiral sugar units make up the sugar phosphate backbone in DNA. The DNA chirality is helical and produces a CD signal. The characteristic spectrum obtained for each sequence of DNA will be explained in the following subchapters; **3.2.1**, **3.2.2**, **3.2.3** and **3.2.4**. CD is a highly sensitive method that allows conformational transitions between complex nucleic acid arrangements to be followed during different experimental conditions.[6] Therefore quadruplex forming DNA will give a different spectrum to duplex DNA. Parallel and antiparallel quadruplex differentiation can also be achieved.[6] To assess whether the small percentage of solvent used in the experiments had any effect on the CD spectroscopy of the DNA, control experiments were carried out. The titrations were carried out normally except omitting the complex from the solvent solution. The controls showed that the small amount of solvent had no effect on the DNA (see appendix section 5 for DMSO controls).

3.2.1 ct-DNA and its Characteristic CD Spectrum

The characteristic CD signal for this type of DNA can be seen in *Fig. 3.5* between 200 - 300 nm. The bands produced in this region are fairly weak and arise from the transitions of purine and pyrimidine bases which are in a weakly chiral environment because of the base pairs being perpendicular to the double helix.[3]
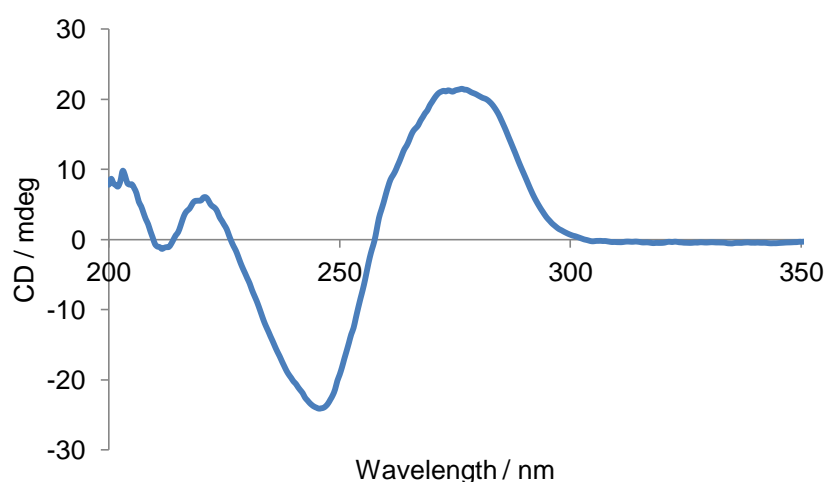
Figure 3.5 Characteristic CD spectrum of ct-DNA (B-DNA conformation) [300 μM, 1cm pathlength cuvette]

In the following titration experiments the concentration of ct-DNA is kept constant whilst an increasing amount of complex is added in order to see how it affects the observed CD spectrum. Any changes to the region 200 - 300 nm may indicate conformational changes in the DNA. If the complexes do bind to the DNA they may acquire some induced chirality from the environment causing the appearance of new CD bands, an effect called induced circular dichroism (ICD). Any new or changing CD bands can provide insight into how the complex is binding to the DNA. Alternatively, binding could induce chirality in the complex if it gets distorted.

3.2.1.1 CD Studies and Binding Constant Determination of 5, 7, 8 and 9

[Pd(ibiq)₂][BF₄]₂ - (5) - (see p176 for UV-vis)

The palladium complex was titrated into a solution of ct-DNA whilst monitoring and recording a CD spectrum after every addition of the complex. The complex generates very intense ICD bands in the MLCT region of the spectrum at 388 nm and 367 nm indicating that binding is occurring between the two species (*Fig. 3.6*). The peaks corresponding to the B-DNA configuration have not moved however they are now much more intense with the addition of the complex indicating complex-DNA interactions are present.

(a)   **(b)**
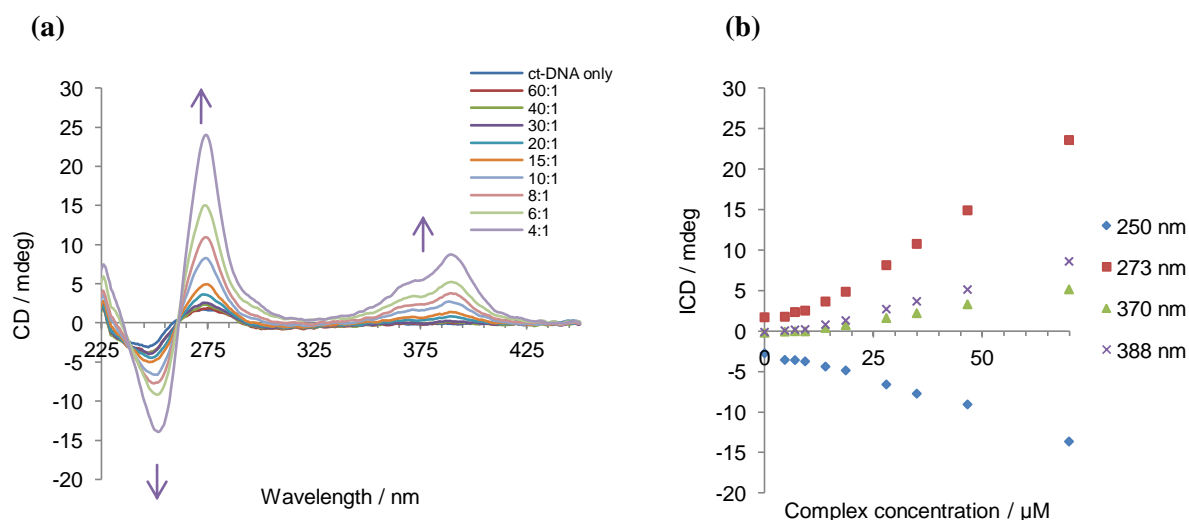
Figure 3.6 **a**. CD spectrum showing the titration of [Pd(ibiq)₂][BF₄]₂ in increasing concentrations to 300 µM ct-DNA (20 mM NaCl, 1 mM Na(CH₂)₂AsO₂.3H₂O, pH 6.8), 1 mm pathlength cuvette. Ratio of DNA:complex shown in the legend (right), **b**. ICD versus concentration of complex at selected λ_{max}.

[Pt(ibiq)₂][PF₆]₂ - (7) (see p178 for UV-vis)

The CD spectrum for the square planar platinum complex is similar to that shown by the palladium complex which is as expected due to the similarity between the two complexes. There are however more transitions occurring in the CD spectrum for the platinum complex (*Fig. 3.7*). The two complexes (**5** and **7**) both have isosbestic points, at 238 nm and 262 nm (Pd complex) and at 242 nm and 265 nm (Pt complex), that arise at relatively

low complex concentrations due to the unbound and bound species. It appears as though further isodichroic points at 297 nm and 317 nm can be seen in the platinum complex CD spectrum when the DNA:complex ratio rises above 8:1. This however is most likely due to the background noise of the CD experiment.[7][8]

Figure 3.7 **a**. CD spectrum showing the titration of [Pt(ibiq)$_2$][PF$_6$]$_2$ in increasing concentrations to 300 uM ct-DNA (20 mM NaCl, 1 mM Na(CH$_2$)$_2$AsO$_2$.3H$_2$O, pH 6.8) with a magnification of the region containing the isosbestic points at 297 nm and 317 nm, 1mm pathlength cuvette. Ratio of DNA:complex shown in the legend (right), **b**. ICD versus concentration of complex at selected λ_{max}.

The mode of binding cannot be determined from the CD spectra alone as groove binding and direct metal base interactions are both possible ways in which the complexes can bind to the ct-DNA. Both the platinum and palladium complexes have a bowed type crystal structure which is likely to put strain on the metal-nitrogen bonds (*Fig. 3.8*). This could be relieved when a ligand is lost from the metal centre and the metal binds instead to either

DNA bases (one or two), water or chloride. Intercalation should be prevented due to the large size of the ligand.
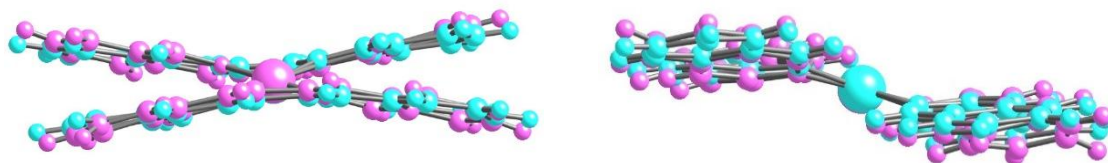
Figure 3.8 Bowed crystal structures of [Pt(ibiq)$_2$][PF$_6$]$_2$ (pink) and [Pd(ibiq)$_2$][BF$_4$]$_2$ (blue) overlaid .

[Re(CO)$_3$(py)(ibiq)][CF$_3$SO$_3$] - (8)

In this complex the 3,3-biisoquinoline ligand is no longer in a square planar environment and instead is part of an octahedral arrangement. The same titration experiment was conducted with the rhenium complex and ct-DNA to give the spectrum in *Fig. 3.9*.

(a) **(b)**
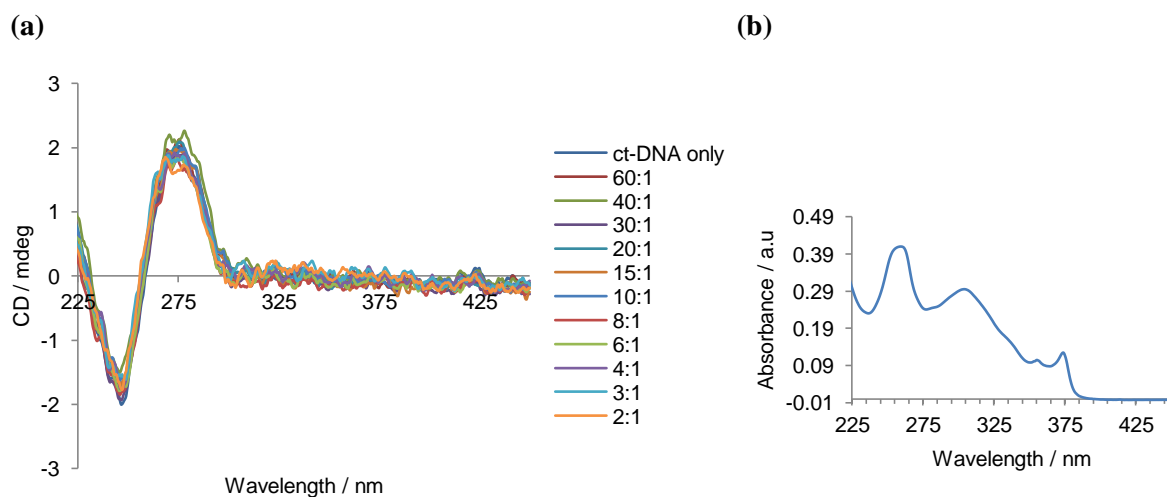
Figure 3.9 **a**. CD spectrum showing the titration of [Re(CO)$_3$(py)(ibiq)][CF$_3$SO$_3$] in increasing concentrations to 300 uM ct-DNA (20 mM NaCl, 1 mM Na(CH$_2$)$_2$AsO$_2$.3H$_2$O, pH 6.8), 1 mm pathlength cuvette. Ratio of DNA:complex shown in the legend (right), **b**. UV-vis spectrum of the [Re(CO)$_3$(py)(ibiq)][CF$_3$SO$_3$].

The spectra gave no evidence for an interaction of the complex with the ct-DNA as no induced circular dichroism peaks or changes in intensity of the DNA peaks could be seen. It seems in the octahedral arrangement the complex cannot groove bind or interact directly with the bases as it is most likely sterically hindered by the other ligands in the complex. Despite this lack of interaction the complex may have a preference for other types of DNA structure which may provide it with a degree of selectivity.

[Rh(COD)(ibiq)]Cl$_2$ - (9)

The CD spectrum obtained from the titration of the rhodium complex (**9**) into a ct-DNA solution clearly shows ICD peaks formed due the interaction between the two species (*Fig. 3.10*). The two ICD peaks at 344 nm and 386 nm may be due to MLCT transitions however the origin of the band at 262 nm is unclear as it could have been induced by the ligand or be the result of a change in DNA conformation.
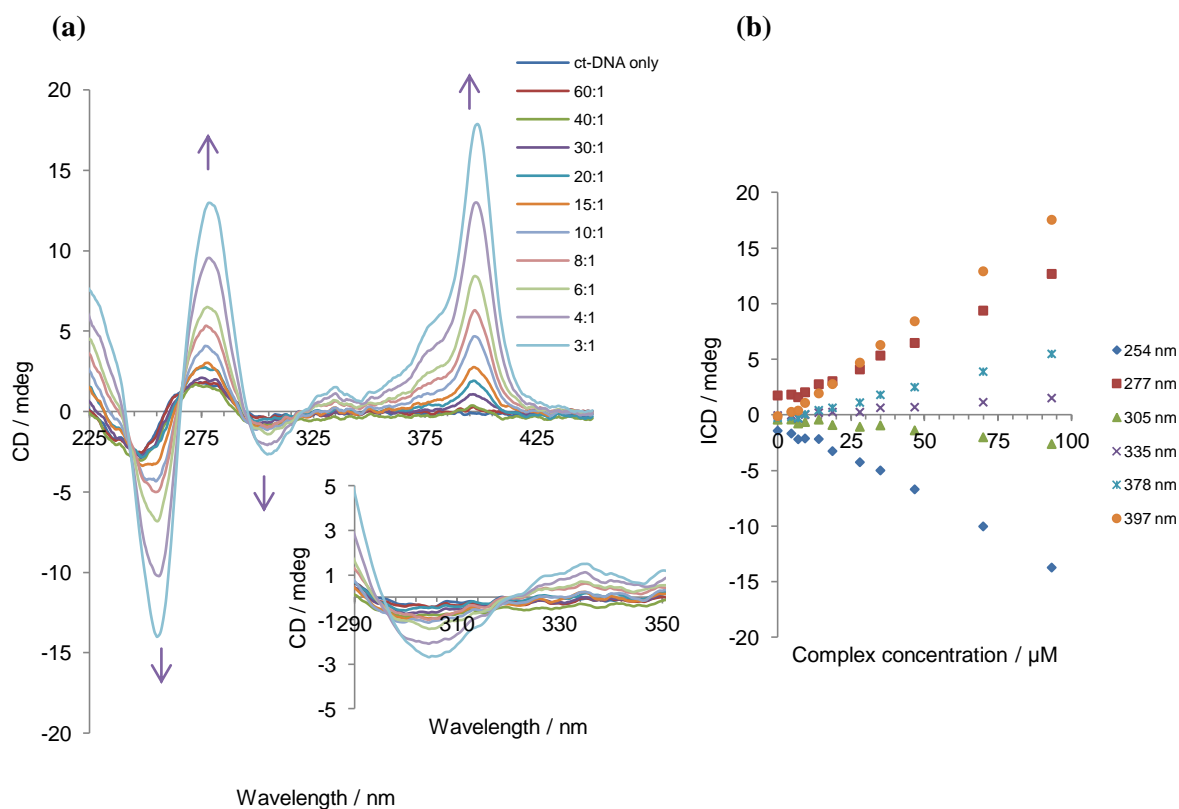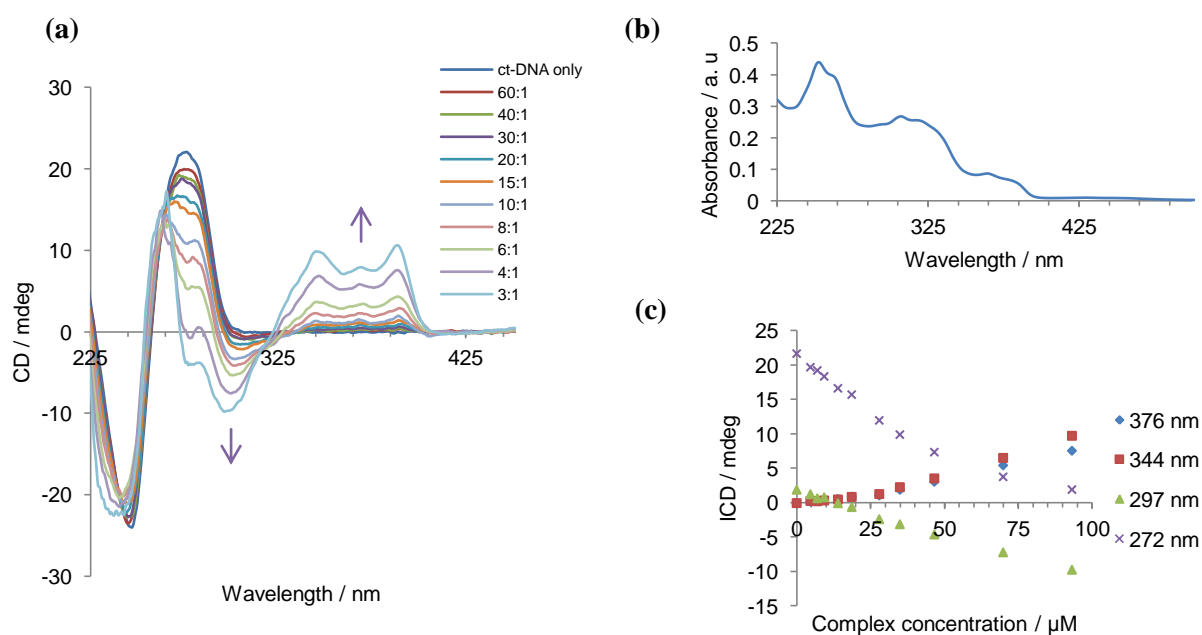

Figure 3.10 **a**. CD spectrum showing the titration of [Rh(COD)(ibiq)]Cl$_2$ in increasing concentrations to 300 μM ct-DNA (20 mM NaCl, 1 mM Na(CH$_2$)$_2$AsO$_2$.3H$_2$O, pH 6.8). Ratio of DNA:complex shown in the legend (right). 1 cm pathlength cuvette, **b**. UV-vis spectrum of [Rh(COD)(ibiq)]Cl$_2$, **c**. ICD versus concentration of DNA at selected λ$_{max}$.

A negative band can be seen at 297 nm, the knowledge of which when combined with the emergence of a band at 262 nm and the disappearance of the band at 272 nm suggests a B → Z conformational DNA transition. B to Z DNA transitions are usually associated with charge quenching and occurs through the groove or backbone. The phosphate groups are located closer in space in the Z conformation causing the destabilisation of the structure through negative repulsion (see *Figure 3.11* for Z-DNA CD spectrum).[9] Cations can shield the negative charges between the phosphate groups stabilising the structure.[9] A complex in the literature with this effect is $[Co(NH_3)_6]^{3+}$ which was studied by CD using poly[d(GC)] DNA.[10]
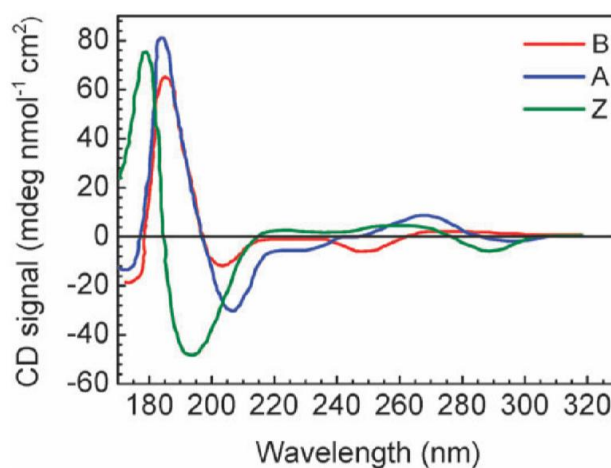
Figure 3.11 CD representation of B, A and Z forms of DNA [Reproduced from Ref [11]]

Binding Constant Determination

The data sets used for each of the binding constant determinations throughout the rest of this sub-chapter were reproducible, however the method of analysis was not therefore the binding constant results can only be given as estimates of binding.

The palladium complex ICD spectrum (*Fig. 3.12 - a*) shows the presence of one potential binding mode at low complex concentrations and another for higher complex

concentrations when comparing the peaks at 250 nm, 273 nm and 388 nm which all follow the same trend. It is possible that the low concentration measurements may not fit with the other data due to the small signal to noise ratio. The platinum complex shows ICD bands at 254 nm, 277 nm, 305 nm, 335 nm, 378 nm and 397 nm, which can be seen in *Fig. 3.12 - b*. Both ICD bands at 254 nm and 277 nm follow a similar trend to the palladium complex however the band at 397 nm shows more of a linear relationship at both low and high complex concentrations.
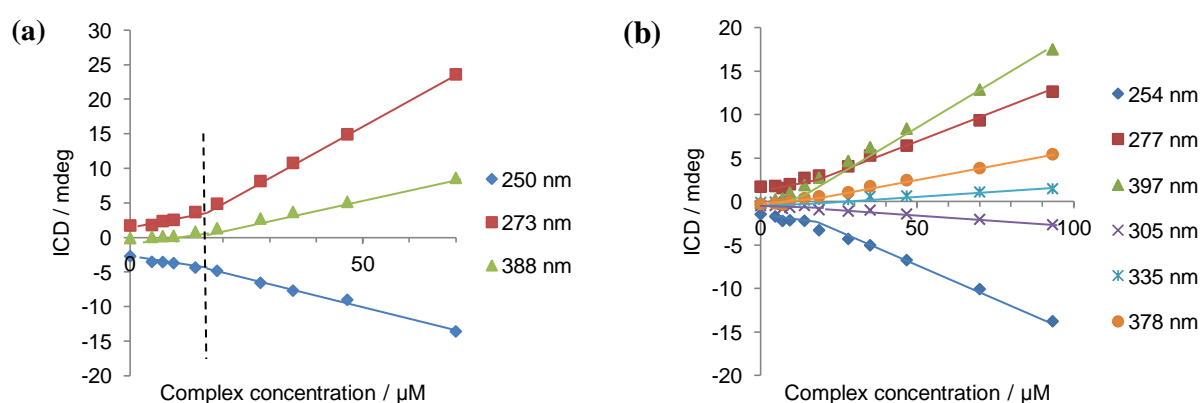
Figure 3.12 ICD of selected λ_{max} shown in the legend to the right of each chart in nm.
a. Palladium complex ICD comparison, **b**. Platinum complex ICD comparison.

The calculation of binding constants was attempted using the intrinsic method described by Rodger and Norden.[12] Generally the ICD signal is proportional to the number of complex molecules that bind to the DNA (if there is only one binding mode) therefore $c_b = \alpha r$ where c_b is the concentration of complex bound, α is the proportionality constant and r is the ICD response.[12] This relationship allows the equilibrium binding constant (K) to be calculated using the following equation where c_f is the free ligand concentration, S is the number of unfilled binding sites, c is [complex]$_{tot}$ and d is [DNA]/n (n = binding site size in bases). A Scatchard plot can be used to calculate the binding constant when binding is complete.[12]

$$K = \frac{c_b}{c_f . S} = \frac{\alpha r}{(c - \alpha r)(d - \alpha r)}$$

From the graphs presented in *Fig. 3.12* the total concentration of complex bound to DNA cannot be read from the graph as the binding curve is incomplete. The intrinsic method uses the difference between two different complex concentrations to calculate α and n which can then be used in a Scatchard plot to calculate K.[12] The equation used to plot the data for the intrinsic method is shown below (where the intercept = α and the gradient = [DNA]/nα and k and j represent all pairs of data points, C_m = [DNA] and L = [complex]):

$$\frac{L_{tot}^k - L_{tot}^j}{r^k - r^j} = \frac{C_m}{\alpha n}\left(\frac{\frac{L_{tot}^k}{r^k} - \frac{L_{tot}^j}{r^j}}{r^k - r^l}\right)$$

The results of the analysis for the palladium complex for both low concentration binding and higher complex concentrations are shown in *Fig. 3.13*. Using the intrinsic method described, no reliable results could be obtained from the two graphs. There are not enough data points for each of the graphs to be conclusive of a linear relationship between x and y. The plots also contain outlier points which further hinder the determination of the binding constant from the analysed data. When analysing the data as a whole and not splitting between high and low concentrations a random scatter of points emerged. The results abstracted from the intrinsic platinum complex graph also showed only a random scatter of points that could not be analysed any further, at any of the ICD wavelengths selected. An explanation for this could be that there are two modes of binding which are occupied at the

same time therefore each particular binding mode constant cannot be calculated. This may also be a possibility for the palladium complex.
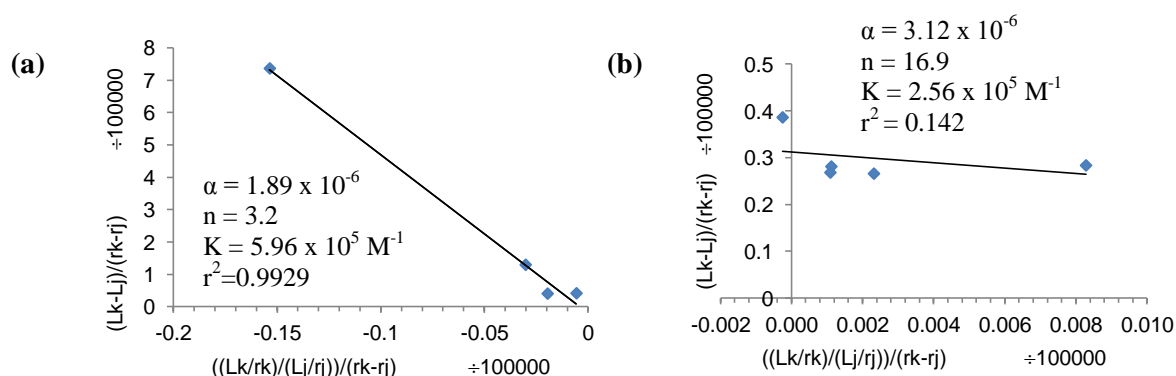
Figure 3.13 Palladium complex: **a**. Intrinsic method used for concentrations 0 μM to 9.3 μM, **b**. Intrinsic method used for concentrations 14.0 μM to 70.0 μM. Calculated for ICD at λ_{277}.

A plot of the rhodium complex ICD bands against concentration is shown in *Fig. 3.14*, where similar binding curves can be seen for the four ICD bands.
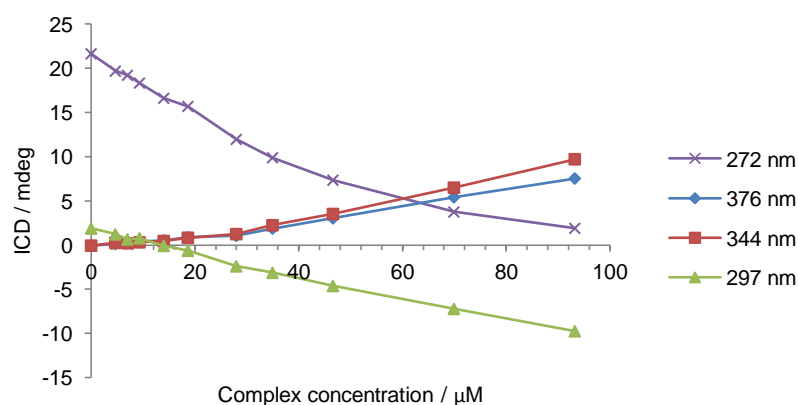
Figure 3.14 Rhodium complex ICD vs. concentration for selected λ_{max}.

Similar analysis using the intrinsic method for each λ_{max} yielded a random distribution of points therefore it is possible that the binding mode is not the same for all concentrations.[12]

3.2.2 ds26-DNA and its Characteristic CD Spectrum

This self complementary strand was chosen as a duplex type DNA control as it has a known sequence unlike the ct-DNA and it will also be used in FRET melting experiments as a competitor. The reason for this is because it has a melting temperature that is around 70°C which is higher than the labelled telomeric sequence (around 50°C) therefore the duplex will not unwind when the quadruplexes unfold (remains a competitor and is not single stranded).[2] It also does not affect the quadruplex forming DNA when the ligand investigated is omitted.

The CD spectrum generated for the ligand binding to ds26 will allow comparisons to be drawn between this system and that of the ct-DNA. A characteristic CD spectrum for the self-complementary ds26 oligo is shown in *Fig. 3.15*.
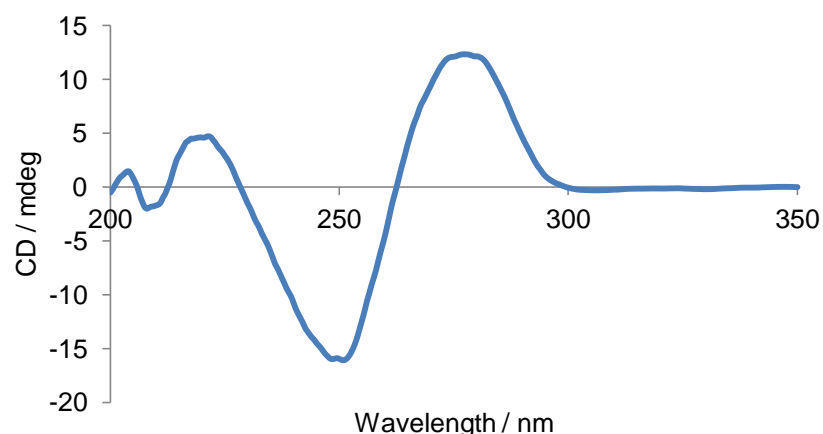
Figure 3.15 Characteristic CD spectrum of ds26 (B-DNA conformation) [300 μM] per base.

3.2.2.1 CD Study and Binding Constant Determination of 7

The platinum complex (**7**) previously tested with ct-DNA was unable to provide a binding constant due to the possible presence of more than one binding mode. In order to rule out

possible binding modes that may occur in various parts of the ct-DNA the same experiment was conducted with ds26 which has a defined structure. The resulting spectrum can be seen in *Fig. 3.16* where very clear ICD peaks can be seen at 397 nm, 332 nm and 306 nm; interestingly, the ICD is proportional to the concentration of the complex added (*Fig. 3.17 - a*).
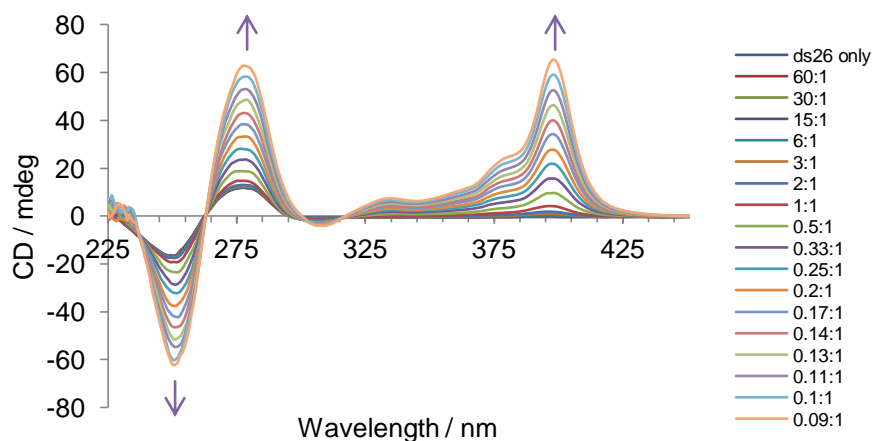
Figure 3.16 CD spectrum showing the titration of $[Pt(ibiq)_2][PF_6]_2$ in increasing concentrations to 300 μM (per base) ds26 (20 mM NaCl, 1 mM $Na(CH_2)_2AsO_2.3H_2O$, pH 6.8). Ratio of DNA:complex shown in the legend (right).

The intrinsic method combined with a Scatchard plot was used to calculate a binding constant for the ICD observed at $\lambda_{397\ nm}$. The first four points at the beginning of the titration were omitted due to the signal to noise ratio at such low concentrations of complex. The resulting binding constant calculated from the Scatchard plot was in the region of $10^5\ M^{-1}$ (*Fig. 3.17 - b*) with a value of n (6.25 bases or 3.13 base pairs).

(a) **(b)**
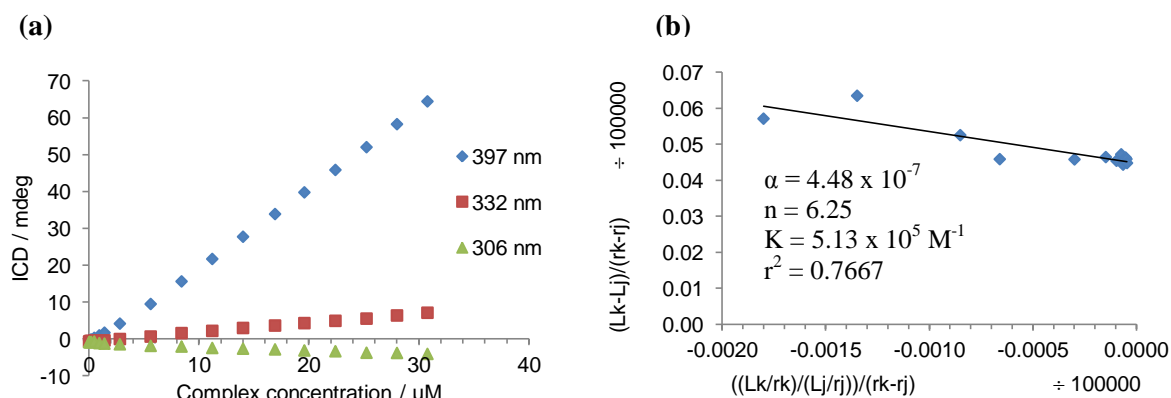
Figure 3.17 **a**. ICD plotted versus concentration for the $[Pt(ibiq)_2]^{2+}$ complex at λ_{max} 397, 332 and 306 nm, **b**. Platinum complex intrinsic plot produced from ICD generated with ds26 at λ_{397} for complex concentrations 0.9 μM to 28.0 μM.

3.2.3 Htelo DNA and its Characteristic CD Spectrum

The guanine rich strand of DNA that mimics the DNA found in the telomeric region of DNA, htelo, can exist in three different conformations depending on the type of cation present in the solution. Potassium and sodium cations are the correct size to be able to coordinate to the hole between the G-tetrads held in place by electrostatic interactions with eight O6 atoms lining the two planes of G-tetrads.[1] The sodium cations generally sit in the central cavity of the quartet while the potassium cations sit between the quartet layers.[1] The three types of structure seen using circular dichroism are shown in *Fig. 3.18*. Before measuring the CD response of the DNA in each cation condition, the DNA was annealed and left to cool slowly to room temperature before placing in a fridge overnight. The DNA preparation ensures that any quadruplexes formed have originated from the specific experimental conditions; the most thermodynamically stable structure would form during the slow cool and would not deteriorate overnight.

When in a potassium rich solution, a characteristic antiparallel hybrid spectrum is seen where the major peak observed at 295 nm originates from its antiparallel character and the smaller side peak at 265 nm represents its parallel nature (*Fig. 3.18*). There is also a small

amount of unfolded DNA represented by the peak at 253 nm. In a sodium rich solution a solely antiparallel conformation is found as now only a peak at 295 nm can be seen, the shoulder of the hybrid is no longer present (*Fig. 3.18*). In the third condition both potassium and sodium ions were omitted to see whether the quadruplex would fold in the absence of cations. There is now a new more defined peak at 253 nm which is due to the unfolded htelo DNA strand, however despite the lack of any cations there is still evidence of the quadruplex formation with the peak at 295 nm demonstrating the stability of the G-quadruplex structure (*Fig. 3.18*).
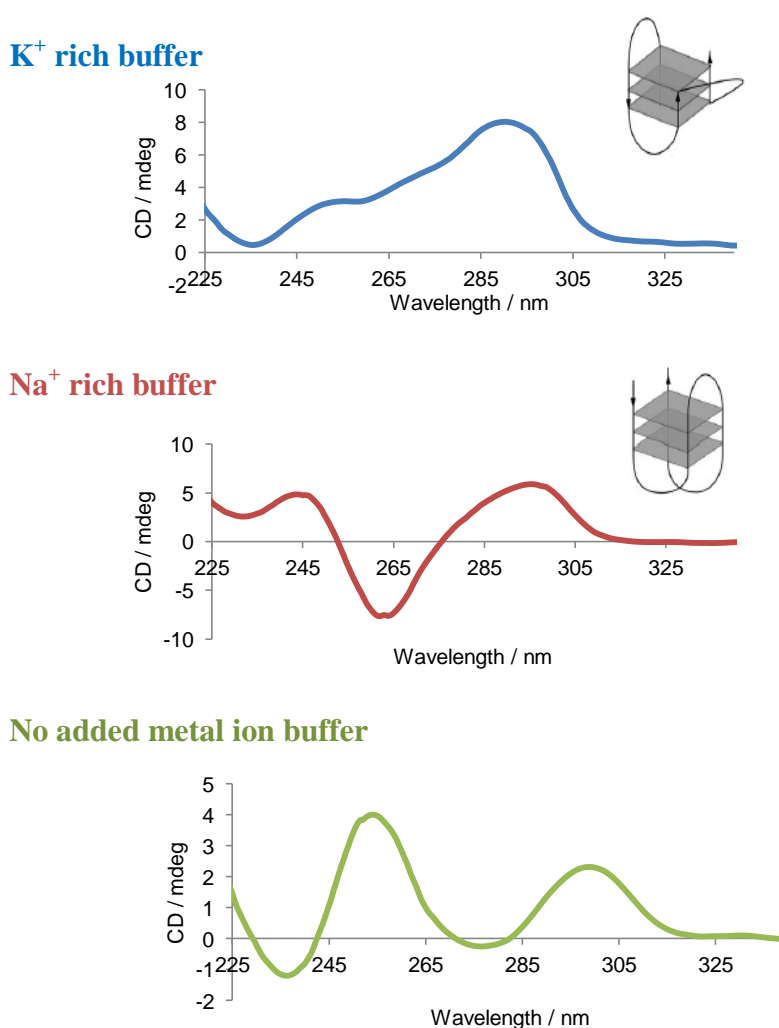
Figure 3.18 Characteristic CD spectra generated from a telomeric strand of DNA in a buffer which is K$^+$ rich, Na$^+$ rich and another without cations present. K$^+$ rich buffer: 3 μM htelo in 100 mM KCl, 10 mM Tris-HCl pH 7.4, Na$^+$ rich: 3 μM htelo DNA in 100 mM NaCl , 10 mM Tris-HCl pH 7.4, No metal ion buffer: 3 μM htelo in 10 mM Tris-HCl pH 7.4. Quadruplex structures where formed shown to the right. [Reproduced from Ref [1]]

All three conditions were used in the titration experiments conducted to investigate whether the initial conformation of the quadruplex in solution affected any potential binding of the platinum, palladium and rhenium complexes (**5**, **7** and **8**).

3.2.3.1 CD Studies and Binding Constant Determination of 5, 7 and 8

The circular dichroism experiment using htelo was conducted in the same way as the CD titrations with ct-DNA. The concentration, however, of DNA is recorded per strand rather than per base so as to give an indication of how many complex molecules bind per strand or quadruplex. In all of the following CD experiments the concentration of DNA (per strand) used was 3 μM.

[Pd(ibiq)$_2$][BF$_4$]$_2$ - (5)

The binding of the palladium complex to the telomeric DNA was examined in K^+, Na^+ and no added metal ion solutions. An attempt was also made to determine a binding constant for each cation condition using the intrinsic method combined with a Scatchard plot (where the Scatchard plot could not be used alone) in order to compare results with those obtained for the duplex forms of DNA.

K^+ Buffer

When the titration is carried out in the potassium rich buffer (*Fig. 3.19 - a*) the addition of the complex to the telomeric DNA sees an ICD peak emerge at 388 nm indicating that binding is occurring between the two species as the complex alone showed no CD response. A peak also arises at 272 nm however its origin is unclear as it could be another ICD band from the complex masking the DNA peaks, or a change in conformation from an

antiparallel hybrid to a parallel quadruplex. The complex has had an effect on the DNA because the peak corresponding to the unfolded DNA strand is no longer present at 253 nm, therefore the complex is either promoting the formation of the antiparallel hybrid (the response of which is hidden by the intense ICD peaks) or forming the parallel quadruplex conformer. The existence of a constant shoulder at 295 nm indicates that the former is occurring.

Figure 3.19 **a**. CD spectrum showing the titration of [Pd(ibiq)$_2$][BF$_4$]$_2$ in increasing concentrations to 3 μM (per strand) htelo (100 mM KCl, 10 mM Tris-HCl, pH 7.4). Ratio of DNA:complex shown in the legend (right). **b**. ICD plotted versus concentration of the palladium complex at λ_{max} 388, 272 and 250 nm, **c.** Palladium complex intrinsic plot (blue) produced from ICD generated with htelo at λ_{388} for complex concentrations 2.1 μM to 10.5 μM, red and green plots represent further attempts that did not show linear relationship.

Examination of the ICD peaks for this system (*Fig. 3.19 - b*) shows that at low complex concentrations a different binding mode may be occurring as the ICD at each wavelength is

not directionally proportional to the concentration. The higher concentration levelling off of the graph could be explained by the possible complete binding of the complex to the DNA followed by the precipitation of the DNA/complex as the concentration further increases (results in the ICD intensity decreasing). Despite this the Scatchard plot alone was not able to yield a satisfactory relationship between ICD and concentration. Reading from the ICD chart the point of complete binding occurs at a complex concentration of ~12 μM indicating a 4:1 complex:DNA binding mode (DNA concentration 3 μM). This however would only be the case if all the complex added was in a bound state with the DNA. The high ratio of complex observed may be a result of the square planar nature of the complex which may stack upon itself whilst bound to the quadruplex.

A binding constant in the region of 2.3×10^6 M^{-1} was calculated for the titration using the ratios of complex:DNA; 1:1, 2:1, 3:1, 4:1 and 5:1 (*Fig. 3.19 - c*). The lower and higher ratios did not fit with the data and yielded randomly scattered points. An error could not be calculated as the three repeats of the experiment did not yield decipherable data when examined by both the Scatchard and intrinsic methods. The value of n when converted to bases becomes 5.5 which correlates closely with the four guanines which are part of the top face of a G-quadruplex.

Na^+ Buffer

When the titration was then conducted in a sodium rich buffer the same ICD peaks appeared upon increasing concentrations of the complex (*Fig. 3.20 - a*). The peak at 388 nm is likely to have arisen from MLCT interactions and the peak at 272 nm shows the same behaviour as that of the potassium rich buffer. Again it is not possible to conclude

whether the peak at 272 nm is due to an overlapping complex ICD peak or a change of conformation from antiparallel to parallel.

A plot of ICD against concentration for the peaks at 388 nm and 272 nm shows that as complex concentration increases above 12 µM no change in the ICD signal occurs. This indicates that at this concentration the complex has saturated the DNA (*Fig. 3.20 - b*). The complex appears to bind in a similar way to both conformations of quadruplex resulting in the same final CD spectrum for both.

Using the ICD at λ_{max} 388 nm the intrinsic and Scatchard methods were used to try to calculate a binding constant for the palladium complex binding htelo DNA in a sodium rich buffer. Despite using the same ratios as the potassium rich buffer experiment omitting the lowest and highest complex concentrations no result could be obtained from the intrinsic method as only a random scatter of points originated from the calculations. The binding of the complex to the two different quadruplex conformations therefore may be more different than first predicted from the matching CD spectra.
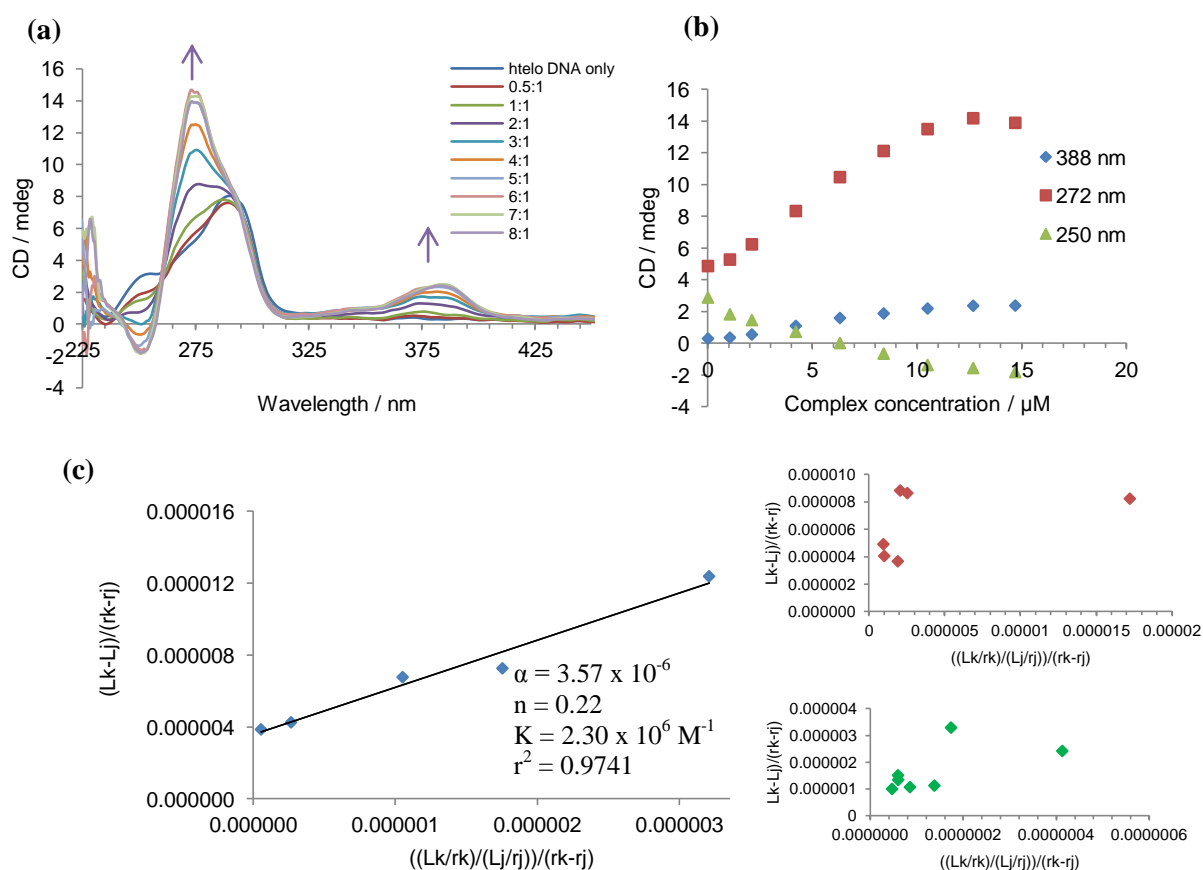

Figure 3.20 **a**. CD spectrum showing the titration of [Pd(ibiq)$_2$][BF$_4$]$_2$ in increasing concentrations to 3 µM (per strand) htelo (100 mM NaCl, 10 mM Tris-HCl, pH 7.4). Ratio of DNA:complex shown in the legend (right). **b**. ICD plotted versus concentration for the palladium complex at λ_{max} 388 and 272 nm.

No Added Metal Ions Present in the Buffer

Finally in order to see the effect on quadruplex formation without the electrostatic stabilisation of the cations the titration was carried out in 10 mM Tris-HCl buffer alone, without any additional cations. The initial spectrum, before the addition of any complex, shows the presence of mainly unfolded htelo DNA but also antiparallel quadruplex formation. Addition of the complex saw the decrease of the peak at 253 nm representing the unfolded DNA strand and the appearance of a peak at 388 nm due to ICD (*Fig. 3.21 - a*). A rapidly rising peak is also seen at 272 nm, the same peak seen in both the K^+ and Na^+ buffer conditions, that is likely to be an ICD peak overshadowing the DNA quadruplex conformational response.

An ICD comparison between the three λ_{max} 388 nm, 272 nm and 250 nm shows a linear increase to ~12 μM followed by a slight decrease in intensity as the concentration of complex increases further and the DNA begins to precipitate out of the solution (*Fig. 3.21 - b*).

Despite the intrinsic method yielding a straight line, after attempting to calculate a binding constant, when its result was used to calculate the binding constant using a Scatchard plot no linear relationship could be established (the Scatchard plot alone also yielded no useable results). Examining the CD spectra it appears that the shape of the quadruplex peak formed when no metal ions are present matches that of the peak formed in the sodium rich buffer which may be why both sets of results fail to produce a binding constant.
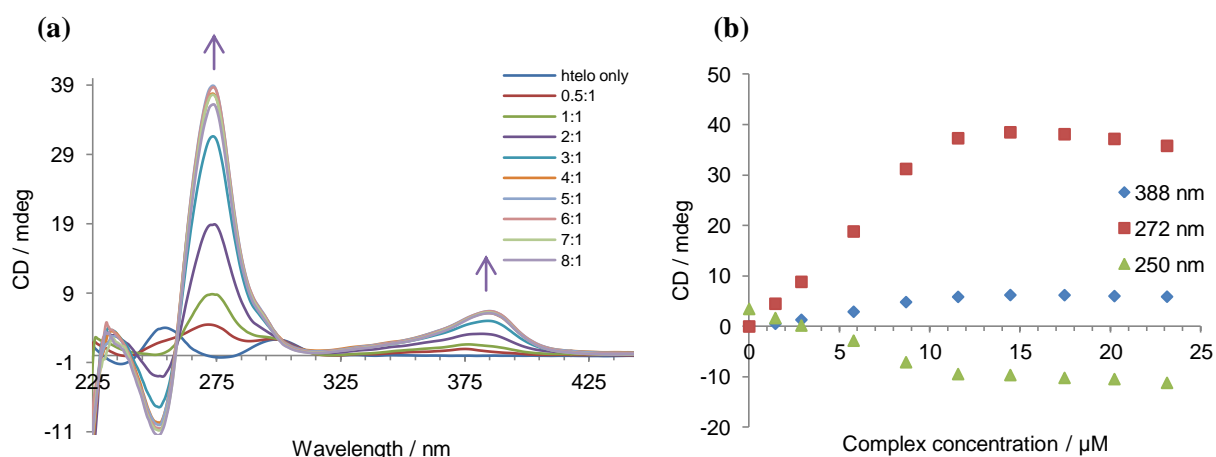
Figure 3.21 **a**. CD spectrum showing the titration of [Pd(ibiq)$_2$][BF$_4$]$_2$ in increasing concentrations to 3 μM (per strand) htelo (10 mM Tris-HCl, pH 7.4). Ratio of DNA:complex shown in the legend (right). **b**. ICD plotted versus concentration for the palladium complex at λ_{max} 388, 272 and 250 nm.

[Pt(ibiq)$_2$][PF$_6$]$_2$ - (7)

K^+ Buffer

When the titration is carried out in a potassium rich buffer the initial antiparallel hybrid CD peak of the DNA becomes dominated by the ICD peaks of the complex at relatively low concentrations of complex (*Fig. 3.22 - a*). The presence of the ICD peaks at 388 nm and 276 nm indicate that the complex is binding to the DNA.

When the ICD is plotted against the concentration for the peaks at 395 nm and 276 nm it is observed that they do not follow the same trend (*Fig. 3.21 – b*). The ICD at 276 nm peaks at 19 μM before starting to descend as the concentration increases further whereas the ICD at 395 nm continues to increase and only begins to start levelling off as the concentration of complex increases giving an approximate binding ratio of 10:1 (complex:DNA). Such a high binding ratio could be rationalised by the ability of the platinum complex to stack upon itself as with every titration addition the complex isn't solely binding to the DNA.

The ICD at 395 nm was chosen to calculate the binding constant as this alone is due to the complex binding however no linear relationship could be attained using the data.
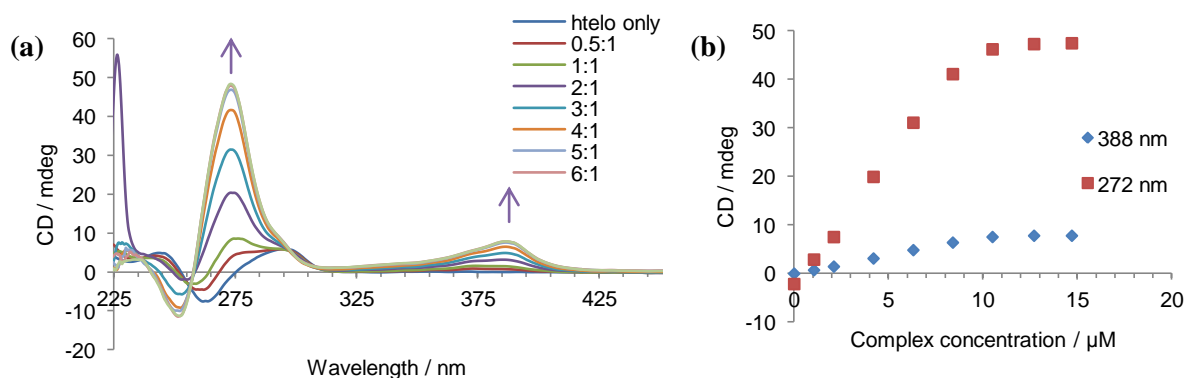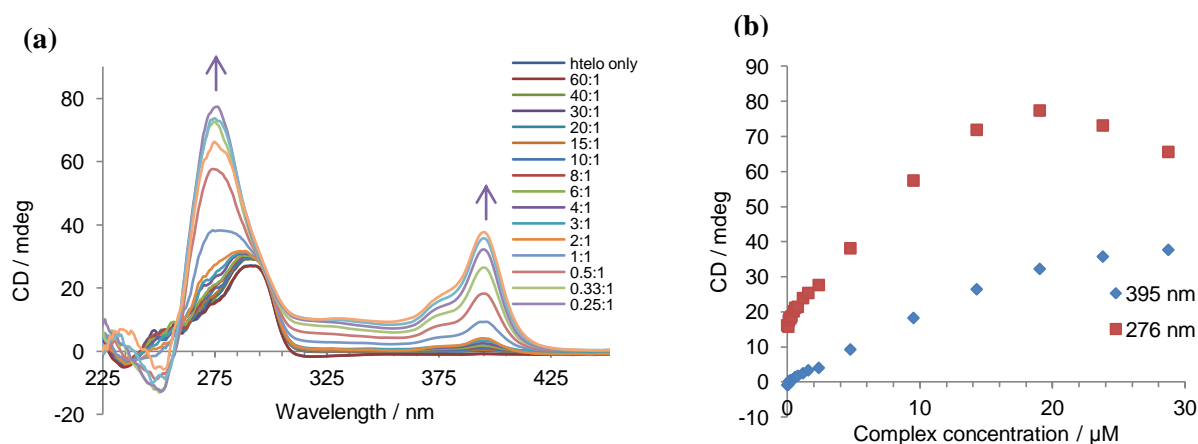

Figure 3.22 **a**. CD spectrum showing the titration of $[Pt(ibiq)_2][PF_6]_2$ in increasing concentrations to 3 μM (per strand) htelo (100 mM KCl, 10 mM Tris-HCl, pH 7.4). Ratio of DNA:complex shown in the legend (right). **b**. ICD plotted versus concentration for the platinum complex at λ_{max} 395 and 276 nm.

Na^+ Buffer

The sodium rich buffer with the initial antiparallel quadruplex conformer generated similar ICD peaks, as seen with the potassium rich buffer, at 395 nm and 272 nm (*Fig. 3.23*). A plot of the ICD versus the concentration gave the same result as the potassium buffer therefore once again no binding constant could be calculated.
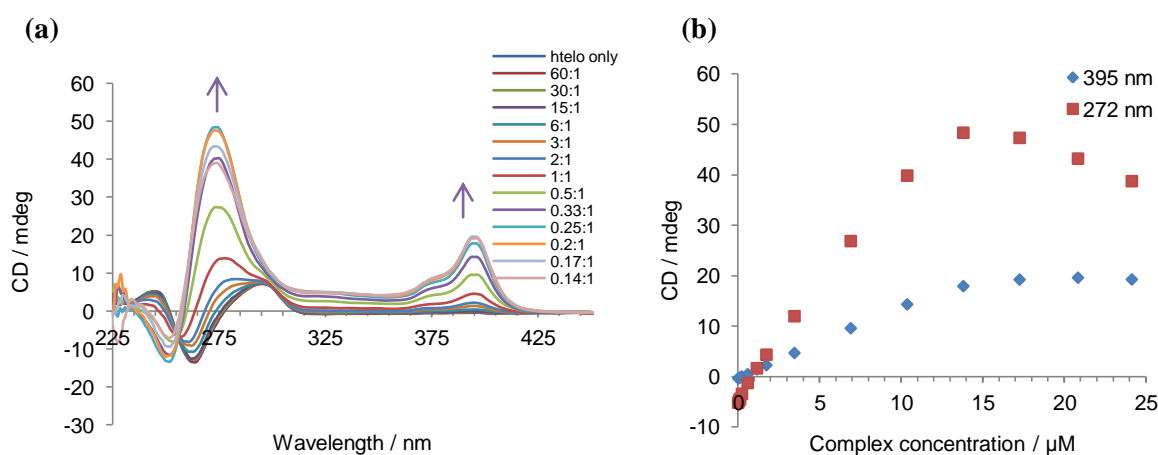
Figure 3.23 **a**. CD spectrum showing the titration of $[Pt(ibiq)_2][PF_6]_2$ in increasing concentrations to 3 μM (per strand) htelo (100 mM NaCl, 10 mM Tris-HCl, pH 7.4). Ratio of DNA:complex shown in the legend (right). **b**. ICD plotted versus concentration for the platinum complex at λ_{max} 395 and 272 nm.

No Added Metal Ions Present in the Buffer

In the absence of both potassium and sodium there is a definite transformation of the DNA as before the addition of any complex the majority of the telomeric DNA is unfolded however the peak corresponding to the unfolded strand is no longer apparent when the complex is added (*Fig. 3.24*). This indicates that the complex is changing the conformation of the DNA; the actual structure formed however is still hidden by intense ICD peaks that form in the same region. The ICD peaks have been compared at 395 nm and 272 nm against the concentration giving a similar result to the other two buffer conditions. The only difference is that the ICD at 272 nm does not start to decrease at very high concentrations of complex.

(a)

(b)
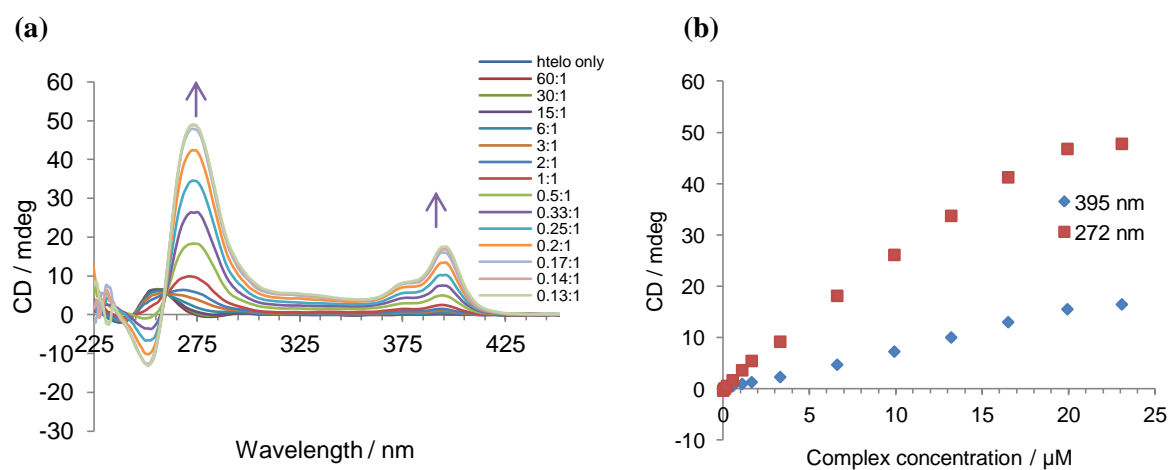
Figure 3.24 **a**. CD spectrum showing the titration of $[Pt(ibiq)_2][PF_6]_2$ in increasing concentrations to 3 μM (per strand) htelo (10 mM Tris-HCl, pH 7.4). Ratio of DNA:complex shown in the legend (right). **b**. ICD plotted versus concentration for the platinum complex at λ_{max} 395 and 272 nm.

For the htelo DNA strand it appears that the ICD peaks generated by both the palladium and platinum complexes remain the same for all types of buffer used. The majority of the titrations yielded no binding constant which indicates that there is no single binding mode in operation.[12]

Evidence in the literature has shown that the potassium cation is preferred due to the relative energies of hydration therefore under cellular conditions it is most likely that the telomeric DNA adopts the quadruplex conformation observed in the potassium cation solution.[13] It is also worth noting computational analysis results (using cation positions suggested by the crystal structure) reported by Jiande Gu and Jerzy Leszczynskiof suggest that the G-tetrads have a slightly distorted structure when optimising the bond distances between the potassium cation and the O_6 atom from the guanine bases (*Fig. 3.25*).[13] The slightly distorted nature of the platinum and palladium complex may make them an ideal fit for the top of a G-tetrad and may be how the complexes are binding to the telomeric DNA indicated by the strong ICD peaks in titration experiments.

*Figure 3.2*5 Side view of a slightly distorted G-tetrad and a potassium cation in its optimal position between O_6 atoms of the guanine bases. [Reproduced from Ref [13]]

[Re(CO)$_3$(py)(ibiq)][CF$_3$SO$_3$] - (8)

K$^+$ Buffer and No Metal Ion Buffer

The rhenium complex did not show any interaction with the telomeric DNA as seen in *Fig. 3.26*, just as it showed no interaction with the ct-DNA. The titration carried out in potassium rich buffer shows the antiparallel hybrid quadruplex which doesn't change upon titration of the complex. When the titration is carried out without the potassium (or sodium) the mostly unfolded htelo DNA remains in its unfolded state.

(a)

(b)
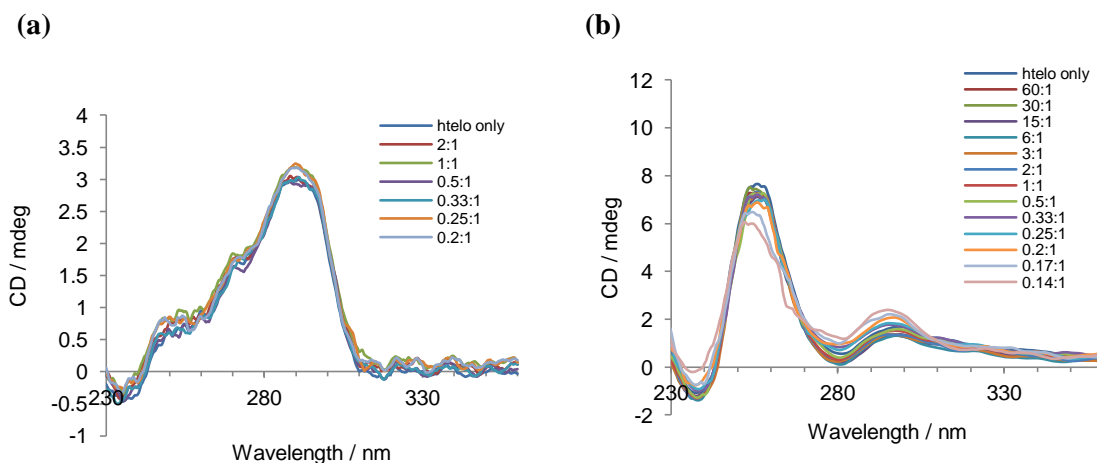
Figure 3.26 **a**. CD spectrum showing the titration of [Re(CO)$_3$(py)(ibiq)][CF$_3$SO$_3$] in increasing concentrations to 3 µM (per strand) htelo (100 mM KCl, 10 mM Tris-HCl, pH 7.4).   **b**. CD spectrum showing the titration of [Re(CO)$_3$(py)(ibiq)][CF$_3$SO$_3$] in increasing concentrations to 3 µM (per strand) htelo (10 mM Tris-HCl, pH 7.4). For both ratio of DNA:complex shown in the legend (right).

3.2.4 C-myc DNA and its Characteristic CD Spectrum

Another example of a guanine rich DNA sequence that has the potential to fold into a G-quadruplex is found in the promoter region of the c-myc gene. The base sequence differs to that found in the telomeric region and as a consequence has different loops that link the G-quartet layers resulting in the formation of a parallel conformer. When the structure of the G-quadruplex formed from the c-myc DNA strand was investigated in different cation buffers, the structure remained the same for all three conditions (K$^+$ rich, Na$^+$ rich and no metal cations present) imposed upon the DNA.

The characteristic CD spectrum of a parallel G-quadruplex is shown in *Fig. 3.27* where a peak can be seen at 265 nm. The spectrum differs from that of the anitparallel response because all of the guanines are now in an anti position about the glycosidic bond where in the antiparallel quadruplex both syn and anti guanine conformations were present.

152
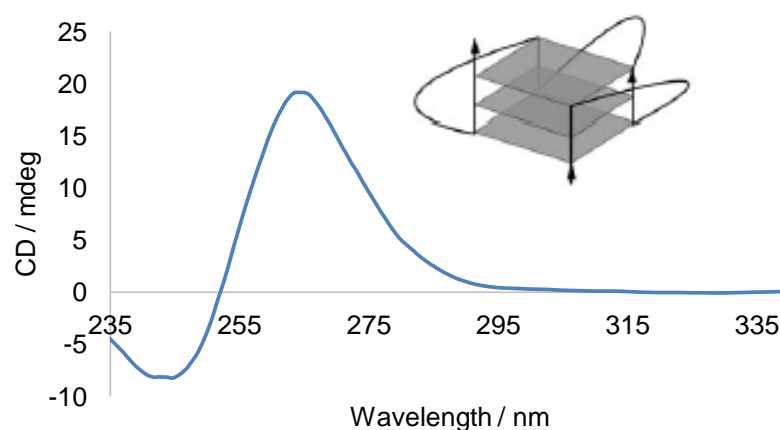
*Figure 3.2*7 CD spectrum of c-myc alone after annealing and leaving overnight forming a parallel G-quadruplex conformer (3 μM (per strand) htelo in 100 mM KCl, 10 mMTris-HCl, pH 7.4).

3.2.4.1 CD Studies and Binding Constant Determination of 5 and 7

[Pd(ibiq)₂][BF₄]₂ - 5

K⁺, Na⁺ and No Cation Buffer Comparison

The CD spectra for c-myc DNA differ much more between the different buffer conditions than for the telomeric DNA. In the K^+ rich buffer a very small ICD peak can be seen at 374 nm, and at 265 nm there is a small decrease in intensity of the DNA peak (*Fig. 3.28*). Potential binding isn't as evident in this system which may be because of the different DNA structure formed by the c-myc DNA strand which is preventing the palladium complex from binding and inducing the same extent of circular dichroism.

An ICD peak at 380 nm is present at a slightly higher intensity (compared with the potassium buffer) when the titration is carried out in the sodium rich buffer however this can only be noticed at very high concentrations of complex.

The buffer without the potassium or sodium cation influence sees a CD spectrum which is more similar to those seen with the telomeric DNA with an ICD peak at 374 nm which red shifts at higher concentrations to 382 nm (*Fig. 3.28*). The other peak seen at 265 nm intensifies as the complex concentration increases and also shifts as the ICD of the complex begins to hide the DNA peak. A binding constant couldn't be calculated as the intrinsic method yielded only a random scatter of points.

The apparent binding in the absence of the cations indicates the importance they have on ligand quadruplex binding in the c-myc system. It is possible that the interaction between the palladium complex and the quadruplex DNA is not an end stacking one and the palladium is instead interacting with the quadruplex loops. The antiparallel loops maybe more accessible hence why binding is seen with the antiparallel hybrids and not the parallel conformer. A possible way the palladium complex could bind to the DNA bases is through coordinative bonding which may occur after the loss of one of the biisoquinoline ligands. Work reported by Teulade-Fichou has shown through mass spectrometry studies that palladium terpyridine chloride complexes predominantly interact with G-quadruplexes by direct co-ordination to the bases after hydrolysation.[14] Binding to the terminal G-quartets (N7 position) is hindered due to the stacking of the aromatic ligand and the presence of Hoogsteen hydrogen bonding therefore it is postulated that the complexes co-ordinate to the thymine bases linking the G-quartets.[14]
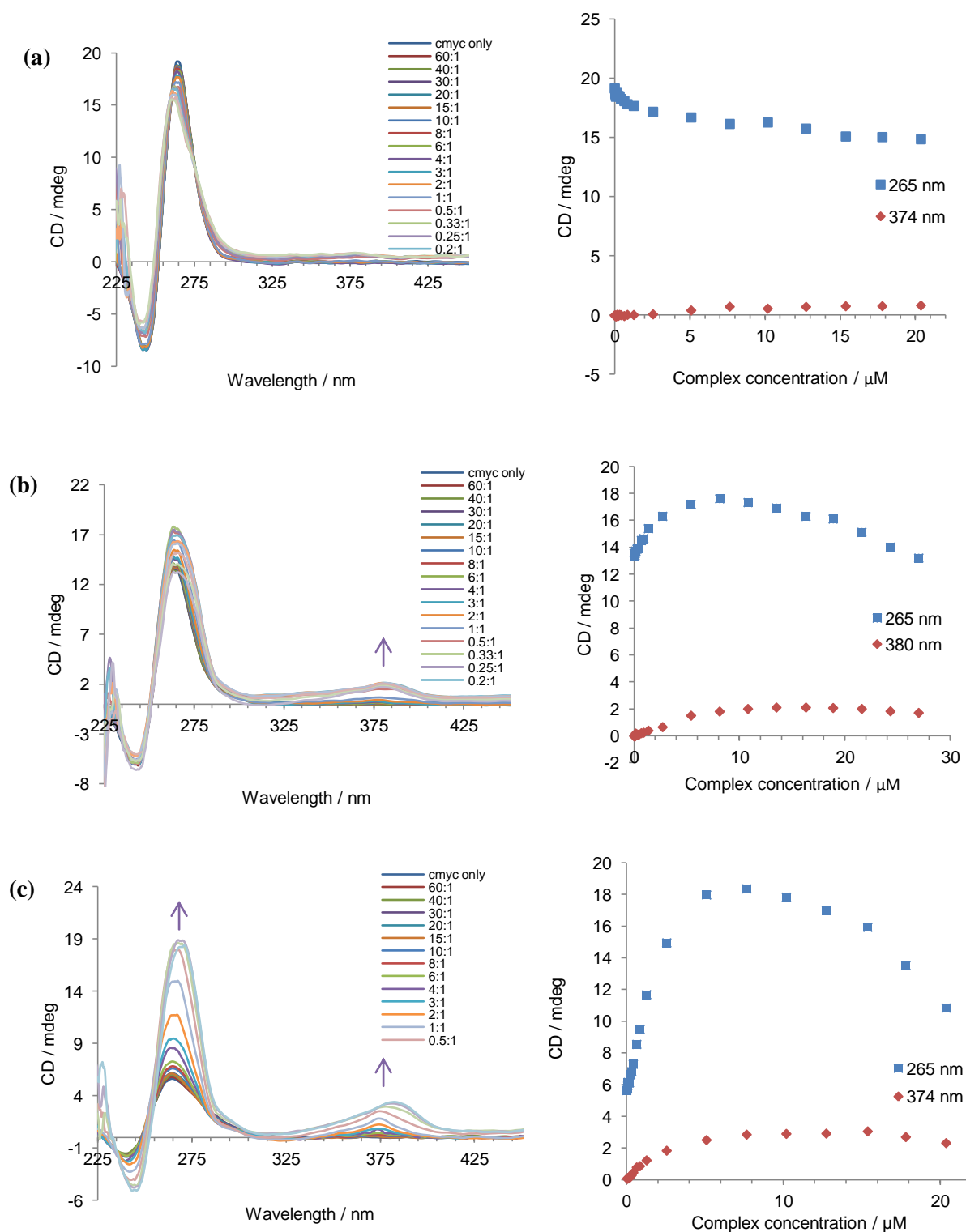
Figure 3.28 **a**. CD spectrum showing the titration of [Pd(ibiq)$_2$][BF$_4$]$_2$ in increasing concentrations to 3 μM (per strand) cmyc (100 mM KCl, 10 mM Tris-HCl, pH 7.4) and the corresponding ICD versus concentration. **b**. CD spectrum showing the titration of [Pd(ibiq)$_2$][BF$_4$]$_2$ in increasing concentrations to 3 μM (per strand) cmyc (100 mM NaCl, 10 mM Tris-HCl, pH 7.4) and the corresponding ICD versus concentration, **c**. CD spectrum showing the titration of [Pd(ibiq)$_2$][BF$_4$]$_2$ in increasing concentrations to 3 μM (per strand) cmyc (10 mM Tris-HCl, pH 7.4). pH 7.4) and the corresponding ICD versus concentration.

[Pt(ibiq)$_2$][PF$_6$]$_2$ - 7

K$^+$, Na$^+$ and No Cation Buffer Comparison

The CD spectra produced from the platinum complex titrations were unexpectedly very different from those obtained for the palladium complex despite the complexes being very similar in structure. In the potassium rich buffer where the palladium complex showed very little interaction with the c-myc DNA, the platinum complex produced many ICD peaks of high intensity, with both negative and positive peaks, at 405 nm, 353 nm and 300 nm (*Fig. 3.29 - a*). The DNA peak at 265 nm shifts to 260 nm before it loses intensity indicating that the structure of the DNA has changed. The negative ICD band at 300 nm is more unusual and hasn't been seen in any of the DNA-complex systems so far therefore its origin cannot be explained.

The CD spectrum obtained from the titration carried out in the sodium rich buffer doesn't contain any of the negative peaks that the complex produced when carrying out the titration in the potassium rich buffer. The DNA peak in this spectrum increases in intensity until it reaches the ratio 0.17:1 where the λ_{max} shifts from 265 nm to 268 nm and the intensity of the peak begins to decrease (*Fig. 3.29 - b*). The ICD peak at 396 nm follows the same trend with a red shift of 2 nm. It appears that when subjected to high concentrations of the complex in Na$^+$ rich buffer a new binding event occurs which causes the differences observed in the CD spectrum.

The CD spectrum of the titration carried out without either of the cations is particularly interesting as the whole CD signal reverses helicity (*Fig. 3.29 - c*). The final titration sees the CD trace as almost a mirror image of its former self at lower concentrations. The

presence of more than one binding mode is even more apparent for this system as the intensity of the ICD peak at 396 nm increases up to a ratio of 0.25:1 (DNA:complex) before the peak shifts to 400 nm and decreases in intensity. At the ratio of 0.14:1, as the peak begins to descend into the negative region of the spectrum, a new peak can be seen emerging at 392 nm.

Attempts at recording a binding constant using a Scatchard plot with and without the intrinsic method were unsuccessful and no results could be obtained for any of the CD experiments carried out with c-myc DNA.
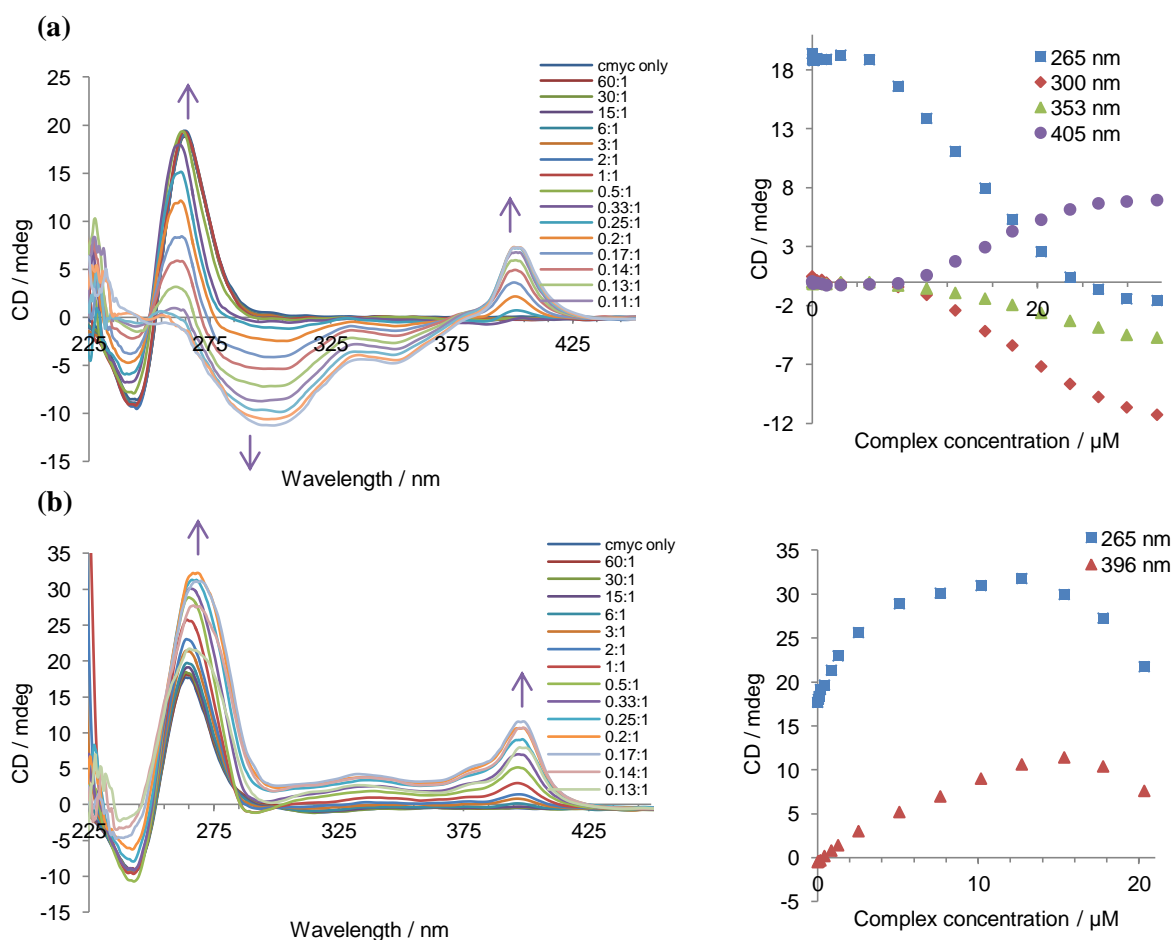
Figure 3.29 **a**. CD spectrum showing the titration of $[Pt(ibiq)_2][PF_6]_2$ in increasing concentrations to 3 μM (per strand) cmyc (100 mM KCl, 10 mM Tris-HCl, pH 7.4) and the corresponding ICD versus concentration **b**. CD spectrum showing the titration of $[Pt(ibiq)_2][PF_6]_2$ in increasing concentrations to 3 μM (per strand) cmyc (100 mM NaCl, 10 mM Tris-HCl, pH 7.4) and the corresponding ICD versus concentration.

(c)
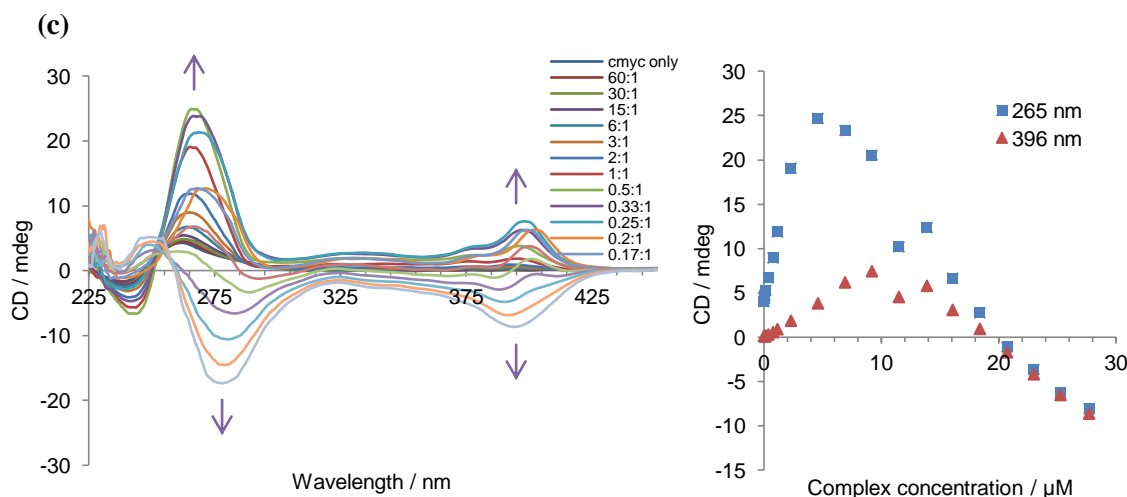
Figure 3.29 continued **c**. CD spectrum showing the titration of [Pt(ibiq)$_2$][PF$_6$]$_2$ in increasing concentrations to 3 μM (per strand) cmyc (10 mM Tris-HCl, pH 7.4) and the corresponding ICD versus concentration .

Both the palladium and platinum complex CD plots show that binding is occurring between the complexes and the htelo DNA with all spectra showing the same type of response to the binding event(s). This could be because of binding to the loops and/or end stacking to the antiparallel hybrid quadruplex structure (see *Fig. 3.30* for the different quadruplex structures all with differing loops).

With the c-myc DNA it is more apparent that different binding modes are occurring for each complex and the ability of the complex to end stack determines the CD response seen. The palladium complex shows very little induced chirality with the c-myc DNA when cations are present as the CD spectrum changes very little therefore it seems that it is no longer to bind to the DNA loops or the G-quartet surface whilst in the parallel conformation. It is possible that the main binding mode of the palladium complex is through direct metal-base binding which occurs after the loss of one of the biisoquinoline ligands. When the accessibility of the loops is restricted, binding does not occur. The

platinum complex on the other hand appears to be end stacking as the loop size has not affected its binding ability.
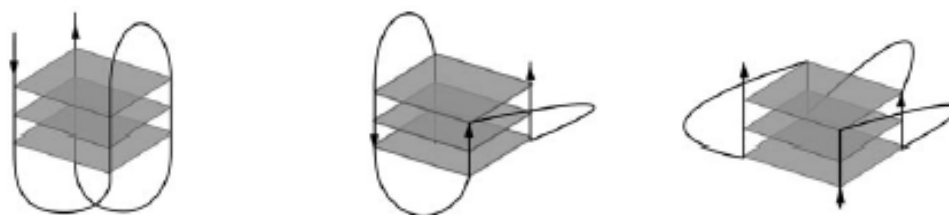
Figure 3.30 Possible loops that can form in a G-quadruplex structure. [Reproduced from Ref [1]]

3.2.5 Comparison of Binding Constants calculated from CD data

As most of the CD spectra produced were not able to produce a linear intrinsic relationship very few binding constants could be calculated. The spectra that did produce a linear relationship after applying the intrinsic method hinted that duplex DNA binding constants were around 10^5 M^{-1} and htelo binding constants around 10^6 M^{-1}.

3.3 Linear Dichroism

Linear dichroism or LD is the result of the difference in the absorbance of light linearly polarised parallel and perpendicular to an orientation axis at a specific wavelength.[15] It can be used to probe DNA conformations and drug-DNA interactions (DNA length permitting, >250 base pairs, as it has to be long enough to be oriented).[4][15]

$$LD(\lambda) = A_{par}(\lambda) - A_{per}(\lambda)$$

The LD signal is measured using a couette cell which orients the sample by viscous drag.[16]   This method of orienting the sample is called flow orientation and is advantageous for biological molecules such as DNA as they need to be hydrated.[16] The viscous drag is created when the DNA in solution is flowed between the narrow walls of the couette in a gap between a cylindrical cell that rotates and causes alignment within another which remains stationary (*Fig. 3.31*).[16] The two perpendicular beams will interact with the oriented DNA producing an LD spectrum.[16]
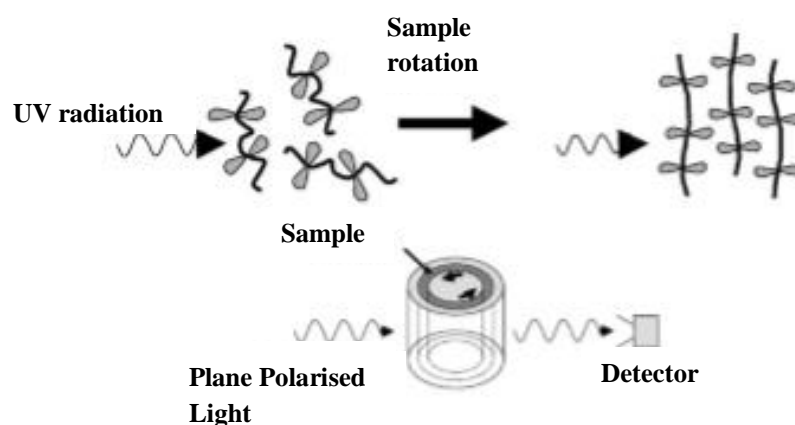
Figure 3.31 Representation of the process which occurs when DNA is placed in a couette and rotated, causing the DNA to align thus allowing a LD signal to be produced when subjected to plane polarised light. [Reproduced from Ref [16]]

Both positive and negative signals can be produced, the former occurring if the transition moment is aligned so that it is more parallel than perpendicular to the orientation axis and the latter if the same moment is less parallel and more perpendicular to the orientation axis.[16]

Generally DNA binding molecules on their own are too small to exhibit a LD signal as they cannot be oriented. They can however contribute to the LD spectrum when they

become oriented through binding to the DNA in a regular arrangement. Induced linear dichroism (ILD) peaks produced from ligand-DNA binding events can help deduce the type of binding occurring as the spectrum is a direct result of how the ligand is orientated with respect to the DNA.

3.4.1 ct-DNA and its Characteristic LD Spectrum

The LD spectrum produced from ct-DNA alone is shown in *Fig. 3.32*. The negative signal at 255 nm arises because of the orientation of the DNA bases with respect to the helix axis. The DNA bases are perpendicular to the helix axis (also the transitions of the bases) therefore the transition moment of the bases is more perpendicular then parallel to the orientation axis hence giving a negative response (LD = A_{par}- A_{per}) .[15][16]
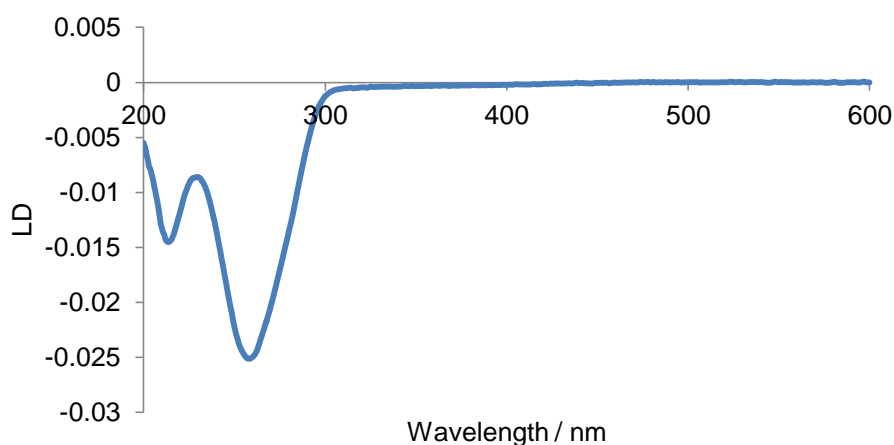
Figure 3.32 LD spectrum of ct-DNA (B-DNA) [300 µM].

In the following titration experiments the concentration of ct-DNA is kept constant whilst an increasing amount of the complex is added in order to see how it affects the observed LD spectrum. Control titrations carried out using a solution of 65% acetonitrile without the complex showed no effect on the DNA. Changes in intensity to the region 200 - 300

nm may indicate kinking or coiling of the DNA. LD peaks that form at longer wavelengths are due to ligand binding and will be oriented in a particular way to the DNA helix.

LD studies using the htelo and c-myc strands of DNA cannot be used as they are not long enough to orient therefore the results reported are for the complexes interaction with ct-DNA only. Solvents such as DMSO could not be used in the couette (because of its construction) therefore the complexes had to be dissolved in acetonitrile (unable to dissolve the complexes in other solvents). Despite the platinum complexes solubility in acetonitrile, when diluted with water the complex was quick to precipitate out even at the highest percentage of acetonitrile permissible for use in the couette. This lack of solubility prevented the examination of the platinum complex (**7**) using LD.

3.2.1.1 LD Studies of 5 and 8

The biisoquinoline complexes used in the LD studies show no peaks in the LD spectrum alone as the complexes are too small to be oriented by the couette cell. Any ILD peaks therefore must be a result of the complex interacting with the oriented ct-DNA.

[Pd(ibiq)$_2$][BF$_4$]$_2$ - 5

When the palladium complex is titrated into the ct-DNA solution there is an initial decrease in the intensity of the LD band corresponding to the DNA at 255 nm which then remains constant up to a ratio of 8:1 (DNA:complex) with no corresponding ILD peaks. At this stage the LD spectrum provides no evidence to indicate that regular complex binding is occurring (*Fig. 3.33*). The complex may be binding but in a random way

162

causing the sum of many different orientations that do not result in a LD peak. As the complex concentration increases from a DNA:complex ratio of 6:1 (44.3 μM) to 3:1 (88.3 μM) an ILD peak is seen at 350 nm and the DNA LD peak at 255 increases in intensity. This indicates that at high concentrations of complex a binding event occurs which is regular enough to produce a peak in the spectrum. The negative sign of the ILD peak produced suggests that the complex is binding by intercalation (binding perpendicularly to the helix orientation) if the absorption transition moment is polarised in the plane of the ligands. The increase in intensity of the DNA LD peak is also consistent with this because the result of intercalation is the lengthening or stiffening of the DNA as it becomes more orientated.[17] A possible explanation for this may be the insertion of an isoquinolyl unit, occurring at high complex concentrations. This however does not rule out coordination.
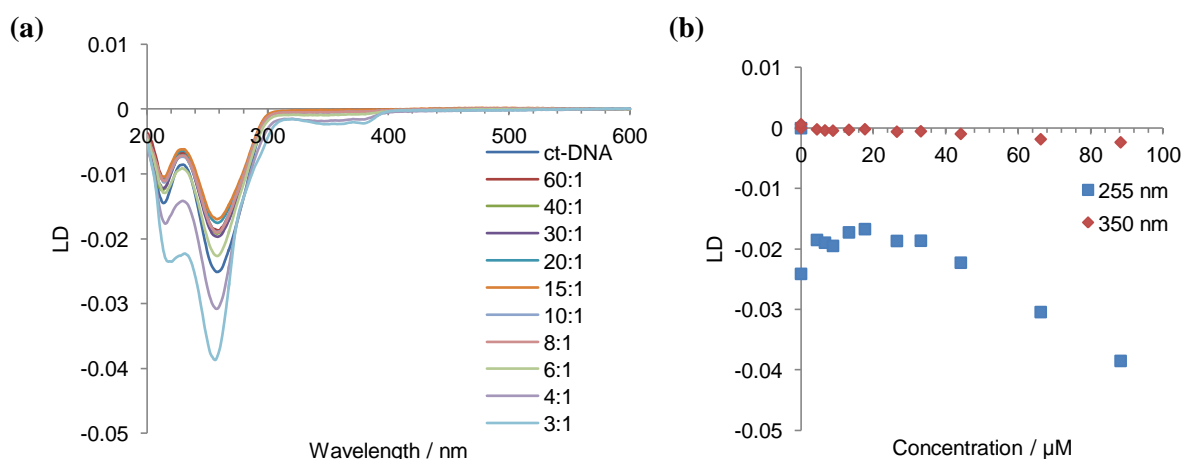
Figure 3.33 **a**. LD spectrum of 300 μM ct-DNA (B-DNA) in 20 mM NaCl and 1 mM Na(CH₂)₂AsO₂.3H₂O (pH 6.8) with the addition of increasing concentrations of [Pd(ibiq)₂][BF₄]₂. Legend to the right shows the ct-DNA:complex ratios. **b**. ILD pattern generated from the complex titration.

[Re(CO)₃(py)(ibiq)][CF₃SO₃] - **8**
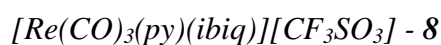
As with the CD analysis of the rhenium complex very little is seen in the LD spectrum (*Fig. 3.34*). There is a slight decrease in the intensity of the DNA peak at 256 nm when the

first titration of complex occurs (40:1, DNA:complex) however as more and more complex is added the intensity remains the same suggesting that the initial small decrease in intensity may be due to the solvent effect. The complex also failed to induce any LD peaks suggesting that the complex does not bind to B-DNA.
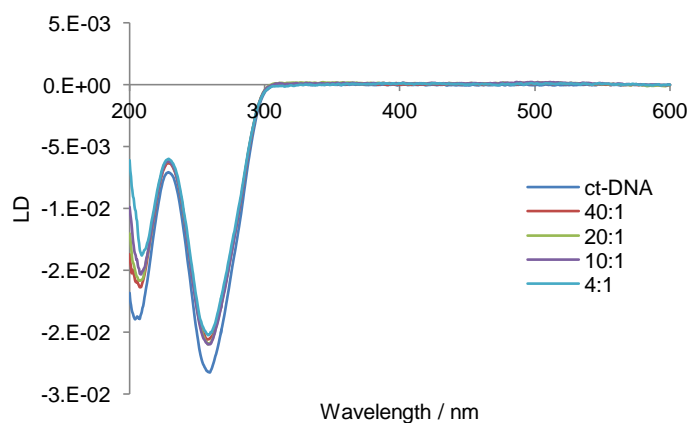
Figure 3.34 LD spectrum of 300 µM ct-DNA (B-DNA) in 20 mM NaCl and 1 mM Na(CH$_2$)$_2$AsO$_2$.3H$_2$O (pH 6.8) with the addition of increasing concentrations of [Re(CO)$_3$(py)(ibiq)][CF$_3$SO$_3$]. Legend to the right shows the ct-DNA:complex ratios.

3.4   Fluorescent Indicator Displacements with complexes 5 and 7

The G-quadruplex fluorescent indicator displacement protocol used by Marie-Paule Teulade-Fichou *et al* [18] is a quick and convenient way to assess the binding affinity of a ligand towards G-quadruplexes. The selectivity of the ligand for quadruplex over duplex DNA can also be investigated. The assay is monitored by the loss of fluorescence caused by the displacement of the dye thiazole orange by the ligand which occurs if the ligand has a stronger binding affinity to the DNA than the dye. Following the titration experiment the concentration at which the total fluorescence has decreased by 50% can then be calculated giving a corresponding DC$_{50}$ value.

Thiazole orange (*Fig. 3.35*) was chosen as the dye of choice because of its highly fluorescent nature when bound to DNA compared with its lack of fluorescence in solution. It has a binding affinity of 2 to 3×10^6 M^{-1} with both quadruplex and duplex DNA showing no selectivity for one structure over the other.[18] TO binds in an intercalative fashion to duplex DNA between base pairs whereas with G-quadruplexes it binds to a tetrad in a single site manner with the loops helping to play a part in its structural accommodation.[19][20] Htelo and c-myc quadruplex forming DNA strands were used to investigate how well the complex displaced the TO from a quadruplex structure and ds26 was used as the duplex comparison (ds12 and ds17 previously investigated by Teulade-Fichou demonstrating that duplex sequence length does not affect binding).[18]
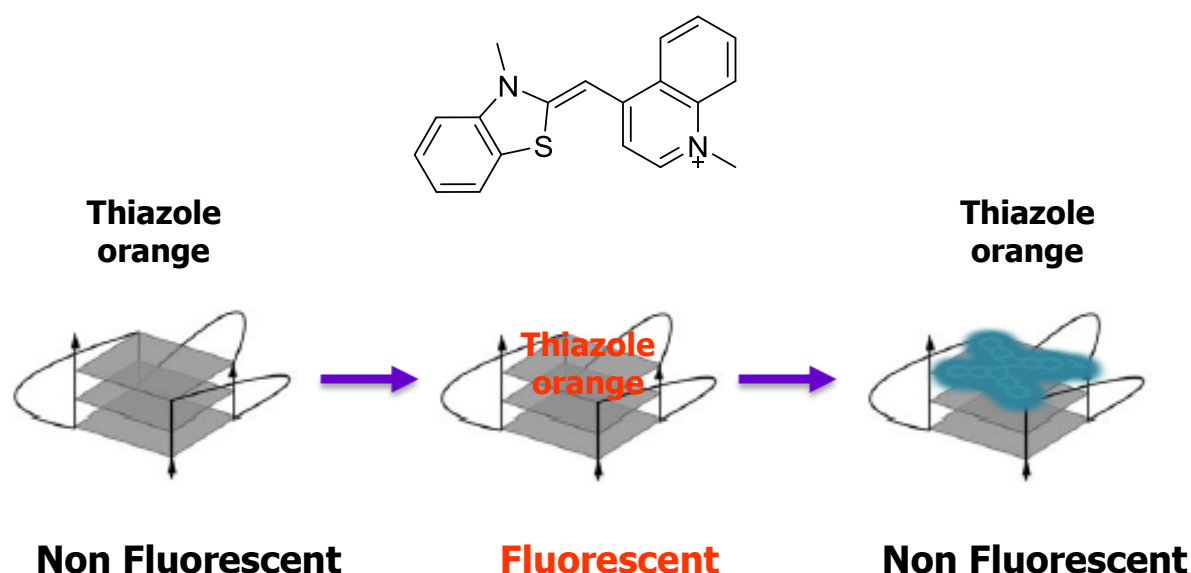
Figure 3.35 Above. Structure of the dye thiazole orange, Below. A schematic of how the ligand tested alters the fluorescence of the solution to indicate binding.

The number of thiazole orange dye molecules that can bind to each type of DNA investigated has also been reported by Teulade-Fichou using a combination of mass spectrometry and fluorescent titration techniques.[19] The mass spectrum corresponding to

the telomeric DNA system is shown in *Fig. 3.36* where the predominant DNA+TO peak is that of the 1:1 ratio.[18] Using the same techniques the ratio of TO and ds26 was found to be 2:1.[18] To achieve competitive displacement by the ligands the experimental ratios of TO:DNA were 2:1 for the telomeric DNA (also c-myc DNA) and 3:1 for the ds26 DNA.[18]
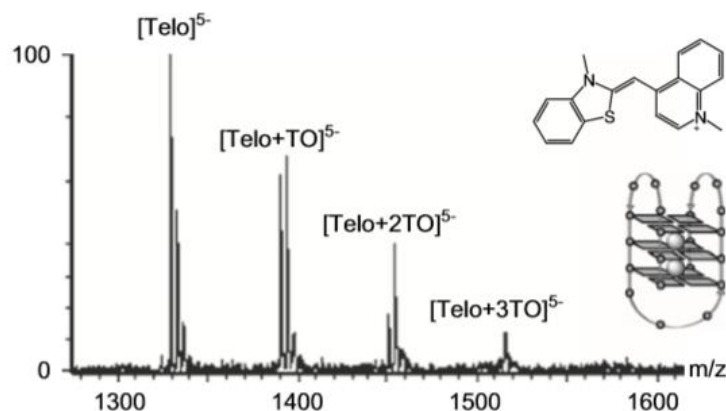
Figure 3.36 ESI-MS profile of the association of TO with htelo DNA obtained with 5 mM of DNA and 10 mM of TO, in 150 mM ammonium acetate, 15% MeOH. [Reproduced from Ref [18]]

The experiment can potentially provide information on the selectivity of the ibiq complexes for quadruplex over duplex DNA and also for one type of G-quadruplex structure over another. This is determined by the amount of complex that is required to reduce the fluorescence intensity of thiazole orange which is read after every titration (TO absorbs light at 501 nm and emits at 550 nm). The thiazole displacement can be calculated by working out the area of the initial emission curve (510 nm - 750 nm) with the DNA and TO only and taking away the fluorescence area of the curve after each time the complex is added. A DC_{50} value is read from the resulting chart which is the concentration at which the TO fluorescence has reduced by 50 %. Terpyridine and salphen complexes in the literature reported by Vilar *et al* have DC_{50} values ranging from 0.17 μM to > 2.5 μM.[14][21] Complexes that can be considered as 'good binders' must have a DC_{50} value that

does not exceed the 0.5 μM 'threshold' that has been established for this type of analysis.[22] The FID experiments were carried out in potassium rich buffer only as this most resembled physiological conditions. Solvent controls showed no decrease in fluorescence when titrated alone into a TO-DNA solution.

3.4.1 Titrations with htelo

When the palladium complex was titrated into the TO-DNA solution there was a significant decrease in the fluorescence on recording the emission spectrum. With subsequent additions of the complex the fluorescence decreased further and the 50 % displacement mark was reached at low levels of complex. The same was true of the platinum complex which had a very similar effect when titrated into the fluorescent mixture. In *Fig. 3.37* the decrease in fluorescence can be seen for the two complex titrations along with a comparison of the two complexes after calculating the percentage displacement after each addition of complex using the following equation (where FA is the fluorescence area and FA_0 is the fluorescence area of bound TO without added complex):

$$\% \, Displacement = 100 - [(FA\text{-}FA_0) \times 100]$$

Both complexes displace the TO initially to similar extents however as the concentration of the complexes increase the platinum complex is able to displace slightly more of the dye before reaching an equilibrium. The overall difference between the complexes is very much as to be expected after considering the CD results where both complexes showed similar spectra upon binding to the htelo DNA.

(a)

(b)

(c)

Figure 3.37 **a**. Emission spectrum for the palladium complex when titrated into 0.25 μM htelo DNA solution containing 100 mM KCl / 10 mM Na cacodylate + 0.5 μM TO, **b**. Emission spectrum for the platinum complex when titrated into 0.25 μM htelo DNA solution containing 100 mM KCl / 10 mM Na cacodylate + 0.5 μM TO. **c**. Percentage TO displacement comparison.

3.4.2 Titrations with c-myc

When the same titrations were carried out using the c-myc DNA strand more of a difference was noted between the palladium and platinum complex, and the decrease in fluorescence of the TO-DNA (*Fig. 3.38*). The platinum complex showed a similar result to the htelo DNA titration where at low concentrations of complex the fluorescence significantly decreased. This was not true for the palladium complex which was unable to displace the TO at such low concentrations indicating that the binding affinity of the

palladium complex towards the c-myc DNA quadruplex is less than that between the same type of DNA and the platinum complex. The CD spectra for the palladium complex with the c-myc DNA also showed a lack of interaction when compared with htelo DNA. The platinum complex on the other hand showed a strong yet different response (negative ICD peaks were now present) showing that there was a good interaction between itself and the c-myc DNA which is consistent with the FID data produced.

Figure 3.38 **a**. Emission spectrum for the palladium complex when titrated into 0.25 μM cmyc DNA solution containing 100 mM KCl / 10 mM Na cacodylate 0.5 μM TO, **b**. Emission spectrum for the platinum complex when titrated into 0.25 μM cmyc DNA solution containing 100 mM KCl / 10 mM Na Cacodylate 0.5 μM TO, **c**. Percentage TO displacement comparison.

3.4.3 Titrations with ds26

When the titrations were carried out with duplex DNA the emission signal decreased very little upon increasing amounts of complex (*Fig. 3.39 and 3.40*). Both of the complexes exhibited similar behaviour with much complex needed to reach the 50 % displacement concentration (the palladium complex failed to reach displacement concentration). The lack of displacement of the TO by the two complexes suggests they bind much more weakly to duplex DNA than the TO. However another explanation could be that the complex is binding to the duplex DNA without displacing the TO. The lack of binding is not reflective of the CD analysis of the complexes with B-DNA where very strong ICD signals are seen indicating the occurrence of binding events. After consideration of both sets of results it appears that the complexes will bind to duplex DNA if there are no competitors, as evidenced by the CD response. The binding affinity however is not high enough to be able displace another binder, like TO, leading to the lack of displacement seen in the FID experiments.
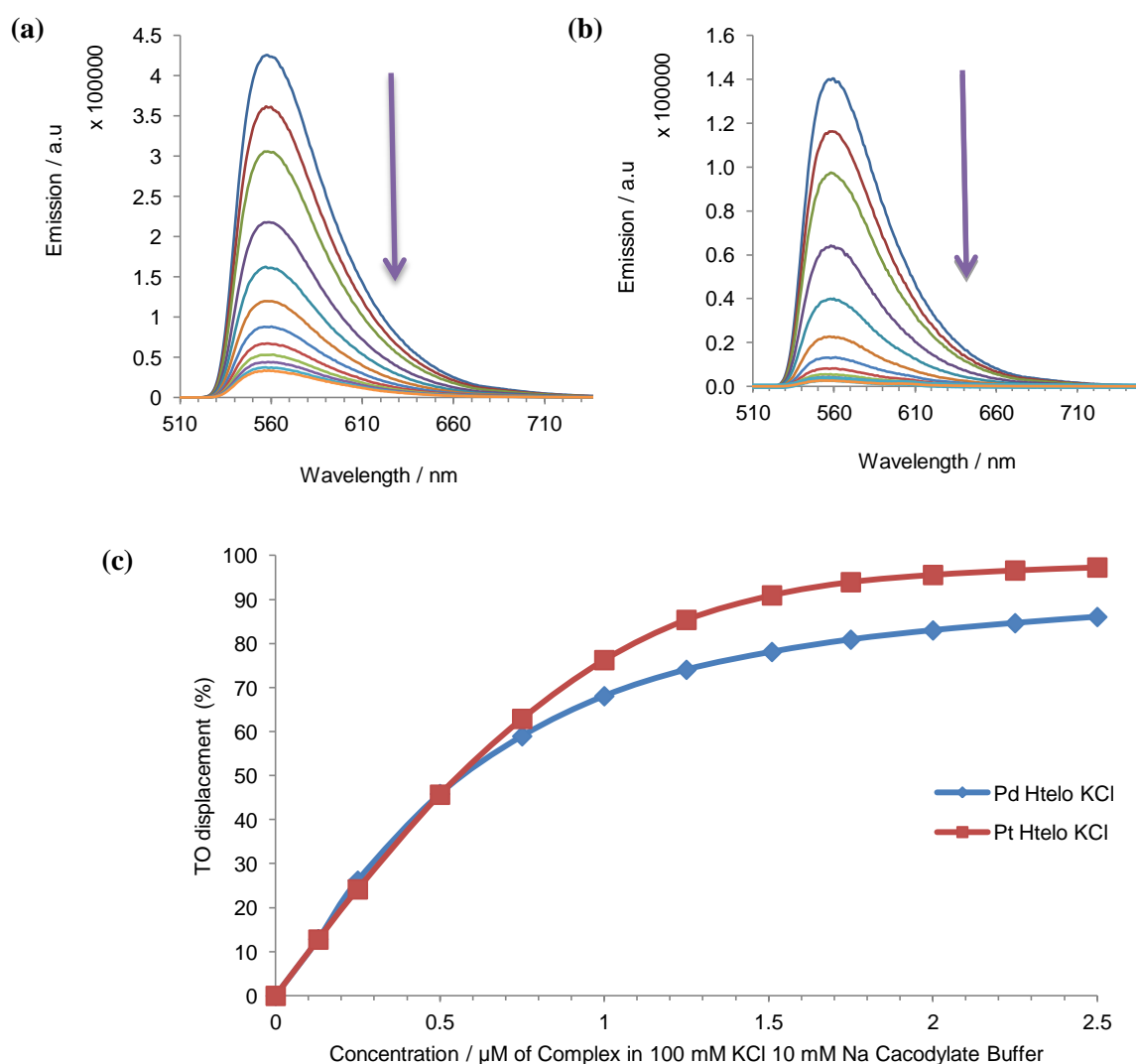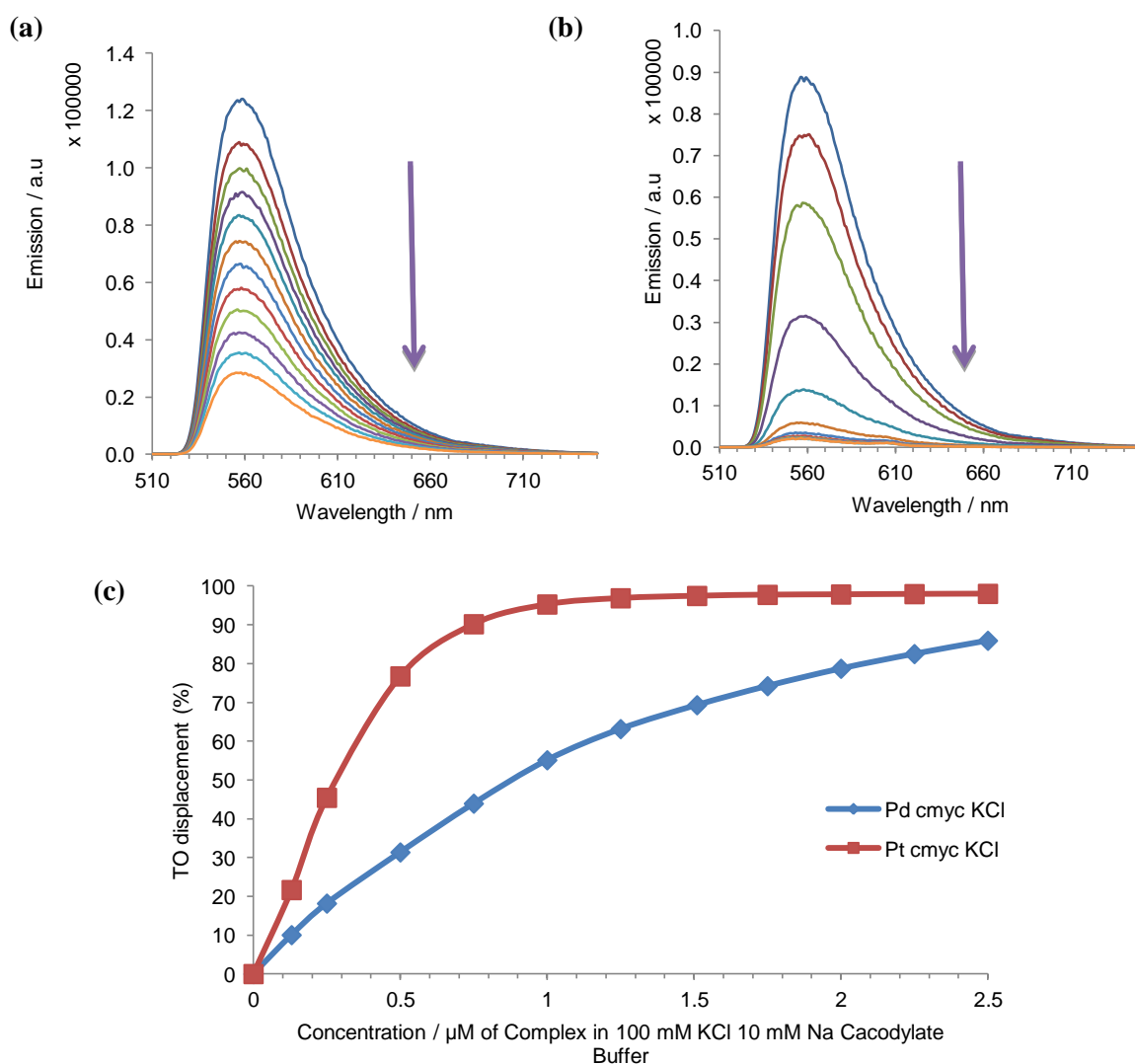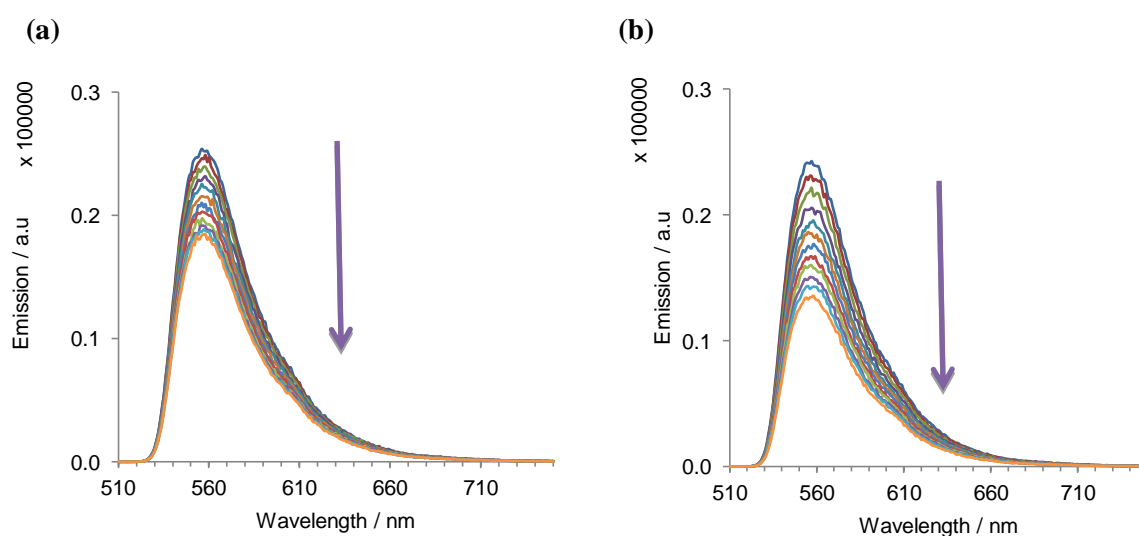

Figure 3.39 **a**. Emission spectrum for the palladium complex when titrated into 0.25 μM ds26 DNA solution containing 100 mM KCl / 10 mM Na cacodylate 0.75 μM TO, **b**. Emission spectrum for the platinum complex when titrated into 0.25 μM ds26 DNA solution containing 100 mM KCl / 10 mM Na Cacodylate 0.75 μM TO.

(c)
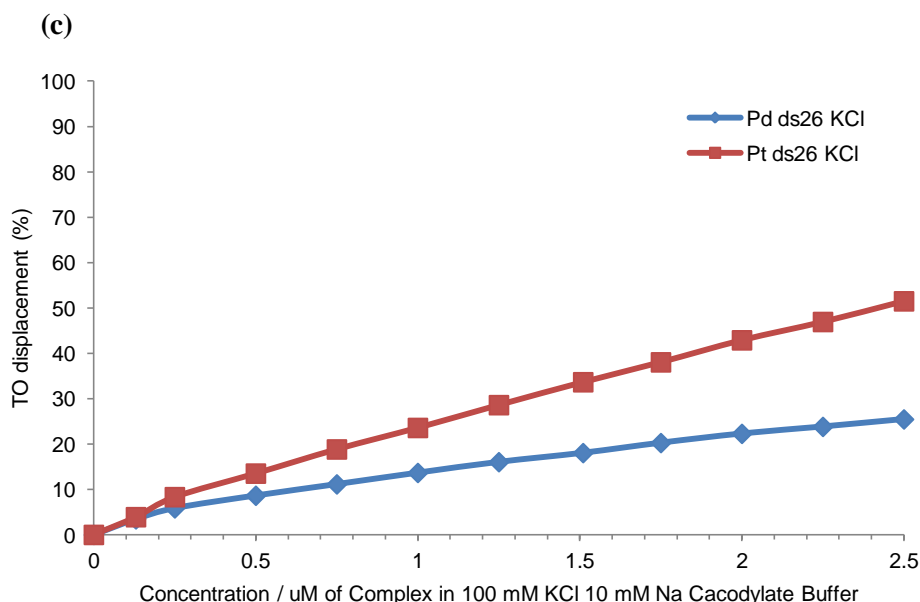
Figure 3.40 % TO displacement comparison for the palladium and platinum complexes with ds26 DNA.

3.4.4 Comparison of DC$_{50}$ Values

The DC$_{50}$ values (concentration at which TO fluorescence has reduced by 50 %) calculated for both complexes with htelo, c-myc and ds26 DNA are shown in *Table 3.1*. With htelo DNA both complexes are just around the '0.5 μM threshold' therefore can be considered as good binders. Results for c-myc DNA show much more of a difference between the two complexes with the palladium complex displaying a DC$_{50}$ value twice the required threshold and the platinum complex showing the lowest displacement concentration seen in the FID experiments conducted. More importantly with regards to selectivity, the DC$_{50}$ values calculated for the ds26 DNA are quite high indicating that the complexes are more selective for quadruplex DNA over duplex DNA based on this analysis.

	DC_{50} / µM		
	htelo	c-myc	ds26
[Pd(ibiq)$_2$][BF$_4$]$_2$	0.57 ± 0.12	1.03 ± 0.49	$6.25 \pm 0.45^{*}$
[Pt(ibiq)$_2$[PF$_6$]$_2$	0.55 ± 0.14	0.31 ± 0.10	2.47 ± 0.48

Table 3.1 DC_{50} values calculated for palladium and platinum FID complex titrations with htelo, cmyc and ds26 DNA. *estimated value as result extrapolated due to 50 % displacement mark not being reached.

The selectivity of the complexes for one type of DNA over another have been calculated in *Table 3.2*. The greatest difference in selectivity, 11 fold, is seen for the palladium complex when comparing the DC_{50} values of the complex with htelo and ds26 DNA. The palladium complex is also more selective for c-myc DNA over ds26 and also shows selectivity between different types of quadruplexes (preferring htelo over c-myc). The platinum complex is also more selective towards quadruplex DNA over duplex with its highest degree of selectivity occurring for c-myc DNA over ds26 DNA.

	Selectivity *[DC$_{50}$(A)/DC50(B)]*			
	ds26/htelo	ds26/c-myc	htelo/c-myc	c-myc/htelo
[Pd(ibiq)$_2$][BF$_4$]$_2$	10.96 ± 2.44	6.07 ± 2.92	-	1.81 ± 0.94
[Pt(ibiq)$_2$[PF$_6$]$_2$	4.49 ± 1.44	7.97 ± 3.00	1.77 ± 0.73	-

Table 3.2 Selectivity comparison between the different types of DNA investigated.

The combination of the CD and FID results suggest that the complexes bind by stacking on top of the G-quartet displacing the TO and lowering the fluorescence. In the case of the palladium complex with the c-myc DNA, displacement of the TO requires higher complex concentrations indicating that it doesn't stack as well on the c-myc quadruplex or the complex is binding to a different site.

3.5 UV-Vis Absorption Spectroscopy Titrations (Complexes 5 and 7)

Ultraviolet-visible absorption spectroscopy titrations are used to investigate how the complexes bind to the DNA by analysing the degree of hypochromicity and measuring red shifts. The presence of both these factors is linked to DNA binding by intercalation, direct metal-base binding and end stacking.[23] The red shift can be the result of a π^* orbital from the ligand coupling with a π orbital from the DNA bases (an energy decrease is associated with the π - π^* transition causing a peak shift to a longer wavelength) or a change of polarity of environment.[23] The stronger the interaction between orbitals the greater the hypochromicity and red shift will be.[24] Hypochromic effects without the additional red shift may be attributed to non-covalent DNA loop (groove) or backbone binding.[14] The UV-vis spectrum may also show hyperchromicity which is linked to electrostatic binding (external contact - DNA backbone) or the denaturing (melting) of the DNA where the DNA bases are more flexible and less shielded from absorbing light.[25] The titration can be used to calculate binding constants on the assumption that the binding between the complex and the DNA is 1:1.

During each experiment the complex UV-vis spectrum is measured first and then monitored whilst DNA is titrated into the solution. A blank titration is also carried out at the same time in order to remove any DNA peaks that absorb in the same region as the complex. The solvent control used in the blank titration showed no effect on the DNA. All titrations were carried out in potassium rich buffer to best match physiological conditions.

3.5.1 [Pd(ibiq)₂][BF₄]₂- Titrations with htelo, c-myc and ct-DNA

When the htelo DNA was added to the palladium complex solution the absorbance at 252 nm, due to ligand π-π* transitions, decreased significantly (43%). A red shift of 5 nm was observed in the presumed MLCT region (at 368 nm) only, which begins to appear at a 1:1 ratio of complex:DNA (*Fig. 3.41* - **a**). The same response occurred when c-myc DNA instead was added to the palladium complex solution. The absorbance peak at 250 nm showed a similar degree of hypochromicity (41 %) and the only red shift (6 nm) was observed in the MLCT region when a new peak emerges at a complex:DNA of 1:1 (*Fig. 3.41* - **b**). The emergence of the new peak in the MLCT region with both types of DNA creates an isosbestic point at 371 nm indicating that interconversion is occurring between two species. Considerable hypochromicity and large red shifts can be indicative of both an end stacking and direct coordination binding mode.[15] The change in the coordination sphere may be due to the loss of a ligand from the palladium centre caused by the bond strain of the bowed structure. This result, however, is surprising for the c-myc DNA interaction because in the CD experiments no ICD peaks relating to binding were seen. Therefore the response could be due to end stacking as it was presumed that the parallel loops wouldn't be as accessible for the [Pd(ibiq)]$^{2+}$ to bind to.

When examining the interaction of the palladium complex with ct-DNA a hypochromic effect was again observed (43 %) with the same magnitude of red shift occurring (6 nm) in the MLCT region (*Fig. 3.42*). It is suspected therefore that the palladium complex again loses a ligand and binds in a coordinative manner to the duplex DNA bases.

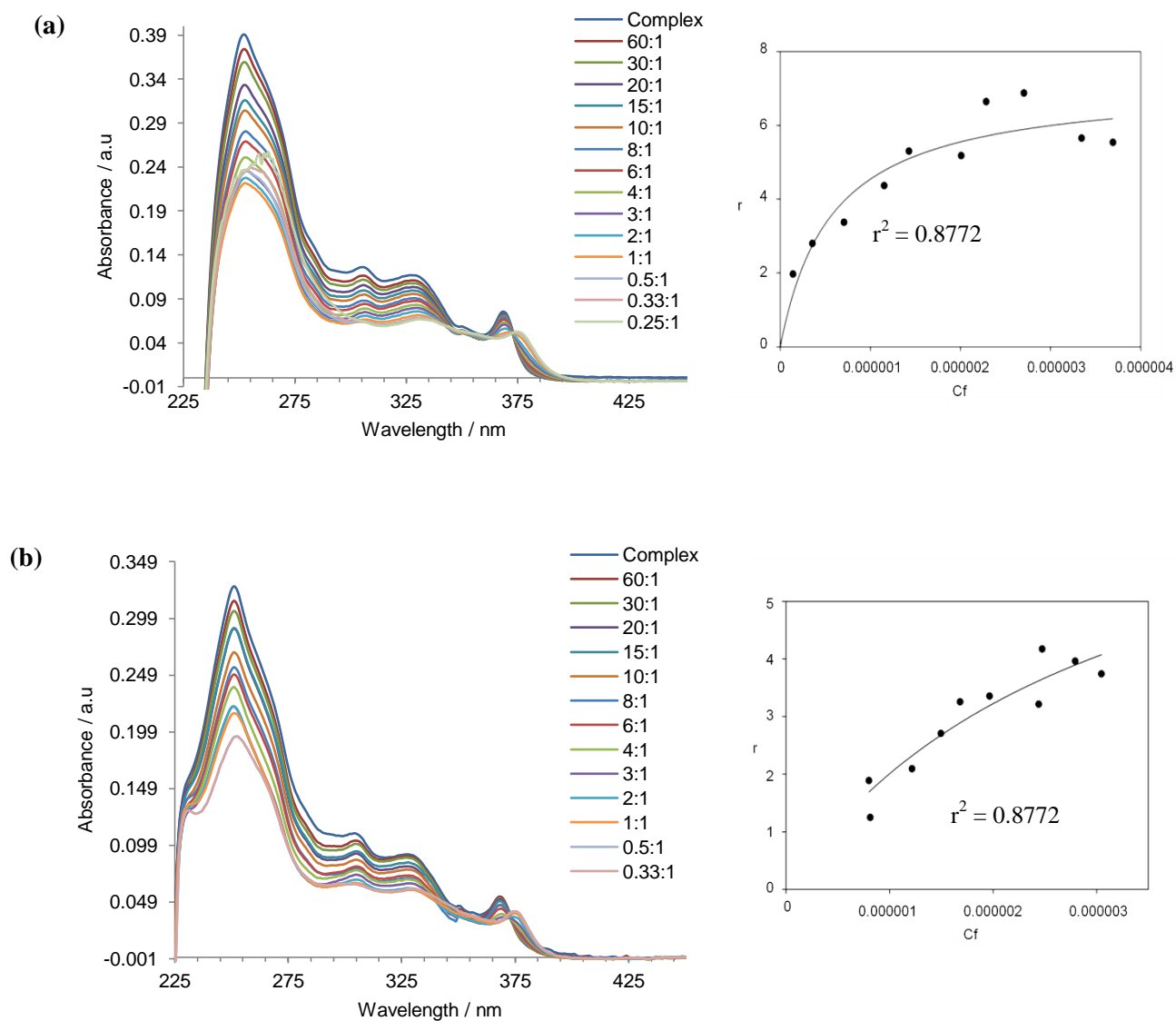*Figure 3.41* **a**. UV-Vis titration of htelo DNA into 7 μM [Pd(ibiq)$_2$]$^{2+}$ solution, ratio of complex:htelo DNA shown in the legend and binding curve plotting Cf versus r. **b**.UV-Vis titration of cmyc DNA into 7 μM [Pd(ibiq)$_2$]$^{2+}$ solution, ratio of complex:c-myc DNA shown in the legend and binding curve plotting Cf versus r.
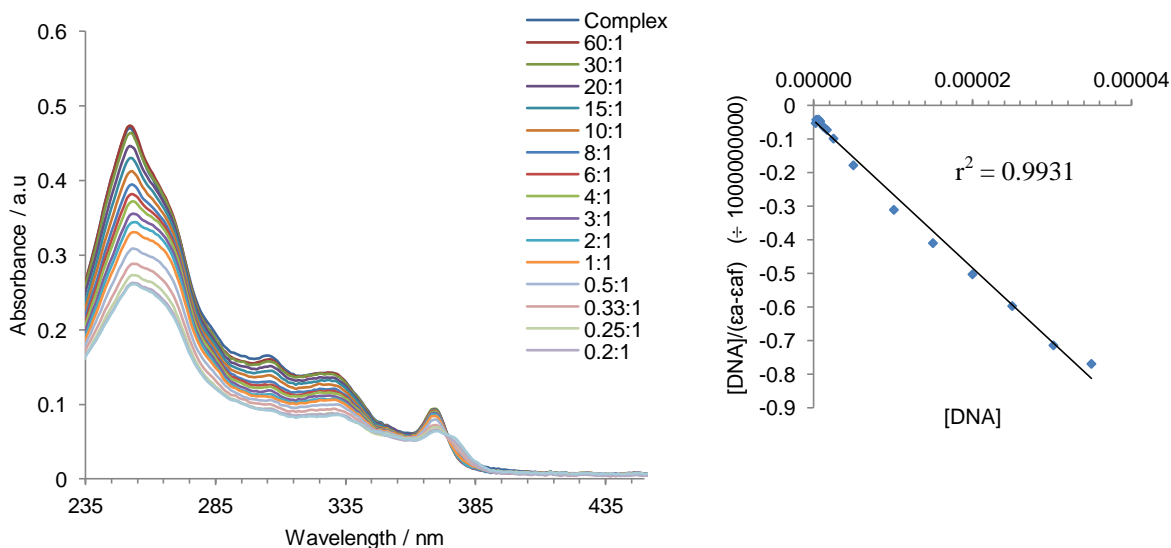
Figure 3.42 Left. UV-Vis titration of ct-DNA into 7 μM palladium solution, ratio of complex:ct-DNA shown in the legend, Right (top) - Scatchard plot for binding constant calculation, Right (bottom) - UV-vis stability solutions showing the red shift of the ct-DNA + Pd complex solution compared with the complex solution alone, both at 0 h.

3.5.2 [Pt(ibiq)$_2$][PF$_6$]$_2$ - Titrations with htelo, c-myc and ct-DNA

The absorbance spectrum for the platinum complex with htelo DNA also displays considerable hypochromicity (48 %) with a loss of absorbance of 15 % after the first addition of DNA at 262 nm (*Fig. 3.43 - a*). The initial titration of DNA also induces an immediate red shift (10 nm) of the MLCT band (380 nm). These changes that occur in the absorbance spectrum after so little addition of the htelo DNA again indicate that end stacking and/or direct coordination are the possible binding modes between the complex and the DNA. End stacking was thought to be the most probable binding mode as the platinum demonstrates slower coordination rates than palladium however the extent of bowing in the structure may lead to a coordination route. Further to this upon increasing amounts of htelo DNA the new red shifted peak at 390 nm increases in absorbance. Despite the apparent conversion of one species to another no isosbestic point could be located as the initial conversion is not a gradual one. This is indicated by the sudden red

shift after adding DNA. Titrations conducted with c-myc DNA show hypochromic changes of 46 % at 262 nm and a red shift of 12 nm in the MLCT region (381 nm - 393 nm) (*Fig. 3.43 – b*). An isosbestic point can be seen in this system at 388 nm. All of these observations indicate that the DNA is most likely binding to the complex in an end stacking mode.

Finally the interaction of the platinum complex with ct-DNA was investigated. The UV-vis spectrum shows the greatest degree of hypochromism of all the DNA-complex systems with a 54 % loss in absorbance (*Fig. 3.43 - c*). A red shift of 10 nm is seen in the MLCT region at a complex:DNA ratio of 1:1 which is very similar to the red shift seen with the quadruplex forming DNA. Both of these effects are consistent with direct coordination of the platinum to DNA bases unless the ligand is intercalating between the base pairs instead. Each type of DNA differs by the ratio of complex:DNA at which the red shift occurs, for the quadruplex systems this is 60:1 (htelo) and 6:1 (c-myc). Hence the interconversion between the two species (bound and unbound) occurs at lower DNA concentrations for htelo and c-myc, and a higher concentration for ct-DNA.

In a hypothesised competitive system, if both types of DNA (quadruplex and duplex) were present, the results indicate that the complex would stack onto the quadruplex DNA at low loading concentrations. This would generate the new species which causes the red shift before the complex could coordinatively bind to the ct-DNA (which has a red shift that occurs at high complex loading concentrations).
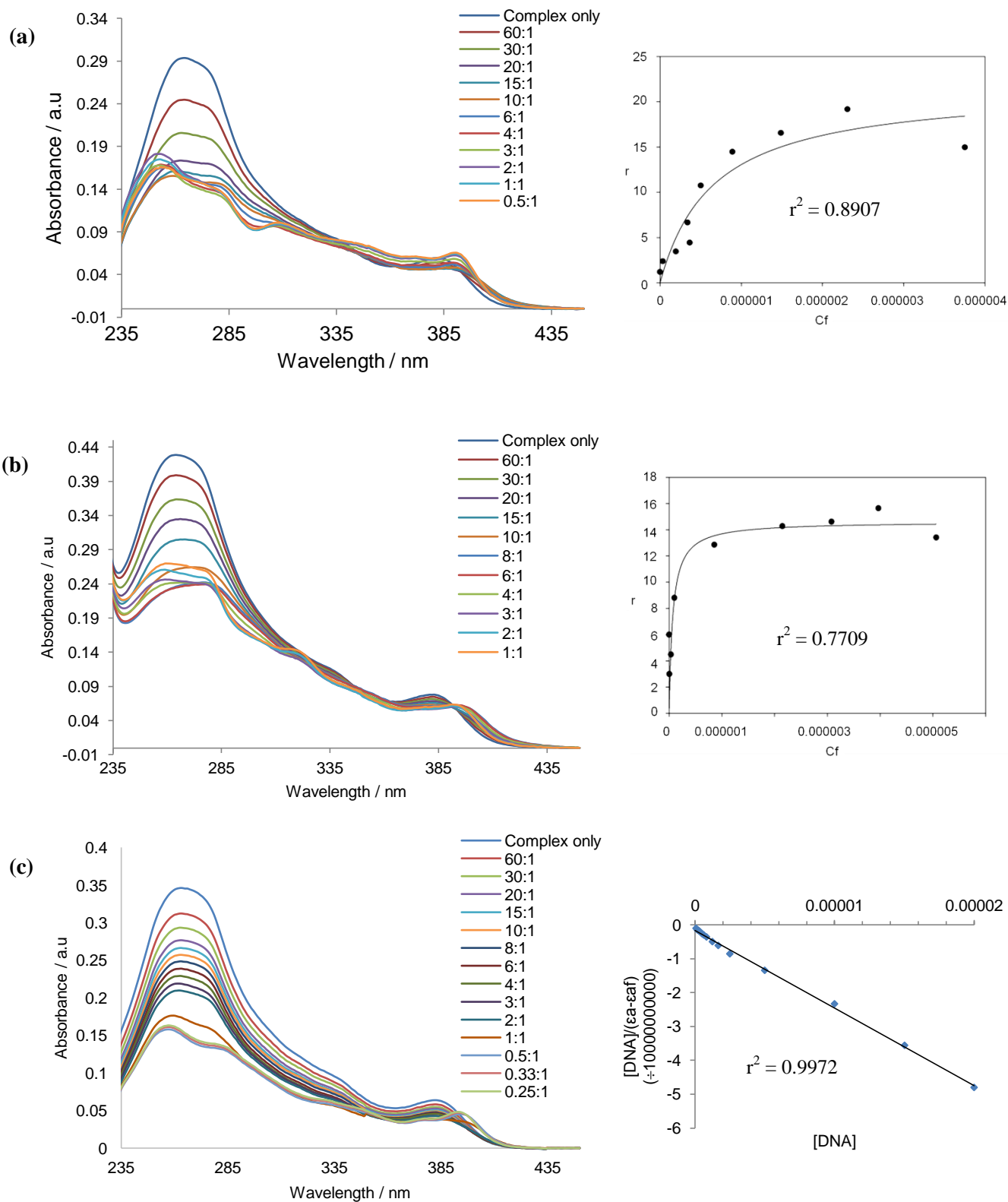
Figure 3.43 **a**. UV-Vis titration of htelo DNA into 7 μM [Pt(ibiq)$_2$]$^{2+}$ solution, ratio of complex:htelo DNA shown in the legend and binding curve plotting Cf versus r. **b**. UV-Vis titration of cmyc DNA into 7 μM platinum solution, ratio of complex:c-myc DNA shown in the legend and binding curve plotting Cf versus r, **c**. UV-Vis titration of ct-DNA into 7 μM platinum solution, ratio of complex:ct-DNA shown in the legend and Scratchard plot to calculate the binding constant.

3.5.3 Binding Constant Comparison

Absorption was measured at 268 nm in each system in order to make a direct comparison between them. The MLCT region would have been the preferred choice to calculate a binding constant however the platinum complex titrations in this region are comprised of overlapping shifts which make it difficult to calculate. Two methods have been used to calculate the binding constant, one for the ct-DNA whose base sequence hence strand concentration is unknown and one for the quadruplex DNA (htelo and c-myc) which have defined sequences with accurately measured strand concentrations. Both methods have been reported in the literature[23], most relevantly in work published by Shankar Balasubramanian.[26]

Method 1:

The method used for ct-DNA systems uses the equation below[23][26]:

$$[DNA] / (\varepsilon_a - \varepsilon_f) = [DNA] / (\varepsilon_b - \varepsilon_f) + [K_b (\varepsilon_b - \varepsilon_f)]^{-1}$$

In this equation [DNA] is measured in bases, ε_a is the observed absorbance/[complex], ε_f is the extinction coefficient for the free complex and ε_b is the extinction coefficient for the complex in its fully bound form. Plotting $[DNA]/(\varepsilon_a - \varepsilon_f)$ versus [DNA] gives the intercept as $[K_b (\varepsilon_b - \varepsilon_f)]^{-1}$. Binding constant determination for the palladium complex binding to ct-DNA can be found in *Fig. 3.42* and for the platinum complex *Fig. 3.43 - c* (pages 176 and 178).

Method 2:

A one site binding isotherm has been used to determine quadruplex DNA binding constants[26]:

$$r = B_{max}C_f/K_d+C_f$$

The above equation can be used after calculating C_f (concentration of free ligand) which is determined from $C_f = (1 - \alpha) \times C$, where C is the [complex]$_{tot}$ and α is the fraction of complex that is bound to the DNA $\{\alpha = (A_f - A) / (A_f - A_b)\}$, A_f = absorbance of free complex and A_b = absorbance of fully bund complex. The binding function **r** (where r = C_b/[DNA] and C_b = C - C_f) is then plotted against [C_f] and analysed by nonlinear regression using Sigmaplot version 10. Graphical results for the palladium complex with htelo and c-myc DNA and the platinum complex with htelo and c-myc DNA can be found in ***Fig. 3.41 - a, 3.41 - b, 3.43 - a and 3.43 - b*** respectively (pages 175 and 178). All the quadruplex DNA data fit the one site binding isotherm.

Results:

The binding results for the complex and DNA systems tested using UV-vis spectroscopy are shown in *Table 3.3*. The ratios of affinity for the palladium complex and the platinum complex to htelo and cmyc are approximately the same but reversed. It appears that all three types of DNA bind well to the platinum complex which again is suggested in the CD results where an intense spectrum is generated in each titration.

DNA Type	Intrinsic binding constant / M^{-1}	
	[Pd(ibiq)$_2$][BF$_4$]$_2$	[Pt(ibiq)$_2$][PF$_6$]$_2$
ct-DNA	$(3.0 \pm 2.0) \times 10^5$	$(1.0 \pm 0.5) \times 10^6$
htelo	$(2.5 \pm 1.0) \times 10^6$	$(1.8 \pm 0.4) \times 10^6$
c-myc	$(4.0 \pm 1.9) \times 10^5$	$(9.7 \pm 6.0) \times 10^6$

Table 3.3 Summary of binding constants calculated using a 1:1 binding isotherm for htelo and cmyc DNA and Scatchard plot for ct-DNA, uncertainty calculated from average of three.

3.6 ^{1}H-NMR Experiments with Complex 7

Work in collaboration with H. Guiset-Miserachs, Dr. D. Donghi and Prof. R. Sigel of the University of Zürich - Experiments run by Dr. D. Donghi and samples prepared by Hannah Pritchard.

Proton NMR spectroscopy is environment sensitive and the presence of binding can be accurately monitored by studying the movement and symmetry of peaks. Two types of analysis were conducted using an AV700 MHz spectrometer that was equipped with a TXI z-gradient CryoProbe which was able to detect a reagent concentration of 100 μM. The experiments were conducted in the NMR facility of the Chemistry Department at the University of Zurich. The platinum complex was chosen for the NMR experiments as it showed the best binding potential in the previous DNA binding experiments. Htelo DNA was used to assess the complex-quadruplex binding interaction.

3.6.1 1D ^{1}H-NMR

The first type of analysis discussed is simply 1D ^{1}H-NMR spectroscopy which with the use of the AV700 MHz spectrometer could produce well resolved NMR spectra requiring very

little amounts of DNA. The concentration of htelo DNA and the platinum complex were kept constant at 100 μM for all experiments (in 85 % H_2O, 15 % d_6-DMSO, 50 mM KCl) to make sure that any changes to the NMR spectrum were not due to concentration effects.

The platinum complex ^{1}H-NMR is shown at the bottom of *Fig. 3.44 - d*, the spectrum above this *(c)* is the htelo DNA alone. In this spectrum imino proton peaks can be seen between 10 ppm and 12 ppm which result from the exchange of protons within the terminal G-quartets. Well defined imino peaks indicate a unique structure has been adopted whereas poorly defined peaks are the result of multiple quadruplex structures; the latter appears to be the case for this system.[27] Imino proton exchange within this region occurs due to the more distorted or flexible nature of the end quartets in the quadruplex structure; the other imino protons from inner quartets exchange much more slowly.[27][28]

Spectrum *b* in *Fig. 3.44* shows the htelo DNA and complex in a 1:1 mixture where new peaks have appeared on the very edge of the imino proton region around 12.8 ppm. Most of the undefined imino proton peaks that were present in the DNA spectrum only, have remained in the same place. The new set of peaks between 8 - 10 ppm are hard to distinguish as they appear too low for imino protons. The complex peaks are no longer present at the same chemical shifts when mixed with the DNA and are also very difficult to locate on the 1:1 spectrum. The addition of one equivalent of complex has generated a further mix of quadruplex structures one of which may be that of the complex bound to the DNA.

In the top spectrum *a* two equivalents of complex have been added causing the initial

imino sequence seen in the DNA only spectrum to disappear leaving a more defined set of

proton peaks between 10.5 - 12.8 ppm. The peaks between 8.0 - 10.5 ppm have remained

constant and therefore may be a combination of complex and other DNA protons. The

shift of imino protons is a good indication that the complex is interacting with the htelo
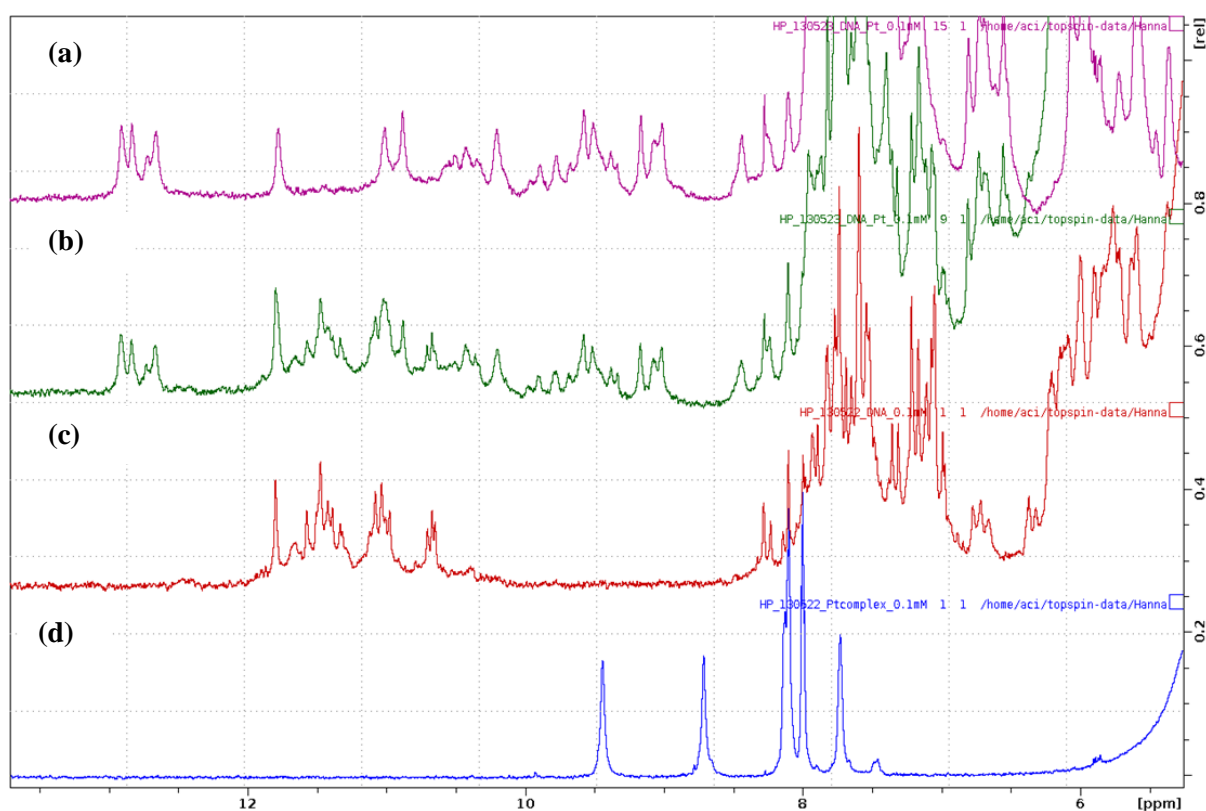
DNA through an end stacking binding mode.

Figure 3.44 1D^{1}H-NMR spectra where the concentration of each species is 100 μM (200 μM for 2 equiv of Pt complex), in 15 % d$_6$-DMSO, 85 % H$_2$O, 50 mM KCl : **a**. Htelo DNA:platinum complex (1:2), **b**. Htelo DNA:platinum complex (1:1), **c**. Htelo DNA alone, **d**. Platinum complex alone.

The same NMR experiments were then conducted in D_2O in order to remove the imino protons from the spectra (due to their fast exchange rates) so an attempt could be made to identify the complex peaks. The resulting spectra can be seen in *Fig. 3.45* where by superimposing the red spectrum (DNA+complex+H_2O+d_6-DMSO) over the blue spectrum (DNA+complex+D_2O+d_6-DMSO) the imino protons could be identified. The peaks that remain could have come from both the complex and the other non imino protons of the DNA.

The symmetry of the complex peaks alone could not be matched anywhere on the spectrum when in the DNA mixture. This indicates the complex is bound to the DNA because if the complex wasn't properly bound and just spinning on the top of the quadruplex the symmetry of the complex would appear exactly the same. Along with the change in symmetry there is a definite chemical shift further indicating that binding has taken place.
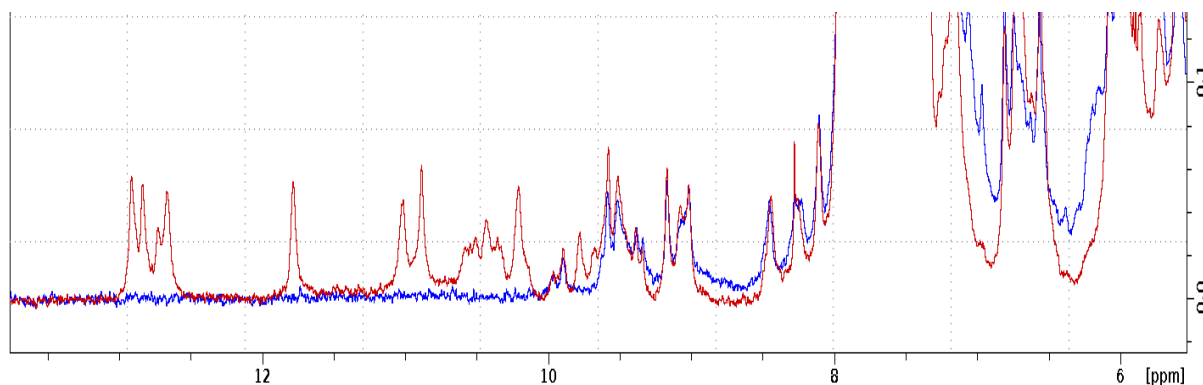

Figure 3.45 Overlaid spectra of blue - DNA:complex (1:2) in D_2O and red - DNA:complex (1:2) H_2O.

3.6.2 DOSY

Diffusion-ordered spectroscopy (DOSY) can be used to separate NMR responses of different compounds by their diffusion coefficient which depends on the size and shape of the molecule, temperature and viscosity of the solution. The technique can also assess aggregate formation and the degree of solvation around the molecule in question.[28] The diffusion coefficient (if shape of the molecule is spherical) can be described by the Stokes-Einstein equation where D (diffusion coefficient) is linked to K_B - Boltzmann constant, T - temperature, η - viscosity and r - radius of the molecule.[29]

$$\textbf{Stokes-Einstein Equation: } D = K_B T / 6\pi\eta r$$

The translational diffusion of the molecules is measured using pulsed magnetic field gradient NMR (PFG-NMR) spectroscopy where the usage of a gradient allows molecules to be labelled depending on their location in the sample tube.[29] Larger molecules will diffuse slowly giving a stronger signal as more nuclei will remain in place that can refocus whereas smaller molecules diffuse quickly and become out of range therefore cannot refocus.[29] An example of a diffusion decay curve is shown in *Fig. 3.46* which generated a diffusion coefficient of 2.787×10^{-10} m^2/s. This was plotted by the Bruker NMR software using the equation below where I - intensity observed, I_0 - unattenuated signal intensity, D - diffusion coefficient, g - gradient strength, δ - gradient length, Δ - diffusion time and γ - gyromagnetic ratio.[29]
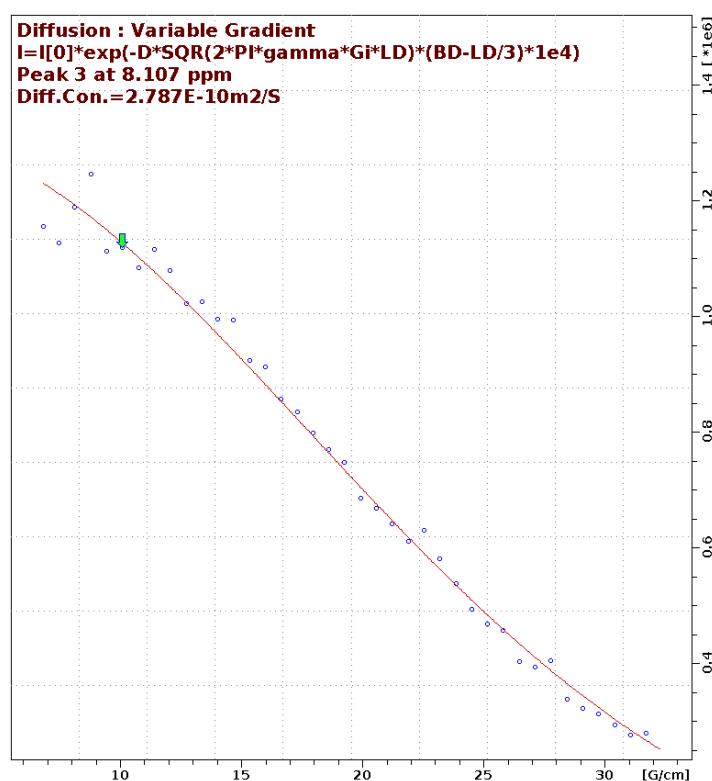
$$I = I_0 e^{-D.(\gamma.g.\delta)^2.(\Delta - \delta/3)}$$

*Figure 3.4*6 Diffusion decay curve for Platinum complex **7** (100 μM) in a 85% H_2O, 15% d_6-DMSO solution.

DOSY spectra were generated for three systems htelo only; (100 μM), htelo (100 μM) + platinum complex (100 μM) and platinum complex only (100 μM). All the experiments were conducted in 85 % H_2O / 15 % d_6-DMSO at 25 °C. In *Fig. 3.47* the three DOSY spectra have been overlaid to show how the diffusion coefficient has changed between each system. The purple trace shows the complex alone displaying the greatest rate of diffusion through the solution as it is the smallest system of the three examined. The peak centred around 4.75 ppm is due to the DMSO which couldn't be reduced or eliminated from the spectra. The system in green is that of the DNA alone which diffuses at a slower rate due to its larger size. Finally the blue DOSY spectrum represents a mixture of the DNA and platinum complex together where only one molecule has been identified as only one diffusion coefficient is shown. If the complex wasn't bound to the DNA it would be

free to diffuse at a faster rate through the solution producing another set of correlation spots on the spectrum. The absence of any additional spots displaying a different diffusion coefficient and the additional spots produced at the diffusion coefficient recorded indicates that the complex has bound to the DNA.
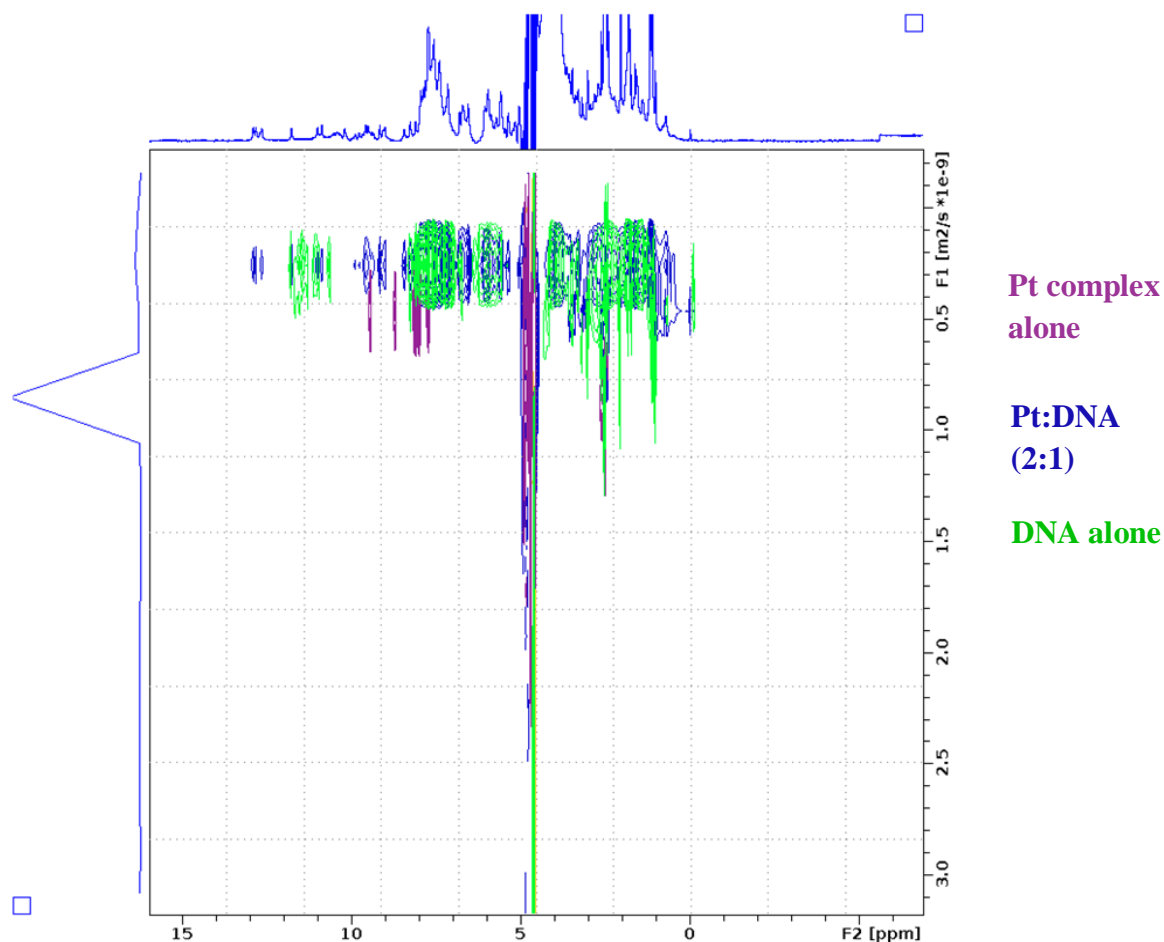
Figure. 3.47 Overlaid DOSY spectra for purple - platinum complex **7** (100 µM) in a 85% H_2O, 15% d_6-DMSO solution, green - htelo DNA (100 µM) in a 85% H_2O, 15% d_6-DMSO solution, blue - Pt:DNA (2:1) (100 µM DNA, 200 µM Pt complex) in a 85% H_2O, 15% d_6-DMSO solution.

The diffusion coefficient estimate for each system is displayed in *Table 3.4* which has been used to calculate the corresponding radii using the Stokes-Einstein equation. The viscosity of this system containing 85 % H_2O and 15 % d_6-DMSO has been previously reported by

Sacco and Matteoli as 0.429 mPa/s at 25°C (obtained from plotting reported ratios versus viscosity to obtain a result for 15 % d_6-DMSO).[30]

System Studied	Diffusion Coefficient Estimate (m^2/s)	Radius (nm)
Pt complex(**7**)	2.8×10^{-10}	1.8
htelo DNA	1.6×10^{-10}	3.3
htelo DNA + Pt complex (**7**) (1:2)	1.3×10^{-10}	3.9

Table. 3.4 Summary of diffusion coefficients and radii estimates calculated using the following constants: $K_B = 1.380 \times 10^{-23}$ J K^{-1}, T = 298 K, $\eta = 4.29 \times 10^{-4}$ Pa s, $\pi = 3.14$.

When the complex is bound to the DNA there appears to be an increase in molecule radius when compared with the DNA alone. The longest reported dimension of the platinum complex alone from its crystal structure is 1.35 nm (diameter) which does not correspond with the estimated experimental radius of 1.82 nm therefore diameter of 3.64 nm.[31] A strong possibility to account for this is the aggregation of the complex in solution. The complex has been designed to effectively stack on a flat planar surface therefore it may be stacking on top of itself giving the appearance of a larger molecule in solution hence a larger radius. It appears though that when binding to the DNA it may no longer be in its aggregated form as the additional length of radius (from DNA alone to DNA with complex) corresponds more closely with the single molecule binding only. The high concentration of DNA and complex in this experiment may be the cause of the aggregation (100 μM DNA, 200 μM [Pt(ibiq)$_2$]$^{2+}$); the CD experiments required much lower concentrations (3 μM DNA) therefore would be less likely to exhibit this effect.

3.7   Gel Electrophoresis Studies

The sugar phosphate backbone of DNA is negatively charged therefore during an electrophoresis experiment the DNA will migrate through the gel matrix towards a positively charged electrode. The speed by which the DNA fragments move through the gel depends upon their size; with smaller fragments moving rapidly through the gel and larger fragments moving more slowly.[32] Overall DNA charge and conformation can also affect how quickly the molecule moves through the gel. Two types of gel electrophoresis experiment have been used to examine how the complexes bind to different types of DNA:

- Agarose gel electrophoresis is used with larger molecules such as plasmid DNA (pBR322 double stranded circular DNA) to investigate the duplex binding ability of the complexes. The technique offers a large separation range but with limited resolution of the DNA.

- Polyacrylamide gel electrophoresis (PAGE) is used for smaller sequences of DNA (22 base htelo sequences) and gives a better resolution of the DNA molecules, however it only has a small range of separation.

3.7.1 Agarose Gel Electrophoresis with Complexes 5 and 7 using Plasmid DNA

In order to probe the interaction between duplex DNA and biisoquinoline complexes **5** and **7** a double stranded supercoiled DNA plasmid was used. The supercoiling nature of DNA has been observed in living cells and is particularly important in processes that require DNA duplex unwinding such as transcription.[33] The negative supercoiled (under wound) DNA in the c-myc promoter region for example enables the formation of G-

quadruplexes.[34]   The closed circular DNA structure is useful for the study of DNA-complex interactions because the plasmid will take on a different form depending on how the complex interacts with the DNA.

For complexes that aren't able to break the sugar phosphate DNA backbone the plasmid will remain in the supercoiled form and any complex binding will be observed by the slower migration of the supercoiled band through the gel.[35]   When the complex is able to cause DNA cleavage of one strand, the supercoiled form relaxes into a nicked circular open form which travels more slowly through the gel; cleavage of both strands leads to the linear form which if present can be found between the supercoiled and nicked circular forms.[35]   This is shown schematically in *Fig. 3.48*.

The experiment is set up so that the agarose gel contains a selection of wells to which are added different ratio's of complex to pBR322 DNA. Once loaded, an electric field is applied which causes the negatively charged DNA to move towards the positive electrode (*Fig. 3.48*). The extent to which the DNA moves depends upon its supercoiled or nicked circular structure and its charge. The supercoiled structure is more compact therefore will have a different migration speed to the larger nicked circular structure .
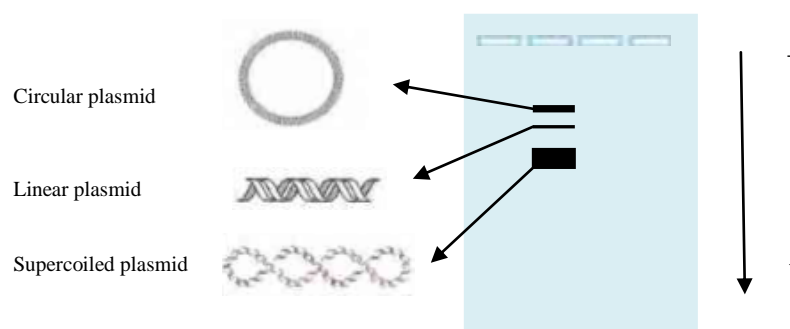
Figure 3.48 Pictorial example of a gel electrophoresis experiment indicating the direction of migration of the DNA and the location of the nicked circular and supercoiled plasmid after visualising using ethidium bromide and UV light.

The forms of the DNA are visualised in the gel using ethidium bromide which binds to DNA through an intercalative mode. This fluorescent stain can be easily detected by UV light thus allowing the position of the DNA in the gel to be seen.

Complex binding to the negatively supercoiled DNA can cause changes in the rate that the DNA migrates across the gel. The effectiveness of the complex-DNA interaction can be investigated by treating the DNA with different ratios of complex and observing any change to the position of the supercoiled band when compared with a control. The negatively supercoiled DNA is underwound so if the complex increases the positive supercoiling then the extent of negative supercoiling is decreased. Intercalators, for example, positively supercoil because the site they bind at is effectively unwound. This causes a stiffening of the DNA when taking up the slack of underwinding.

The following experiments were conducted to assess whether the biisoquinoline complexes would display any significant unwinding behaviour or other binding activity with duplex DNA. The plasmid has no telomeres (as circular) and tetrads are not expected to form in

any promoter regions therefore this experiment is probing intercalation or other duplex binding modes Different ratios of complex to DNA were loaded onto a 1% agarose gel before applying an electric potential. After running the gel the DNA was visualised using ethidium bromide and UV light to assess the extent of complex-DNA interaction.

*[Pd(ibiq)$_2$][BF$_4$]$_2$ - **5***

The pBR322 plasmid DNA was treated with the palladium complex in DNA:complex ratios from 40:1 to 2:1. Due to the insolubility of the complex in water alone a small percentage of DMSO was required to completely dissolve it. Controls using both DMSO and water were used to make sure that the addition of the DMSO had no effect on the unwinding of the DNA. Before the gel was loaded with the samples, the DNA and complex mixtures were left at room temperature for 2 hours.

Very little change can be seen from the UV visualised agarose gel at the end of the experiment (*Fig. 3.49*). A small amount of movement of the supercoiled band (sc) starts to occur at a ratio of 5:1 indicating that there is a small amount of binding to the supercoiled structure slowing the rate of migration through the gel. The separation between the supercoiled (sc) and open circular (oc) bands is reduced at high loading indicating some DNA unwinding but this is a small effect and cannot be readily quantified from this experiment. There is little evidence for a strong interaction with this plasmid DNA which in order for it to be a selective quadruplex binder shows good promise. The result contrasts with the CD data where the strong ICD peaks produced for a linear genomic ct-DNA suggest there is a more significant interaction between the complex and the DNA.
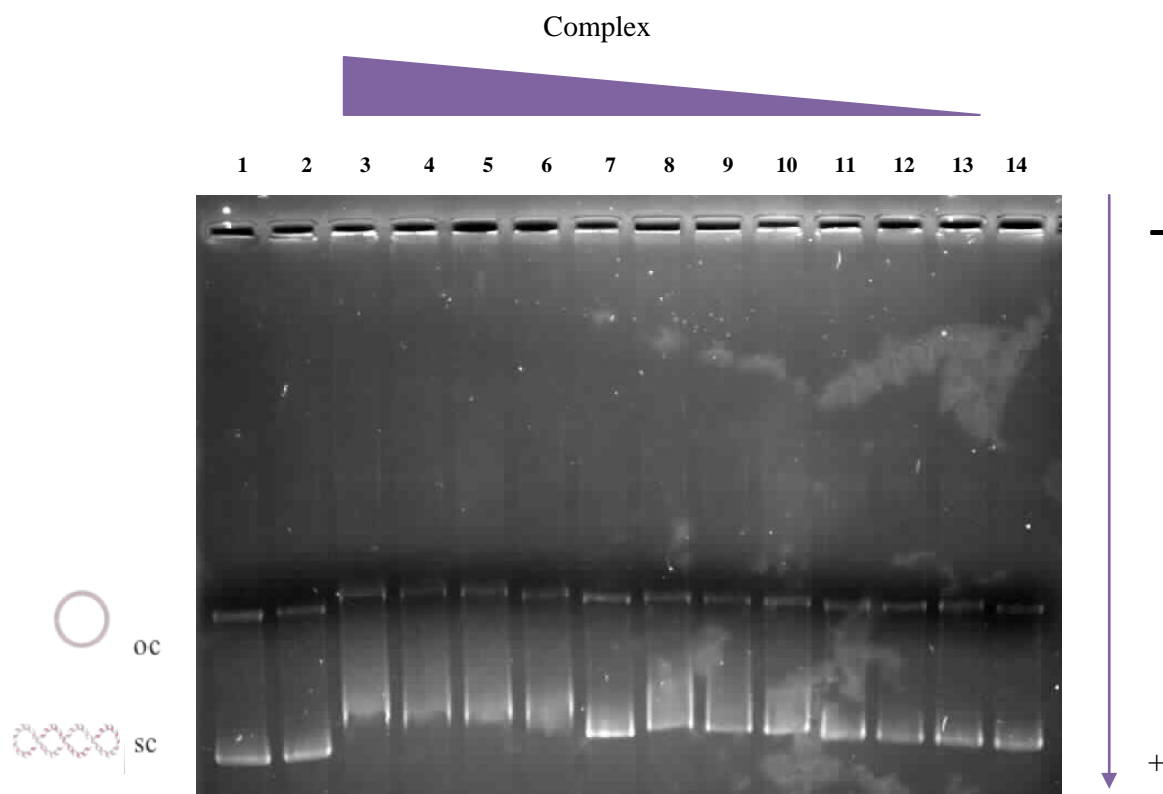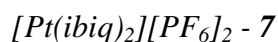
Complex

Figure 3.49 Agarose gel electrophoresis (1% agarose) showing the migration of the supercoiled and nicked circular forms of the DNA plasmid when an electric potential is applied. pBR322 was treated with the complex and then left at 20°C for 2 hours before the gel was run. Control lanes without complex **1**-DMSO, **2**-H_2O, **14**- H_2O, lanes **3-13**, DNA:complex ratios, 2:1, 3:1, 4:1, 5:1, 6:1, 8:1, 10:1, 15:1, 20:1, 30:1, 40:1.

*[Pt(ibiq)₂][PF₆]₂ - **7***

As with the palladium complex the platinum complex required a small amount of DMSO to fully dissolve the complex in H_2O. The gel electrophoresis results show that there is a gradual reduction in the migration rate of the supercoiled band as the concentration of the platinum complex increases (*Fig. 3.50*). Even at the lowest concentration addition of the complex there is an immediate shift of the supercoiled band when compared with the control in lanes 1 and 13. This indicates that either the complex is binding to the supercoiled DNA and unwinding it or binding and retarding its movement. The circular band can also be seen to migrate more slowly through the gel on the addition of the

complex. At a DNA:complex ratio of 8:1, the supercoiled band becomes more strained and can no longer be seen. It appears to have been wound into the circular form however this movement could again be due to band retardation. The increase in concentration of complex from 6:1 to 2:1 sees the further retardation of the circular band and the appearance of a new band in between the original two. It is likely that the charge on the open circular plasmid is quenched through the binding of many positively charged complexes, retarding its movement through the gel.
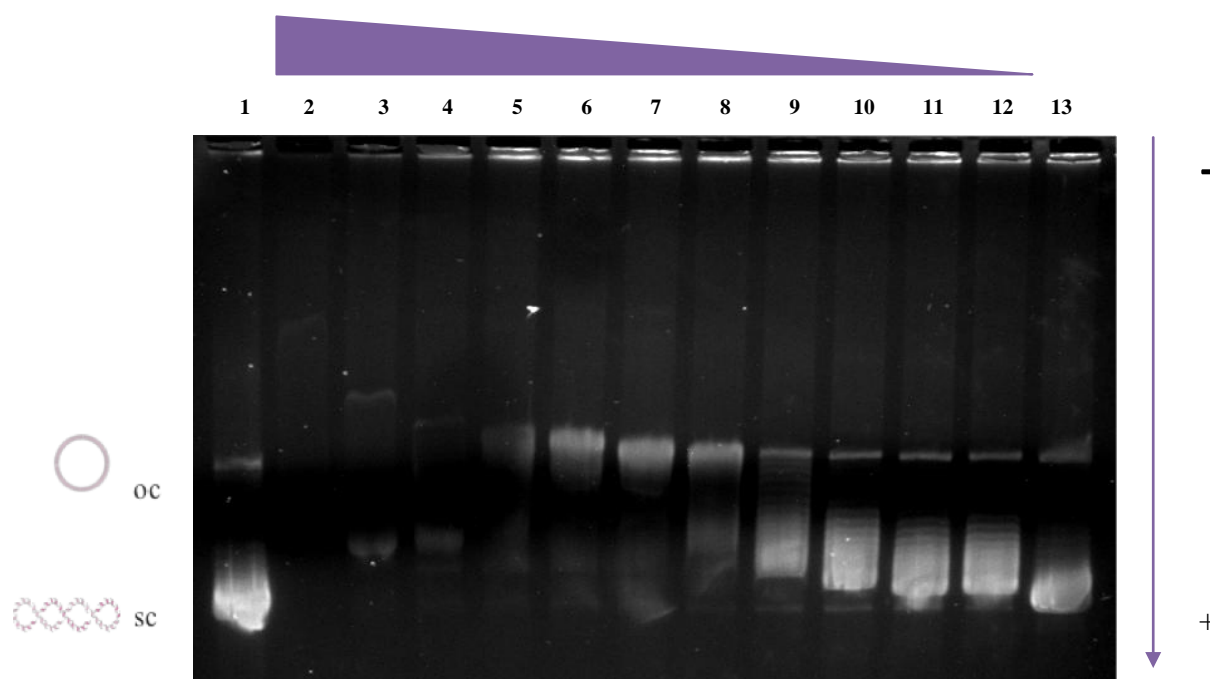

Figure 3.50 Agarose gel electrophoresis (1% agarose) showing the migration of the supercoiled and nicked circular forms of the DNA plasmid when an electric potential is applied. pBR322 was treated with the complex and then left at 20°C for 2 hours before the gel was run. Control lanes without complex **1**-DMSO, **13**-H$_2$O, lanes **2-12**, DNA:complex ratios, 2:1, 3:1, 4:1, 5:1, 6:1, 8:1, 10:1, 15:1, 20:1, 30:1, 40:1.

It is no surprise that the platinum complex has shown that it is able to bind to duplex DNA in the gel electrophoresis experiments as in all other experiments, regardless of the type of DNA, the complex has produced results that indicate significant binding.

3.7.2 Non-denaturing PAGE with Complexes 5 and 7 using htelo and c-myc DNA

Work in collaboration with H. Guiset-Miserachs, Dr. D. Donghi and Prof. R. Sigel of the University of Zürich - Experiments conducted by Hannah Pritchard

Polyacrylamide gel electrophoresis works very much in the same way that agarose gel electrophoresis does but is suited to smaller DNA fragments because of the smaller pore size created by the gel forming process.[36]

The visualisation of DNA in the gel can be achieved using many techniques. In the experiments with the ibiq complexes UV light alone was used to locate the DNA bands however a more widely used way to visualise the DNA involves radiolabelling specific fragments of DNA and recording an autoradiogram.[37] Radioactive labelling is useful as very small quantities of DNA can be used as the technique is highly sensitive.[37] Another labelling technique involves the attachment of a fluorescent label to the DNA strand such as FAM (6-carboxyfluorescein) which again is highly sensitive requiring very little quantities of DNA due to the highly fluorescent nature of the appended ligand. A fluorescent dye used to specifically target quadruplexes called protoporphyrin IX (PPIX) has been used to identify bands linked to quadruplex formation and silver staining has also been used.[38][39]

As mentioned above UV light alone was used to visualise the DNA following the PAGE experiment with the location of the bound complex to the DNA verified by extracting the DNA and complex from the gel spot and recording a UV-Vis spectrum. The technique required a large amount of DNA (3 nmole) to be seen with ease using UV light (λ= 254

nm) due to the lack of sensitivity. The experiment however could be run much more quickly and cheaply without the need to label the DNA which may affect DNA folding and ligand binding. For example the ligand may interact with the fluorescent dye (such as fluorescein) instead of the DNA.[40]

All the quadruplex forming DNAs used in the PAGE experiments were annealed before use in a potassium rich buffer (the running buffer contains 50 mM potassium also). This should ensure that all of the DNA has been folded into its G-quadruplex structure allowing the investigation to determine how well the ibiq complexes bind to existing quadruplexes.

G-quadruplex DNA (after annealing) was mixed with different ratios of each ibiq complex (platinum or palladium) and then incubated before loading the wells on the polyacrylamide gel (15%). The controls used were the quadruplex DNA alone and also with the small percentage of DMSO that was required to dissolve the complexes. Once loaded an electric potential was applied causing the DNA to migrate to the positive electrode. G-quadruplexes migrate fastest through the gel due to their compact structure, the type of quadruplex formed also has an effect on the mobility with antiparallel quadruplexes migrating faster than parallel quadruplexes.[38][41] As with the agarose gel electrophoresis experiments the binding of a complex to the DNA structures will cause the migration across the gel to slow as the size of the structure has increased.

PAGE Results with htelo DNA

The UV image for the gel obtained when loaded with annealed telomeric DNA (htelo) and both complexes; platinum ibiq complex (1:1 and 2:1, complex:DNA) and palladium ibiq complex (1:1) is shown in *Fig. 3.51*. In lane 1 containing the annealed telomeric DNA alone, one band can be seen corresponding to the formation of a G-quadruplex. Lane 2 shows the two bands formed when the DNA is treated with one equivalent of the palladium complex; one corresponding to the G-quadruplex alone and a much lighter band above indicating that a small amount of the palladium complex has bound to the quadruplex lowering its electrophoretic mobility. When treated with one equivalent of platinum complex in lane 3 the darker band is now the slower moving band with very little G-quadruplex alone band visible. This indicates as with the CD and FID experiments that the platinum complex is a better G-quadruplex binder than the palladium complex. The control G-quadruplex DNA treated with DMSO in lane 4 displayed only one band as lane 1 did ruling out any significant contribution of the DMSO to the electrophoretic mobility of the DNA. Finally in lane 5 two equivalents of the platinum complex were added to the quadruplex to investigate the binding stoichiometry of the complex to the DNA. The same bands were produced in both lanes 3 and 5 indicating that only one complex:DNA species is produced. The addition of more complex doesn't appear to form higher ratios of complex:DNA as this would have produced a slower moving band in the gel as the size of the species has increased.
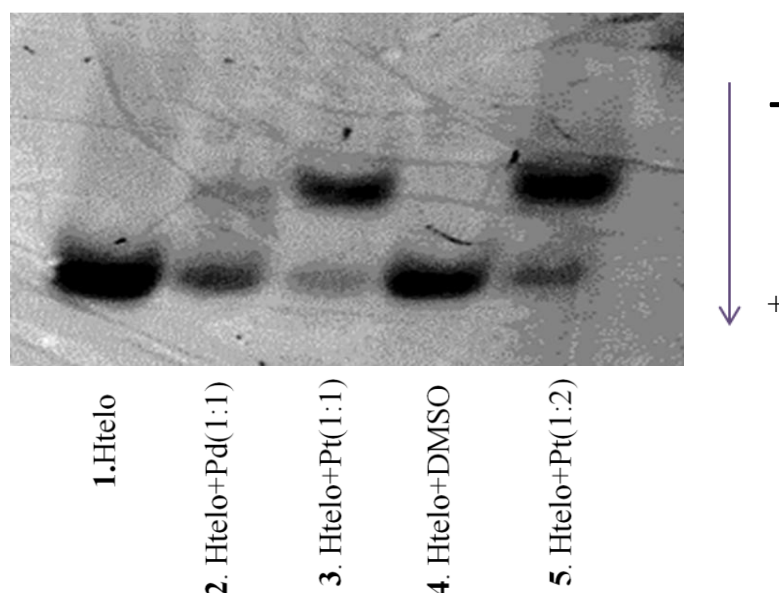
Figure 3.51 UV picture of PAGE (15% polyacrylamide) at 25°C showing the migration of htelo through the gel alone and when mixed with the platinum complex (Pt = [Pt(ibiq)$_2$][PF$_6$]$_2$) and the palladium complex (Pd = [Pd(ibiq)$_2$][BF$_4$]$_2$). Lanes 3 and 5 show the appearance of a new slower migrating band indicative of complex-quadruplex binding.

As a further check to confirm that the presence of the slower band in the gel was caused by the complex binding to the htelo G-quadruplex each of the spots on the DNA were extracted using a crush and soak technique (see *Experimental*). A solution of each spot on the gel was examined by UV-vis absorbance spectroscopy in order to link the presence of the complex with the DNA band on the gel. The complex alone would not be able to move through the gel as it lacks the negative charge of the DNA. Therefore for the complex to be seen with the DNA some form of interaction must be occurring between the two species. This method can only be qualitative as it is difficult to extract all of the DNA from the gel. In *Fig. 3.52 and 3.53* the UV-vis spectra of the slower and faster migrating bands through the gel can be seen respectively. When the slower bands were analysed the platinum complex could clearly be seen in lanes 3 and 5 indicated by the CT peak seen at 388 nm (see Chapter 3.5.2 for original UV-vis spectroscopy analysis). The presence of a

peak around 260 nm could also be observed for lanes 3 and 5 arising from the DNA. In lane 2, where a very faint band appeared after treating the DNA with the palladium complex, a very small amount of DNA can be seen when compared to the blank control taken of a random piece of the gel the experiment was conducted on. This indicates that a small amount of binding may have occurred however the concentration is so weak the palladium UV-vis trace cannot be seen.
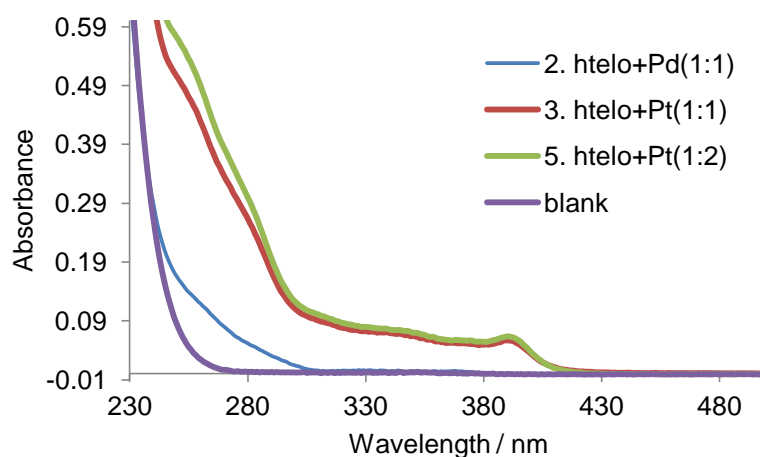

Figure 3.52 Overlaid UV-vis spectra recorded from the slower migrating bands in the gel in *Fig. 3.51*. 2, 3 and 5 correspond to the lanes where a band was present. The spectra match with platinum complex for lanes 3 and 5 indicating that it has bound to the htelo quadruplex.

The faster migrating bands when analysed in the same way saw no metal complex presence in any of the lanes, which was expected as any complex binding would cause the migration across the gel to slow when compared with the G-quadruplex alone. Lane 1 clearly shows the UV peak corresponding to the DNA around 260 nm, lanes 2 and 4 show the presence of DNA again but at a much lower concentration which is a result of the extraction process which is not quantifiable. More importantly very little DNA can be seen in lanes 3 and 5 as they look very similar to the UV-spectrum obtained for the blank control which

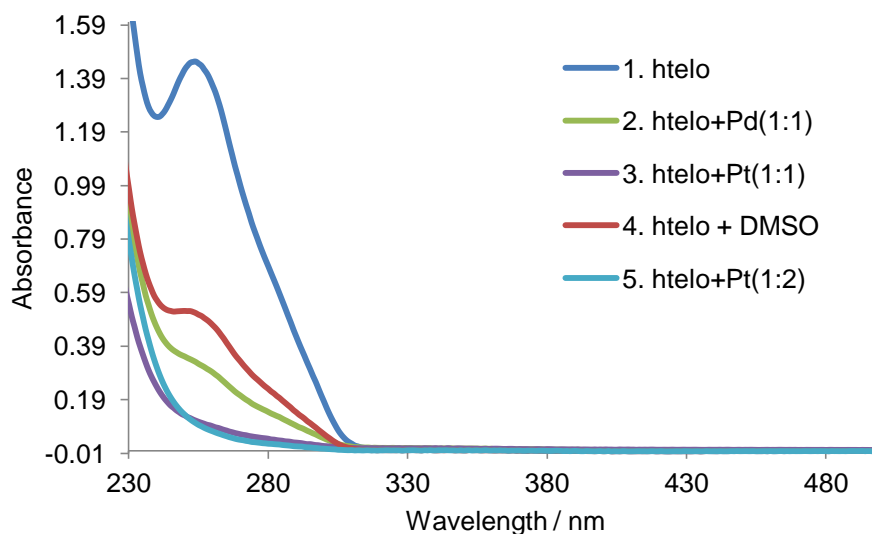indicates that all of the DNA is bound to the platinum complex which migrates slower through the gel.

Figure 3.53 Overlaid UV-vis spectra recorded from the faster migrating bands in the gel in *Fig. 3.50.* 1, 2, 3, 4 and 5 correspond to the lanes where a band was present. DNA found in lanes 1, 2 and 4 however no peak corresponding to DNA could be seen in lanes 3 and 5 which had been treated with the platinum complex indicating that the majority of DNA must be bound to complex in the slower migrating band.

Competitive PAGE Experiments - Work carried out by Hannah Pritchard at the University of Birmingham

Platinum complex, htelo and ds26

Further PAGE experiments were conducted at the University of Birmingham where a competitor in the shape of the duplex forming DNA, self complementary ds26, was used. Both types of DNA (htelo and ds26) were treated with the complex individually and also as a mixture in order to determine whether the complex would preferentially bind to one form of DNA over the other; the results of this PAGE experiment can be seen in *Fig. 3.54*. The duplex DNA ds26 alone is in lane 1 where two bands can be seen; the slower migrating one being that of the duplex form and the faster migrating band is the single stranded form. In lane 3 ds26 has been treated with one equivalent of the platinum

complex causing the slower migrating band to become more diffuse as it moves more slowly through the gel after interacting with the complex. Lane 2 shows the htelo quadruplex DNA which is assumed to be in its quadruplex form and lane 4 shows the quadruplex DNA with the platinum complex and the formation of a new band indicating complex-quadruplex binding. A mixture of both types of DNA can be seen in lane 5 and in lane 6 with the addition of the platinum complex. The quadruplex-complex band can again be seen in the same place as with htelo DNA alone indicating that the presence of ds26 has not prevented this interaction. More importantly when comparing the duplex band of the ds26+complex with the ds26+complex+htelo DNA the same diffuse band is not observed and it appears as it did without the complex present indicating that the complex is binding to the quadruplex DNA over the duplex ds26 DNA. However the fact that the ss DNA (single stranded DNA) and platinum complex+htelo run at a similar position makes quantification impossible.
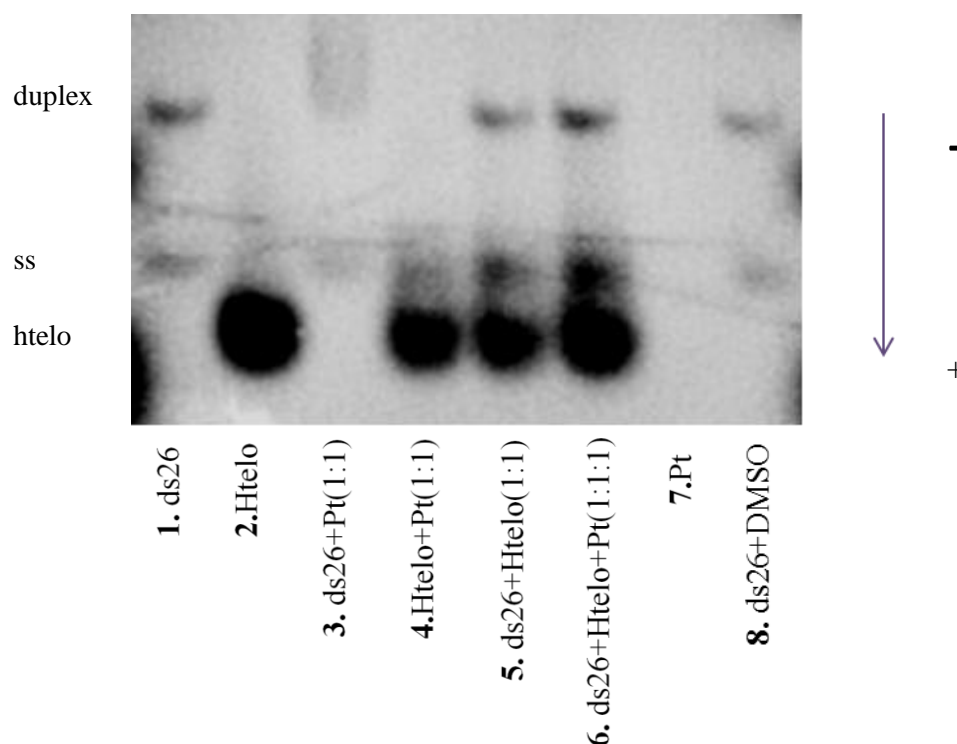

Figure 3.54 UV picture of PAGE (15% polyacrylamide) at 25°C showing the migration of htelo and ds26 when mixed with the platinum complex (Pt = [Pt(ibiq)$_2$][PF$_6$]$_2$).

Platinum complex, c-myc and ds26

When the same experiment was carried out with c-myc DNA a similar result was obtained as for the htelo DNA (*Fig. 3.55*). In lane 5 where there is a mixture of the two types of DNA, two bands are seen; the slower being that of the duplex ds26 and the faster band is a mixture of the quadruplex DNA and the single stranded ss26. Lane 6, which contains c-myc DNA, ds26 and the platinum complex, sees the emergence of three bands where the duplex form of ds26 matches that without the complex added (lane 1) and the c-myc bands can be matched with the c-myc+complex lane 4 indicating that the platinum complex binds to c-myc DNA over duplex DNA.
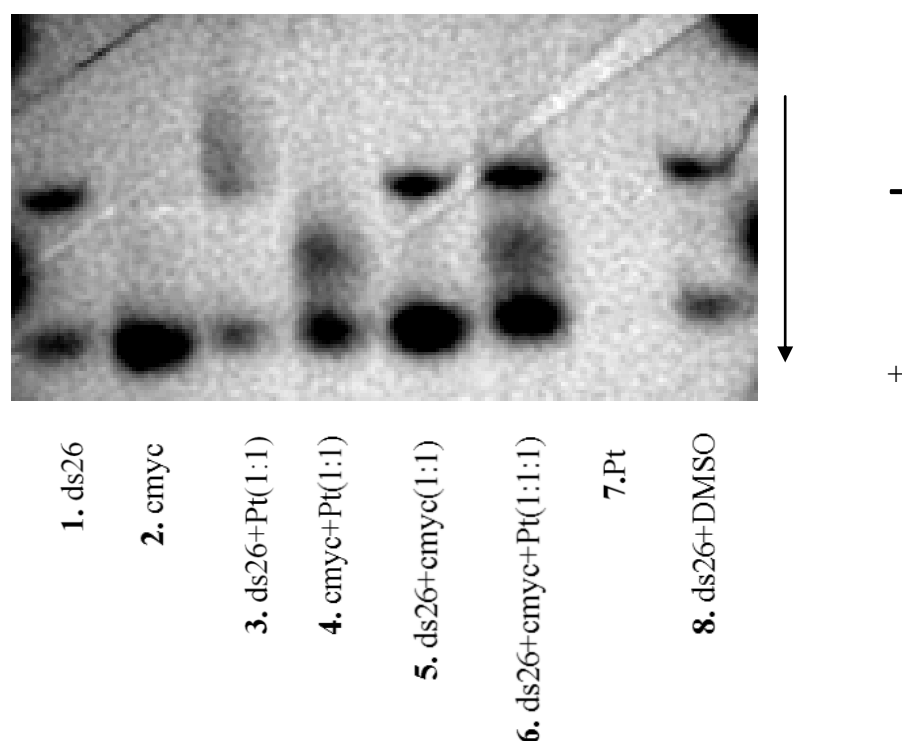

Figure 3.55 UV picture of PAGE (15% polyacrylamide) at 25°C showing the migration of c-myc and ds26 when mixed with the platinum complex (Pt = [Pt(ibiq)$_2$][PF$_6$]$_2$).

The co-running of ss26 and the c-myc DNA again prevent quantification however an attempt at quantification was still made in order to get an idea of the amount of quadruplex

DNA in its bound state. This was achieved using the software ImageJ where the gel analysis tool was used to obtain the ratio of ss to ds in lane 8. The software is able to display the density of the bands and plots distance in pixels versus grey value producing a series of peaks from which the area can be calculated. After calculating the ratio of ds to ss DNA (which came out as 1:1) the ratio was applied to lane 6 where the known area of the ds26 peak allowed the area of the hidden ss26 peak to be calculated. This value was then subtracted from the area of the quadruplex combined with the ss26 band to give the area of the quadruplex only. The area of the band corresponding to the quadruplex and complex was then added to the area of the quadruplex (G_4) alone to give the total area of quadruplex DNA which should equate to 100 μM. Dividing the concentration by the total area and then multiplying by the individual areas gave a 42 μM result for unbound G_4 and 58 μM for complex bound G_4 indicating that 58 % of the c-myc DNA interacts with the complex in the presence of ds and ss 26 DNA (for data see Appendix 3).

3.8   Förester Resonance Electron Transfer (FRET) using Complexes 5 and 7

Work in collaboration with Dr. D. Rusling and Prof. K. Fox of the University of Southampton - Experiments prepared and conducted by Hannah Pritchard and D. Rusling.

FRET can be used to investigate the distances between two different sites on a macromolecule such as DNA. One part of the structure can be labelled with a donor whilst another part can be labelled with an acceptor. The transfer efficiency between the donor and acceptor units can be monitored by measuring the quenching of the donor by the acceptor.[43] In order for FRET to occur the emission spectrum of the donor must overlap

with that of the acceptor with the efficiency of this process depending on the degree of overlap, donor and acceptor orientations and distance, and donor quantum yield.[43]

The phenomenon of fluorescence resonance energy transfer can be explained by considering what happens to a molecule when it absorbs light. At the correct energy corresponding to the energy gap between its ground and excited states the molecule is excited from its ground state (S_0) to its excited singlet state (S_1) (*Fig. 3.56*).[42] Although many excited states are open to the donor most of the emission occurs from the S_1 state due to rapid vibrational relaxation by internal conversion from the other energy states.[42] The excited donor under circumstances where an acceptor isn't present within range could then return to the ground state resulting in fluorescence.[43] When an acceptor is within range (10 - 90 Å away) the excited donors' energy can then be transferred non-radiatively to the acceptor fluorophore.[42] This energy transfer is possible when the energy of the $S_1 \rightarrow S_0$ emission from the donor matches with the $S_0 \rightarrow S_1$ energy gap of the acceptor.[42] The excited acceptor can then return to the ground state with the observance of fluorescence.
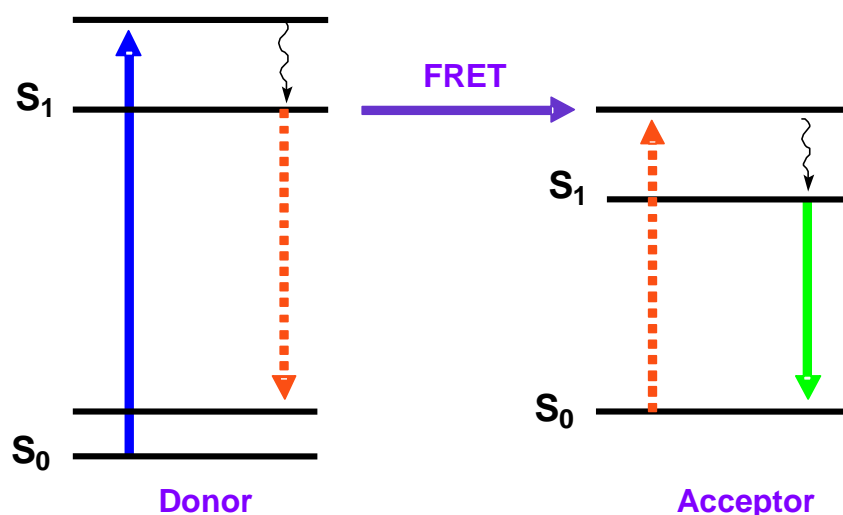

Figure 3.56 Jablonski diagram showing the absorption, vibrational relaxation, non-radiative transfer and emission steps involved in FRET.

Manipulating FRET systems can be advantageous as fluorescence detection is very sensitive therefore will only require small amounts of labelled product. The energy transfer between a donor and an acceptor occurs over a short timescale (nanosecond) and can be applied over a range of distances.[42] The technique can be used to investigate the secondary structure (G-quadruplex) of guanine rich DNA sequences that have been labelled with the donor 6-carboxyfluorescein (FAM) at the 5' end and the acceptor 6-carboxytetramethylrhodamine (TAMRA) at the 3' end.[2]

6-Carboxyfluorescein

6-Carboxytetramethylrhodamine
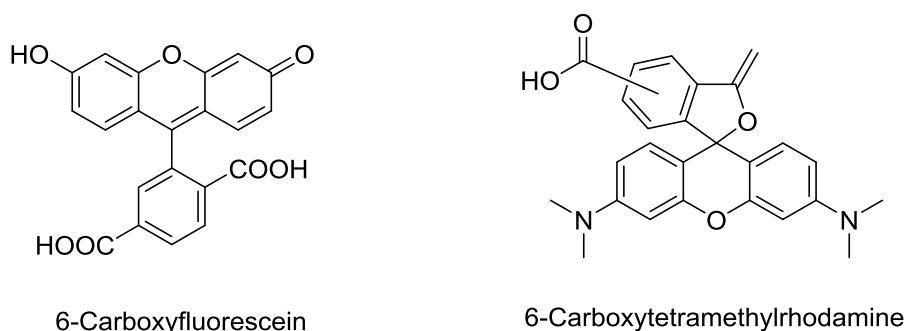
Figure 3.57 Chemical structures of FAM (6-carboxyfluorescein) and TAMRA (6-carboxytetramethylrhodamine.

The labelled DNA strand is annealed in the presence of a cation such as potassium and left to cool slowly allowing the most thermodynamically stable G-quadruplex to dominate. When the DNA is folded in its quadruplex form the two fluorophores, FAM and TAMRA will be relatively close to each other allowing FRET to occur. The fluorescein is excited around 490 nm and its emission is recorded at 530 nm which is monitored throughout the experiment with the use of a Roche Lightcycler.[2] TAMRA emits at 588 nm which could only be monitored at 640 nm using the same machine.[2][40] The temperature of the DNA sample will then be gradually increased between 25 °C to 95 °C which will cause the DNA to unfold. When the quadruplex melts becoming a single strand once more the donor and

acceptor (FAM and TAMRA) will be far apart in space from each other hindering any FRET (*Fig. 3.58*). This can be detected by observing an increase in the fluorescence of the donor as non-radiative transfer to the acceptor is prevented.[42] If a G-quadruplex binding ligand is added and the system requires higher temperatures to unfold the quadruplex, the ligand is deemed able to bind to and stabilise a G-quadruplex. The extent of the melting temperature change denotes the stabilising strength of the binding ligand. The melting temperature or T_m can be taken as the half way point on the melting curve where 50 % of the DNA is denatured (*Fig. 3.59*). A more accurate determination can be achieved by plotting the first derivative of the melting curve.[2]
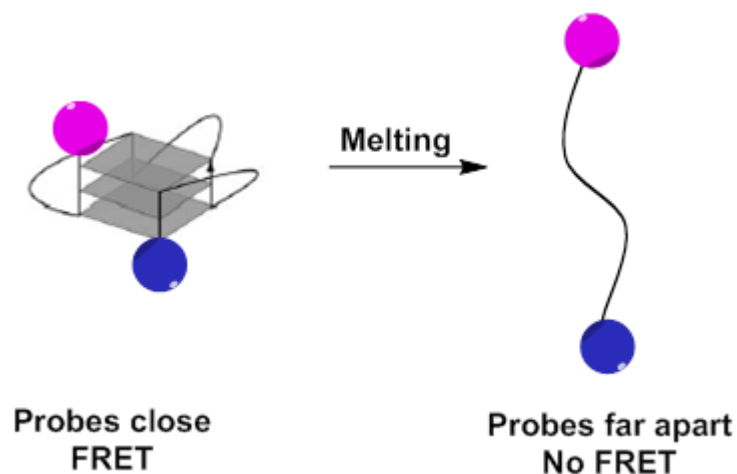

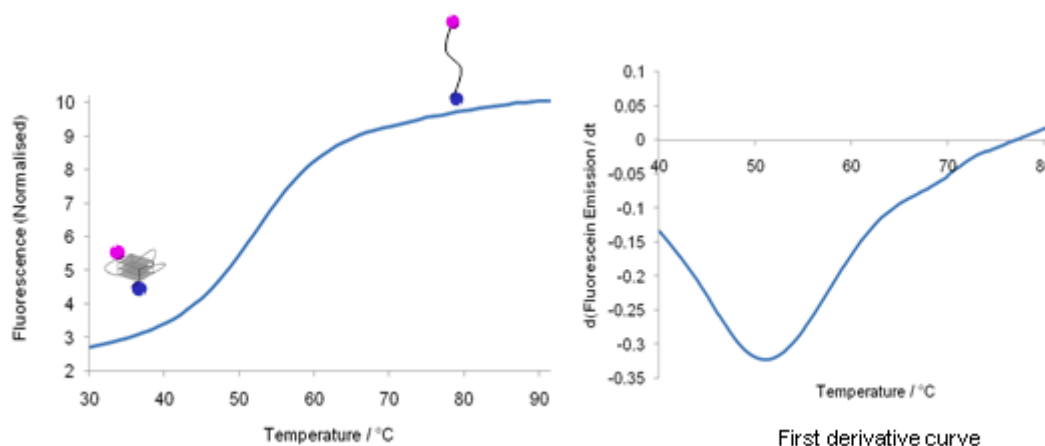*Figure 3.58* Folding of a labelled quadruplex forming oligonucleotide.

Figure 3.59 General melting curve and first derivative of the melting curve that are produced by performing FRET melting experiments.

The htelo DNA sequence used in the experiments was chosen as it has been frequently reported in the literature to evaluate the folding of guanine rich oligos in the presence of compounds such as terpyridine and bis-indolecarboxamides (reported by Teulade-Fichou and Balasubramanian respectively).[2][26] It has a melting temperature between 50 - 55°C that allows complete folding at lower temperatures and the analysis of stability within a viable temperature range when G-quadruplex stabilising complexes are added (quadruplex systems that are too stable will not melt within the measureable range). It also offers a comparison of FRET melting temperatures with other G-quadruplex binding complexes currently in the literature.

F21T: 5'-*FAM* - **GGGTTAGGGTTAGGGTTAGGG** - *TAMRA*-**3'** (htelo)
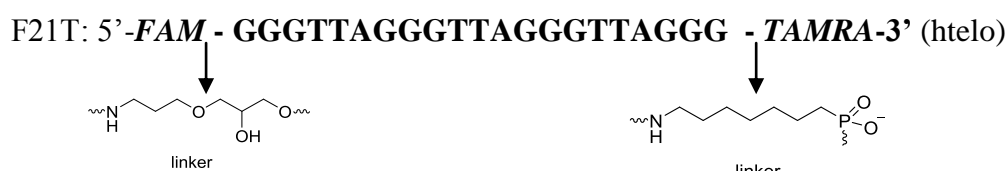
The duplex competitor ds26 (self complementary strand) will also be used in the FRET melting experiments which has a higher melting temperature (70 °C). If the presence of the competitor results in a decrease in melting temperature when with the complex and the

207

labelled quadruplex forming oligo (when compared with the system without the competitor); it is possible that the complex is binding to the duplex DNA instead of the quadruplex. The complex is no longer stabilising the G-quadruplex hence the labelled oligo unfolds at a lower temperature.

The ability the palladium and platinum ibiq complexes to stabilise the quadruplexes formed by the dual labelled htelo sequence was investigated using the FRET melting assay. Both of the complexes required DMSO-H_2O mixtures in order to fully dissolve them and to ensure accurate melting temperatures were recorded, each experiment was carried out with two sequences of melt and anneal stages which were repeated three times. A DNA concentration of 0.25 μM was treated with a range of complex concentration between 0.1 - 2.0 μM. The solvent alone did not affect the melting temperature of the DNA.

3.8.1 [Pd(ibiq)₂][BF₄]₂ FRET Melting Curves with htelo (F21T)

The stabilisation effect the palladium ibiq complex had on G-quadruplexes formed with htelo DNA was very little. Observation of the melting curve in *Fig. 3.60* shows little movement of the curve with increasing amounts of the complex and in the first derivative plot of the curve in *Fig. 3.61* the change in melting temperature (ΔT_m) is only 2°C at 2 μM, with a T_m of 54.1 °C. The results of the FRET melting experiment indicate that the palladium complex is a poor G-quadruplex stabiliser. They also suggest that the complex may be quenching the fluorescence by binding to the fluorophores (see insert in *Fig. 3.60*) as the emission signal seen decreases as the complex concentration increases. Thus introducing the fluorophores may have created a competitor binding site.
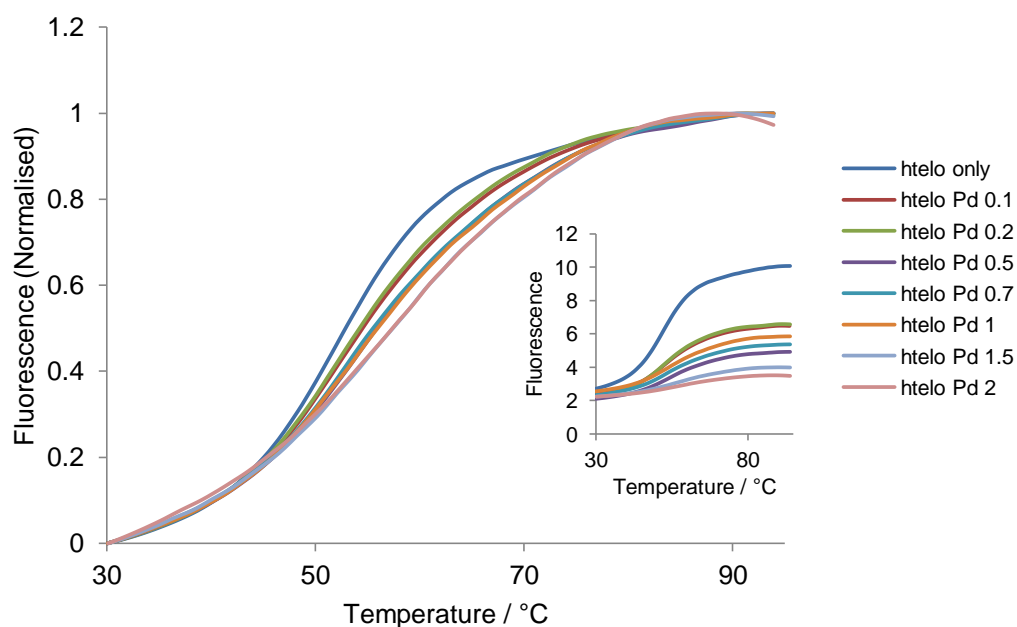
Figure 3.60 FRET melting curve generated from 0.25 μM of htelo DNA with different concentrations of the palladium complex (μM). Inset image shows the raw data where a decrease in emission intensity can be seen as the concentration of the complex increases.
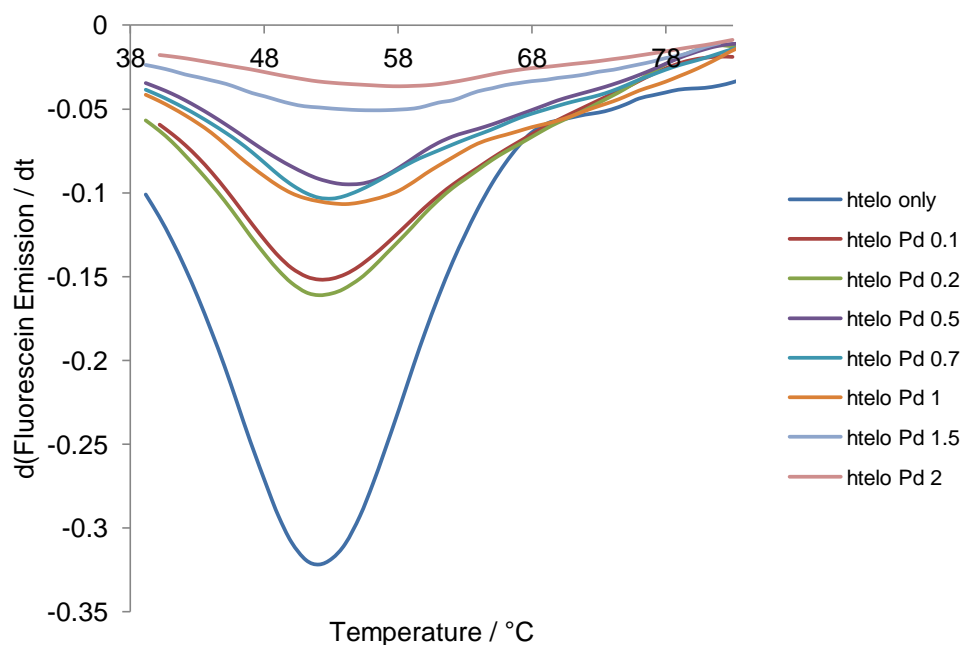

Figure 3.61 First derivative plot of the palladium melting curves where the peaks represent the melting temperature T_m.

3.8.2 [Pt(ibiq)$_2$][PF$_6$]$_2$ FRET Melting Curves with Htelo (F21T)

The platinum complex, after initial observation of the normalised melting curve (*Fig. 3.62*), appears to stabilise the G-quadruplex formed by the labelled oligo as the curve shifts to higher temperatures when the concentration of complex increases. There is however, as for the palladium complex, a quenching of fluorescence upon each sequential addition of the complex making the effect more difficult to see. Further analysis of the melting curve shows very little movement with increasing amounts of the complex in the first derivative plot (*Fig. 3.63*), where ΔT_m is 2°C at 2 μM, with a T_m of 54. 1 °C. Interestingly however, there is another peak which emerges after 0.7 μM of the complex has been added to the DNA whose apex cannot be seen as it is out of range of the recorded temperature range (>83°C). The appearance of this peak could be the consequence of another highly stabilised quadruplex structure which forms alongside the other quadruplex with a melting temperature of 54.1 °C in a biphasic transition.
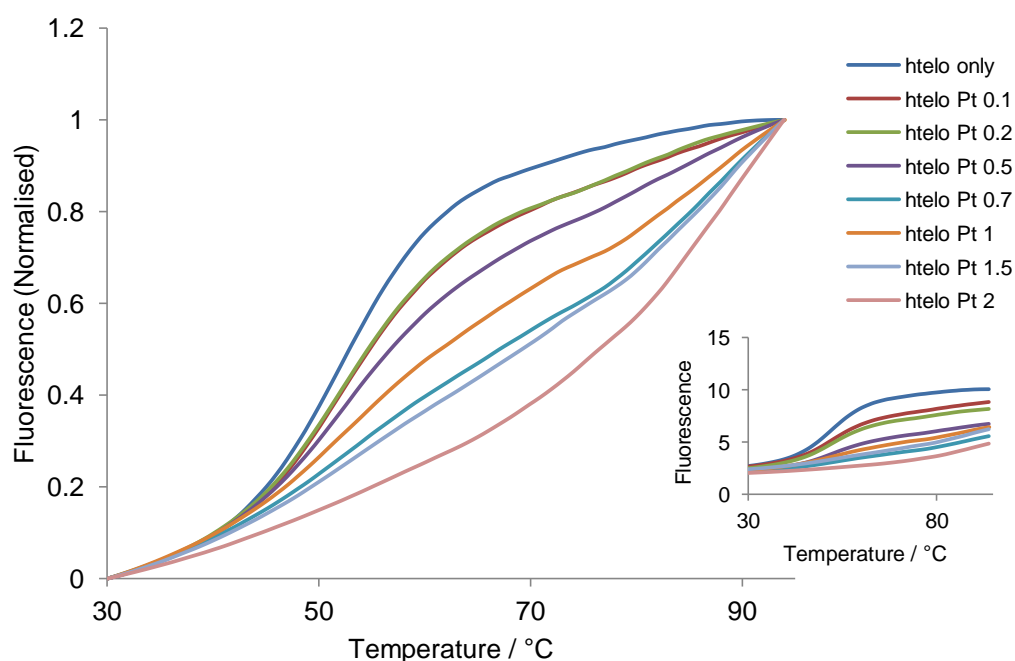

Figure 3.62 FRET melting curve generated from 0.25 μM of htelo DNA with different concentrations of the platinum complex. Inset image shows the raw data where a decrease in emission intensity can be seen as the concentration of the complex increases.
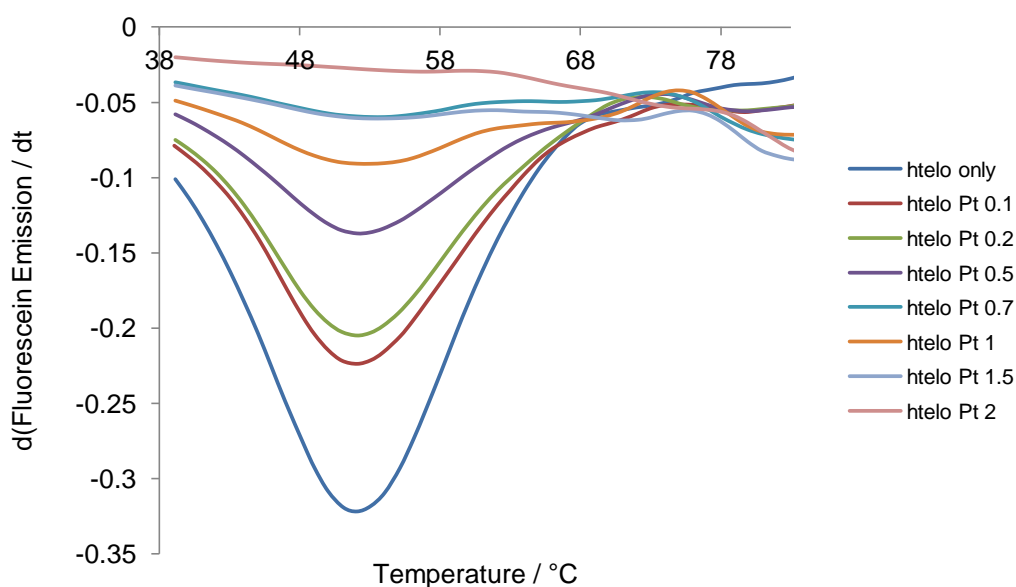
Figure 3.63 First derivative plot of the platinum melting curves where the peaks represent the melting temperature T_m.

3.8.3 Competitor ds26 Addition

At a complex concentration of 1 μM, 10 μM of ds26 (duplex forming DNA) was added in order to assess how or if the FRET melting would change in its presence. The results were ultimately disappointing for both complexes as both complexes saw a decrease in T_m when in a solution with duplex DNA. Chart (**a**) in *Fig. 3.64* shows the effect of duplex DNA addition to the palladium complex and labelled oligo mix where very little change has occurred to the melting curve of the two systems. A new melting temperature of 52.1 °C ($\Delta T_m = -2$ °C) was recorded for the palladium complex with the additional duplex. In chart (**b**), for the platinum complex, the same change of melting temperature, $\Delta T_m = -2$ °C to 52.1 °C, occurs and the biphasic peak ~85 °C no longer appears in the first derivative plot of the melting curve.
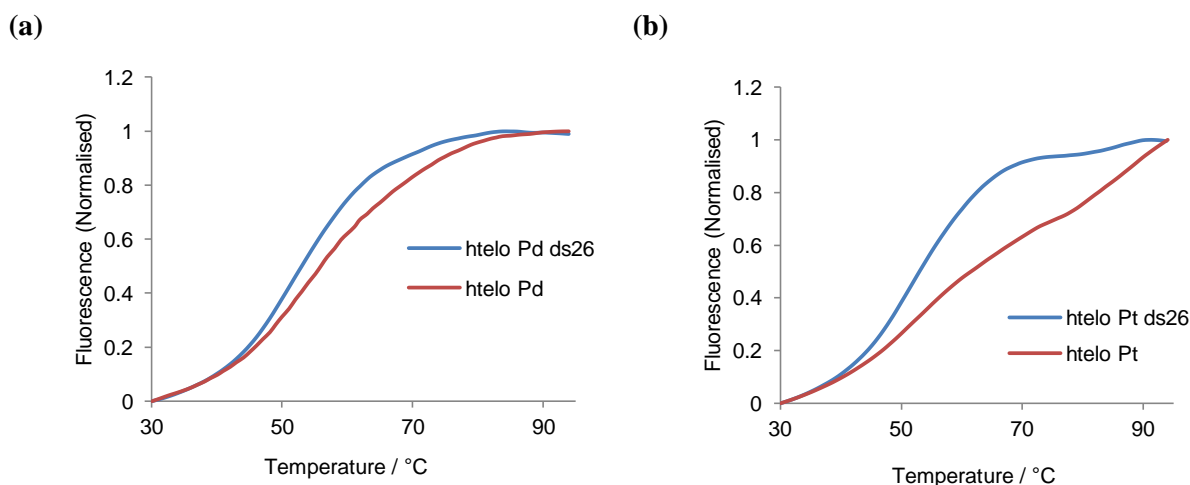
(a)

(b)

Figure 3.64 FRET melting curves of; **a.** Palladium complex (1 μM) with htelo DNA (0.25 μM) compared with the palladium complex (1 μM) with both htelo (0.25 μM) and ds26 DNA (10 μM), **b.** Platinum complex (1 μM) with htelo DNA (0.25 μM) compared with the platinum complex (1 μM) with both htelo (0.25 μM) and ds26 DNA (10 μM).

Both complexes exhibit π stacking surfaces therefore the possibility of fluorophore quenching is enhanced as the fluorophores also possess large aromatic surfaces which the stacking ibiq complex could interact with. This may be the reason why the stabilisation abilities of the complexes do not live up to the ΔT_m values of 29.5 °C and 17.3 °C reported by Vilar and Teulade-Fichou for their metal based salphen and terpyridine complexes respectively.[15][22] As with all DNA binding experiments the response to complex-DNA binding activity is more pronounced for the platinum complex suggesting the platinum complex binds more favourably to quadruplexes than the palladium complex.

3.9 Conclusions

Presented in this chapter were the binding abilities of the synthesised palladium, platinum, rhenium and rhodium ibiq complexes to different types of DNA (quadruplexes and duplexes). The extent of response seen is influenced by the geometry of the complex with

the octahedral rhenium complex showing very little DNA interaction and the square planar palladium, platinum and rhodium complexes giving more positive indications of binding.

The palladium and rhodium complexes showed good stabilities with the ct-DNA when examined by UV, compared with their less stable nature without the DNA presence, indicating that complex-DNA binding was occurring for these two complexes. The platinum and rhenium complexes showed good stability results without the DNA which didn't change on the addition of the ct-DNA.

Circular dichroism was used to investigate how each complex interacts with ct-DNA, htelo DNA, c-myc DNA and in some cases ds26 DNA. The palladium complex showed a strong ICD response with both the ct-DNA and the htelo DNA in all buffer conditions. It didn't however produce such a response when titrated into c-myc DNA and hence shows a degree of selectivity for antiparallel hybrid quadruplexes over parallel conformers. The platinum complex interacted well with all types of duplex and quadruplex DNA with a negative ICD response seen for the c-myc interaction indicating that the mode of interaction with quadruplexes is end stacking. The rhenium complex showed no response to either duplex or quadruplex DNA by CD and after examination using LD, which also yielded no induced signal, was investigated no further.

Fluorescent indicator displacements (FID) and PAGE experiments were used to try to assess the selectivity of the palladium and platinum complexes for one type of DNA over another. The platinum complex was able to displace the fluorescent indicator (thiazole orange) at fairly low concentrations (< 0.5 μM) from htelo and c-myc quadruplex DNA.

Displacement from duplex DNA however took considerably higher complex concentrations demonstrating the potential lack of binding affinity the complexes have for duplex DNA. In the PAGE experiments when both types of DNA (quadruplex and duplex) were in a mixture the platinum complex could be seen to bind to the quadruplex DNA causing the formation of a new band in the gel without causing the dispersion of the duplex band which occurred when the duplex DNA was subjected to the complex alone.

The palladium and platinum complexes bind to both duplex and quadruplex DNA, the platinum complex binding very well. The bulky nature of the ibiq ligand was hoped would prevent duplex interaction as it is too big to intercalate however it is possible that the complexes are binding directly to the bases instead. LD however, suggests that intercalation may be occurring between the palladium complex and duplex DNA. End stacking is the proposed binding mode that is occurring between the platinum complex and the quadruplex DNA as evidenced by the strong ICD signal and the large red shifts seen in the UV-vis spectroscopy titrations. For the palladium complex this is a little less clear as it interacts differently with each of the quadruplexes. Coordinative loop binding is a possible binding mode which may explain the CD results where a stronger response is seen for the antiparallel hybrid quadruplex over the parallel conformer.

3.10 Experimental

General Methods

In all of the DNA binding studies Ultrapure water (18.2 MΩ) purchased from Fisher Scientific was used to carry out the experiments. Calf thymus DNA (ct-DNA) was

purchased from Sigma Aldrich. The htelo, c-myc and ds26 oligos were bought from Eurofins and the pBR322 plasmid DNA from New England Biolabs. All types of DNA were kept frozen until use. The Tris-acetate-EDTA and Tris-HCl buffer were purchased from Fisher and agarose from USB Corporation. The DNA oligonucleotides were purified using a NAP column (packed with Sephadex G-25 DNA Grade) before using in the NMR studies. UV-Vis spectra were recorded on a Varian Cary 5000 UV-Vis spectrometer.

Circular Dichroism Experiments

ct-DNA

A Jasco J-810 spectropolarimeter was used to record the CD measurements of the titration mixture contained within a quartz cuvette with a pathlength of 1cm (750-200 nm). Ct-DNA was prepared in a stock solution of 3000 μM which was kept frozen until the day of use. A 300 μM solution of DNA was required for carrying out the experiment which was made by diluting the stock solution with sodium chloride (1 M) and sodium cacodylate ($Na(CH_2)_2AsO_2.3H_2O$) buffer stock solutions, resulting in a 20 mM sodium chloride and 1 mM sodium cacodylate solution (pH 6.8). Accurate DNA concentrations were determined by UV-Vis analysis using the molar extinction coefficient of $\varepsilon_{260} = 6600$ mol^{-1}dm^{3}cm^{-1} calculated per DNA base. In total three solutions are required to conduct the CD titrations which are; solution A (300 μM of ct-DNA which contains sodium cacodylate (1 mM) and sodium chloride (20 mM)), solution B (600 μM ct-DNA which contains sodium cacodylate (2 mM) and sodium chloride (40 mM)) and solution C (500 μM of complex solution). When carrying out the titration a CD spectrum is initially recorded of solution A and then to this equal volumes of solution B and solution C are added. This keeps the ct-DNA

concentration constant over the course of the experiment whilst increasing the complex concentration from a DNA:complex ratio of 60:1 to 3:1.

htelo, c-myc and ds26 DNA

The titrations using the shorter oligos were carried out in a similar way to the ct-DNA titrations however the DNA concentration for each oligo was calculated per strand instead of per base. The UV-Vis molar extinction coefficients for the oligos htelo, c-myc and ds26 are as follows; ε_{260} = 228000, 231000 and 414000 (duplex) $mol^{-1}dm^{3}cm^{-1}$ and they were made into 3 μM solutions in 10 mM Tris-HCl with either 100 mM KCl, 100 mM NaCl (pH 7.4) or no other metal ions depending on the salt condition used (solution A). Prior to recording their concentration they were annealed at 95 ℃ for 5 minutes. Solution B was a 6 μM DNA solution with 20 mM Tris-HCl and 200 mM of the required salt and solution C was a 150 μM complex solution.

Linear Dichroism Experiments

A flow couette cell (Krometek) with a 0.1 cm pathlength was used to carry out the LD experiments. They were carried out with ct-DNA only following the same method as that for the CD measurements with the same solutions of A, B and C.

Fluorescent Indicator displacements

Experiments were carried out using a Shimadzu spectrofluorimeter in a 3 ml quartz cuvette with a 1 cm pathlength. Htelo, c-myc and ds26 oligos were used in the experiments and prior to carrying out the titration they were diluted to 0.25 μM in a 10 mM Na cacodylate (pH 7.4) solution with 100 mM KCl and then annealed to 95 °C before leaving to cool to

room temperature. A 1 mM stock solution of thiazole orange was prepared in milliQ water which was then diluted to the corresponding concentration with 10 mM Na cacodylate solution. $[Pd(ibiq)_2][BF_4]_2$ and $[Pt(ibiq)_2][PF_6]_2$ solutions were made by diluting 1000 μM DMSO stock solutions with the 10 mM Na cacodylate solution to 20 μM. The concentrations of TO required for each type of DNA (all at 0.25 μM) are as follows: htelo - TO = 0.5 μM, c-myc - TO = 0.5 μM and ds26 - TO = 0.75 μM. Competitive displacements of the TO resulted in a ratio of 2:1 for quadruplex DNA and 3:1 for ds26 (TO:DNA).[19] These ratios favour the occupation of one binding site for the quadruplex DNA and two binding sites for ds26 helping to prevent the formation of mixtures of complexes in solution.[19]

To conduct the experiment the DNA and TO mixture are placed in the cuvette before adding increasing amounts of the complex being investigated (0.12 to 10 μM, which is 0.5 to 40 equivalents). After each addition of complex the mixture was left to equilibrate for 3 minutes before recording an emission spectrum between 510 and 700 nm, exciting at 501 nm. The trapezium rule[44] was used to calculate the fluorescence area after each titration which was then converted into TO % displacement using % TO displacement = 100 - [(fluorescence area of sample/fluorescence area of DNA+TO alone) × 100].

UV-Vis Absorption Spectroscopy Titrations

The htelo and c-myc oligos were made into 300 μM solutions in 10 mM Tris-HCl / 100 mM KCl and annealed to 95 °C before use (solution B). The complexes were diluted to 7 and 14 μM solutions also using 10 mM Tris-HCl (pH 7.4) / 100 mM KCl (solution A and solution C). Blank solutions were also made up to run alongside the DNA into complex

titration in order to subtract the DNA peaks from the complex spectra. The experiment was carried out by placing solution A into a 1 ml cuvette and titrating in solutions B and C in equal amounts in order to keep the complex concentration constant. The concentration of DNA was increased from 60:1 to 0.2:1. All UV-Vis spectra were recorded on a Varian Cary 5000 UV-Vis spectrometer.

1D ^{1}H-NMR and DOSY Experiments

DNA:complex NMRs were run in shigemi tubes on a Bruker AV700 instrument. 100 μM of the purified htelo DNA was prepared in a 50 mM KCl, 15 % d_6-DMSO solution (and then annealed before use) which was kept constant in all the experiments. The platinum complex was prepared using the same conditions, without annealing. The proton spectra were recorded with a sweep width of 25 ppm, an acquisition time of 0.5 s, WATERGATE water suppression and 35 k scans. The data was processed using the Bruker NMR software and analysed using TOPSPIN.

Agarose Gel Electrophoresis

To create the agarose gel 2 grams of agarose was heated in 1x Tris-acetate-EDTA buffer. Once fully dissolved the solution was then poured into a gel tray measuring 210 × 150 nm, with a 15 tooth comb already in place enabling the formation of sample wells, before leaving to set for 30 minutes. The pBR322 plasmid DNA was prepared in a 93.3 μM solution and the complexes made into 60 μM stock solutions (also containing 15 % DMSO for the platinum and palladium complexes). The two lots of solutions (DNA and complex) were then mixed together in ratios ranging from 100:1 to 2:1. The samples were then left for 2 hours at room temperature before adding 4 μl of loading buffer (30% glycerol, 0.25%

bromophenol blue) and mixing again. They were then loaded into the gel wells, transferring 16 μl into each. An electric potential was then applied to the gel in an electrophoresis submarine kit (Amersham Biosciences HE99X) submerged in 1 × Tris-acetate-EDTA running buffer using an electrophoresis power supply-EPS 301 system set at a constant voltage of 120 V and 400 mA. The gel was run for 3 hours after which time the gel was stained with a solution of ethidium bromide (0.5 mg ml^{-1}, 200 ml) and left for a further 20 minutes. The gel was then visualised using a UVtec-uvipro platinum 2.0 camera at a wavelength of 312 nm.

Polyacrylamide Gel Electrophoresis (PAGE)

Polyacrylamide gel preparation

52.5 ml of ultra pure water, 10 ml of 10 × TB buffer (890 mM tris(hydroxyl)amino methane and 890 mM boric acid) and 37.5 ml of 40 % acrylamide (29:1) were mixed together to form the basis of a 15 % native polyacrylamide gel. Potassium chloride was also added to achieve a concentration of 50 mM. To initiate the cross linking which solidifies the gel 500 μl of 10% (w/v) ammonium persulfate and 75 μl tetramethylenediamine (TEMED) were added before pouring onto a set of glass plates and leaving to set for 40 minutes. Once the gel had polymerised the wells were washed with running buffer and pre-run at 200 V for 5 minutes before starting the experiment with the samples.

PAGE electrophoresis experiment

Solutions of htelo, c-myc and/or ds26 with the complexes were prepared in TBN buffer (89 mM tris(hydroxymethy)amino methane, 89 mM of boric acid and 100 μM KCl) to give

100 µM DNA and complex solutions (to be used together in a 1:1 ratio). 15 % DMSO solutions were required to fully dissolve the complexes. When the competitor DNA was used the ratio of ds26:quadruplex DNA:complex was 1:1:1. The sample solutions were left to equilibrate for 1 hour at room temperature. Before the samples were loaded into the gel 5µl of 30 % glycerol was added. Each well of the gel was then loaded with 13 µl of each sample. The gel was run for 5 hours at 120 V, 150 mA using Gel System equipment (Thermo Scientific UK) and then visualised using UV light. To perform the UV-vis experiments the DNA and complexes were extracted from the gel using a crush and soak technique where the gel bands containing the DNA are cut out using a razor blade under UV light and then suspended in 500 µl of the running buffer. The gel pieces were left over night on a rotating wheel before centrifuging to remove the gel pieces. The supernatant was then placed in a UV cuvette (0.1 ml) to measure its absorbance.

FRET Melting Experiments

A Roche Lightcycler 1.5 was used to run the experiments and the Roche Molecular BiochemicalsLightCycler Software Version 3 was used to process and analyse the data. The buffer used in the experiments was a 10 mM LiOH, 10 mM KCl, with H_3PO_4 pH 7.4. 1 µM stock concentrations of the labelled oligos were prepared and protected from the light and 20 µM complex solutions were prepared by diluting a 1 mM stock solution in DMSO with buffer. The competitor duplex DNA (ds26) was also prepared in a 20 µM concentration. The concentration of labelled DNA in each experiment was kept constant at 0.25 µM and treated with a range of complex concentrations from 0.1 µM to 10 µM. Using a Roche Lightcycler 1.5 holding 32 capillary tubes each containing 20 µl of sample, the fluorescence of the samples was measured every 1 °C from 30 - 95 °C. The experiment

consisted of a 1 hour slow melt followed by holding the temperature at 95 °C for 10 minutes before conducting a 1 hour slow anneal followed by holding the temperature at 30 °C for 10 minutes. The melting temperature of melting and annealing curves could then be compared to check for any sign of hysteresis. The fluorescence was recorded at wavelengths of 530 nm and 640 nm which monitors the increase in FAM emission and decrease in TAM fluorescence respectively.

3.11 References

1. T. Ou, Y. Lu, J. Tan, Z. Huang, K. Wong, L. Gu. *Chem. Med. Chem.*, 2008, **3**, 690.

2. A. De Cian, L. Guittat, M. Kaiser, B. Saccà, S. Amrane, A. Bourdoncle, P. Alberti, M. P. Teulade-Fichou, L. Lacroix, J. L. Mergny. *Methods,* 2007, **42**, 183.

3. J. Kypr, I. Kejnovska, D.Renciuk, M.Vorlıckova. *Nucleic Acids Res.,* 2009, **37**, 1713.

4. B. M. Bulheller, A. Rodger, J. D. Hirst. *Phys. Chem. Chem. Phys.,* 2007, **9**, 2020.

5. I. Warnke, F. Furche. *WIREs Comput. Mol. Sci.,* 2012, **2**, 150.

6. M. Vorlickova. *Chirality,* 2012, **24**, 691.

7. K. K. Patel, E. A. Plummer, M. Darwish, A. Rodger, M. J. Hannon. *J. Inorg. Biochem.,* 2002, **91**, 220.

8. K. M. Sovenyhazy, J. A. Bordelon, J. T. Petty. *Nucleic Acids Res.,* 2003, **31**, 2561.

9. M. Guéron, J.-Ph. Demaret, M. Filoche. *Biophys. J.,* 2000, **78**, 1070.

10. C. Bauer, A. Wang. J. Inorg. Biochem., 1997, **68**, 129.

11. A. I. S. Holm, L. M. Nielsen, S. V. Hoffmannc, S. Nielsend. Phys. Chem. Chem. Phys., 2010, **12**, 9581.

12. A. Rodger, I. S. Blagbrough, G.Adlam, M. Carpenter. *Biopolymers,* 1994, **34**, 1583.

13. J. Gu, J. Leszczynski. *J. Phys. Chem., A,* 2002, **106**, 529.

14. E. Largy, F. Hamon, F. Rosu, V. Gabelica, E. De Pauw, A. Guedin, J. Mergny, M. Teulade-Fichou. *Chem. Eur. J.,* 2011, **17**, 13274.

15. B. Norden, T. Kurucsev. *J. Mol. Recogn.,* 1994, **7**, 141.

16. A. Rodger, R. Marrington, M. A. Geeves, M. Hicks, L. de Alwis, D. J. Halsall, T. R. Dafforn. *Phys. Chem. Chem. Phys.,* 2006, **8**, 3161.

17. A. Rodger. *Circular Dichroism and Linear Dichroism.* Oxford University Press, Oxford, 1997.

18. D. Monchaud, C. Allain, H. Bertrand, N. Smargiasso F. Rosu, V. Gabelica, A. De Cian, J. L. Mergny, M. P. Teulade-Fichou. *Biochimie,* 2008, **90**, 1207.

19. J. Nygren, N. Svanvik, M. Kubista. *Biopolymers,* 1998, **46**, 39.

20. D. Monchaud, C. Allain, and M. P. Teulade-Fichou. *Nucleos. Nucleot. Nucl.,* 2007, **26**, 1585.

21. N. H. Campbell, N. H. Abd Karim, G. N. Parkinson, M. Gunaratnam, V. Petrucci, A. K. Todd, R. Vilar, S. Neidle. *J. Med. Chem.,* 2012, **55**, 209.

22. K. Suntharalingam, A. J. P. White, R. Vilar. *Inorg. Chem.,* 2010, **49**, 8371.

23. F. L. Thorp-Greenwood, M. P. Coogan, L. Mishra, N. Kumari, G. Rai, S. Saripella. *New. J. Chem.,* 2012, **36**, 64.

24. H. Chao, W. Mei, Q. Huang, L. Ji. *J. Inorg. Biochem.,* 2002, **92**, 165.

25. N. Shahabadi, S. Mohammadi, R. Alizadeh. *Bioinorg. Chem. Appl.,* 2011, **2011**, 1.

26. J. Dash, R. Nath Das, N. Hegde, G. Dan Pantos, P. S. Shirude, S. Balasubramanian. *Chem. Eur. J.,* 2012, **18**, 554.

27. P. A. Rachwal, I. S. Findlow, J. M. Werner, T. Brown, K, R. Fox. *Nucleic Acids Res.,* 2007, **35**, 4214.

28. M. Adrian, B. Heddi, A. T. Phan. *Methods,* 2012, **57**, 11.

29. C.S. Johnson Jr. *Prog. Nucl. Magn. Reson. Spectrosc.,* 1999, **34**, 203.

30. A. Sacco, E. Matteoli. *J. Solution Chem.,* 1997, **26**, 527.

31. M. Kato, K. Sasano, C. Kosuge, M. Yamazaki, S. Yano, M. Kimura. *Inorg. Chem.,* 1996, **35**, 116.

32. M. Yılmaz, C. Ozic, İ. Gok. *Principles of Nucleic Acid Separation by Agarose Gel Electrophoresis, Gel Electrophoresis - Principles and Basics,* Dr. Sameh Magdeldin (Ed.), InTech, Rijeka, 2012.

33. L. F. Liu, J. C. Wang. *Proc. Nati. Acad. Sci. USA,* 1987, **84**, 7024.

34. D. Sun, L. H. Hurley. *J. Med. Chem.,* 2009, **52**, 2863.

35. M. F. Shubsda, J. Goodisman, J. C. Dabrowiak. *J. Biochem. Biophys. Methods,* 1997, **34**, 73.

36. N. C. Stellwagen. *Electrophoresis,* 2009, **30**, 1.

37. J. Malina, M. J. Hannon, V. Brabec. *Chem. Eur. J.,* 2007, **13**, 3871.

38. D. M. Engelhard, R. Pievo, G. H. Clever. *Angew. Chem. Int. Ed.,* 2013, **52**, 12843.

39. H. Yu, X. Wang, M. Fu, J. Ren, X. Qu. *Nucleic Acids Res.,* 2008, **36**, 5695.

40. A. Guédin, L. Lacroix, J. Mergny. *Methods Mol. Biol.,* 2010, **613**, 25.

41. V. Dhamodharan, S. Harikrishna, C. Jagadeeswaran, K. Halder, P. I. Pradeepkumar. *J. Org. Chem.,* 2012, **77**, 229.

42. A. Periasamy, R. N. Day. *Molecular Imaging: FRET Microscopy and Spectroscopy.* Academic Press, New York, 2005.

43. P. Atkins, J. de Paula. *Elements of Physical Chemistry 4th ed.* Oxford University Press, Oxford, 2005.

44. A. Bevan. *Statistical Data for the Physical Sciences.* Cambridge University Press, New York, 2013.

Chapter 4: RNA Binding Studies

4.1 Introduction

G-quadruplexes not only form in guanine rich strands of DNA, but also in guanine rich strands of RNA (within genomes).[1] Early investigations found the RNA G-quadruplexes to be actively present in viral genomes (translational recoding in herpes and genome dimerisation in HIV) where selective binding of a viral protein to a RNA G-quadruplex structure was reported.[1] More recently they have been found experimentally to be present in telomeric (TERRA) and non-coding sequence transcripts (5'-untranslated regions) playing essential roles in important cellular functions such as telomere regulation and gene expression.[2] As with DNA the formation of the RNA G-quadruplexes can affect the binding of proteins and therefore control the regulatory mechanisms they are associated with.[2] Both of the RNA sequences, TERRA and 5'-untranslated regions (UTRs), have potential links with cancer biology therefore there is much research into the biological effects of these structures along with the ability of small binders to selectively target them.[1]

4.1.1 RNA G-Quadruplex Structure and Stability

The structure of RNA is closely related to that of DNA, however there are differences between the two which result in the type of structure seen for each. There are three main differences: RNA exists as a relatively short single stranded entity whereas DNA is primarily double stranded and very long; ribose replaces deoxyribose in RNA which has an additional hydroxyl group at position C2'; the base thymine is replaced by uracil which is the unmethylated version of thymine *(Fig. 4.1 - a)*.[1]

G-rich sequences of RNA *in vivo* are more likely to fold into a G-quadruplex structure as they primarily exist as single stranded sequences, with no complementary strand to interact with, and also form very stable G-quadruplex structures (more so than DNA).[2] The increased stability exhibited by the RNA quadruplexes stems from the ribose C2' hydroxyl groups which form hydrogen bonds with the phosphate and oxygen atoms, N2 groups of the guanine bases (H-bond acceptors) and O4' sugar oxygen (*Fig. 4.1 - b*).[3]
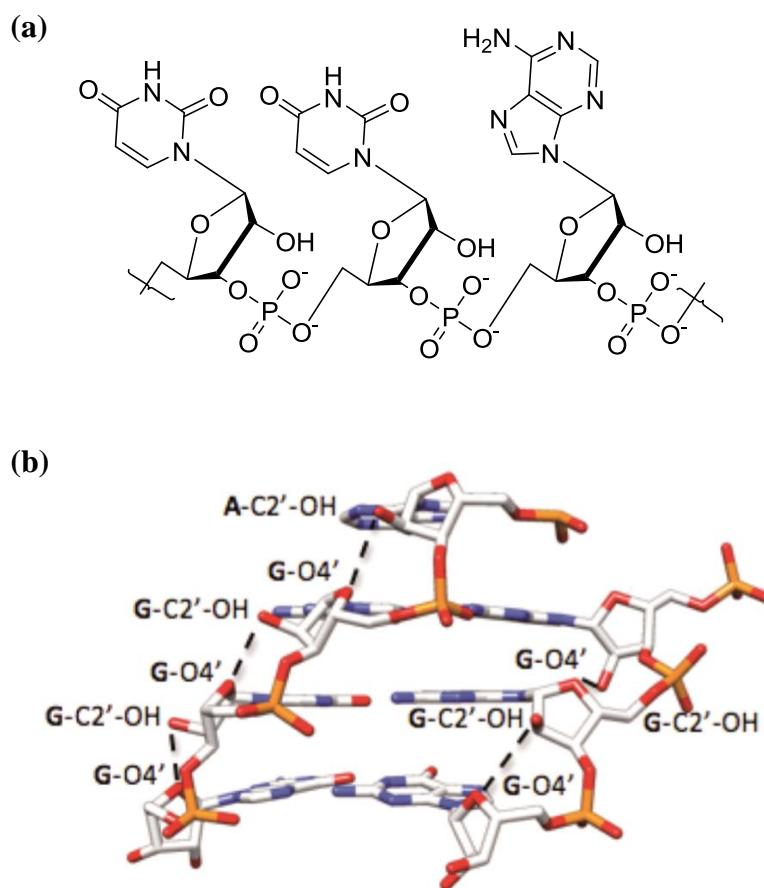
Figure 4.1 **a**. Example of RNA sequence UUA showing the sugar phosphate backbone, **b**. RNA G-quadruplex showing the H-bonds between C2'-OH and O4' which help stabilise the structure PDB: 3IBK. [Reproduced from Ref [3]]

All of the additional interactions, when compared with DNA quadruplexes, increase the thermodynamic stability of the RNA quadruplex by:

- Lowering the cost of entropy as the ribose hydroxyl groups prefer to interact intramolecularly rather than with the surrounding water molecules. This results in a decrease of ordered water molecules within the grooves of the RNA quadruplex.[1]

- Increasing the enthalpic addition to the free energy of RNA G-quadruplex formation with the additional hydrogen bonding.[3]

DNA and RNA G-quadruplexes also differ in the number of topologies that they can exist in.[3] DNA G-quadruplex structures are polymorphic and a single G-rich sequence can fold into a variety of quadruplex conformers depending on the concentration of the oligonucleotide and the buffer conditions. RNA G-quadruplexes on the other hand prefer to exist in parallel quadruplex conformers regardless of the oligonucleotide concentration or the buffer conditions.[3] This is because of the steric hindrance inflicted by the C2' hydroxyl group in the RNA quadruplex which favours anti-glycosidic torsion angles hence a parallel quadruplex conformer.[1]

4.1.2 RNA Quadruplexes in Telomeric Regions

The guanine rich sequence that exists at the end of a DNA strand is shortened after every cell division unless counteracted by the enzyme telomerase which acts to extend the G-rich telomeric sequence.[2] The telomerase works by extending the 3' end of DNA by the reverse transcription of a small region of RNA called TERC or hTR producing an encoded version of the sequence.[2] DNA-dependent RNA polymerase II transcribes the C-rich strand of the DNA resulting in the formation of a non-coding G-rich RNA strand called TERRA which

has been implicated in the regulation of telomere length and telomerase inhibition (*Fig. 4.2*).[2]

The guanine rich TERRA RNA sequence is also able to fold into a G-quadruplex structure like its DNA equivalent sequence however it only exists as the parallel conformer.[3][4] The transcription of TERRA is regulated by RNA surveillance mechanisms and reacts to changes in the telomere length.[5] The overproduction of TERRA can cause problems with telomere replication resulting in an abrupt loss of telomere tracts.[5]
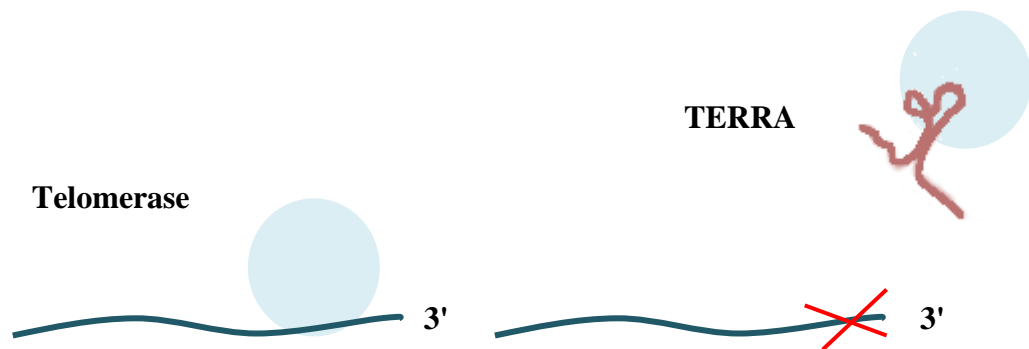
Figure 4.2 Inhibition of telomerase by RNA TERRA sequence.

4.1.3 RNA Quadruplexes in 5' Untranslated Regions

Three important steps are involved in the translation of mRNA into its corresponding protein product which are:

- Initiation; ribosome assembly on the mRNA

- Elongation; synthesis of protein

- Termination; removal of the ribosome

The most regulated and rate limiting step of the entire process is thought to be initiation which occurs in the 5'-untranslated region (UTR) of the mRNA strand.[3] In this region translation initiation occurs where the small (40S) ribosomal subunit binds to the 5' end of the mRNA and scans the region in a 5' → 3' direction until the initiation codon (AUG) is reached.[2] At this point the larger subunit of the ribosome (60S) joins the smaller unit to form the 80S ribosome to start the translation leading to gene expression.[2]

Many 5'-UTR regions are predicted to contain G-rich sequences which are able to fold into G-quadruplexes.[2] The presence of secondary structures, such as G-quadruplexes, in these regions of RNA help to regulate translational processes for growth factors, transcription factors and oncoproteins as their formation is able to block initiation preventing gene expression.[2][6] One particular 5'-UTR is that of the neuroblastoma RAS viral oncogene (NRAS) whose encoded protein is responsible for cell proliferation and differentiation.[6] Mutations that are activated in the coding region of NRAS result in an elevated level of cell growth causing the development of tumours.[6] As the NRAS 5'-UTR region is guanine rich, G-quadruplexes have the potential to form in this area and repress translation preventing the formation of the protein that causes cell proliferation.[7]

4.1.4 Small Molecule RNA G-Quadruplex Binding

The formation of G-quadruplexes in G-rich regions of RNA and their link with regulatory systems make them ideal targets in order to combat cancers caused by the up regulation of specific genes. As with DNA, the formation and stabilisation of G-quadruplexes by small molecules can prevent the binding of proteins required for processes such as telomere extension or gene translation. Small molecules that are designed to target 5'-UTR RNA G-

quadruplexes can control or alter mRNA translation by: Stabilising the existing G-quadruplex structure preventing the ribosomal subunit from scanning the untranslated region for the initiation codon; Destabilising the existing RNA quadruplex to allow translation or interfering in a G-quadruplex-protein binding event.[3]

Two types of G-quadruplex binders that have been explored with both DNA and RNA quadruplexes are BRACO-19 and three tetrasubstituted naphthalene diimides (*Fig. 4.3*) where in each case the side chains are composed of two or more CH_2 groups that terminate with an amine.[8]

1. $R_1 = R_2 =$ -$(CH_2)_3$-NMe_2
2. $R_1 = R_2 =$ -$(CH_2)_3$-pyrrolidino
3. $R_1 =$ -$(CH_2)_3$-NMe_2 $R_2 =$ -$(CH_2)_3$-OH
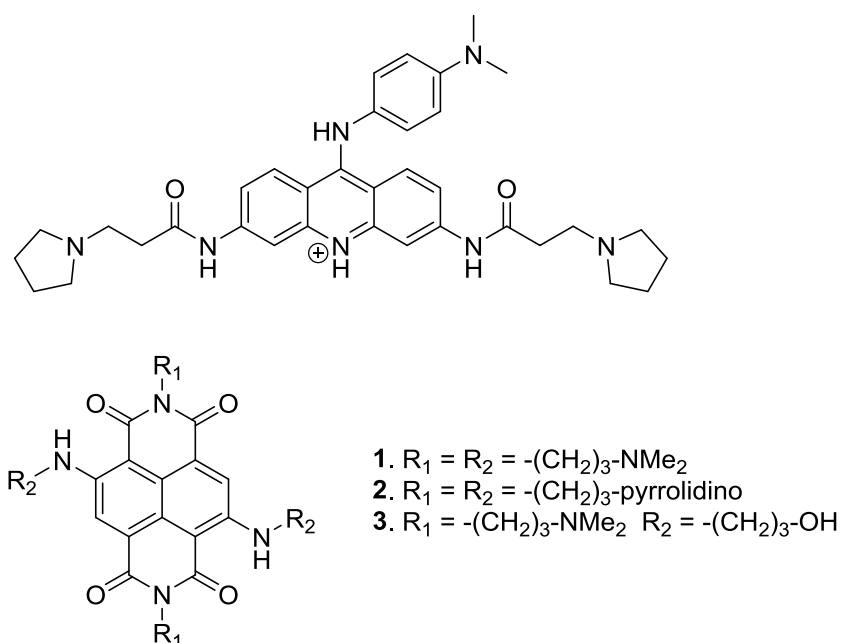
Figure 4.3 DNA and RNA G-Quadruplex binders. Top. BRACO-19, Bottom. Tetrasubstituted naphthalene diimides.

BRACO-19 was found to bind to DNA G-quadruplexes with a higher affinity than RNA G-quadruplexes. This was also true for the naphthalene diimide ligands except for ligand 3 where the RNA showed a similarly strong response to that of DNA.[8] The extra stability of

the DNA quadruplex - BRACO-19 complex arises from interactions between the 3'
thymine O4 atom with an amide group in the side chain of BRACO-19.[8] The same
stabilising interaction does not occur in the RNA quadruplex - BRACO-19 complex
because electrostatic repulsion is felt between the 2'-OH group on guanine (G17) and the
O4 atom on uracil (U24).[8] The side chain of the BRACO-19 ligand in this complex is
situated between the terminal uracil O4 atom and the 2'-OH (G17).[8] The repulsion
prevents the amide nitrogen of BRACO-19 interacting with the carbonyl atom, O4 (*Fig.
4.4*).[8]
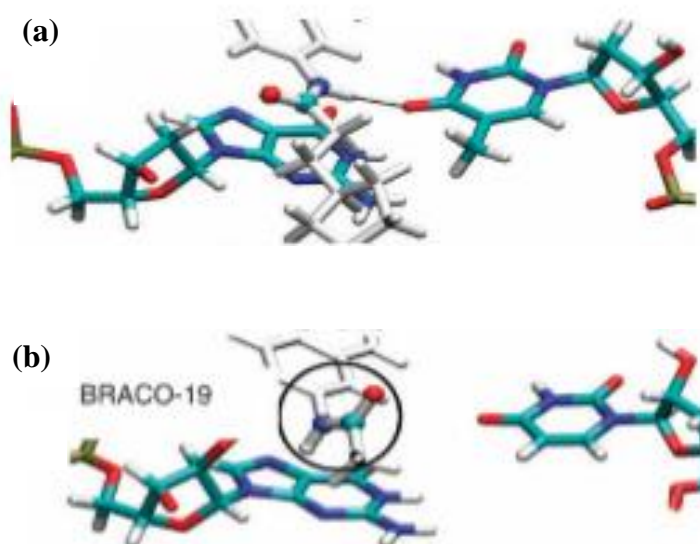
Figure 4.4 Interactions between BRACO-19 (white) with; **a**. DNA - showing the amide O4
interaction stabilising the structure, **b**. RNA - where the amide O4 interaction is prevented due to
the presence of the 2'-OH group on the guanine (G17) base the ligand is stacking on top of.
[Reproduced from Ref [8]]

The three naphthalene ligands which all bound to DNA quite well did not all bind to RNA
with similar success.[8] Naphthalene ligands 1 and 2 both contain a similar amide side
chain which interacts with the RNA like the BRACO-19 ligand.[8] Naphthalene ligand 3 on
the other hand gave a 15 fold increase in ligand binding when compared with the amide
versions indicating that the presence of a hydroxyl group in a ligand side chain may be

important for RNA quadruplex binding.[8] Only a 3 fold increase was seen when using the hydroxyl ligand with DNA.[8]

When a human telomeric RNA sequence was treated with a triazoleacridine ligand a bimolecular G-quadruplex structure was formed from two strands of RNA with two acridine ligands.[9] The RNA G-quadruplexes formed were parallel in conformation with UUA loops.[9] The presence of the additional 2'-OH groups means the loops are more constricted in space which in some cases (BRACO-19) may hinder some ligand side chain interactions.[9] The two acridine ligands in this system are stacked on each other in between two terminal G-quartets of two quadruplexes and stabilised by interactions with the 2'-OH groups in the RNA parallel loops (*Fig. 4.5*).[9]
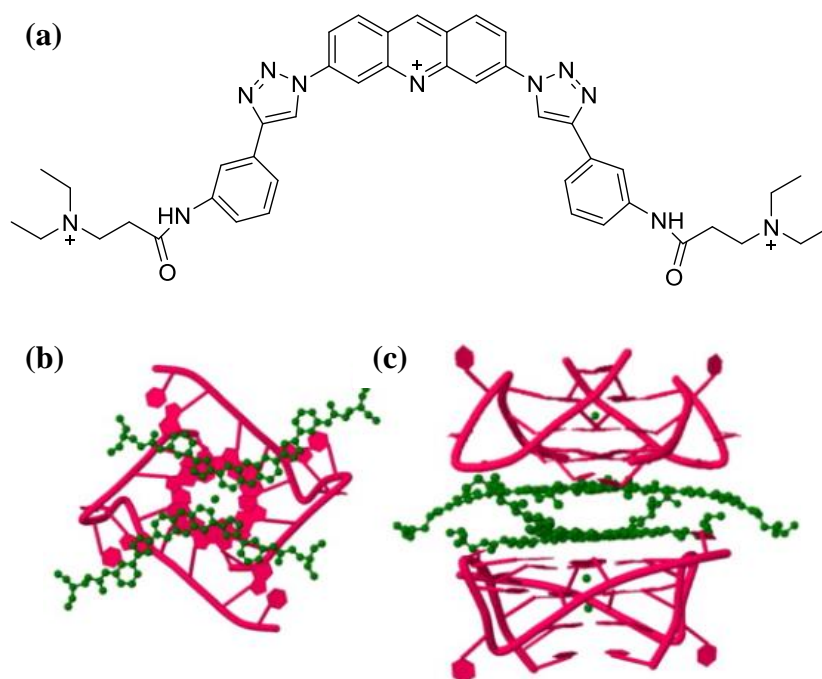
Figure 4.5 **a**. Acridine compound *N,N'*-((1,1'-(acridine-3,6-diyl)bis(1H-1,2,3-triazole-4,1-diyl))bis(3,1-phenylene))bis-(2-(diethylamino)acetamide), **b**. Crystal structure of acridine molecules on top of terminal G-quartet, **c**. Schematic of two RNA G-quadruplex structures with two acridine molecules in between them. [**b** and **c** Reproduced from Ref [9]]

4.1.5 Interaction of Biisoquinoline Complexes with RNA G-Quadruplexes

Two G-quadruplex forming strands of RNA were used in the following CD and FID experiments to investigate how they interacted with the palladium and platinum biisoquinoline complexes in comparison with DNA G-quadruplexes. The RNA strands chosen were TERRA (telomeric linked) and NRAS (5′-UTR linked), shown below, both of which fold into G-quadruplexes in a parallel conformation .

TERRA: 5'-**UUA GGG UUA GGG UUA GGG UUA GGG**-3'

NRAS: 5'-**GGG AGG GGC GGG UCU GGG**-3'

The biisoquinoline complexes were not designed with additional side arms to potentially react with the loops therefore will hopefully avoid any 2'-OH group interference from the ribose sugar. The mode of interaction is likely to be end stacking, as with the DNA G-quadruplexes, onto the terminal G-quartet with the complex being able to maximise its coverage on the whole guanine quartet surface. The results of the circular dichroism and fluorescent indicator displacement experiments were expected to give an indication of the possible specificity of each complex for RNA or DNA. The constriction of the loops in the RNA quadruplexes may; help binding by being closer in space to the G-quartet surface and hence the end stacking complexes (maximising interactions between the two) or hinder by being too restrictive for the complex to fit on top of the G-quartet making it a too tight a fit to sit planarly.

4.2 Circular Dichroism with Complexes 5 and 7

The principles of circular dichroism can be found in Chapter 3.2 which relate to the experiments carried out using RNA instead of DNA. RNA G-quadruplexes are inherently more stable than their DNA analogues, due to their additional hydroxyl hydrogen bonding substituent and closer loop structure minimising water association, therefore are able to form in very dilute salt concentrations. Despite this the same salt conditions were used in the RNA experiments as for the DNA in order to obtain a more accurate comparison of binding in solution. Two buffer solutions were used to investigate the TERRA RNA oligo, 10 mM Tris-HCl with 100 mM KCl and 10 mM Tris-HCl only. The NaCl based buffer was omitted from these experiments as the potassium buffer is more biologically relevant. The RNA concentration used in each experiment was 1 μM (calculated per strand). Control titrations found the solvent to have no effect on the CD spectrum where the ICD peaks are found.

4.2.1 [Pd(ibiq)$_2$][BF$_4$]$_2$ - 5

- TERRA RNA + 10 mM Tris-HCl + 100 mM KCl

The initial peak seen with the TERRA RNA alone occurs at 262 nm which agrees with the formation of a parallel quadruplex conformer (*Fig. 4.6*). The addition of the palladium complex resulted in a gradual decrease in the intensity of the peak at 262 nm which may have been due to the precipitation of RNA out of solution as more of the complex solution was added. There is no sign of any induced circular dichroism peaks even at 12:1 equivalents of complex:RNA which is very similar to what was seen for the palladium complex interaction with c-myc DNA quadruplexes. Both the c-myc and TERRA

233

quadruplexes form parallel conformers that the palladium complex is not able to interact with in the same way it does with antiparallel quadruplex hybrids. This leads to the assumption that the palladium complex is not interacting with the terminal G-quartet in an end stacking mode because if so it would be able to stack like this onto the parallel conformer also, as there are no loops hindering access across the top of the end quartet.

- TERRA RNA + 10 mM Tris-HCl

The same result was observed for the same titration conducted without the presence of potassium cations. The stable nature of the RNA parallel quadruplex conformer allows its formation even without the extra stabilising central cation as shown by the initial peak in the spectrum with TERRA RNA alone at 262 nm (*Fig. 4.7*). A weak negative peak may be emerging at 292 nm however this may be a consequence of the broad base line produced by the apparatus that is more pronounced due to the low magnitude of CD signal observed.

A CD titration using NRAS RNA could not be performed due to the lack of stock and time whilst in Zurich. Based on previous results it is predicted that the palladium complex would show very little interaction with the parallel quadruplex formed from this type of RNA.
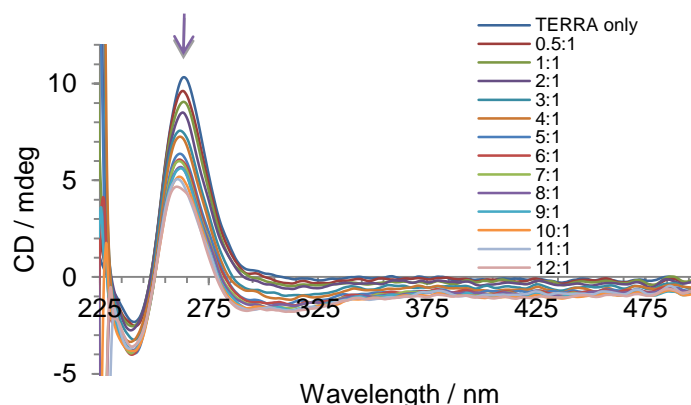
Figure 4.6 CD spectrum for 1 μM TERRA RNA in 10 mM Tris-HCl + 100 mM KCl titrated with Pd complex in ratios shown in the legend to the right.
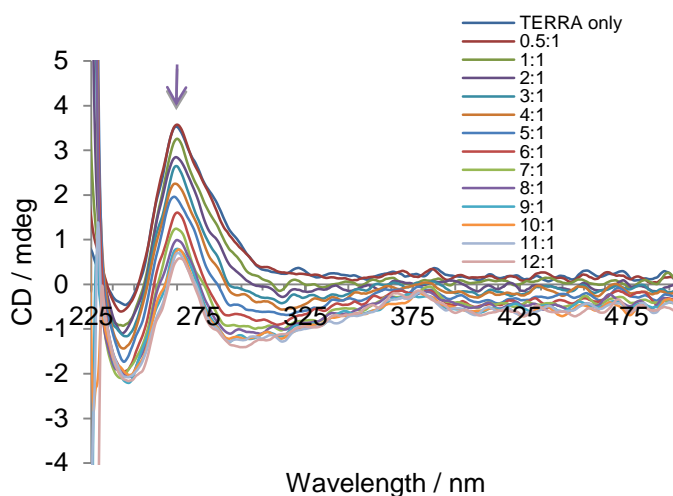
Figure 4.7 CD spectrum for 1 μM TERRA RNA in 10 mM Tris-HCl titrated with Pd complex in ratios shown in the legend to the right.

4.2.2 [Pt(ibiq)$_2$][PF$_6$]$_2$ - 7

- TERRA RNA + 10 mM Tris-HCl + 100 mM KCl

The parallel quadruplex conformer is seen for the TERRA RNA when alone in the potassium rich buffer solution as evidenced by the CD peak at 262 nm (*Fig. 4.8 - a*). When the platinum complex is titrated into the RNA solution two negative ICD peaks begin to emerge at 282 nm and 392 nm after a complex:RNA ratio of 2:1. As for the palladium complex the platinum complex shows a similar CD spectrum to that obtained for the same experiment with c-myc quadruplex forming DNA; which is as expected when considering they both form parallel type quadruplexes. A great degree of similarity between the two spectra also assumes a lack of interaction with the loops. The RNA loops are more constricted having a smaller width and depth when compared with the DNA loops. Therefore if the complex was interacting with them this may have caused more of a difference to be seen between the CD responses.

235

- TERRA RNA + 10 mM Tris-HCl

Without the presence of potassium ions in solution there is much more of a decrease in the intensity of the ICD signal at 277 nm and 390 nm as the platinum complex is added (*Fig. 4.8 - b*). A positive peak at 250 nm emerges whilst the positive peak at 264 nm disappears at a complex:RNA ratio of 4:1. As with the c-myc DNA quadruplex, the platinum complex is believed to be interacting through an end stacking mode.

- NRAS RNA + 10 mM Tris-HCl + 100 mM KCl

When investigating the NRAS RNA quadruplex forming strand a much less intense response can be seen when compared with the TERRA RNA titrations. Both of the RNA strands fold into parallel quadruplex conformers. The initial peak for NRAS RNA alone in *Fig. 4.8 - c* at 260 nm is characteristic for this type of quadruplex. However the NRAS quadruplex structure has different sized loops to the TERRA RNA quadruplex which may restrict access to the terminal G-quartet. Nevertheless negative ICD peaks emerge at 286 nm and 387 nm similar to those seen for the TERRA RNA with KCl rich buffer (although much less intense) which means that the complex may be interacting with the RNA in a similar way (most probably by end stacking).
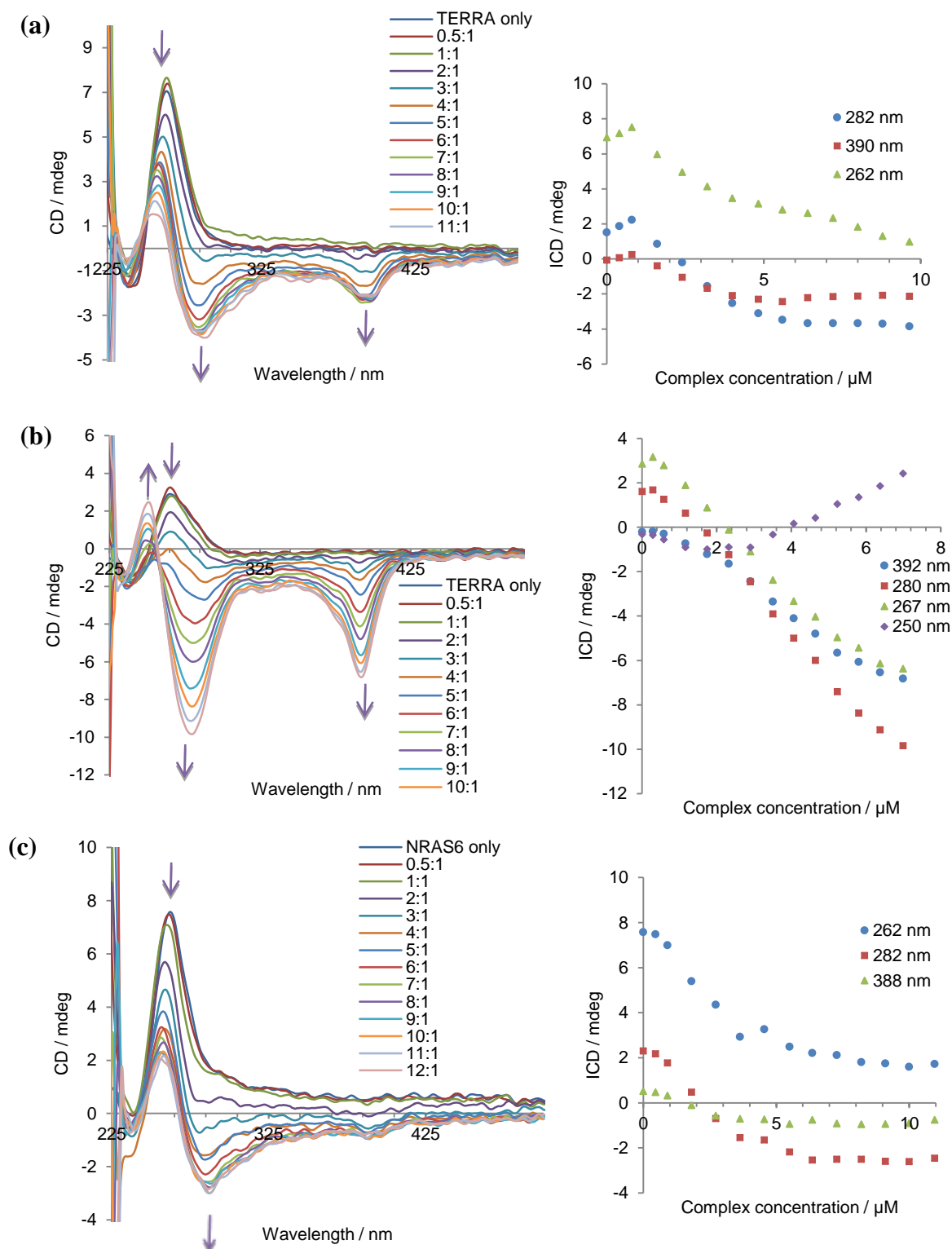
Figure 4.8 **a**. CD spectrum for 1 μM TERRA RNA in 10 mM Tris-HCl + 100 mM KCl titrated with Pt complex, **b.** CD spectrum for 1 μM TERRA RNA in 10 mM Tris-HCl titrated with Pt complex, **c**. CD spectrum for 1 μM NRAS RNA in 10 mM Tris-HCl + 100 mM KCl titrated with Pt complex. ICDs for selected wavelengths are shown to the right of each CD spectrum.

4.3 Fluorescent Indicator Displacements for Complexes 5 and 7

The same fluorescent indicator displacement experiment (protocol used by Marie-Paule Teulade-Fichou[10]) conducted in Chapter 3.4 was used to investigate the displacement of thiazole orange (TO) from RNA quadruplex structures also, using both the palladium and platinum biisoquinoline complexes. The binding constant for the thiazole orange to the RNA quadruplexes has not been investigated. However due to the similarities between the DNA and RNA quadruplex structures it was expected that the affinity would be similar for both. This would be apparent from the results obtained because if the thiazole orange bound much more strongly to the RNA than DNA the biisoquinoline complex would not be able to displace it and vice versa (if the thiazole orange binds very weakly, little complex would be needed to completely displace it). The conditions used for the RNA experiments were exactly the same as for the DNA experiments therefore a direct comparison could be made between the two systems.

4.3.1 Titrations with TERRA RNA

When the palladium complex was added to the TERRA RNA-thiazole orange mixture the emission decreased by only small amounts upon each titration increment. After adding the total amount of complex to make the concentration the full 2.5 μM the 50 % displacement mark was not reached therefore the results had to be extrapolated. The platinum complex however was able to quench the fluorescence of the system after very little had been added to the titration mixture (at 1 μM nearly 100 % of the emission signal had been quenched). The ability therefore of the platinum complex to displace the thiazole orange from the RNA TERRA quadruplex appears to be much greater than that of the palladium complex.

This may be because of the topology of the quadruplex formed which is similar to the c-myc DNA quadruplex studied in Chapter 3.4.2. The platinum complex is able to interact with parallel quadruplex conformers (like c-myc and TERRA) whereas the palladium complex is less able to displace TO from this type of quadruplex. This is probably due to its poorer binding affinity which most likely relates to how accessible the loops are for it to coordinatively bind. The percentage displacement after the addition of each of the complexes was plotted using the equation below; the plot shown in *Fig. 4.9* shows the results.

$$\% \, Displacement = 100 - [(FA-FA_0) \times 100]$$
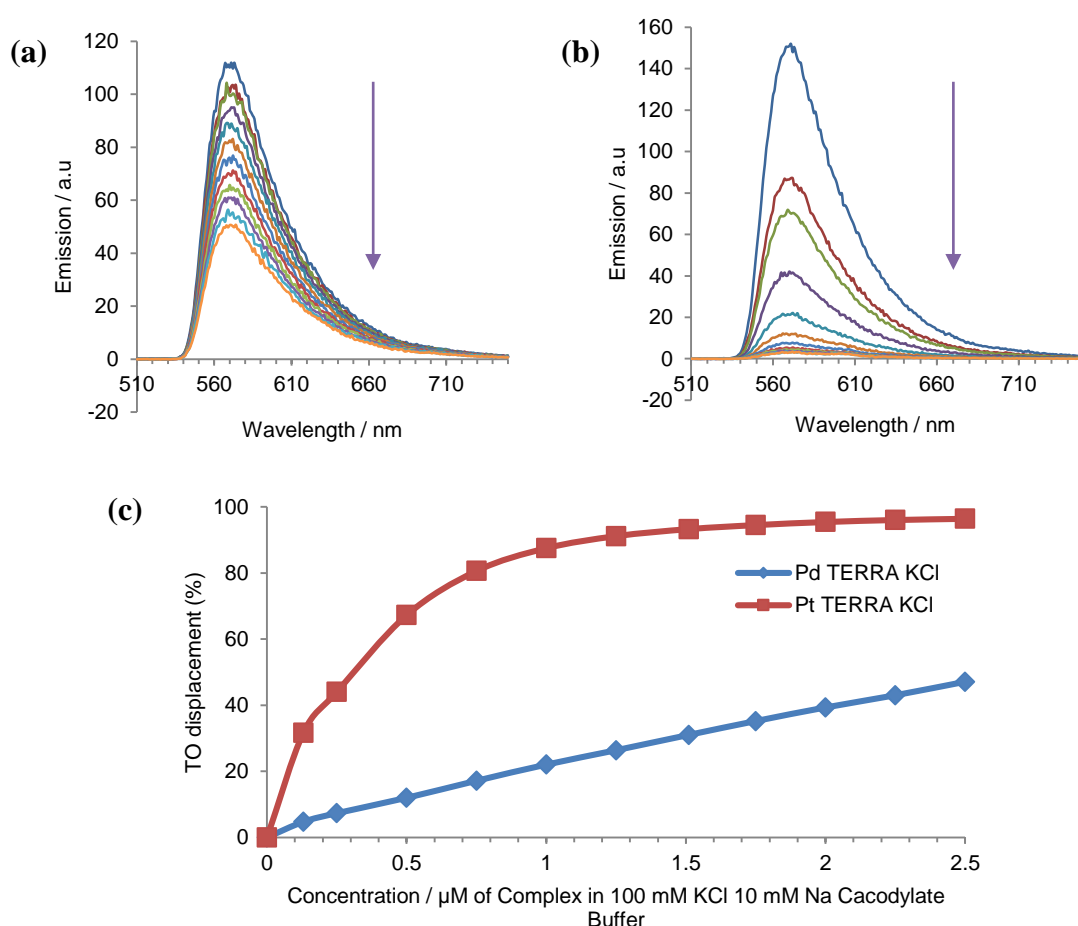
Figure 4.9 **a**. Emission spectrum for the palladium complex when titrated into 0.25 μM TERRA RNA solution containing 100 mM KCl / 10 mM Na cacodylate + 0.5 μM TO, **b**. Emission spectrum for the platinum complex when titrated into 0.25 μM TERRA RNA solution containing 100 mM KCl / 10 mM Na cacodylate + 0.5 μM TO. **c**. Percentage TO displacement comparison.

4.3.2 Titrations with NRAS RNA

The FID results for the palladium complex show that it binds slightly better to NRAS quadruplexes when compared with TERRA quadruplexes even though both form parallel quadruplex conformers. Despite this it is still a poor binder when compared with the platinum complex which was able to quench the fluorescence at much a lower concentration and hence ratio of complex:RNA (at a complex concentration of 1 μM the emission had decreased by nearly 100 %). The plot of the concentration of complex versus TO percentage displacement in *Fig. 4.10* shows the large difference in displacement between the two complexes.
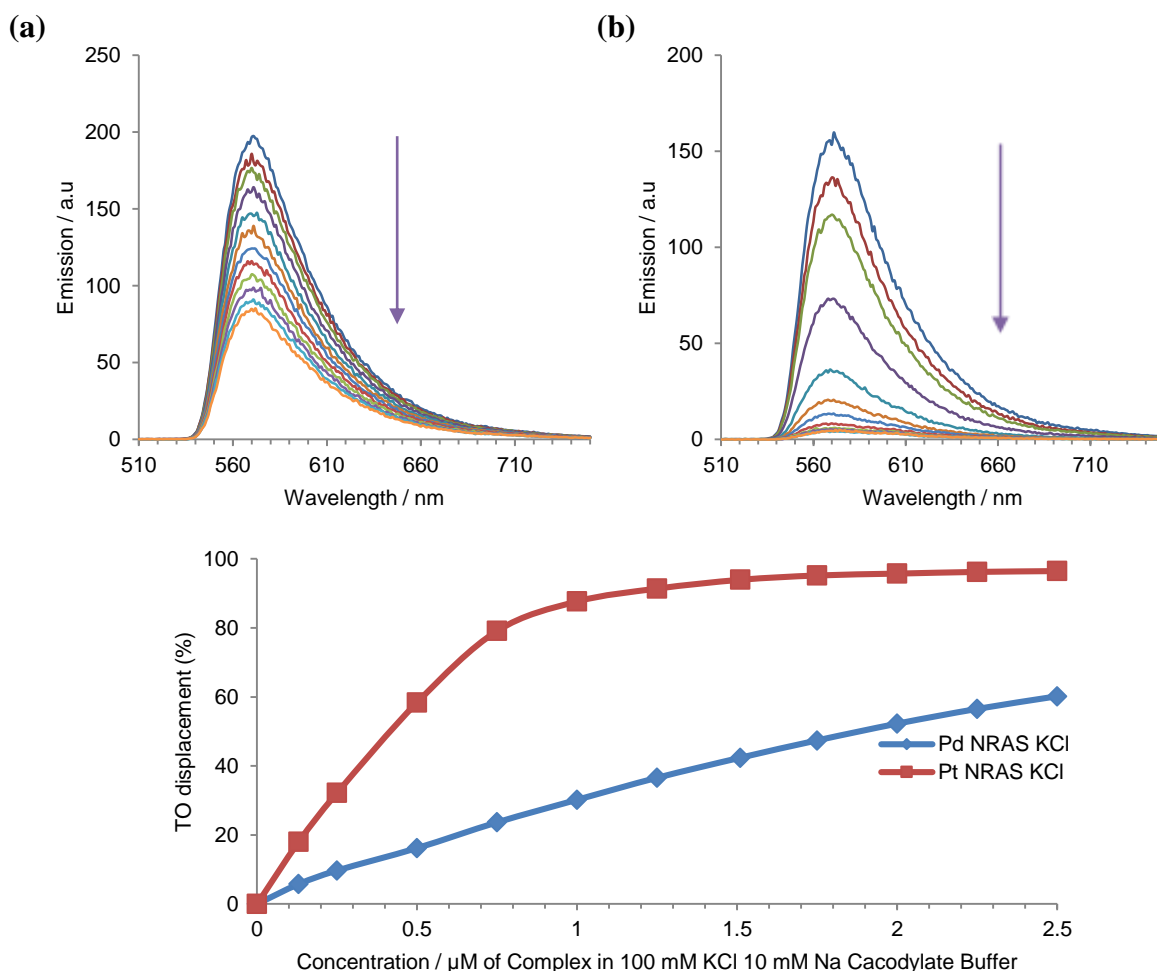
Figure 4.10 **a**. Emission spectrum for the palladium complex when titrated into 0.25 μM NRAS RNA solution containing 100 mM KCl / 10 mM Na cacodylate + 0.5 μM TO, **b**. Emission spectrum for the platinum complex when titrated into 0.25 μM NRAS RNA solution containing 100 mM KCl / 10 mM Na cacodylate + 0.5 μM TO, **c**. Percentage TO displacement comparison.

240

4.3.3 *Comparison of DC$_{50}$ Values*

In *Table 4.1* the DC$_{50}$ values (concentration at which TO fluorescence has reduced by 50 %) calculated for the palladium and platinum complexes, with TERRA and NRAS RNA, have been calculated. As this is a direct comparison with DNA quadruplex binding the 0.5 µM threshold will still be used to decide whether a complex can be considered as a good quadruplex binder or not. The palladium complex for each of the types of RNA had DC$_{50}$ values which far exceed the limit and therefore is a poor RNA quadruplex binder. The platinum complex on the other hand showed DC$_{50}$ values below the threshold making it an excellent potential RNA quadruplex binder. Despite the excellent binding results obtained for the platinum complex it suffers with regards to its selectivity as it has very similar DC$_{50}$ values to those obtained for DNA quadruplexes (c-myc 0.31 µM and htelo 0.55 µM).

	DC$_{50}$ µM	
	TERRA	NRAS
[Pd(ibiq)$_2$][BF$_4$]$_2$	$2.57 \pm 0.40^*$	1.90 ± 0.14
[Pt(ibiq)$_2$[PF$_6$]$_2$	0.30 ± 0.10	0.41 ± 0.03

Table. 4.1 DC$_{50}$ values calculated for palladium and platinum FID complex titrations with TERRA and NRAS RNA. *estimated value as result extrapolated due to 50 % displacement mark not being reached.

An overview of the selectivity of the complexes for one type of quadruplex over another is displayed in *Table 4.2*. On comparing how each of the complexes interact with each type of RNA they both show very little difference between the two types, showing how the complexes cannot discriminate one type of RNA quadruplex from another. This however is no surprise as the RNA sequences both form parallel conformers. More interestingly the

palladium complex shows a degree of selectivity for htelo DNA quadruplexes over TERRA RNA complexes. The main reason for this is likely to be the type of quadruplex conformer formed, antiparallel hybrid (DNA) versus parallel (RNA).

	Selectivity $[DC_{50}(A)/DC50(B)]$			
	NRAS / TERRA	TERRA / NRAS	htelo / TERRA	TERRA / htelo
[Pd(ibiq)$_2$][BF$_4$]$_2$	-	1.35 ± 0.23	-	4.51 ± 1.18
[Pt(ibiq)$_2$[PF$_6$]$_2$	1.37 ± 0.47	-	1.83 ± 0.77	-

Table. 4.2 Selectivity comparison between the different types of RNA and DNA investigated.

4.4 Conclusions

The binding abilities of each of the biisoquinoline complexes to the RNA quadruplexes, after studying with circular dichroism and fluorescent indicator displacement experiments, compares very closely with the DNA quadruplex binding results.

The ability of each of the complexes to bind depends on how well they are able to stack onto the terminal G-quartet of a G-quadruplex or bind to the loops. There is very little difference between the structure of the platinum and palladium complex when examined by x-ray crystallography (Chapter 2). The difference in binding between the two complexes highlighted here stems from how available the loops are for the palladium complex to coordinatively bind. RNA quadruplexes form parallel conformers like the c-myc DNA which the palladium complex (after losing a ligand) cannot bind to as the loop size is too restrictive (RNA tetrad loops more so than DNA tetrad loops). It is likely that

that the platinum complex does not dissociate from one of its ligands and therefore binds through end stacking generating the response seen in both the CD and FID experiments.

4.5 Experimental

General Methods

In the RNA binding studies Ultrapure water (18.2 MΩ) purchased from Fisher Scientific was used to carry out the experiments. The TERRA and NRAS oligos were bought from Microsynth and kept frozen until use. All other reagents were purchased from Fisher Scientific.

Circular Dichroism Experiments

A Jasco J-810 spectropolarimeter was used to record the CD measurements of the titration mixture contained within a quartz cuvette with a pathlength of 1 cm (750-200 nm). The concentration of each RNA oligo was calculated per strand. The UV-Vis molar extinction coefficients for the oligos TERRA and NRAS are ε_{260} = 281,200 and 202,300 mol^{-1} dm^3 cm^{-1} respectively which were made into solutions A, B and C. Solution A contained a 1μM solution of the RNA in 10 mM Tris-HCl (pH 7.4) with 100 mM KCl or no other metal ions depending on the salt condition used. Before recording the concentration they were annealed to 95 °C. Solution B was a 2 μM RNA solution with 20 mM Tris-HCl plus 200 mM of the required salt and solution C was a 150 μM complex solution made from the dilution of a 1000 μM stock solution for each complex. When carrying out the titration a CD spectrum is initially recorded of solution A and then to this equal volumes of solution B and solution C are added. This keeps the RNA concentration constant throughout the

experiment whilst increasing the complex concentration from a RNA:complex ratio of 0.5:1 to 0.08:1.

Fluorescent Indicator displacements

Experiments were carried out using a Perkin Elmer luminescence spectrometer L55OB in a 3 ml quartz cuvette. TERRA and NRAS oligos were used in the experiments and prior to carrying out the titration they were diluted to 0.25 μM in a 10 mM Na cacodylate solution (pH 7.4) with 100 mM KCl and then annealed to 95 °C before leaving to cool to room temperature. A 1 mM stock solution of thiazole orange was prepared in milliQ water which was then diluted to the corresponding concentration with 10 mM Na cacodylate solution. $[Pd(ibiq)_2][BF_4]_2$ and $[Pt(ibiq)_2][PF_6]_2$ solutions were made by diluting 1000 μM DMSO stock solutions with the 10 mM Na cacodylate solution to 20 μM. The concentrations of TO required for each type of DNA (all at 0.25 μM) are as follows: TERRA - TO = 0.5 μM and NRAS - TO = 0.5 μM.

The experiments were conducted by placing the RNA and TO mixture in a cuvette before adding increasing amounts of the complex being investigated (0.12 to 10 μM, which is 0.5 to 40 equivalents). After each addition of complex the mixture was left to equilibrate for 3 minutes before recording an emission spectrum between 510 and 700 nm, exciting at 501 nm. The trapezium rule[11] was used to calculate the fluorescence area after each titration which was then converted into TO % displacement using % TO displacement = 100 - [(fluorescence area of sample/fluorescence area of DNA+TO alone) × 100].

4.6   References

1. G. W. Collie, G. N. Parkinson. *Chem. Soc. Rev.,* 2011, **40**, 5867.

2. S. Millevoi, H. Moine, S. Vagner. *WIREs RNA,* 2012, **3**, 495.

3. A. Bugaut, S. Balasubramanian. *Nucleic Acids Res.,* 2012, **40**, 4727.

4. H. Martadinata, A. T. Phan. *Biochemistry,* 2013, **52**, 2176.

5. B. Luke, J. Lingner. *EMBO J.,* 2009, **28**, 2503.

6. S. Kumari, A. Bugaut, J. L Huppert, S. Balasubramanian. *Nat. Chem. Biol.,* 2007, **3**, 218.

7. S. Kumari, A. Bugaut, S. Balasubramanian. *Biochemistry,* 2008, **47**, 12664.

8. G. Collie, A. P. Reszka, S. M. Haider, V. Gabelica, G. N. Parkinson, S. Neidle. *Chem. Commun.,* 2009, **48**, 7482.

9. Y. Xu, M. Komiyama. *Methods,* 2012, **57**, 100.

10. D. Monchaud, C. Allain, H. Bertrand, N. Smargiasso F. Rosu, V. Gabelica, A. De Cian, J. L. Mergny, M. P. Teulade-Fichou. *Biochimie,* 2008, **90**, 1207.

11. A. Bevan. *Statistical Data for the Physical Sciences.* Cambridge University Press, New York, 2013.

Chapter 5: Cellular Studies

5.1 Introduction

There is much interest in the development of complexes that do not demonstrate genotoxic or mutagenic behaviour. Although a successful anticancer agent, cisplatin is unspecific and can damage healthy DNA causing mutations within the cell by coordinately binding to two adjacent guanine bases.[1] The targeting of another type of DNA or RNA structure such as the G-quadruplex offers a different mode of action to the duplex binding cisplatin which is useful when circumventing cisplatin resistance.[2] G-quadruplexes are formed during active processes such as translation and replication which make them ideal targets when considering proliferative cancer cells where the frequency of these processes is up-regulated.[2]
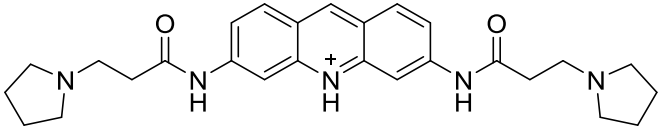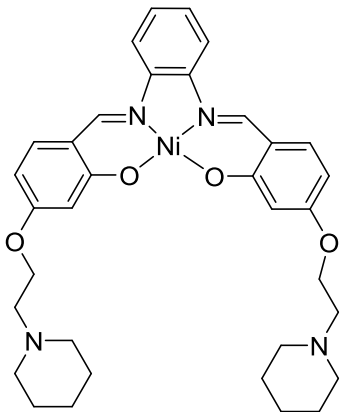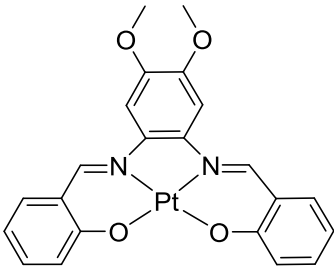
Complexes intended for use in cells must be able to get into the cell in order to reach their desired target, which means the complex will need to cross cell membranes and also the nuclear membrane when DNA is the cellular target.[3] The complex can enter the cell through the cell membrane by several pathways, the choice of which will affect how fast the complex uptake occurs and also how it will be distributed within the cell.[3] Three examples of how complexes could be transported into the cell include:

- Passive diffusion: The movement of molecules through the phospholipid bilayer which occurs down a concentration gradient. [3]

- Transport proteins: Expression in cells varies and carry only particular substituents.[3] The transport can be energy dependent (ATP powered pumps) or energy independent (channels and passive carriers). [3]

- Endocytosis: Complex uptake will involve vesicles formed from the plasma membrane. [3]

The phospholipid membrane is hydrophobic therefore complexes with lipophilic substituents will be able to cross more easily into the cell.[3] Covalently attaching conjugated moieties to complexes such as B vitamins, hormones and peptides can also be used to help with the cellular uptake of the complex by exploiting uptake mechanisms used for these biomolecules. [3]

There are a variety of G-quadruplex binders which have been studied in various cancer cell lines to study their cytotoxic effects. A few of these include (shown in *Table 5.1* with their IC$_{50}$ values in selected cancer cell lines); 3,6,9-trisubstituted acridine inhibitors (**a**) which are predicted to interact specifically with human G-quadruplexes in the telomeric region of DNA[4], metal salphen complexes (**b**) prohibit cell proliferation through telomeric quadruplex binding and also through binding to other genomic quadruplex sites[5], platinum Schiff base complexes (**c**) which have been found to bind to the c-myc G-quadruplex DNA by end stacking onto the terminal G-quartet using NMR, UV-vis absorption and emission molecular docking experiments[6], and palladium terpyridine complexes (**d**) that interact with quadruplexes through end stacking and metal to base binding.[7]

Complex	Cell line investigated and IC$_{50}$ / μM
(a)	IC$_{50}$ = 2.65 uM Cell line = A2780 [4]
(b)	<table><tr><td>IC$_{50}$[5]</td><td>Cell Line [5]</td></tr><tr><td>2.3 μM</td><td>MCF7</td></tr><tr><td>2.3 μM</td><td>A549</td></tr><tr><td>2.3 μM</td><td>RCC4</td></tr><tr><td>2.3 μM</td><td>RCC4-VHL</td></tr><tr><td>2.3 μM</td><td>786-0</td></tr><tr><td>2.3 μM</td><td>Mia-PaCa-2</td></tr><tr><td>**2.4 μM**</td><td>**W138**</td></tr></table>
(c)	<table><tr><td>IC$_{50}$[6]</td><td>Cell Line [6]</td></tr><tr><td>1.28 ± 0.33 μM</td><td>HeLa</td></tr><tr><td>1.09 ± 0.14 μM</td><td>HepG2</td></tr><tr><td>1.04 ± 0.21 μM</td><td>SUNE-1</td></tr><tr><td>4.8 ± 0.56 μM</td><td>NCI-H460</td></tr><tr><td>**46.11 ± 0.53 μM**</td><td>**CCD-19 Lu**</td></tr></table>
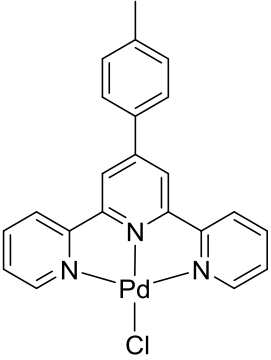
(d)		
	IC$_{50}$[7]	Cell Line [7]
	0.10 ± 0.02 μM	KB
	0.065 ± 0.021 μM	A549
	0.12 ± 0.021 μM	MCF7

Table 5.1 G-quadruplex binding complexes and their IC$_{50}$ values in a number of different cell types. Cancer cell lines include; A2780 (ovarian), MCF7 (breast), A459 (lung), RCC4 (renal), 786-0 (renal), Mia-PaCa-2 (pancreatic), HeLa (cervical), HepG2 (hepatocellular), SUNE-1 (nasopharyngeal), NCI-H460 (lung), KB (keratin forming tumour cell line of HeLa). **Normal cell lines; W138 (human fibroblast), CCD-19 Lu (lung fibroblast).**

All the reported complexes show a good interaction with G-quadruplex DNA in some or all of the following techniques; CD, UV-Vis, FRET and FID. It is hoped that the observed toxicity levels are a result of the complexes binding to the DNA quadruplex structure. It is still possible however that the activity of the complex in the cell may be due to interactions with other cellular targets with a different mode of action not yet examined.

The cytotoxicity of the palladium and platinum biisoquinoline complexes (*Fig. 5.1 - **a** and **b***) were investigated with two different cancer cell lines, A2780 (ovarian) and T47D (breast) by conducting an MTT assay to obtain an IC$_{50}$ value for each of the complexes. Cisplatin (Fig. 5.1 - **c**) was also used as a well studied comparison.
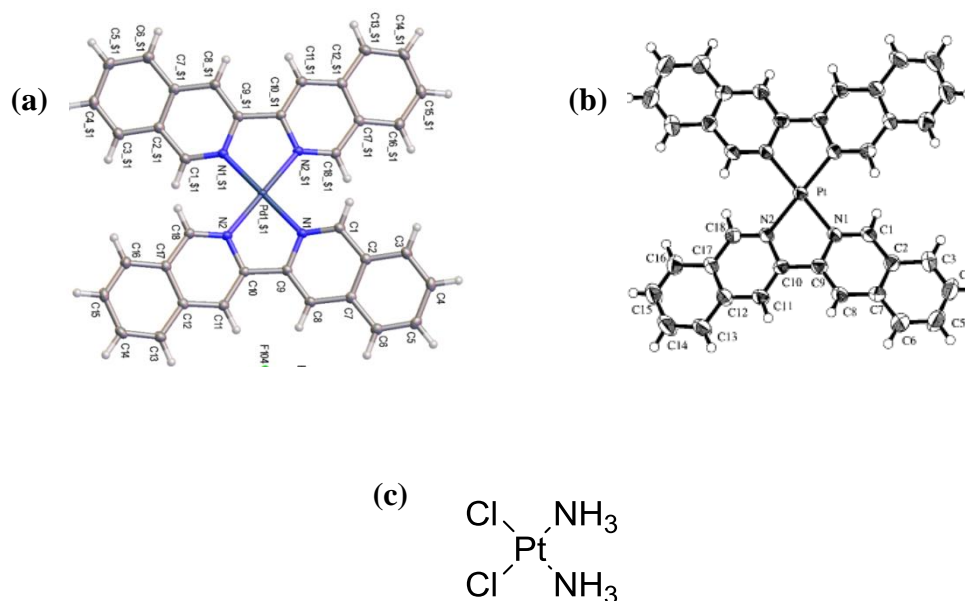
Figure 5.1 Crystal structures of; **a**. [Pd(ibiq)$_2$][BF$_4$]$_2$, **b**. [Pt(ibiq)$_2$][PF$_6$]$_2$ [Reproduced from Ref [8]], **c**. Structure of cisplatin.

5.2 MTT Cytotoxicity Assay

A MTT (or a 3-(4,5-dimethylthiazol-2-yl)-2,5-diphenyltetrazolium bromide) assay can be used to investigate how toxic a complex is to a particular cell line by measuring the value of its half maximal inhibitor concentration (IC$_{50}$). The IC$_{50}$ value will be the measure of the complex concentration it takes to reduce the cell viability by 50 % therefore the lower this value is the more potent the complex will be.

When cells are treated with the yellow complex MTT, the cells that are able to respire will be able to reduce the MTT compound (by electron transport processes involving mitochondrial reductase) forming violet formazan crystals within the cells (*Fig. 5.2*).[9] The results for the MTT assay are determined colourimetrically as the intensity of the

colour produced, by dissolving the formazan crystals, is an indicator of the proportion of functional mitochondria and therefore the proportion of living cells.[9] Details of the assay including cell growth and incubation can be found in the experimental section, subchapter 5.5.
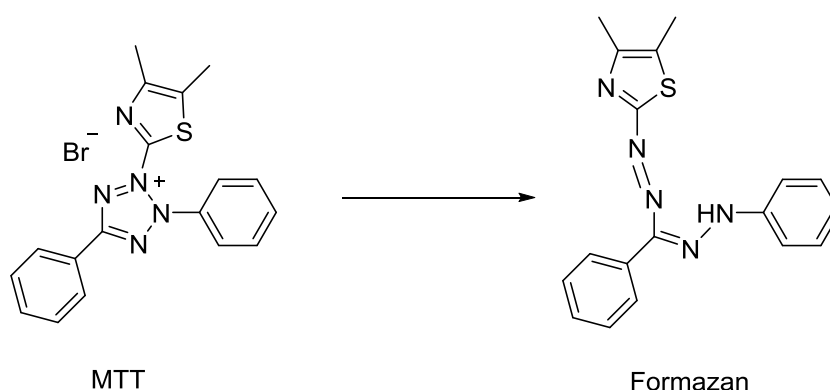
Figure 5.2 The reduction of MTT to formazan in living cells by mitochondrial reductase.

5.3 IC$_{50}$ Results for Complexes **5**, **7** and Cisplatin

The human cancer cell lines (A2780 and T47D) were treated with complexes **5** (palladium complex), **7** (platinum complex) and cisplatin. The results of the MTT assay for each are shown in both *Chart 5.1* and *Table 5.2* where the IC$_{50}$ value is reported in μM. A solution of 2% DMSO PBS was also used to treat the cells as a control, as well as PBS only, in all repeats. Both controls showed no significant cytotoxic effects on either of the cell lines investigated. See appendix section 4, for examples of raw cytotoxicity data.

251
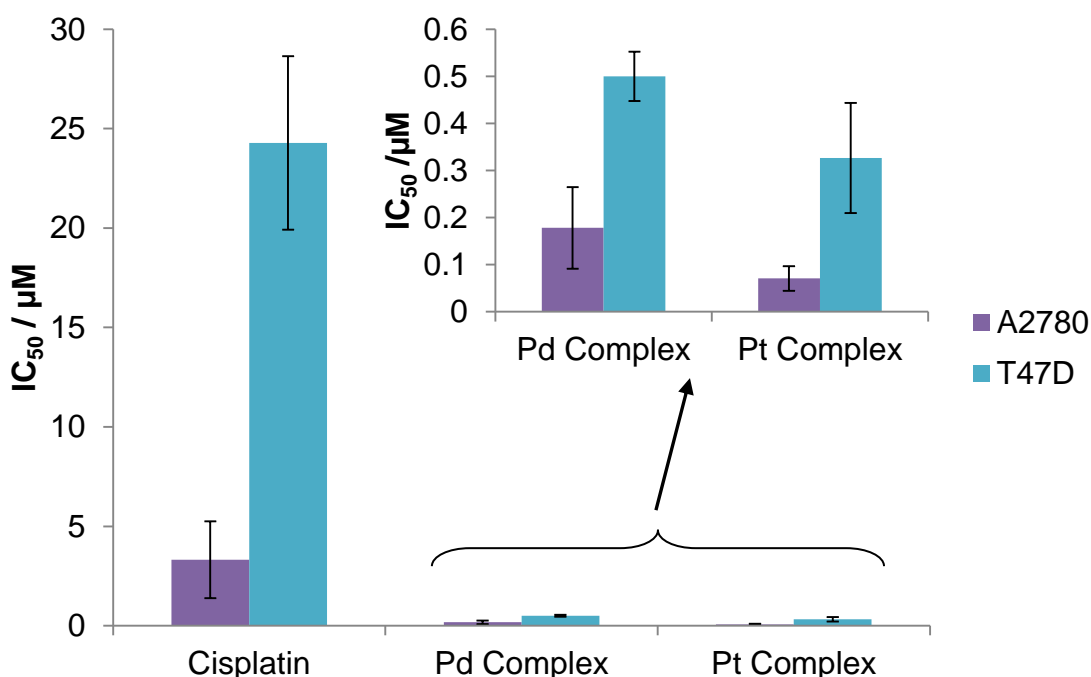
Chart 5.1 IC$_{50}$ results for complexes **5** (Pd), **7** (Pt) and cisplatin, smaller image shows the results for the Pd and Pt complexes enlarged.

Immediately a striking difference can be seen between the activity observed when the cells were treated with cisplatin compared to when they were treated with the biisoquinoline complexes (*Chart 5.1*).   The cytotoxicity effects of the biisoquinoline complexes far surpass those seen for the cisplatin as they are in nanomolar range when compared with cisplatin which is in the micromolar range.   The greatest difference in cytotoxicity is seen between the platinum complex and cisplatin in the T47D cell line with the platinum complex being 81 times more cytotoxic than cisplatin.   An explanation for this could be the difference in DNA targets of each complex where the cisplatin is interacting with duplex DNA and the biisoquinoline complexes are interacting with G-quadruplexes.   This would indicate that binding to G-quadruplexes has a greater cytotoxic effect however from the other spectrographic studies conducted in Chapter 3 the biisoquinoline complexes also bind to duplex DNA.   The binding of the complex to both types of DNA could be the

reason for its heightened cytotoxicity value as it is able to stop DNA replication in two ways. The experimental research in Chapter 3 has also revealed that when the two types of DNA are in the same system (in the PAGE studies) the biisoquinoline complexes bind to quadruplex DNA over duplex. A stronger binding affinity to quadruplexes is also demonstrated in the FID experiments where the complex was able to displace the TO at a much lower concentration when compared with duplex DNA. Further explanations for the cytotoxicity results seen could be linked to the mechanism of uptake, the extent of complex degradation and how toxic the degradation products are or interactions with other cellular structures such as proteins.

When comparing the palladium and platinum complexes the cytotoxicity values obtained are very similar, with the platinum complex being only slightly more cytotoxic than the palladium complex. This result was surprising as the platinum complex displayed more encouraging results for binding to quadruplex DNA in the CD and PAGE studies. A possibility for the similar activity may be because of the conditions in the cell which are different to those used for the other experiments. The molecular crowding effects in the cell were not accounted for. This may alter how the complex exists and may change the extent of aggregation in the cell. The other cellular components also provide potential binding platforms which may, when disrupted, have a cytotoxic affect on the cell. The majority of experiments with telomeric DNA gave similar results for both palladium and platinum complexes therefore a telomeric quadruplex binding mode may be responsible for their cytotoxic nature.

Complex	IC$_{50}$ A2780 / μM	IC$_{50}$ T47D / μM
[Pd(ibiq)$_2$][BF$_4$]$_2$	0.2 ± 0.1	0.5 ± 0.1
[Pt(ibiq)$_2$][PF$_6$]$_2$	0.1 ± 0.02	0.3 ± 0.1
Cisplatin	3.3 ± 1.9	24.3 ± 4.4

Table 5.2 IC$_{50}$ results for complexes **5** ([Pd(ibiq)$_2$][BF$_4$]$_2$), **7** ([Pt(ibiq)$_2$][PF$_6$]$_2$) and cisplatin.

In general, when compared with similar quadruplex binders, the biisoquinoline complexes show lower IC$_{50}$ values hence high cytotoxicity levels. This prompts the future investigation of the complexes synthesised in this thesis in order to find out where they localise in cells, how they get into cells and other methods to determine cell viability. The cytotoxic effect of the complexes on primary cell lines is also important in establishing how selective the complex will be. For example it is hoped that it is targeting processes where DNA replication is high (proliferating cancers) therefore having a minimal effect on healthy cells which will replicate at a slower rate.

5.4 Conclusions

Complexes, such as the terpyridine and salphen based structures discussed in the introduction of this chapter, that are designed to target G-quadruplexes can have a significant cytotoxicity effect. This makes them an exciting prospect when treating cancers, especially those which are cisplatin resistant.

Both biisoquinoline complexes were found to have IC_{50} values lower than that of cisplatin and therefore are potent anticancer agents. This is likely to be due to them binding to other secondary DNA structures other than duplex DNA as determined by other spectrographic techniques. There is little difference in activity between the palladium and platinum complexes which was not predicted as the platinum complex showed a better response in the DNA binding experiments. This leads to the possibility that the cytotoxicity may not be due to G-quadruplex binding alone and there is another target within the cell which both complexes have a similar affinity for.

Despite the cytotoxic success of the biisoquinoline complexes the actual mode of action cannot be proven as localisation of the complex was not be monitored in these experiments. Therefore future development of this structure would involve modification with a fluorescent marker that would allow the use of confocal microscopy to help determine this.

5.5 Experimental

All cellular experimental supplements were purchased from Sigma Aldrich with the exception of the media which was obtained from PAA-The Culture Company and the fetal bovine serum (FBS) purchased from Invitrogen. The actual cell lines were sourced from the European Collection of Cell Cultures (ECACC) which is a health protection agency culture collection. Both the A2780 (human ovarian cancer cells) and T467D (human breast cancer) cell lines were grown in Roswell Park Memorial Institute (RPMI-1640)

media to which was added further reagents to make a 10 % FBS, 1 % L-glutamine, 1 % sodium pyruvate, 1 % hepes buffer and an antibiotics-antimycotic (1×) solution.

The two cell lines were cultured in T75 flasks, kept in an incubator at 37 °C, 5% CO_2 in a humid environment, and grown as monolayers. Once cell coverage had reached 70 % confluency (cell optimum growth phase) the cells were unadhered from the flask using 1% tryspin-EDTA in PBS leaving single cell suspensions. The density of cells in the suspensions were determined using a hemocytometer using the trypan blue exclusion test to determine the cell viability. The cells were then seeded into 96 well microtiter plates (Corning Costar) transferring 100 μl of complete media cell suspension to each well; 4,000 cells per well for A2780 and 25,000 cells per well for T47D. The microtiter plates were then placed in the controlled incubator for 24 hours before treating in order to give the cells time to adhere to the bottoms of the wells. The two biisoquinoline complexes $[Pd(ibiq)_2][BF_4]_2$ and $[Pt(ibiq)_2][PF_6]_2$ both required a small amount of DMSO (2 %) to aid the solubility in the complete medium, cisplatin dissolved in complete media alone. Five different complex concentrations were prepared before adding 100 μl of complex to the 100 μl cell solution in each of the wells (A2780 6.25 μM - 0.10 μM and T47D 100 μM - 0.39 μM). Control lanes were prepared by treating with complete media (control 1) and 2 % DMSO 98% complete media (control 2). Every experiment was run in quadruplicate and repeated over three times. The treated microtiter plates were then placed back into the controlled incubator and left for 72 hours which were checked daily for signs of contamination. After this time the cell viability was then established by administering 20 μl of a 5 mg/ml MTT solution in PBS to each well, except to half of each control set of wells, and leaving for a further 2 hours in the incubator. The medium was then removed

from the wells before adding 200 μl of DMSO to each to dissolve any formazan crystals produced from the MTT. The plates were then left for 20 minutes and using a microplate reader (Bio-Rad) the absorbance of the DMSO and MTT solutions in each well were read at 590 nm.

5.6   References

1. Y. Ho, S. C. F. Au-Yeung, K. K. W. To. *Med. Res. Rev.,* 2003, **23**, 633.

2. T. Ou, Y. Lu, J. Tan, Z. Huang, K. Wong, L. Gu. *Chem Med Chem.*, 2008, **3**, 690.

3. C. A. Puckett, R. J. Ernst, J. K. Barton. *Dalton Trans.,* 2010, **39**, 1159.

4. M. Read, R. J. Harrison, B. Romagnoli, F. A. Tanious, S. H. Gowan, A. P. Reszka, W. D. Wilson, L. R. Kelland, S. Neidle. *Proc. Nati. Acad. Sci. USA,* 2001, **98**, 4844.

5. N. H. Campbell, N. H. Abd Karim, G. N. Parkinson, M. Gunaratnam, V. Petrucci, A. K. Todd, R. Vilar, S. Neidle. *J. Med. Chem.,* 2012, **55**, 209.

6. P. Wu, D. Ma, C. Leung, S. Yan, N. Zhu, R. Abagyan, C. Che. *Chem. Eur. J.,* 2009, **15**, 13008.

7. E. Largy, F. Hamon, F. Rosu, V. Gabelica, E. De Pauw, A. Géudin, J. Mergny, M. P. Teulade-Fichou. *Chem. Eur. J.,* 2011, **17**, 13274.

8. M. Kato, K. Sasano, C. Kosuge, M. Yamazaki, S. Yano, M. Kimura. *Inorg. Chem.,* 1996, **35**, 116.

9. F. M. Freimoser, C. A. Jakob, M. Aebi, U. Tuor. *Appl. Environ. Microbiol.,* 1999, **65**, 3727.

Chapter 6: Further Synthesis and Development of the Biisoquinoline

Complex

6.1 Introduction

This chapter describes some initial synthetic attempts to introduce side arms onto the complex structure. Although the desired target was not achieved the routes show potential for future development.

The incorporation of side arms into the structure of a G-quadruplex binder provides another potential mode of binding between the DNA and the complex. Complexes that initially π-stack onto the terminal G-quartet can now, with the correctly positioned side arms, interact with the loops and grooves of the G-quadruplex also. Ideally the new linkages would be able to be protonated under cellular conditions providing electrostatic interactions between them and the DNA backbone.

An example of a complex designed with potentially interactive side arms is the copper(II) salphen complex (*Fig. 6.1 - a*) reported by Vilar *et al* [1]. Despite being a symmetrical complex the two side chains interact differently with the quadruplex.[1] One of them interacts with a quadruplex groove by extending downwards, causing the piperidine ring to be close enough to the quadruplex backbone to set up a water hydrogen bonding bridge (*Fig. 6.1 - b*).[1] The piperidine side arm on the other side of the molecule is close in space to the TTA loop however no interactions between the two have been reported.[1]
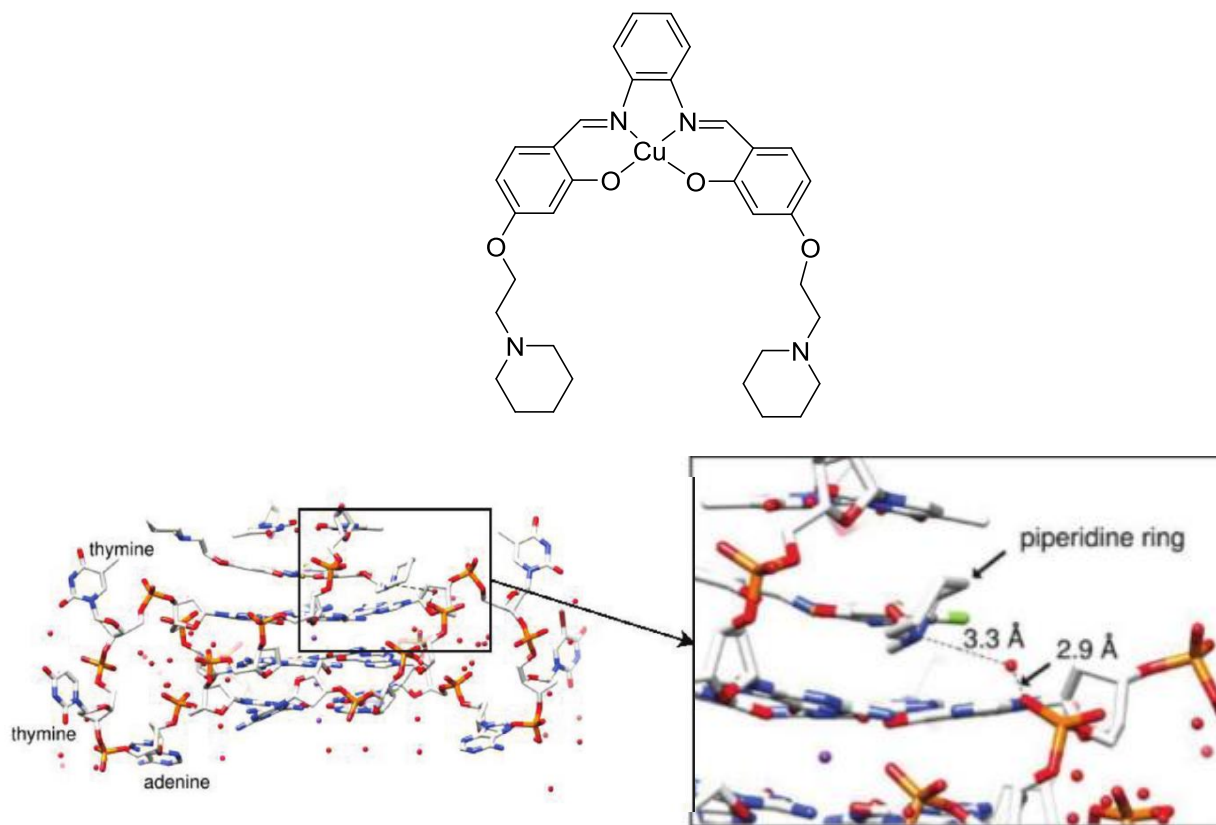
Figure 6.1 **a**. Structure of copper(II) salphen complex, **b**. Crystal structure of the copper(II) salphen complex with a telomeric G-quadruplex showing the positions of the two side chain piperidine rings with the groove binding side chain interaction enlarged to the right with the location of the water bridged H-bonding.[1]

In order to provide a better interaction with the TTA loops future work with this complex involves the lengthening of one of the side chains.[1]   This will allow the binding established with the groove to be maintained whilst a further interaction can be exploited to create a better and more specific binder.[1]

The biisoquinoline complexes presented in this thesis have the potential to be developed by incorporating additional side chains into the structure of the complex. At present they show good interactions with G-quadruplex DNA however they also interact with duplex DNA. The selectivity of the complexes as determined by PAGE and TO FID show good indications that the platinum complex binds more specifically to G-quadruplexes over duplex DNA. This selectivity however could be further enhanced by incorporating side chains that can interact with specific quadruplex loops.

The initial side chain chosen to be incorporated into the biisoquinoline structure was piperidine which is the same side chain used in the salphen work. Instead of providing two side chains to interact with the loops and grooves, attaching piperidine ligands to the biisoquinoline complexes will result in four side chains. The method of attaching each side arm involves the formation of a triazole linked product (*Fig. 6.2*) through click chemistry. Using the click chemistry mechanism allows the incorporation of a variety of side groups to quickly build up a library of complexes to investigate DNA and RNA quadruplex binding. [2][3][4]
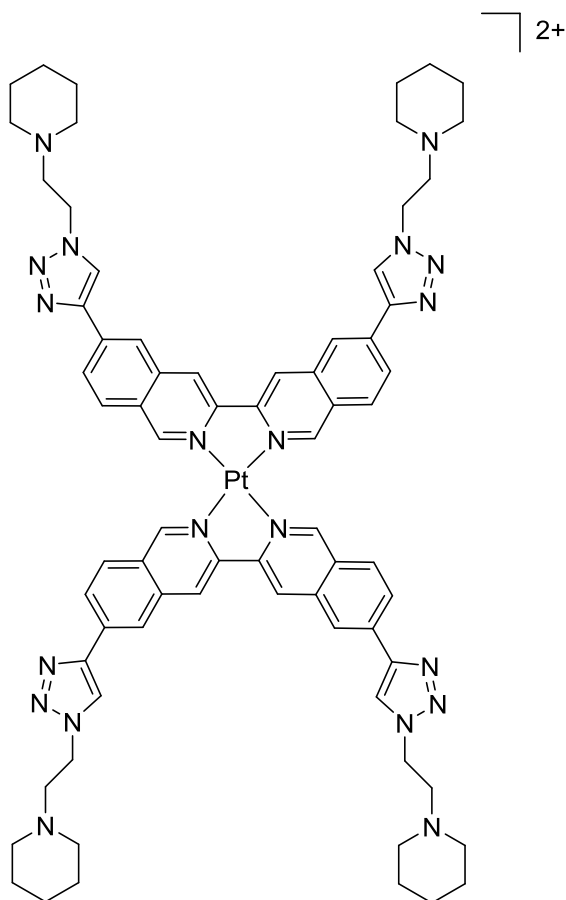
Figure 6.2 Target structure of platinum(II) biisoquinoline complex with additional triazole piperidine ligands.

6.2 Molecular Design

The synthesis of the biisoquinoline ligand with incorporated piperidine side arms requires a different synthesis route to that of the initial ligand covered in Chapter 2. At present there is no means to attach an additional group therefore a new synthesis route was developed, shown in *Scheme 6.1,* which ends with the precursor required for the click reaction to attach the piperdine side arms. The proposed reaction mechanisms can be found in section 2 of the Appendix.
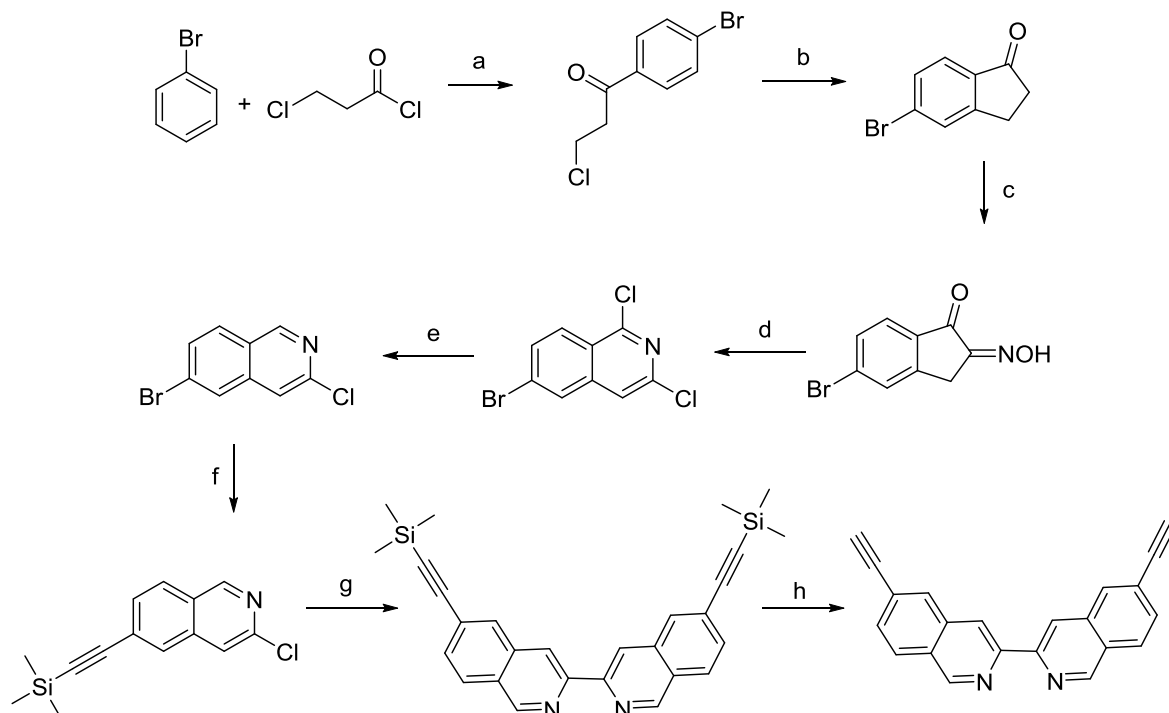
Scheme 6.1 Synthesis of 6-ethynyl-3,3-biisoquinoline under the following conditions; **a** - AlCl₃, CH₂Cl, **b** - AlCl₃, NaCl, 200 °C, **c** - n-butylnitrite, EtOH, HCl, **d** - POCl₃, PCl₅, gaseous HCl, 6 h 60 °C, **e** - P (red), HI, AcOH, 6 h 130 °C, **f** - PdCl₂(PPh₃)₂, CuI, Et₃N, (CH₃)₃SiC≡CH , N₂, **g** - [NiCl₂.6H₂O], Zn dust, PPh₃, DMF, 70°C 4 h, **h** - THF, MeOH, 1 M NaCl.

Step a: The synthesis begins with the readily available 3-chloropropionyl chloride (acid chloride) and bromobenzene compounds which undergo a Friedel-Crafts acylation in the presence of aluminium chloride (Lewis acid).[5] A stable acylium ion is formed from the acid chloride with Lewis acid catalysis before the attack on the bromobenzene through an electrophilic substitution mechanism producing an aromatic ketone (*Appendix 2.1*).[5] The ortho-para directing bromo group on the benzene ensures that the major product is para as bromine sterically hinders the ortho groups.[5]

Step b: The product is then subjected to harsh intramolecular ring closing conditions that once again involve a Fridel-Crafts alkylation (*Appendix 2.2*). High temperatures and

excess $AlCl_3$, combined with NaCl generate an ionic melt with 'latent acidity', which is required to remove the terminal chloride resulting in the creation of an unstable carbocation.[6] The NaCl is added to create a neutral buffered melt; for example if more acidic $AlCl_3$ is added the NaCl dissolves and reacts to generate $[AlCl_4]^-$.[6] If a strongly basic compound is added the Na^+ dissolved in the solution reacts to reform NaCl and precipitates out of the neutral solution.[6] When a weak Lewis base is added to the melt (such as 4-Bromophenyl 2-Chloroethyl Ketone) if the Na^+ concentration is greater than the base concentration all of the base will react to form an $AlCl_3$ adduct (*Scheme 6.2*).[6] The reaction of Na^+ and Cl^- drives the formation of the adduct which is generated when $[AlCl_4]^-$ forms an $AlCl_3$ adduct with the base.[6] Ring closure can then follow through an electrophilic substitution mechanism with the formation of a 5 membered ring producing the indoline product.

$$B: (l) + [AlCl_4]^- (l) + Na^+ (l) \rightarrow B \cdot AlCl_3 (l) + NaCl (s)$$
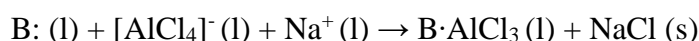
Scheme 6.2 Reaction occurring between NaCl and $AlCl_3$ when a weak Lewis base is added to the neutral melt mixture.

Step c: The corresponding oxime is formed through the nitrosation of the indoline product produced in **step b** using n-butyl nitrite in ethanol under acid catalysis (*Appendix 2.3*).[7] The reaction proceeds through the tautomeric enol form (structure is subject to keto-enol tautomerism) generated under the acidic conditions and reacts with the nitrite in a reaction analogous to the halogenation of ketones.[8] The nitrosation agent is generated from the hydrolysis of RONO under acid catalysis (effectively nitrous acid in its protonated form) shown in *Scheme 6.3*.[9]

RONO + HA → [A--H--O--N=O]‡ → ROH + A⁻ + NO⁺

$$RONO + HA \longrightarrow \left[A\text{-}\text{-}H\text{-}\text{-}\underset{\underset{R}{|}}{O}\text{-}\text{-}N{=}O \right]^{\ddagger} \longrightarrow ROH + A^{-} + NO^{+}$$
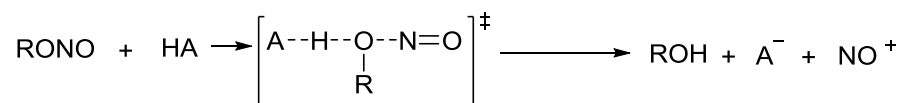
Scheme 6.3 Hydrolysis of RONO to produce nitrosation product NO⁺

Step d: The indone species can be converted into an isoquinoline through a modified Beckman rearrangement involving the expansion of the 5 membered ring into a 6 membered ring with the inclusion of nitrogen through the formation of nitrillium ion.[7] Once the diketone product is generated further PCl$_5$ is required in substitutive chlorination reactions to convert the ketone moieties into chlorides (*Appendix 2.4*).[7]

Step e: The 1-chloro group can be removed by a selective hydrogenolytic reaction using HI (57 % wt in H$_2$O) and red phosphorus heated to reflux in acetic acid.[7] The reduction mechanism by hydriodic acid is composed of two steps the first being the nucleophilic substitution of the chloride by iodide and the second the reduction of the alkyl iodide by hydriodic acid (*Scheme 6.4*).[10] The regioselective reaction ensures that the 3-chloro group and bromo group are not reduced as the chloride situated in position 1 is the most electron deficient (disruption of aromaticity is required for positive charge to rest on the other positions).
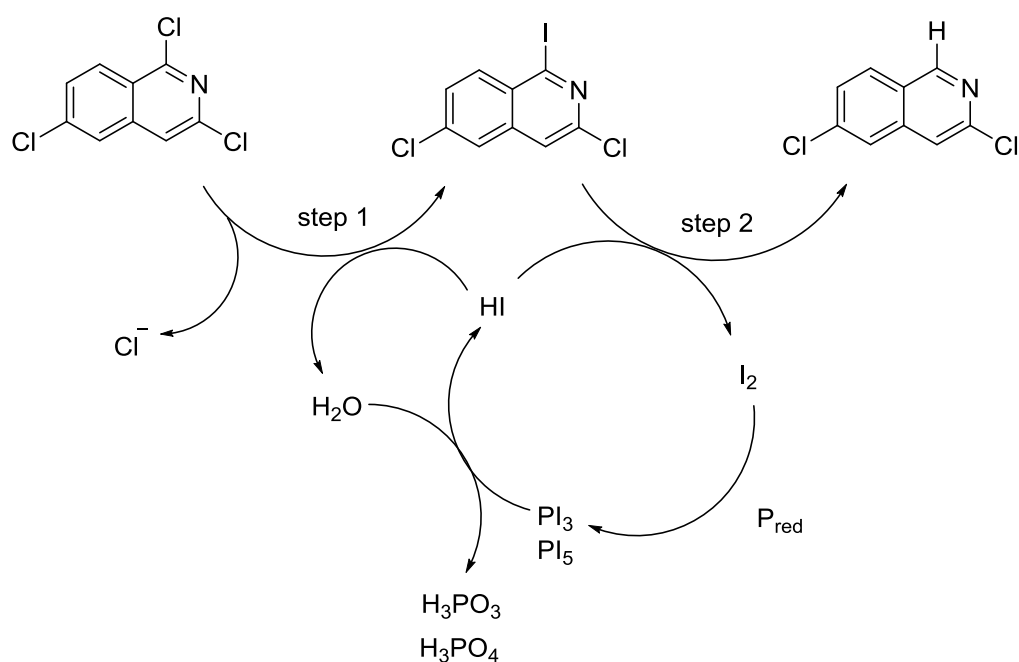
Scheme 6.4 Mechanism of chloride reduction and the reuse of iodine, (HI 57 % wt solution is the source of H_2O).[10]

Step f: A Sonogashira coupling reaction is able to substitute the bromide group for the more useful alkyne group protected with TMS (ethynyltrimethylsilane).[11] The catalytic cycle shown in *Scheme 6.5* involves the oxidative addition of 6-bromo-3-chloro isoquinoline to a Pd(0) catalyst.[11] The next step involves the transmetallation reaction between the newly formed Pd-alkyl halide complex and the Cu-alkyne resulting in a Pd complex containing both the alkyne and alkyl halide.[11] Reductive elimination then sees the formation of the coupled product and the palladium in its initial oxidation state.[11] The use of triethylamine in the reaction is important as it is involved in the deprotonation step that forms the alkyne anion, which can then bind to the oxidised copper.[11]
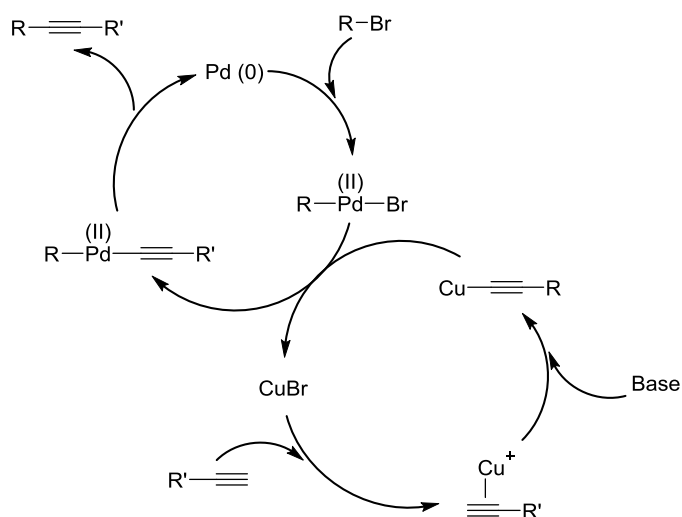
Scheme 6.5 Catalytic cycle of Sonogashira coupling.[11]

Step g: Before deprotecting, the 6-(2-trimethylsilyl)ethynyl-3-chloro isoquinoline compound is coupled with itself using the same conditions as for the 3-chloro isoquinoline compound to produce 3,3-biisoquinoline (nickel templated cycle - see Chapter 2).

Step h: In the final step of the modified biisoquinoline unit it is proposed that the alkyne groups can be deprotected by removal of the TMS group using either potassium carbonate and methanol or THF, methanol and 1 M NaOH.[12][13]

The addition of a piperidine ligand to each of the alkyne groups can then potentially be achieved using click chemistry.[2][3][4] This involves the synthesis of an azide appended to the piperidine ligand which can then be clicked into place through a copper-catalyzed azide–alkyne cycloaddition with the formation of a triazole moiety linking the isoquinoline block to the piperidine side arm (*Scheme 6.6*).
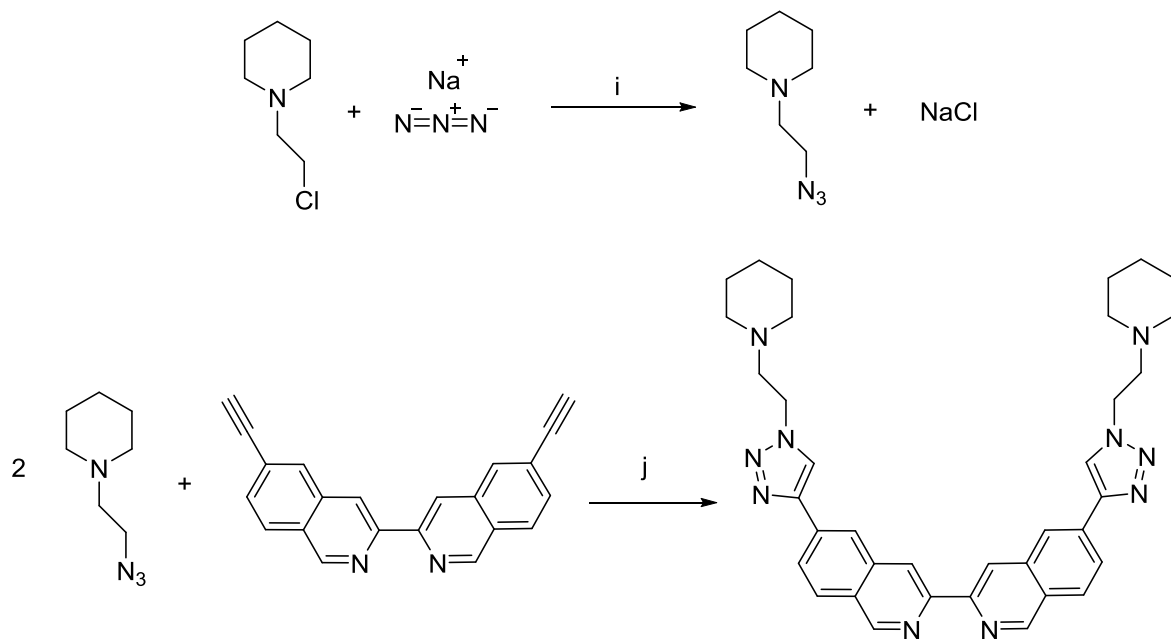
Scheme 6.6 Proposed synthesis of 6-piperidine-1,2,3-triazole-3,3-biisoquinoline under the following conditions; **i** - H_2O 15 h 80 °C, KOH/Et_2O, **j** - $CuSO_4$, Na ascorbate, H_2O:t-butyl alcohol (1:1) 15 h.

The copper catalysed reaction produces only one isomer, 1,4-disubstituted-1,2,3-triazole, and proceeds through the formation of a 5-triazolyl copper intermediate.[14]   As shown in *Scheme 6.7* a carbon-nitrogen bond is formed between the nucleophilic β-carbon of the newly formed copper(I) acetylide and the electrophilic terminal nitrogen of the bound azide.[14]
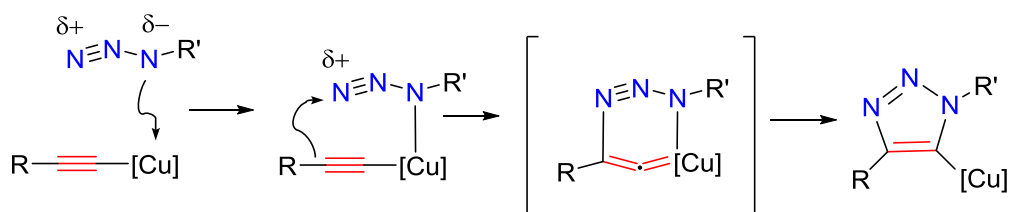
Scheme 6.7 Mechanism of triazole formation between an azide and an alkyne.[14]

Platinum and palladium metal centres can then potentially be utilised in the same way as the unmodified biisoquinoline complexes to produce the metal complexes that would go forward in further DNA binding experiments.

6.3   Synthesis and Characterisation of Ligand Building blocks

This section reports only the synthesis and characterisation for the building blocks shown in *Scheme 6.1*.   Difficulties in the deprotection of the modified biisoquinoline compound and time constraints prevented the completion of the fully modified compound and subsequent reactions to produce the palladium and platinum complexes.   The aim was to provide full analysis for each of the compounds however as compounds A, B, C, D, E and F have all been previously synthesised in the literature[15][16][17][18] this was not essential.

6.3.1   4-Bromophenyl 2-Chloroethyl Ketone (A)

Bromobenzene and 3-chloropropionyl chloride were individually mixed with dichloromethane and reacted together in the presence of aluminium chloride according to a literature procedure.[15]   After the reaction work up the product required purification by column chromatography giving a final yield of 82 %.   The reaction scheme for this reaction is shown in *Scheme 6.8*.
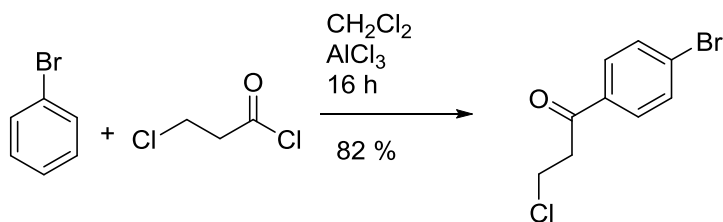
Scheme 6.8 Synthesis of 4-bromophenyl 2-chloroethyl ketone.

The electron ionisation mass spectrum shows the fragmented compound at the following m/z peaks; 212.0 $[C_9H_8OBr]^+$, 183.0 $[C_7H_4OBr]^+$ and 157.0 $[C_6H_4Br]^+$ (further fragments can be seen in the mass spectrum found in the *Appendix 1.10*). The ^{1}H-NMR spectrum (*Fig 6.3*) was assigned using 2D COSY and NOESY (see *Appendix 1.10*). The two groups of alkyl protons were easily distinguishable from the aromatic protons as they were seen at a much lower ppm as triplets. The full assignment was deduced using NOESY where only protons H_3 and H_2 showed long range couplings between each other.
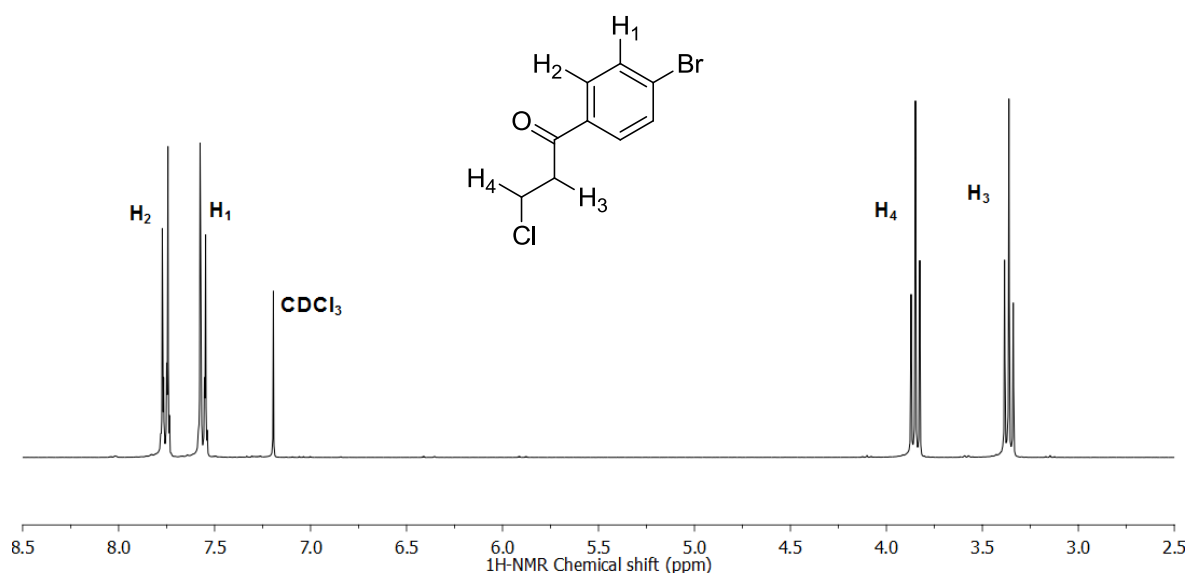
Figure 6.3 H-NMR spectrum (300 MHz, CDCl₃, 298 K) of 1,3-dione 4-bromophenyl 2-chloroethyl.

6.3.2 5-Bromoindan-1-one (B)

The next step of the building block synthesis involved the formation of an indoline following an intramolecular ring closing reaction (*Scheme 6.9*). The reaction required a mixture of AlCl₃ and NaCl to be melted by heating them to 200 °C before adding reagent **A** (4-bromophenyl 2-chloroethyl ketone), carried out according to literature procedure.[15] No further purification of the product after work up was required giving a 58 % yield.

269
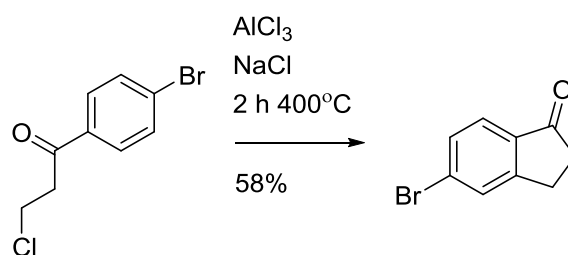
Scheme 6.9 Synthesis of 5-bromoindan-1-one.

Electron ionisation mass spectrometry resulted a number of fragmented peaks corresponding to the compound, the most abundant peaks being found at a m/z of 210.0 $[C_9H_7OBr]^+$ corresponding to the intact compound and 103.1 $[C_8H_7]^+$ (see *Appendix 1.11*). The ^{1}H-NMR spectrum (*Fig. 6.4*) was partly assigned using the splitting pattern of the aromatic peaks and comparison with the NMR spectra for its precursor (**A**). Proton H_1 would exist as a singlet as it has no adjacent protons whilst both protons H_2 and H_3 form doublets which couldn't be accurately assigned. Both protons H_2 and H_3 would be identified at a later stage of the synthesis as it was not necessary to formally identify them at this step in order to proceed to compound **C**. The proton NMR provides insight into the purity of the compound whereas the mass spectrum shows evidence of the compound formation.
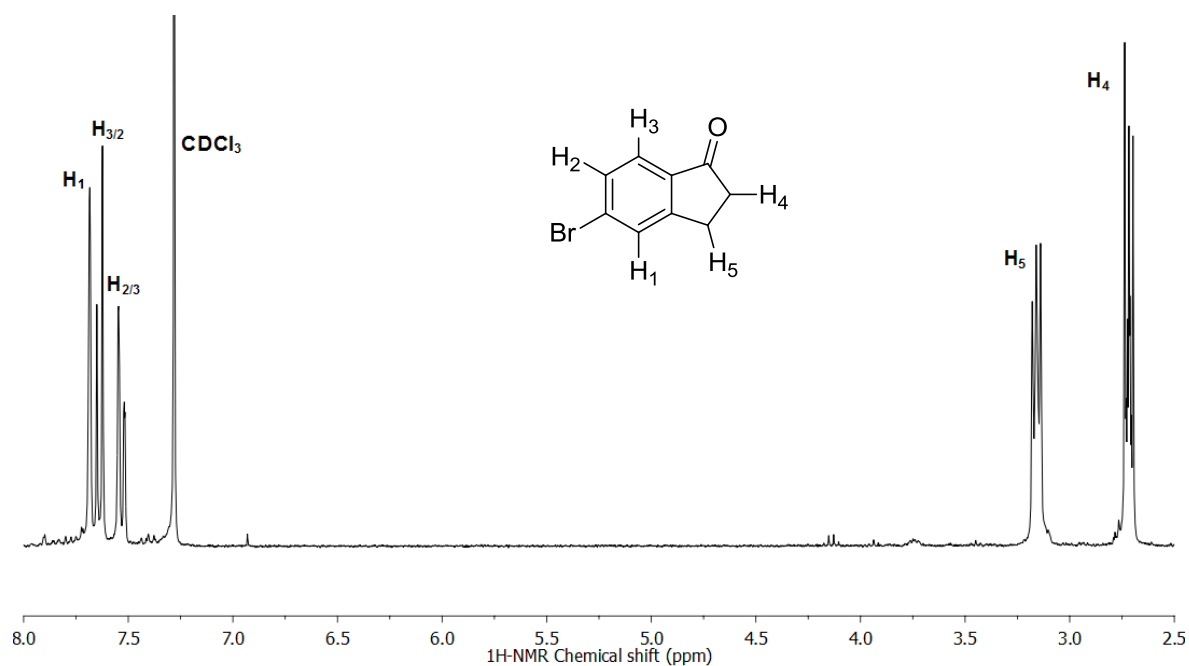
Figure 6.4 H-NMR spectrum (300 MHz, CDCl₃, 298 K) of 5-bromoindan-1-one ketone.

6.3.3 6-Bromo-Indan-1,2-Dione-1-Oxime (C)

The nitrosation of indoline (**B**) using n-butyl nitrite under acid catalysis resulted in the formation of the oxime shown in *Scheme 6.10*. The reaction proceeds through compound **B**'s tautomeric enol form whose formation is also the rate determining step of the reaction.[8] The synthesis was adapted from the literature and required no further purification generating a yield of 60 %.[16]
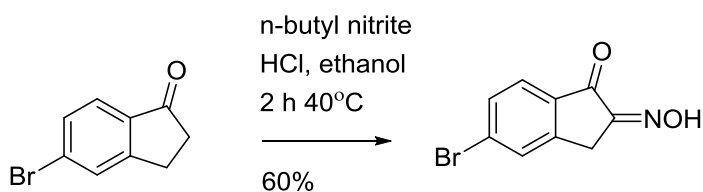
Scheme 6.10 Synthesis of 6-bromo-indan-1,2-dione-1-oxime.

The molecular ion peak at m/z 238.0 corresponding to $[C_9H_6O_2NBr]^+$ was found when analysing the compound by electrospray ionisation mass spectrometry (see *Appendix 1.12*). In the ^{1}H-NMR spectrum (*Fig. 6.5*) there is only one alkyl proton present which is no longer a triplet and instead a singlet (H_4) as it can no longer couple to an adjacent proton. The newly added NOH group is in the place of proton H_5. Protons H_1, H_2 and H_3 are in similar positions with the same multiplicity to precursor compound **B**.
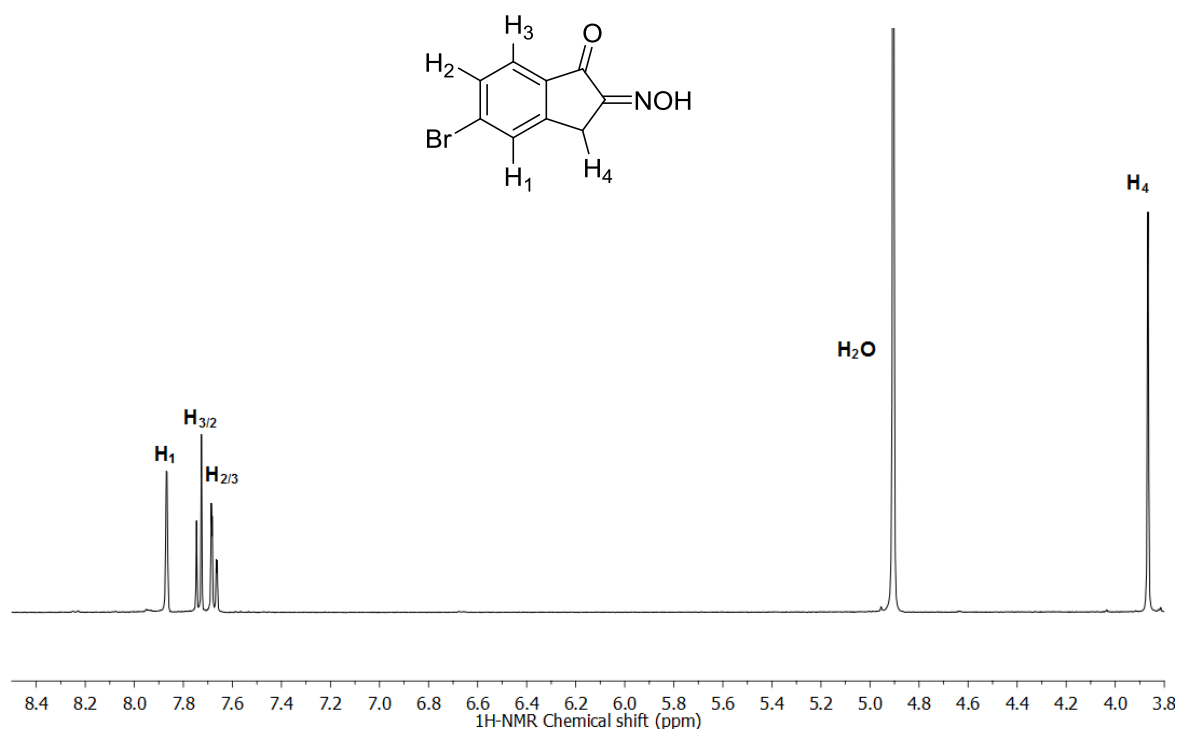
Figure 6.5 H-NMR spectrum (300 MHz, MeOD, 298 K) of 6-bromo-indan-1,2-dione-1-oxime.

6.3.4 6-Bromo-1,3-Dichloro-Isoquinoline (D)

The oxime was converted into the dichlorinated isoquinoline in a modified Beckmann rearrangement using an excess of phosphorus pentachloride in phosphorus oxychloride (*Scheme 6.11*).[7][17] The reaction mixture was saturated with gaseous hydrogen chloride which was produced in situ by the careful addition of concentrated HCl onto calcium carbonate. Extra care was taken to avoid any contact of water with reagents during the

reaction and when reducing *in vacuo*. The yield obtained from this stage of the reaction after purification using column chromatography was a disappointing 18 %. This may have been due to a leakage in the apparatus which after saturating with gaseous hydrogen chloride allowed air to leak into the system.

POCl$_3$, PCl$_5$
HCl gas
4 h 60°C
2 h 80°C (after excess PCl$_5$ addition)

18%
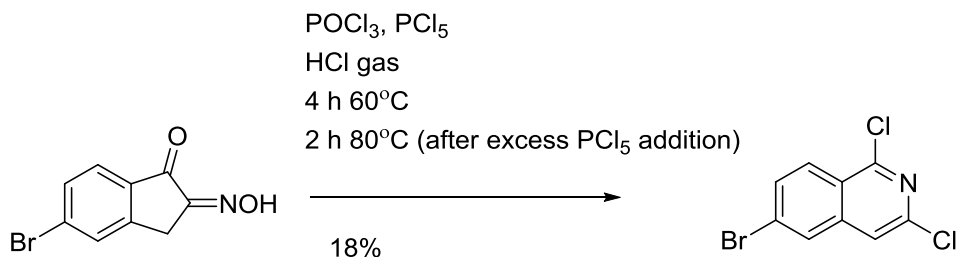
Scheme 6.11 Synthesis of 6-bromo-1,3-dichloro-isoquinoline.

The electron ionisation mass spectrometry spectrum displayed a molecular ion peak at a m/z of 276.9 consistent with the product formation (*Appendix 1.13*). The ^{1}H-NMR spectrum can be assigned by taking into account the ortho and meta contributions for each proton. Short range couplings to ortho positions exhibit larger coupling constants whereas long range couplings to meta exhibit smaller coupling constants. H$_3$ has one proton ortho to it (para proton is too far away to make a contribution) and has a J-coupling value of 6.9 Hz while H$_1$ which has one proton meta to it has a J-coupling value of 2.0 Hz (*Fig. 6.6*). H$_2$ meanwhile has a proton both ortho and meta to it therefore produces a doublet of doublets in the spectra with J-coupling values of 6.9 Hz and 2.0 Hz. Proton H$_4$ is part of the other aromatic ring and has no ortho or meta protons to interact with, therefore is seen as a singlet in the spectrum.
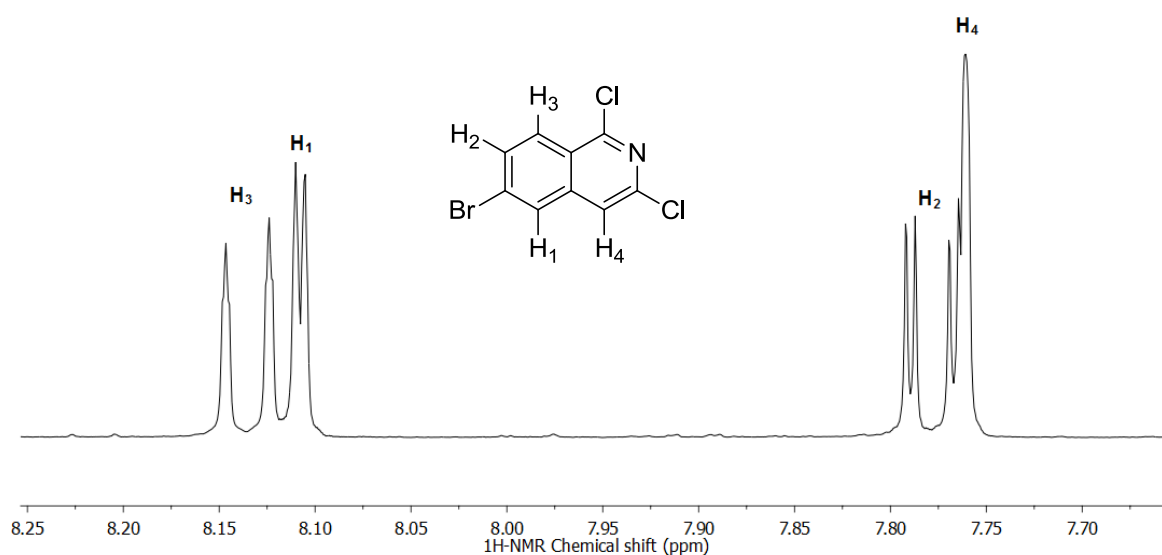
Figure 6.6   H-NMR spectrum (300 MHz, MeOD, 298 K) of 6-bromo-1,3-dichloro-isoquinoline.

6.3.5   6-Bromo-3-Chloro-Isoquinoline (E)

The method used in Chapter 2 to abstract the same chloro substituent using tin from 1,3-dichloroisoquinoline was not repeated due to very little product being produced that was also heavily contaminated with tin salts. In this experiment the dichlorinated product (**D**) was refluxed with hydriodic acid and red phosphorus in acetic acid in order to remove the 1-chloro substituent (*Scheme 6.12*).[7][17] The product synthesised required purification by column chromatography producing the product in a 27 % yield. Despite the % yield being very low the unreacted starting materials were more easily obtained than for the synthesis using tin.
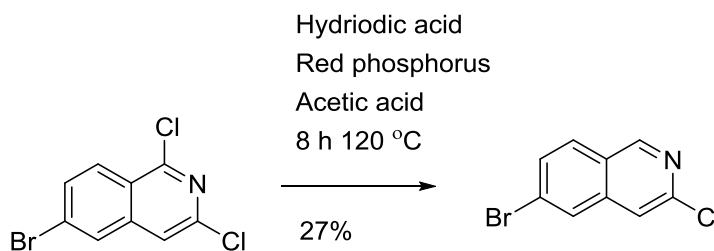
Scheme 6.12 Synthesis of 6-bromo-3-chloro-isoquinoline.

The molecular ion peak corresponding to the formation of he compound was found at a m/z of 242.9 [H + C_9H_5NClBr]$^+$ (see *Appendix 1.14*). The ^{1}H-NMR spectrum in *Figure 6.7* shows the emergence of a fifth proton environment after the removal of the 1-chloro substituent. Proton H_5 is seen furthest downfield (singlet peak) as it is closest to the electronegative nitrogen atom. H_4 is also shown as a singlet due to lack of coupling protons further upfield as it is further from nitrogen. H_1, H_3, and H_2 exist in a similar pattern to that seen in compound **D** where ortho and meta proton couplings dictate the magnitude of peak splitting.
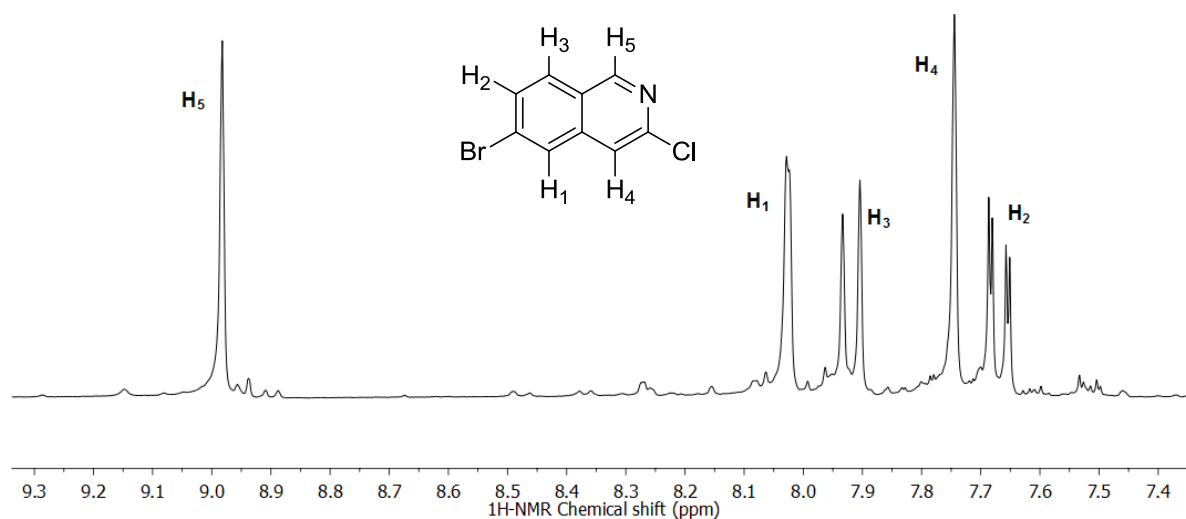
Figure 6.7 H-NMR spectrum (300 MHz, MeOD, 298 K) of 6-bromo-3-chloro-isoquinoline.

6.3.6 6-(2-Trimethylsilyl)Ethynyl-3-Chloro-Isoquinoline (F)

The bromide group in position 6 was removed and replaced with ethynyltrimethylsilane in the palladium catalysed cycle, shown at the beginning of this subchapter, in a reaction mixture containing $PdCl_2(PPh_3)_2$, copper(I) iodide and triethylamine (*Scheme 6.13*).[11][18]

Operating in an inert atmosphere the Sonogashira coupling reaction produced, after column chromatography using silica gel, a 63 % yield.
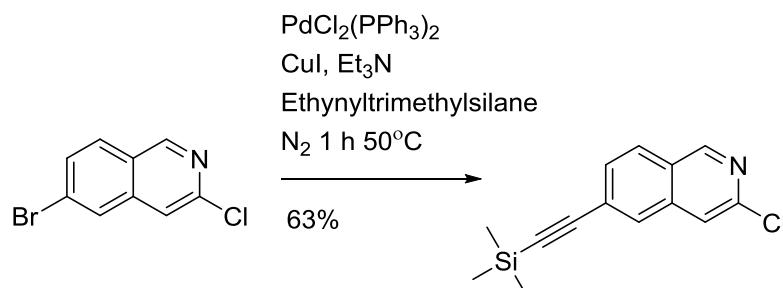
Scheme 6.13 Synthesis of 6-(2-trimethylsilyl)ethynyl-3-chloro-isoquinoline.

Electron ionisation mass spectrometry data produced a molecular ion peak at 259.1 corresponding to $[C_{14}H_{14}NClSi]^+$ (see *Appendix 1.15*). Clear evidence is seen in the ^{1}H-NMR spectrum in *Figure 6.8* for the formation of the required product. The singlet peak at 0.27 ppm has an integration of nine and is representative of the trimethylsilane part of the newly added substituent. The protons H_3 and H_1 have also switched places when compared with compound **E.** The bromine atom would have had a more significant deshielding effect on the adjacent proton than the carbon replacing it hence H_1 seen slightly further upfield. Protons H_3 and H_2 can be assigned based on their ortho and meta coupling patterns (H_3 is a doublet and H_2 is a doublet of doublets).
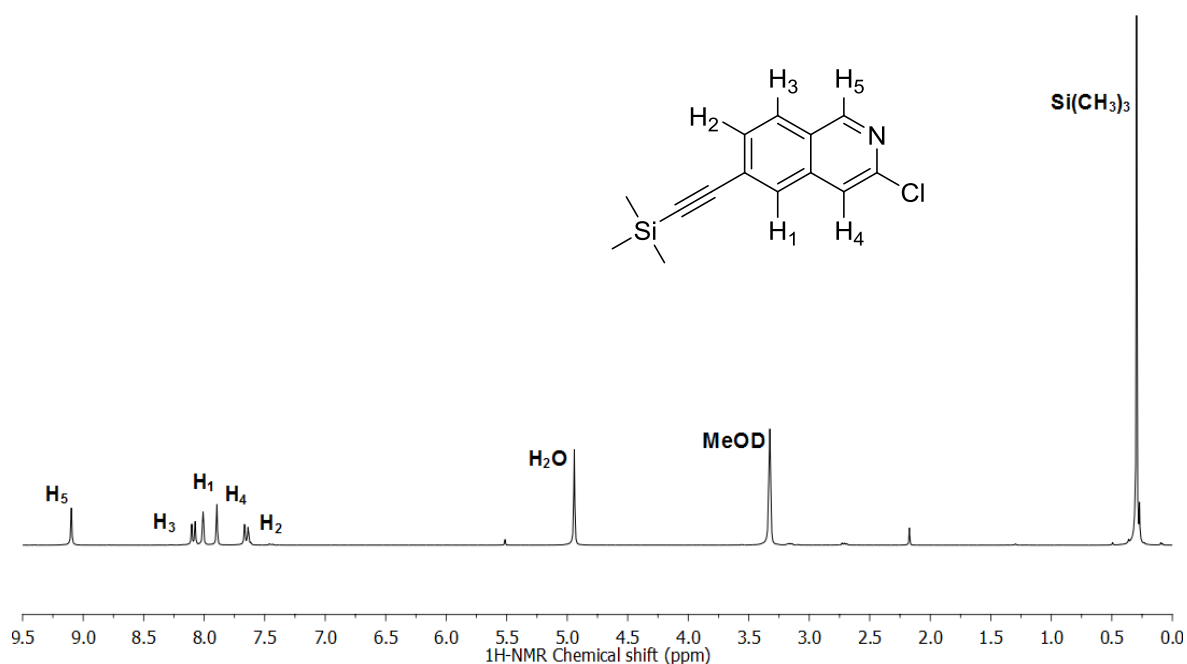
Figure 6.8 H-NMR spectrum (300 MHz, MeOD, 298 K) of 6-(2-trimethylsilyl)ethynyl-3-chloro-isoquinoline.

6.3.7   6-Ethynyl-3,3-Biisoquinoline (G)

The coupling of the two modified isoquinoline units was carried out using a nickel complex as a template with triphenylphosphine and zinc dust in DMF (*Scheme 6.14*).   The experiment proceeded as for the unmodified isoquinoline units with the reduction of the nickel complex by the zinc dust (turning the solution from green to red) and then adding the compound and leaving it to react for four hours.   Column chromatography was used to purify the product, the main contaminant being triphenylphosphine oxide, before deprotecting using a 18 ml solution of THF:MeOH (2:1) and 1 M NaOH (6 ml).[13] Unfortunately the deprotection step was not completely successful and the product contained a mixture of protected and deprotected biisoquinoline compounds. The probable cause of this was the lack of solubility of the compound and length of reaction time, both of which could be addressed in further experimental work.   The overall yield for the mixture of protected and deprotected compound was 0.4 % which although a little bit

277

disappointing, was only the first attempt at this synthesis which with more starting material

may be optimised.
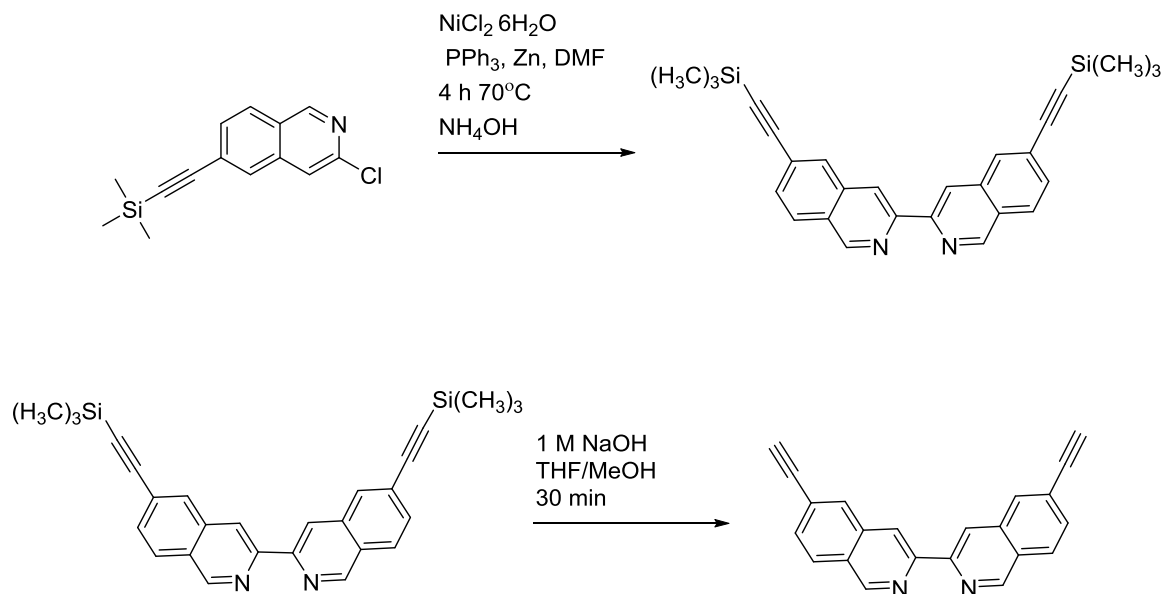
Scheme 6.14 Synthesis of 6-ethynyl-3,3-biisoquinoline.

The final ^{1}H-NMR spectrum contains a mixture of the deprotected and protected modified

biisoquinoline compounds (*Fig. 6.9*) which can also be seen in the mass spectrum

(*Appendix 1.16*) with molecular ion peaks at 449.2 and 305.1 (protected and deprotected

respectively). There is also a small amount of monodeprotected compound which has a

molecular ion peak at 399.1. An attempt at assigning the ^{1}H-NMR peaks was made by

considering the integration of the newly formed alkyne peak and comparing with both

peaks belonging to proton H_5. Only one of these peaks matches the integration therefore

the other peak must be from the protected compound and hence will correlate with the

integrated TMS peak. The protons H_2 and H_3 could not be fully assigned for each

compound as they shift very little between forms and therefore have too great an overlap to

integrate separately. The presence of the monodeprotonated compound will also have an

effect on the spectrum (however the concentration of this species is much lower) which

278

further prevents the full assignment of the spectrum. This can only be acheived upon purification of the mixture.
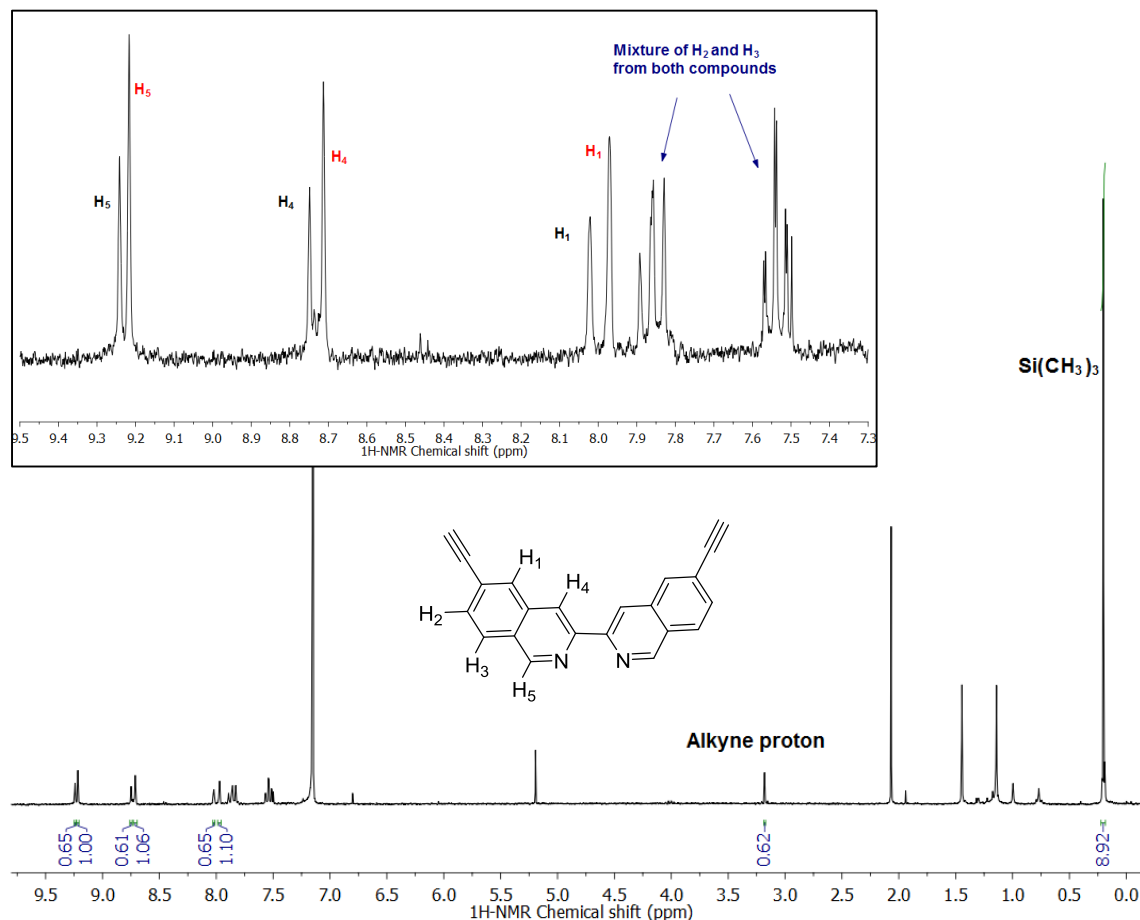
Figure 6.9 H-NMR spectrum (300 MHz, CDCl$_3$, 298 K) of the protected (red) and deprotected (black) forms of 6-ethynyl-3,3-biisoquinoline, only deprotected structure displayed.

6.4   Conclusions

The development of the biisoquinoline complex used in the DNA and RNA binding and cell toxicity experiments was explored resulting in a molecular design incorporating protonatable side arms that have the potential to interact with the loops of a G-quadruplex. Piperidine type appendages have been used in other quadruplex binding complexes in the

literature therefore work was started to combine them with the well fitting stackable biisoquinoline complex unit

The same synthetic route for the unmodified biisoquinoline ligand could not be followed as to incorporate the new side arms a 6-bromo moiety was required, therefore a new reaction scheme was designed. Despite the synthesis requiring many steps, once the ethylene modified biisoquinoline compound can be synthesised a whole host of possibilities for side arm addition can be considered by utilising click chemistry.

Unfortunately due to lack of time the synthesis of the completed ligand with the additional clicked piperidine side arms was not achieved. Despite this 6-ethynyl-3,3-biisoquinoline was produced and characterised by mass spec and ^{1}H-NMR, although not in an entirely pure form due to the presence of the TMS protected compound. The presence the deprotected compound suggests the deprotection step was partially successful and can be modified in order to produce a pure yield.

6.5 Experimental

General Methods

All characterisation techniques took place within the University of Birmingham. NMR spectra were recorded in $CDCl_3$ and CD_3OD. 1D ^{1}H NMR and COSY spectra were recorded on BrukerAV(III) 300 and AV(III) 400 instruments operating at 300 MHz and 400 MHz respectively. ^{13}C NMR and HSQC spectra were recorded on a BrukerAV(III) 400 instrument operating at 100 MHz. Electrospray ionisation was performed on a Waters

LCT Time of Flight Spectrometer and electron impact mass spectrometry on a VG

ZabSpec mass spectrometer. A Varian Cary 5000 UV-Vis spectrometer was used to

obtain UV-Vis spectra for the complexes and infrared spectra were recorded on a Perkin

Elmer Spectrum 100 FT-IR spectrometer. Full characterisation, although aimed for, was

not necessary for compounds A - F as they have been previously synthesised in the

literature.[15][16[17][18]

The compounds and solvents used were obtained from Fisher, Sigma Aldrich, Scientific

Laboratory Supplies and Acros organics. All the solvents were of a laboratory reagent

grade and were used without further purification

4-Bromophenyl 2-Chloroethyl Ketone (A) [15]

Molecular weight = 247.52 gmol^{-1}

Molecular Formula = C_9H_8OClBr
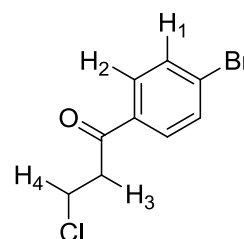
To a suspension of aluminium chloride (26.1 g, 0.2 mol) and dichloromethane (45ml) was

added a solution of 3-chloropropionyl chloride (20 ml, 0.2 mol) in dichloromethane (13

ml). The mixture was allowed to stir at room temperature for 15 minutes before adding a

solution of bromobenzene (20 ml, 0.2 mol) in dichloromethane (13 ml) portion wise over

the course of 1 h. After stirring at room temperature for 16 h the mixture was poured onto

a mixture of ice and 1M hydrochloric acid. The organic phase was then washed with water

and then an aqueous solution of sodium bicarbonate, dried over magnesium sulfate and

dried *in vacuo*. The residue was then purified by column chromatography (silica gel, 15:1,

petroleum ether:ethyl acetate, Rf 0.2) to leave a pale orange powder, 40.5 g, 82 % yield.

^{1}H NMR (400 MHz, CDCl$_3$): δ 7.82 (d, 2H, J = 8.8, H$_2$), 7.63 (d, 2H, J = 8.4, H$_1$), 3.91 (t, 2H, J = 6.8, H$_4$), 3.43 (t, 2H, J = 6.8, H$_3$).

^{13}C NMR (100 MHz, CDCl$_3$): δ 132.1 (C$_{H1}$), 129.6 (C$_{H2}$), 41.2 (C$_{H3}$), 38.5 (C$_{H4}$).

IR (Solid): ν = 1612 (s), 1507 (m), 1463 (s), 1126 (s), 1088 (s), 1036 (s), 860 (w), 757 (s) cm^{-1}.

Mass analysis (EI, +ve): m/z = 212.0 [C$_9$H$_8$OBr]$^+$, 183.0 [C$_7$H$_4$OBr]$^+$, 157.0 [C$_6$H$_4$Br]$^+$.

5-Bromoindan-1-one (B) [15]

Molecular weight = 210.15 gmol^{-1}

Molecular Formula = C$_9$H$_7$OBr
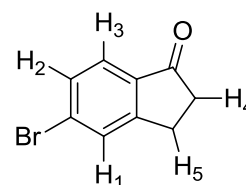
Aluminium chloride (54.0 g, 0.4 mol) and sodium chloride (11.8 g, 0.2 mol) were mixed together and heated to 200°C. When the compounds had melted 4-bromophenyl 2-chloroethyl ketone (**A**) (10 g, 0.04 mol) was added over a period of 10 min before leaving to react at 200°C for 2 h. The hot mixture was poured into a beaker of ice and 1M hydrochloric acid and extracted with ethyl acetate. It was washed with a sodium bicarbonate solution, followed by water, dried over magnesium sulfate and then dried *in vacuo*. 4.86 g, 58 % yield.

^{1}H NMR (400 MHz, CDCl$_3$): δ 7.66 (s, 1H, H$_1$), 7.61 (d, 1H, J = 8.4, H$_{3/2}$), 7.51 (d, 1H, J = 8.4, H$_{2/3}$), 3.14 (t, 1H, J = 5.6, H$_5$), 2.70 (t, 1H, J = 6.0, H$_4$).

^{13}C NMR (100 MHz, CDCl$_3$): δ 131.0 (C$_{H2}$), 130.0 (C$_{H1}$), 125.0 (C$_{H3}$), 36.2 (C$_{H4}$), 25.5 (C$_{H5}$).

IR (Solid): ν = 1698 (m), 1571 (w), 1435 (w), 1318 (w), 1267 (w), 836 (w), 813 (w) cm^{-1}.

Mass analysis (EI, +ve): m/z = 210.0 $[C_9H_7OBr]^+$, 103.1 $[C_8H_7]^+$.

6-Bromo-Indan-1,2-Dione-1-Oxime (C) [16]

Molecular weight = 238.05 gmol^{-1}

Molecular Formula = $C_9H_6O_2NBr$
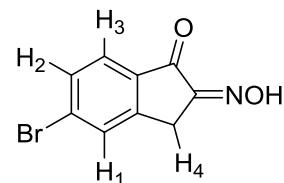
A solution of 5-bromoindan-1-one (**B**) (3.1 g, 0.015 mol) in ethanol (250ml) was heated to 40°C before adding drop wise n-butylnitrite (1.9 ml, 0.016 mol) followed by the drop wise addition of concentrated HCl (1.3 ml). The solution was then left to stir for 1.5 h at 40°C before reducing *in vacuo*. The resulting orange solid was washed with water and left to dry under vacuum. 2.12 g, 60% yield.

^{1}H NMR (300 MHz, MeOD): δ 7.87 (s, 1H, H_1), 7.73 (d, 1H, J = 8.0, $H_{3/2}$), 7.67 (d, 1H, J = 8.0, $H_{2/3}$), 3.87 (s, 2H, H_4).

^{13}C NMR (100 MHz, MeOD): δ 132.6 (C_{H2}), 131.6 (C_{H1}), 126.4 (C_{H3}), 29.0 (C_{H4}).

IR (Solid): ν = 3251 (br, m), 1730 (m), 1655 (w), 1598 (m), 1419 (w), 1316 (m), 1258 (m), 1035 (w), 903 (s), 827 (m), 741 (m) cm^{-1}.

Mass analysis (ESI, +ve): m/z = 238.0 $[C_9H_6O_2NBr]^+$.

6-Bromo-1,3-Dichloro-Isoquinoline (D) [17]

Molecular weight = 276.94 gmol^{-1}

Molecular Formula = $C_9H_4Cl_2NBr$
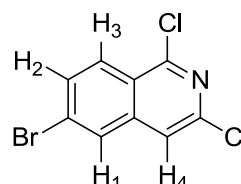
6-Bromo-Indan-1,2-Dione 1-Oxime (**C**) (1.6 g, 6.7mmol) was suspended in POCl$_3$ (41.5 ml) before carefully treating with PCl$_5$ (1.6 g, 7.7 mmol). A stream of HCl gas was generated by dripping hydrochloric acid onto calcium carbonate which was then introduced to the solution until it was saturated. Only then was the mixture heated to 60°C and left to stir for 6 h. The dark brown solution generated was reduced in *vacuo,* taking care not to bring the solution into contact with water, before hydrolysing the residue with water, extracting with ethyl acetate, washing with brine then water, drying over magnesium sulphate and finally reducing *in vacuo*. The crude product was purified by column chromatography (silica gel, 9:1, hexane: ethyl acetate, Rf 0.7). 0.34 g, 18 % yield.

^{1}H NMR (300 MHz, MeOD): δ 8.24 (d, 1H, J = 9.2, H$_3$), 8.22 (d, 1H, J = 2.0, H$_1$), 7.89 (dd, 1H, J = 9.2, 2.0, H$_2$), 7.87 (s, 1H, H$_4$).

^{13}C NMR (100 MHz, MeOD): δ 133.8 (C$_{H2}$), 130.1 (C$_{H1}$), 129.1 (C$_{H3}$), 120.4 (C$_{H4}$).

IR (Solid): ν = 1607 (m), 1549 (m), 1471 (m), 1336 (w), 1286 (m), 1155 (w), 1060 (m), 980 (s), 891 (s), 854 (m), 809 (s) cm^{-1}.

Mass analysis (EI, +ve): m/z = 276.9 [C$_9$H$_4$Cl$_2$NBr]$^+$.

6-Bromo-3-Chloro-Isoquinoline (E) [17]

Molecular weight = 240.93 gmol^{-1}

Molecular Formula = C$_9$H$_5$NClBr
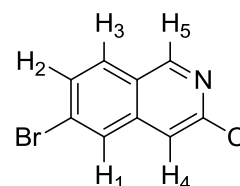
6-Bromo-1,3-dichloro-isoquinoline (**D**) (2.87 g, 0.01 mol (from multiple batches of **D**), red phosphorus (0.77 g, 0.02 mol), hydriodic acid (4.7 ml, 0.10 mol) and acetic acid (17 ml) were mixed together and heated at reflux for 8 h. The mixture was then hot filtered

through celite and then reduced *in vacuo*. A 1 M sodium hydroxide solution was used to basify the residue before extracting with ethyl acetate, washing with brine, drying over magnesium sulfate and reducing again *in vacuo*. The crude product was then purified by column chromatography (silica gel, 7:3, hexane: ethyl acetate, Rf 0.6). 0.64 g, 27 % yield.

^{1}H NMR (300 MHz, MeOH): δ 9.09 (s, 1H, H$_5$), 8.15 (s, 1H, H$_1$), 8.03 (d, 1H, J = 8.7, H$_3$), 7.86 (s, 1H, H$_4$), 7.78 (d, 1H, J = 8.7, H$_2$).

IR (Solid): ν = 1615 (m), 1479 (m), 1383 (m), 1269 (w), 1058 (m), 943 (s), 805 (m), 788 (m) cm^{-1}.

R$_f$ value: 0.6 (7:3, hexane: ethyl acetate)

Mass analysis (EI, +ve): m/z = 242.9 [H + C$_9$H$_5$NClBr]$^+$.

6-(2-Trimethylsilyl)Ethynyl-3-Chloro Isoquinoline (F) [18]

Molecular weight = 259.06 gmol^{-1}

Molecular Formula = C$_{14}$H$_{14}$NClSi
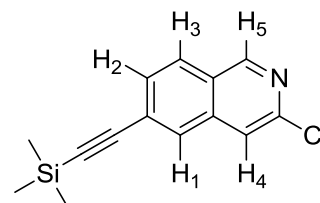
PdCl$_2$(PPh$_3$)$_2$ (22.6 mg, 0.03 mmol) and copper(I) iodide (18 mg, 0.1 mmol) were added to a solution of 6-bromo-3-chloro-isoquinoline (**E**) (0.64 g, 2.7 mmol) in triethylamine (13 ml). Nitrogen was bubbled through the solution for 1 minute to degas it before adding ethynyltrimethylsilane (0.2 ml, 1.4 mol) and heating the mixture to 50°C for 1 h. The solvent was then removed *in vacuo* before purifying by column chromatography (silica gel, 5:95, ethyl acetate: hexane, Rf 0.2). 0.44 g, 63 % yield.

285

^{1}H NMR (300 MHz, MeOD): δ 9.09 (s, 1H, H$_5$), 8.08 (d, 1H, J = 8.7, H$_3$), 8.00 (s, 1H, H$_1$), 7.89 (s, 1H, H$_4$), 7.64 (d, 1H, J = 8.4, H$_2$), 0.28 (s, 9H, Si(CH$_3$)$_3$)

^{13}C NMR (100 MHz, MeOD): δ 153.9 (C$_{H5}$), 131.7 (C$_{H2}$), 130.7 (C$_{H1}$), 129.4 (C$_{H3}$), 121.0 (C$_{H4}$).

IR (Solid): ν = 2967 (w), 1619 (m), 1611 (w), 1481 (m), 1430 (m), 1372 (m), 1242 (m), 1191 (m), 1072 (m), 839 (s) cm^{-1}.

Mass analysis (EI, +ve): m/z = 259.1 [C$_{14}$H$_{14}$NClSi]$^+$, 244.1 [C$_{13}$H$_{11}$NClSi]$^+$

6-Ethynyl-3,3-Biisoquinoline (G)

Molecular weight = 302.84 gmol^{-1}

Molecular Formula = C$_{22}$H$_{12}$N$_2$
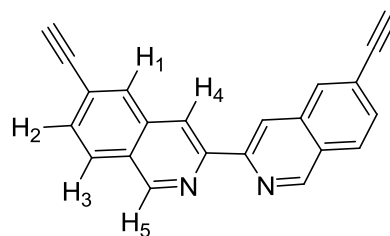
Part 1

As for 3,3-biisoquinoline, under an argon atmosphere [NiCl$_2$.6H$_2$O] (826 mg, 3.48 mmol), PPh$_3$ (3.67 g, 14.0 mmol) and (washed) zinc dust (246 mg, 3.76 mmol) were added to a Schlenk tube. DMF (39 ml) was then added by syringe into the sealed vessel. The brick red solution that formed was left to stir at 70°C for an hour before adding a degassed solution of 6-(2-trimethylsilyl)ethynyl-3-chloro isoquinoline (**F**) (0.9 g, 3.47 mmol) in DMF (20 ml). The mixture was then left to heat at 70°C for 4 h. After heating, the mixture was allowed to cool to room temperature before pouring onto a 7 % ammonium hydroxide solution (19 mL) – a small amount of concentrated (28 %) ammonium hydroxide was added to ensure all the ligand has been removed from the metal. The product was then extracted in dichloromethane and diethyl ether (2:1, 3 x 65 ml) before removing the solvent from the organic layer *in vacuo*. The brown oil that remained was

diluted with dichloromethane (40 ml) and washed with water (4 x 13 ml) and brine (26 ml) before drying over MgSO₄ and reducing *in vacuo* to a brown solid. This was purified by column chromatography (silica gel, CH₂Cl₂ followed by ethyl acetate, Rf 0.4) to give a yellow solid. This was followed by another column to remove any traces of triphenylphosphine oxide (silica gel, diethyl ether) which again left a yellow solid.

Part 2[13]

The coupled product was immediately taken through to the de-protection step by dissolving the product in THF (12 ml) and then diluting this with methanol (6 ml). 1 M NaOH solution (6 ml) was then added to the reaction mixture and it was left to stir for 30 min. After this time diethyl ether was added (30 ml) and the solution left to stir again for a further 15 min. The product was then extracted, washed with brine and dried over sodium sulfate. The product still remained a mixture of protected and de-protected products. 2 mg, 0.4 % yield.

Protected Compound
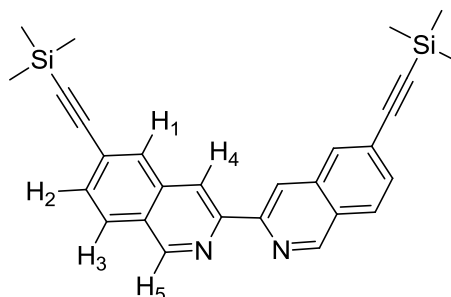
^{1}H NMR (300 MHz, CDCl₃): δ 9.22 (s, 1H, H₅), 8.71 (s, 1H, H₄), 7.97 (s, 1H, H₁), 7.89 - 7.83 (m, 1H, H₂ or 3), 7.57 - 7.51 (m, 1H, H₃ or 2), 0.20 (s, 9H, Si(CH₃)₃).

Mass analysis (ESI, +ve): m/z = 449.2 [H(C₂₈H₂₈N₂Si₂)]⁺, 471.1 [Na(C₂₈H₂₈N₂Si₂)]⁺.

287

De-protected Compound
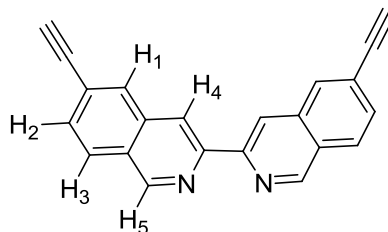
^{1}H NMR (300 MHz, CDCl$_3$): δ 9.24 (s, 1H, H$_5$), 8.75 (s, 1H, H$_4$), 8.02 (s, 1H, H$_1$), 7.89 - 7.83 (m, 1H, H$_{2\,or\,3}$), 7.57 - 7.51 (m, 1H, H$_{3\,or\,2}$), 3.18 (s, 1H, alkyne).

Mass analysis (ESI, +ve): m/z = 305.1 [H(C$_{22}$H$_{12}$N$_2$)]$^+$, 327.1[Na(C$_{22}$H$_{12}$N$_2$)]$^+$.

6.6 References

1. N. H. Campbell, N. H. Abd Karim, G. N. Parkinson, M. Gunaratnam, V. Petrucci, A. K. Todd, R. Vilar, S. Neidle. *J. Med. Chem.,* 2012, **55**, 209.

2. R. Rajaganesh, P. Ravinder, V. Subramanian, T. Mohan Das. *Carboydr. Res.,* 2011, 346, 2327.

3. V. V. Rostovtsev, L. G. Green, V. V. Fokin, K. B. Sharpless. *Angew. Chem. Int. Ed.,* 2002, **41**, 2596.

4. Z. Liang, L. Zhang, L. Li, J. Lui, H. Li, L. Zhang, L. Chen, K. Cheng, M. Zheng, X. Wen, P. Zhang, J. Hao, Y. Gong, X. Zhu, J. Chen, H. Liu, H. Jiang, C. Luo, H. Sun. *Eur. J. Med. Chem.,* 2011, **46**, 2011.

5. *Organic Chemistry, third edition.* M. Jones Jr, W. W. Norton and Company, Inc, New York, 2005.

6. R. A. Mantz, P. C. Trulove, R. T. Carlin, T. L. Theim, R. A. Osteryoung. *Inorg. Chem.,* 1997, **36**, 1227.

7. W. Bartmann, E. Konz, W. Rüger. *J. Heterocyclic Chem.,* 1987, **24**, 677.

8. Alan Graham, *PhD Thesis,* Durham University, 1991.

9. M. J. Crookes, D. Lyn H. Williams. *J. Chem. Soc. Perkin. Trans. II,* 1998, **7**, 1339.

10. M. Dobmeier, J. M. Herrmann, D. Lenoir, B. König. Beilstein *J. Org. Chem.,* 2012, **8**, 330.

11. R. A. D. Arancon, C, Sze Ki Lin, C. Vargas, R. Luque. *Org. Biomol. Chem.,* 2014, **12**, 10.

12. E. Merkul, F. Klukas, D. Dorsch, U. Grädler, H. E. Greiner, T. J. J. Müller. *Org. Biomol. Chem.*, 2011, **9**, 5129.

13. J. Li, M. Hu, S. Q. Yao. *Org. Lett.*, 2009, **11**, 3008.

14. J. E. Hein, V. V. Fokin. *Chem Soc Rev.,* 2010, **39**, 1302.

15. T. G. C. Bird, W. L. Reims, P. Ple. US Pat., 005332757A, 1994.

16. A. Nakao, H. Suzuki, R. Tatsumi, T. Setsuta, M. Seki, H. Iwasaki, M. Tanaka. US Pat., 20120196824A1, 2012.

17. Q. Li, K. W. Woods, G. Zhu, J. P. Fischer, J. Gong, T. Li, V. Gandhi, S. A. Thomas, G. K. Packard, X. Song, J. N. Abrams, R. Diebold, J. Dinges, C. Hutchkins, V. S. Stoll, S. H. Rosenberg, V. L. Giranda. US Pat., 20030187026A1, 2003.

18. S. Hoelder, J. Blagg, J. Cheung, B. Rash, P. Sheldrake. WO., 2014037751A1, 2014.

Chapter 7: Conclusions and Future Work

7.1 Conclusions

Specific targeting of cellular processes by complexes has led to designs based on the associated DNA. Notable examples of such complexes include the supramolecular iron helicate which targets three way and Y-shaped junctions and $[Rh(bpy)_2chrysi]^{3+}$ which targets DNA mismatches.[1][2] G-quadruplexes are another type of DNA structure that have been linked to processes that control replication and transcription. Complexes seen in research conducted by Vilar and Teulade-Fichou are designed to target G-quadruplexes by incorporating a large end stacking surface area with an overall positive charge (from a central metal ion) to maximise interactions with the terminal G-quartet of the quadruplex. Quadruplex only binders will prevent the B-DNA structure from being unnecessarily damaged by unspecific targeting. The synthesis of a highly specialised complex that can prevent the continuous replication of cancerous cells (by preventing telomerase action) or stop oncogene promoter regions from over producing transcription factors is advantageous. This is especially true if the complex can offer specific binding to mutated DNA whilst maintaining the health of B-DNA; offering an effective anticancer alternative to conventional duplex binders.

The aim of this thesis was to focus on the targeting of the G-quadruplex structure by synthesising a simple metal complex capable of specifically binding to a G-quartet. Biisoquinoline was chosen as the aromatic ligand to form 2:1 complexes with palladium and platinum that potentially have an excellent size and shape match for a G-quartet. This

was hoped to result in enhanced selectivity as the ligands should be too bulky to interact by intercalating between base pairs. Rhodium and rhenium biisoquinoline complexes were also investigated. The interactions of the complexes with both duplex and quadruplex forming DNA were investigated using DNA binding experiments. This helped to determine how the complexes bound to G-quadruplexes and if they were selective for one type of DNA over another.

Both of the square planar complexes [Pd(ibiq)$_2$][BF$_4$]$_2$ and [Pt(ibiq)$_2$][PF$_6$]$_2$ were shown to interact well with duplex DNA and antiparallel hybrid quadruplex forming htelo DNA when examined by circular dichroism. Strong ICD peaks were seen in each of the titrations conducted with the two types of DNA. When the same titrations were carried out using a c-myc oligo, which forms parallel quadruplex forming DNA, the platinum complex was observed to interact more than the palladium complex with the DNA. Interestingly when the platinum complex was titrated in the c-myc DNA without the additional K$^+$ or Na$^+$ cations in the buffer the CD spectrum became a mirror image of itself at high complex concentrations. The octahedral rhenium complex showed no interaction with either ct-DNA or htelo DNA which demonstrated how important the square planar geometry was for efficient binding.

The platinum biisoquinoline complex does bind to quadruplex forms of DNA as hypothesised in Chapter 2. The formation of quadruplexes before the addition of the complex could be observed using CD therefore it is believed that the complex binds to preformed quadruplexes resulting in the presence of the intense CD bands in the MLCT region. Work has been presented in this thesis that suggests an end stacking binding mode

is occurring (red shifts in UV-vis titrations). However without the crystal structure of the complex with the DNA this mode of binding cannot be fully established.

Unfortunately the platinum and palladium complexes also bind to duplex DNA as seen in the CD titration spectra with ct-DNA. The size of the biisoquinoline ligand was expected to be too big to interact significantly with duplexes through an intercalative mode of action. The strong ICD bands and the red shift observed in the UV-vis titration indicate both of the complexes are able to directly coordinate to the duplex DNA. Groove binding is a possibility at low complex concentrations as the red shift is only observed at high complex loading. This is especially true for the palladium complex in the gel electrophoresis where changes in the bands occur only at high complex loadings.

The palladium biisoquinoline complex differs from the platinum complex in its response to c-myc DNA (which forms a parallel G-quadruplex conformer). The reason for this may be that the palladium is actually binding co-ordinatively to the bases in the loops instead of end stacking and cannot bind to the loops when in this conformation. However further analysis using UV-vis titrations found the complex to produce a similar response with both types of quadruplex forming DNA (htelo and c-myc). The large red shifts can indicate both an end stacking and coordinative mode of interaction.

To further investigate the selectivity of the complexes for quadruplex forming DNA over duplex DNA fluorescence indicator displacements (FID) and polyacrylamide gel electrophoresis experiments (PAGE) were carried out. The complexes were both able to displace the thiazole orange at concentrations below the 0.5 μM threshold in both types of

quadruplex forming DNA. More significantly the same complexes were less able to displace the TO from the duplex forming DNA, ds26, requiring concentrations above 2 μM. The palladium complex struggled to displace the TO from the c-myc quadruplex which again may be linked to how it binds. If in solution with the DNA, the majority is in its dissociated form it is no longer going to be able to successfully displace the TO as it becomes a poorer π stacker and cannot access the parallel quadruplex loops to coordinate. The PAGE experiments, for the platinum complex only, demonstrated that when both types of DNA are present (duplex and quadruplex) the complex appears to bind to the quadruplex DNA over the duplex DNA. Evidence lies in the undisturbed duplex band that is seen when combined with the complex and the quadruplex forming DNA. The band seen with duplex DNA and the complex only is more dispersed suggesting that binding is occurring.

Another possible difference between the binding ability of the platinum complex and the palladium complex may be linked to the extent of planarity each complex is able to achieve and how this fits with the surface of the terminal G-quartet. Only very subtle differences however were actually found between the platinum and palladium complex crystal structures. The platinum complex appears to be the better match of the two despite it actually being slightly less planar than the palladium complex (26° between planes instead of 24°), indicating that the G-quartet is slightly distorted too. The anions present may have also contributed to the difference in binding however this wasn't investigated in this thesis.

In Chapter 4 the interactions of the palladium and platinum complex were investigated with RNA oligos TERRA and NRAS which fold into parallel quadruplex conformations, as the c-myc DNA did. Unsurprisingly, the platinum complex showed a similar interaction to that observed with the c-myc DNA and the palladium complex showed very little response in both the CD and FID experiments. This further suggests that the platinum interacts in an end stacking mode whilst the palladium complex loses a ligand. Instead of targeting the quadruplex in an end stacking mode the palladium prefers to bind coordinatively with the loops which is hindered in parallel quadruplex conformations.

In the cell work reported in Chapter 5 both of the platinum and palladium complexes show cytotoxicity values in the nM range against ovarian and breast cancer cell lines. The similar cytotoxic abilities of the two complexes suggests that they both have the same mode of action. When considering the preceding binding investigations the platinum complex was expected to have the greatest cytotoxic effect upon binding to DNA. The complexes cytotoxic effect therefore may be due to a combination of duplex DNA and htelo DNA binding events as well as the possible disruption of other cellular processes that haven't been investigated in this work.

The experimental work conducted in Chapter 6 aimed to develop the biisoquinoline complex by including additional side arms that have been seen to promote binding in the literature.[3] The design and synthesis of the new ligand was reported; however due to the number of steps in the reaction scheme the modified ligand could not be completed on time.

7.2 Future Work

The biisoquinoline complex in its present state lacks the visibility required for it to be seen in cells. Therefore the appendage of a fluorescent arm would enable the localisation of the complex to be observed, which could be added to the complex in a similar way to the 'clicked on' side arms in Chapter 6. Confocal microscopy would then be used to visualise the complex in the cells where it would hopefully be found in the nucleus. Further work into the overall synthesis of the biisoquinoline ligands is required in order to increase the yield of the final metal complexes.

An attempt at calculating the binding constant was made using the circular dichroism and UV-vis spectroscopy results for some of the complex-DNA titrations. A useful technique that could be used to confirm this is surface plasmon resonance (SPR). The technique involves the immobilisation of DNA on a gold chip that is treated with the complex. The chip is exposed to incident light causing the oscillation of gold surface electrons (which are influenced by the mass at the surface).[4] The association and dissociation rates of the ligand to the DNA can be recorded which are used to calculate the binding constant.

Another biological assay that could determine the target of the complex is the scratch assay (or wound healing assay) where cells are grown until confluent before scratching the surface so that there is an area where no cells are present. The cells would then be treated with the complex and if the complex is able to inhibit the SRC gene required to produce the SRC protein required for cell mobility, the cells would not be able to regrow over the

scratch formed. The SRC proto-oncogene is G-quadruplex rich and quadruplex formation and stabilisation in this area can be linked to the inhibition of the mobility protein.[5]

Further toxicity assays either monitoring ATP or using an enzyme linked immunosorbant assay (ELISA) need to be performed in order to be confident of the MTT assay results attained in Chapter 5. It is thought that the media and its components can affect the amount of formazan produced giving an inaccurate cell viability determination. Cell work using primary cell lines is also required to determine how toxic the complexes are.

The platinum complex, [Pt(ibiq)]Cl$_2$, here synthesised with limited solubility could be developed into a carboplatin type complex by replacing the chloride ligands with 1,1-cyclobutanedicarboxylate (*Fig. 7.1*). This exchange is hoped to increase the solubility of the complex that could then be used in further DNA binding experiments.
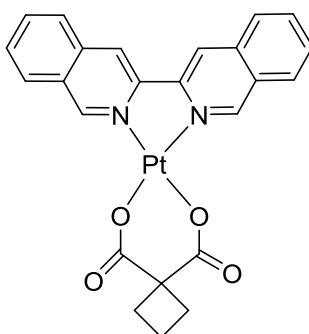
Figure 7.1. Platinum biisoquinoline complex with a bidentate carboxylate group substituting the original chloride ligands.

The long term aim of this work would be to fully understand the interactions that occur between the biisoquinoline complexes and the quadruplex DNA in a cellular environment. This also involves the development of the biisoquinoline modifications so that the binding is specifically between quadruplexes and the complex, and targeted to towards cancerous cells.

7.3 References

1. R. J. Ernst, H. Song, J. K. Barton. *J. Am. Chem. Soc.,* 2009, **131**, 2359.

2. M. J. Hannon. *Chem. Soc. Rev.,* 2007, **36**, 280.

3. N. H. Campbell, N. H. Abd Karim, G. N. Parkinson, M. Gunaratnam, V. Petrucci, A. K. Todd, R. Vilar, S. Neidle. *J. Med. Chem.,* 2012, **55**, 209.

4. S. Zeng, K. Yong, I. Roy, X. Dinh, X. Yu, F. Luan. *Plasmonics,* 2011, **6**, 491.

5. R. Rodriguez, K. M. Miller, J. V. Forment, C. R. Bradshaw, M. Nikan, S. Britton, T. Oelschlaegel, B. Xhemalce, S. Balasubramanian, S. P. Jackson. *Nat. Chem. Biol.,* 2012, **8**, 301.

Appendix

1. 2D-COSY, NOESY and Mass Spectrometry Spectra (Including Crystallographic data for Pd and Re complexes)

1.1 Isoquinoline 1,3-dione (**1**)
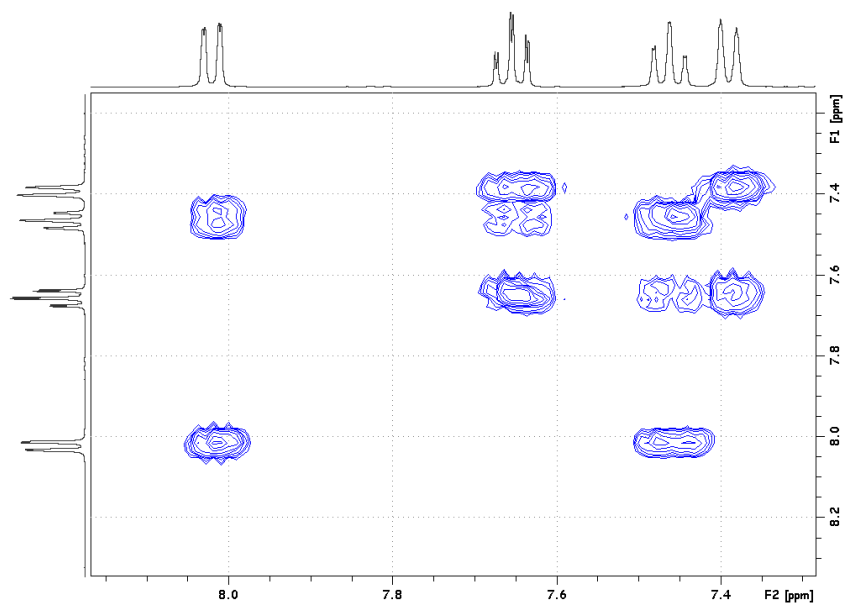
COSY NMR (400 MHz, d_6-DMSO, 298 K).
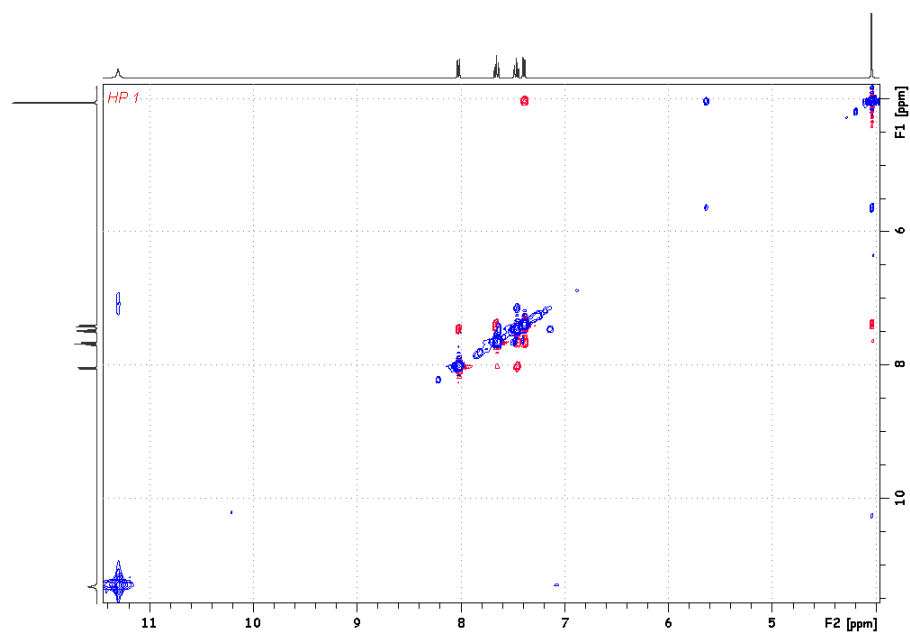
NOESY NMR (400 MHz, d_6-DMSO, 298 K).
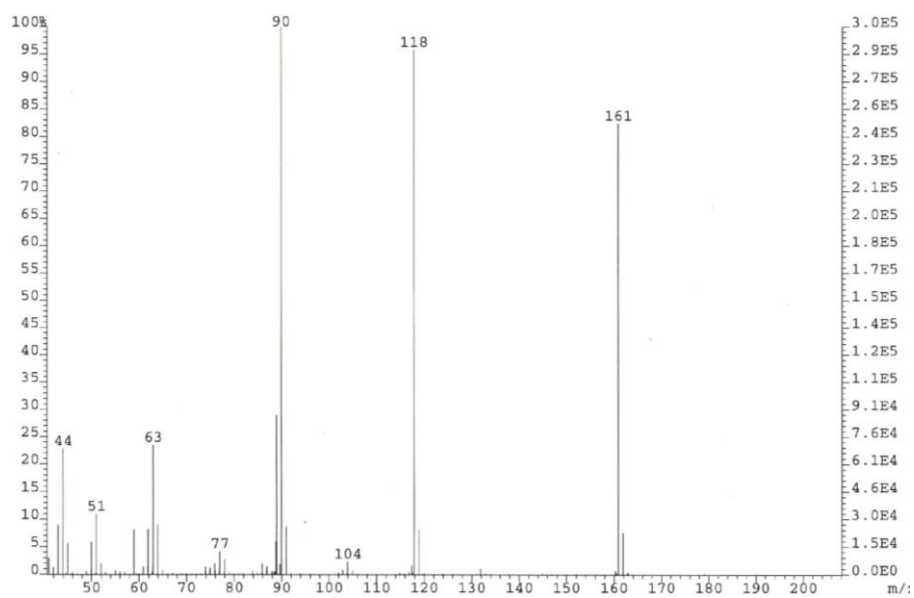
EI Mass spectrum.

1.2 1,3-Dichloroisoquinoline (2)
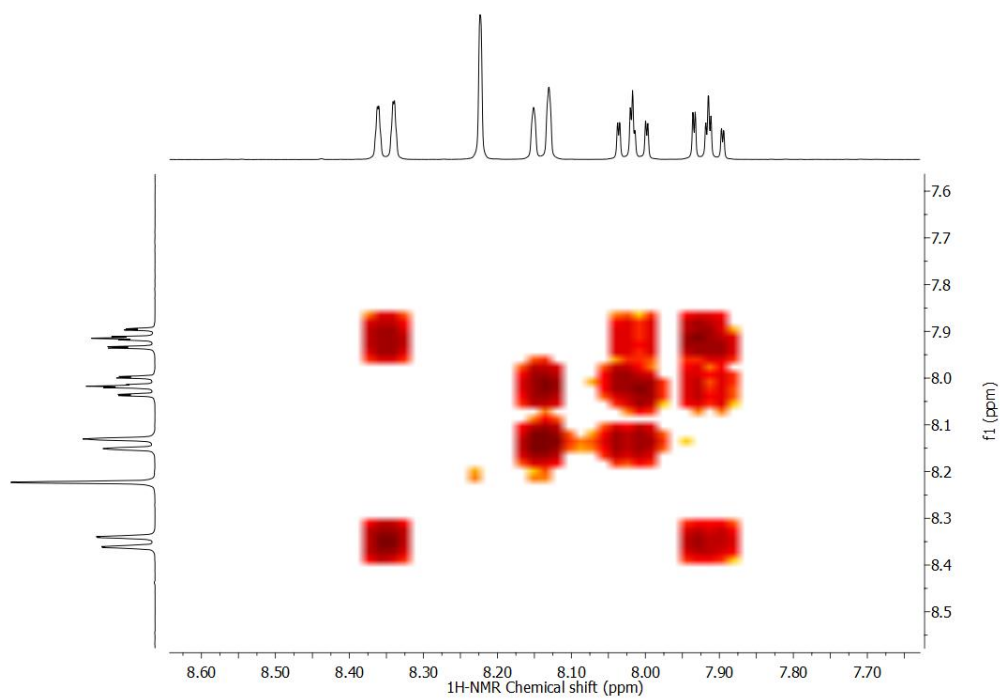
COSY NMR (400 MHz, d$_6$-DMSO, 298 K).
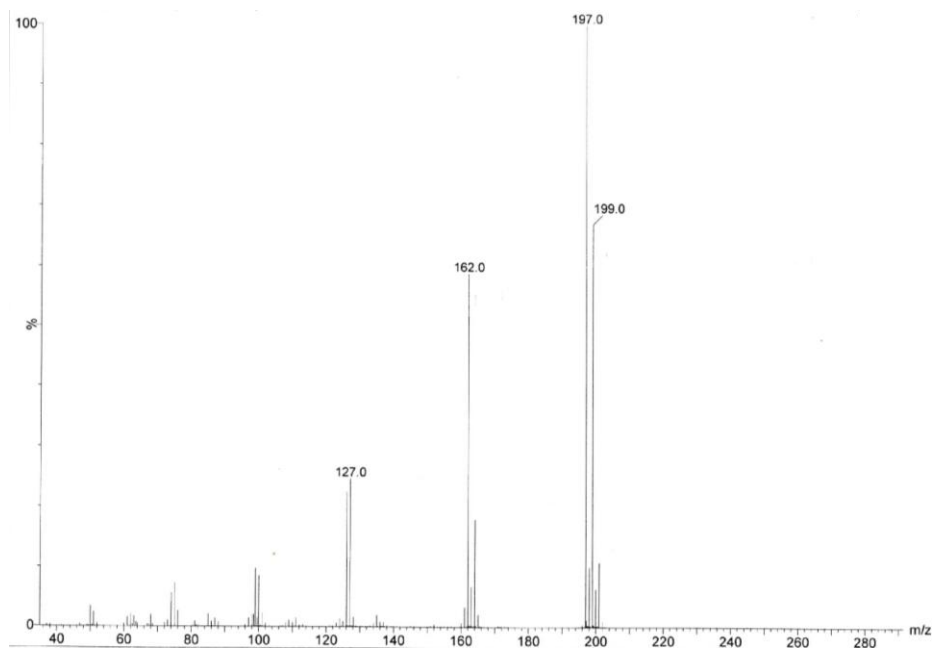
EI Mass spectrum.

1.3 3-Chloroisoquinoline (**3**)
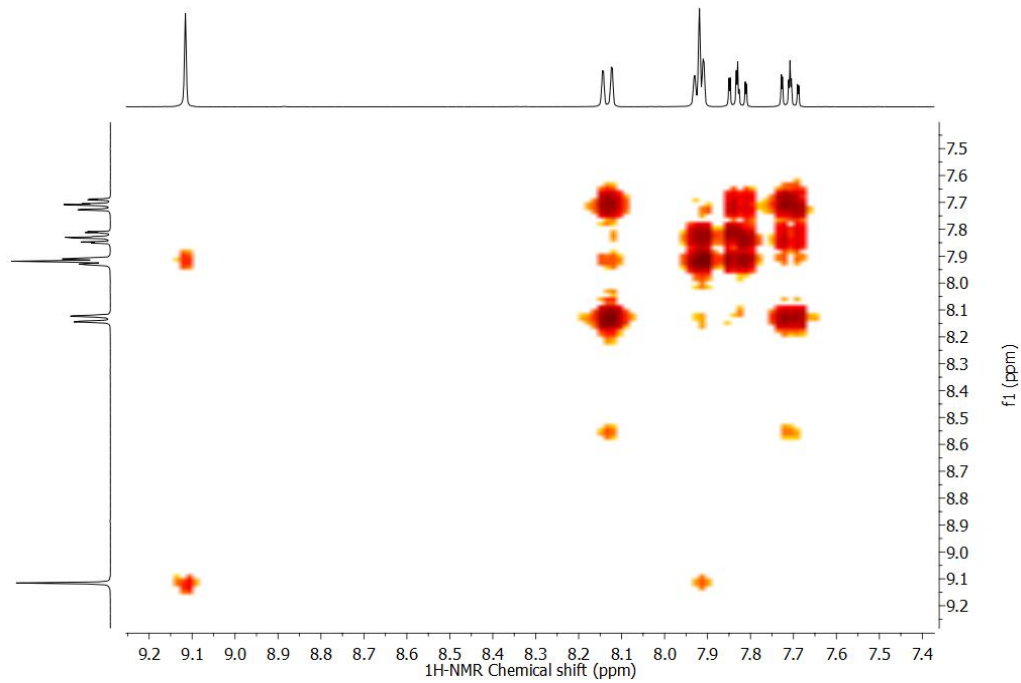
COSY NMR (400 MHz, MeOD, 298 K).
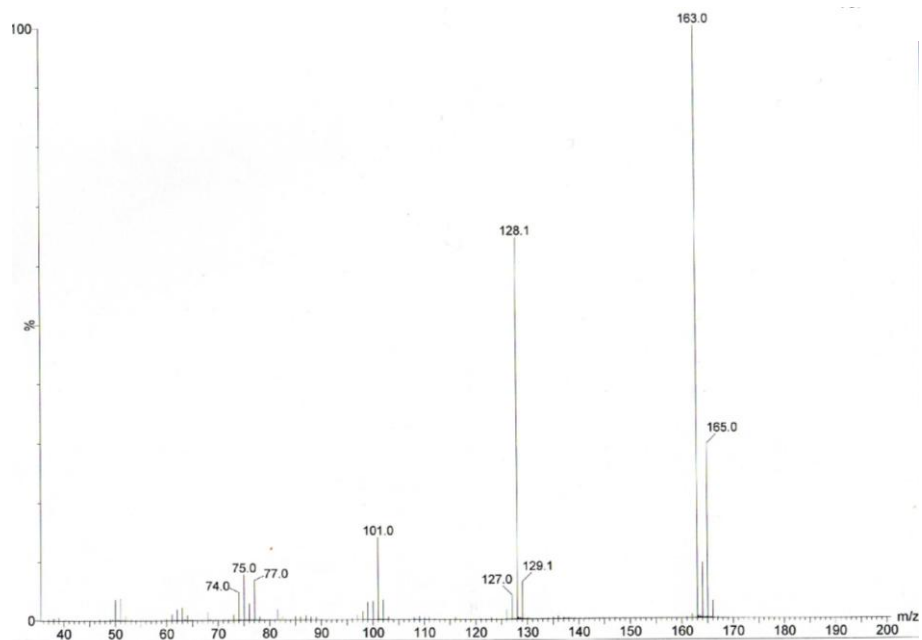
EI Mass spectrum.

1.4 3,3-Biisoquinoline (ibiq) (**4**)
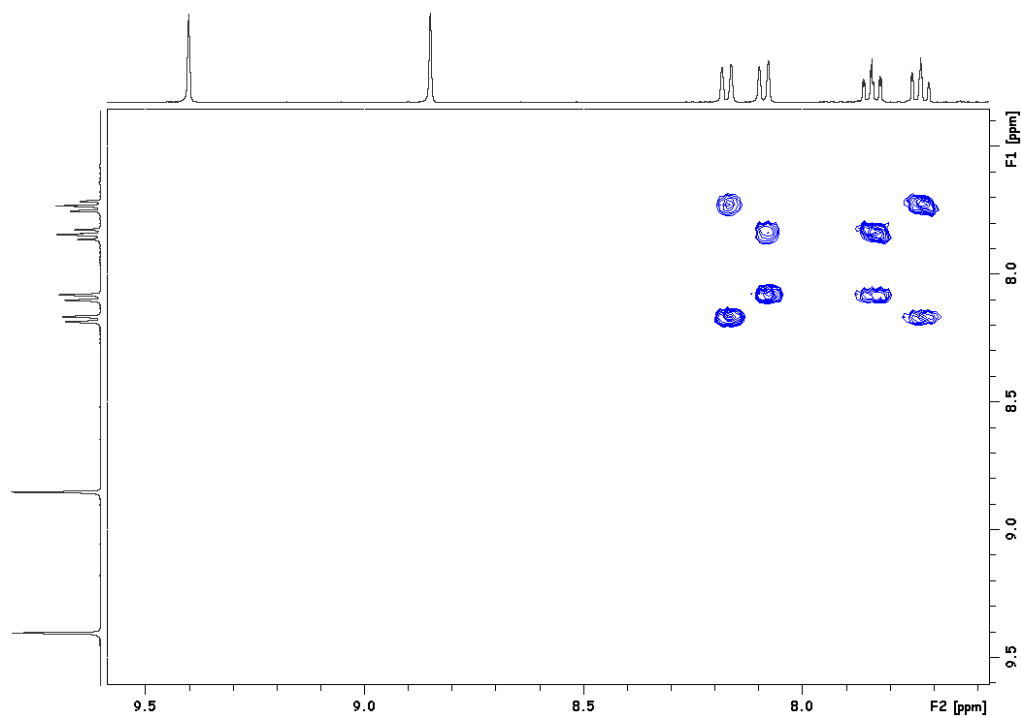
COSY NMR (400 MHz, MeOD, 298 K).
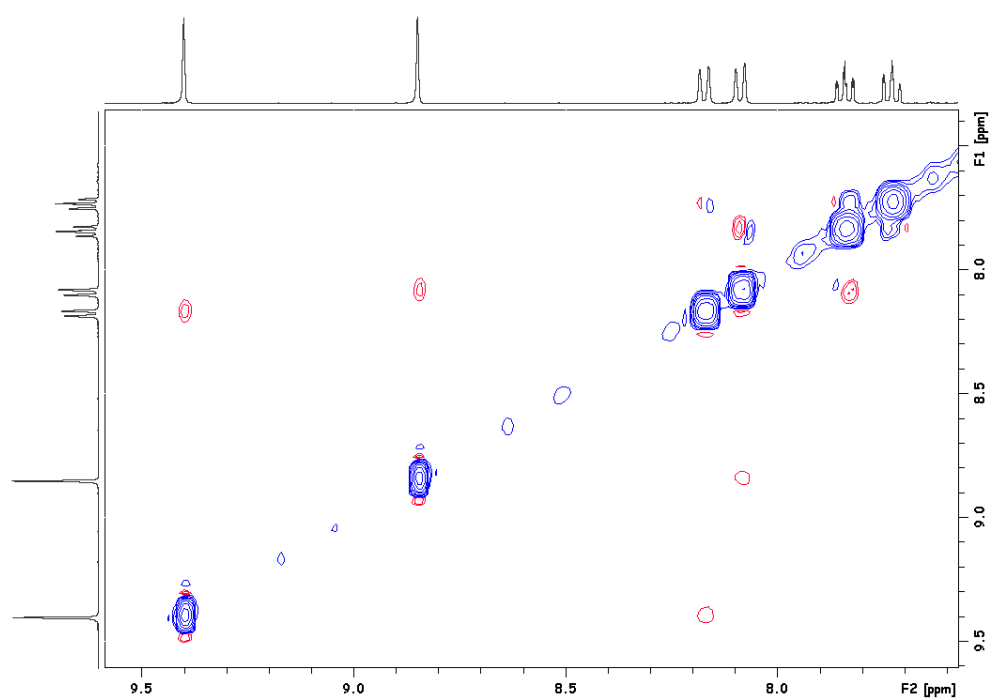
NOESY NMR (400 MHz, MeOD, 298 K).
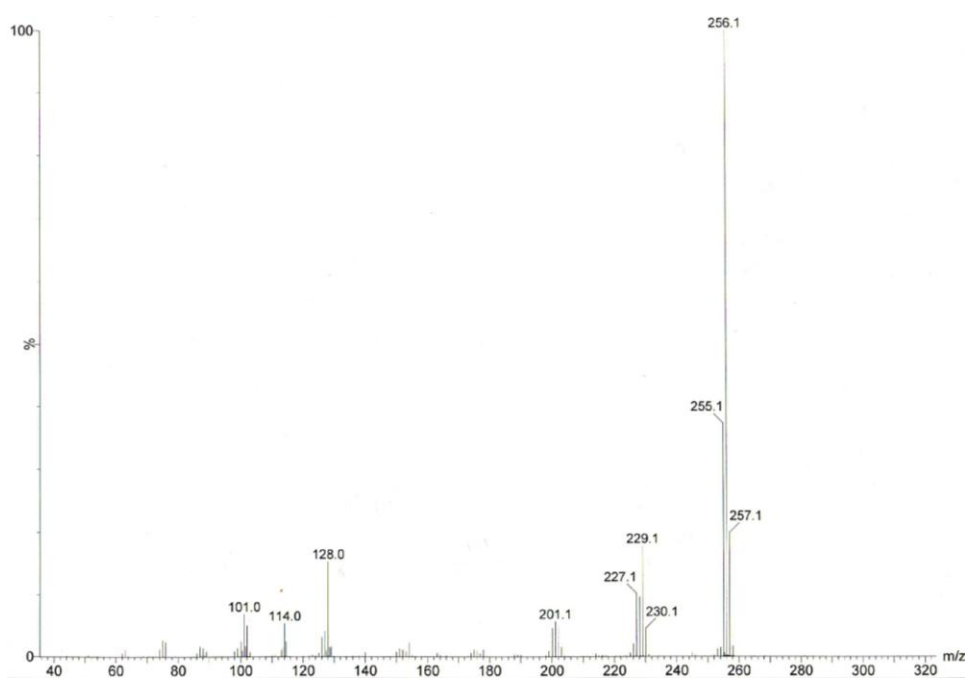
EI Mass spectrum.

1.5 [Pd(ibiq)$_2$][BF$_4$]$_2$ (**5**)
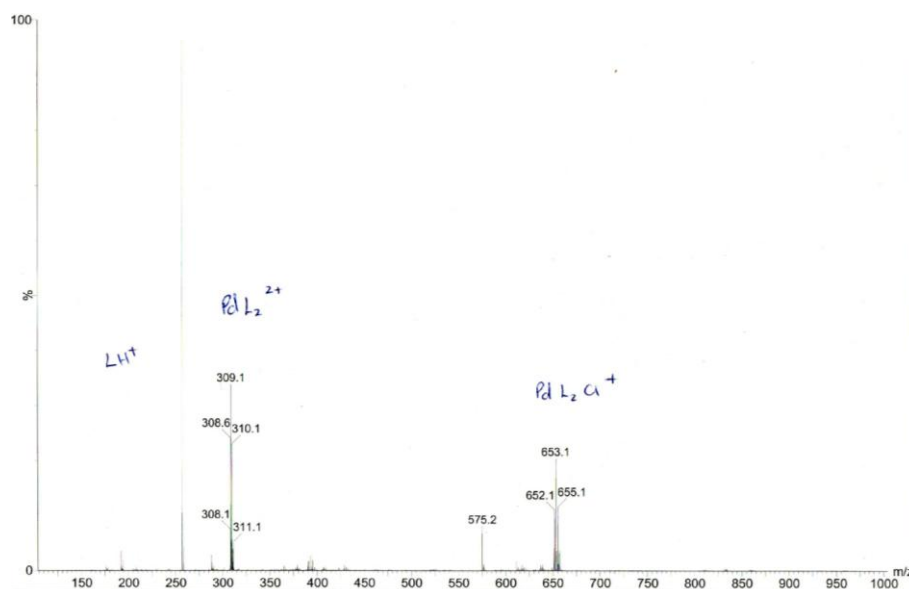
ESI Mass spectrum.

Crystallographic Data

Empirical formula	C$_{36}$H$_{24}$N$_4$Pd, 2(BF$_4$), C$_6$H$_6$
Mr	870.72
T [K]	100.00(10)
Crystal system	Triclinic
Space group	P -1
Unit cell dimensions	a = 7.3309(3) Å α= 84.443(3)°
	b = 8.4090(3) Å β= 89.964(3)°
	c = 14.3651(5) Å γ = 76.153(3)°
V [Å^3]	855.54(6) Å^3
Z	1
Density(calc) (Mg/m^3)	1.690 Mg/m^3
Absorption coefficient (mm-1)	5.114 mm^{-1}

Reflections collected	16249
Independent reflections	3460 [R(int) = 0.0270]
Goodness of fit on F^2	1.059
Final R indices [I>2σ(I)]	R1 = 0.0202, wR2 = 0.0533
R indices (all data)	R1 = 0.0203, wR2 = 0.0534

1.6 [Pt(ibiq)Cl$_2$] (**6**)
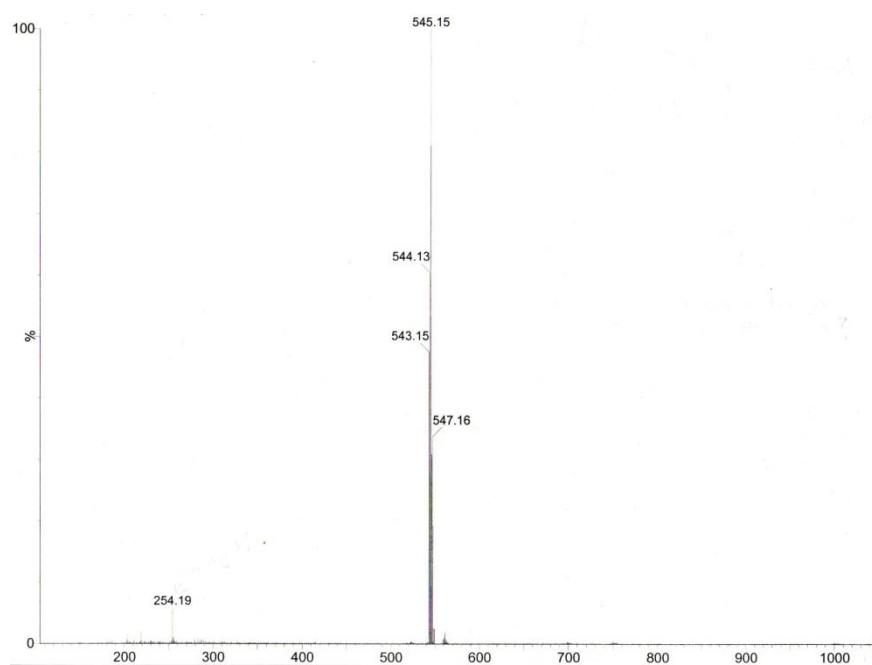
ESI Mass spectrum.

1.7 [Pt(ibiq)₂][PF₆]₂ (**7**)
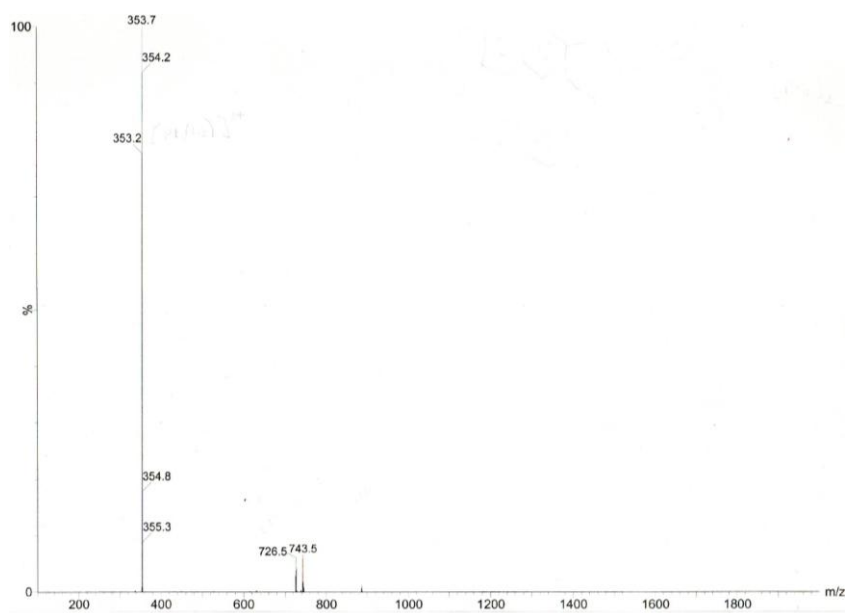
ESI Mass spectrum.

1.8 [Re(CO)₃(ibiq)(Py)][CF₃SO₃] (**8**)
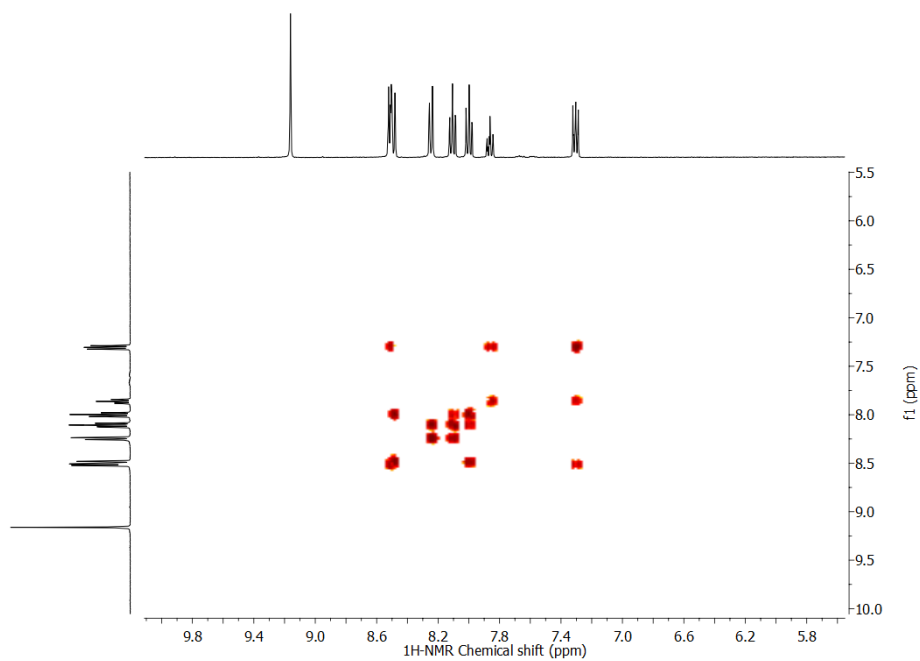
COSY NMR (400 MHz, MeOD, 298 K).
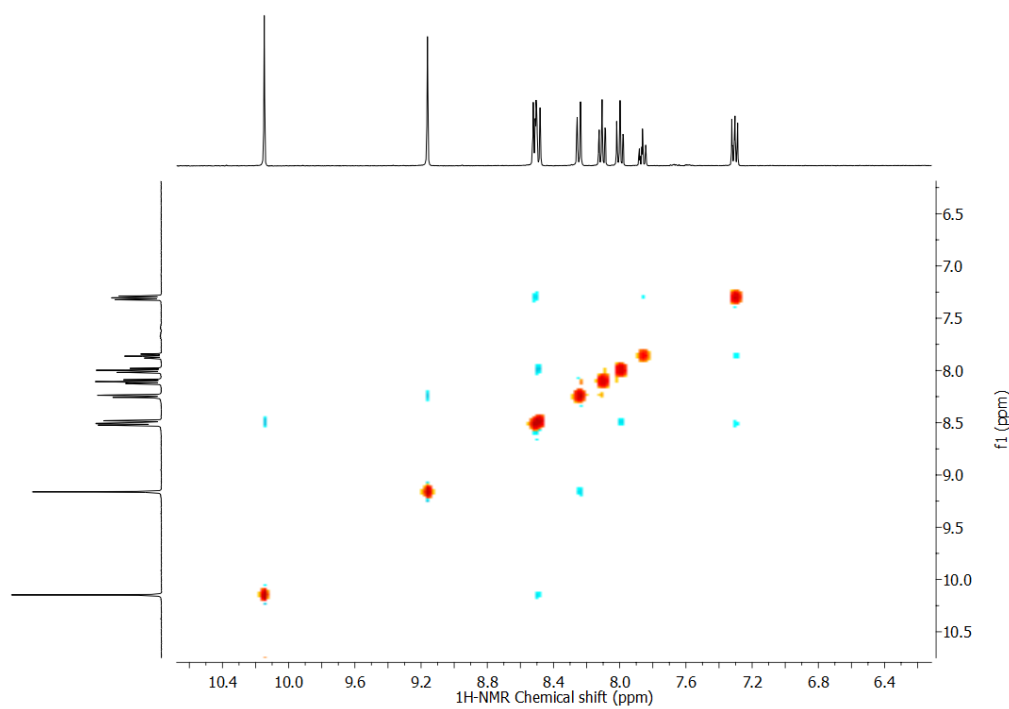
NOESY NMR (400 MHz, MeOD, 298 K).
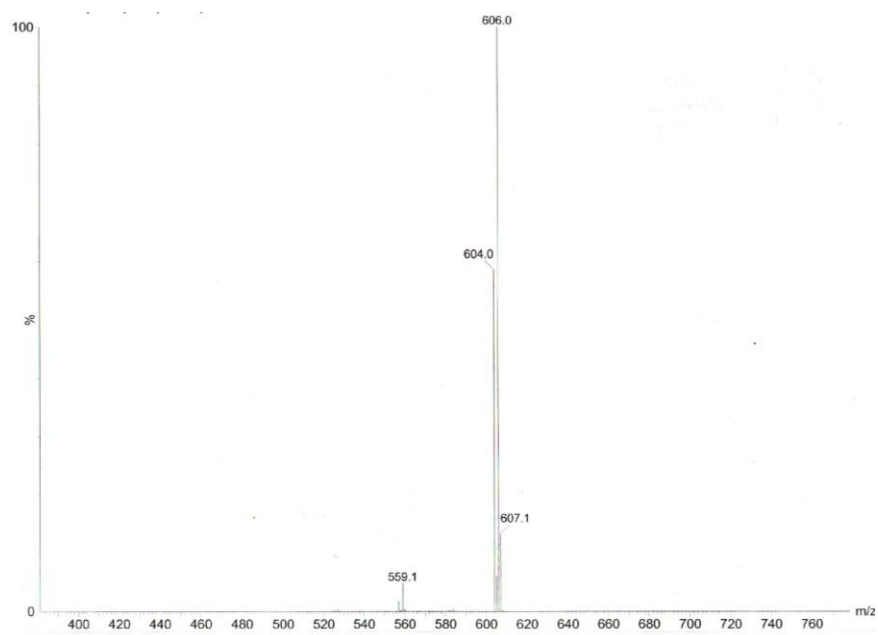
ESI Mass spectrum.

Crystallographic Data

Empirical formula	$C_{26}H_{17}N_3O_3Re$, CF_3O_3S, $0.5(C_6H_6)$, $0.5(C_6H_6)$
Mr	832.80
T [K]	100.00(10)
Crystal system	Triclinic
Space group	P -1
Unit cell dimensions	a = 11.2393(5) Å α= 66.417(4)°
	b = 11.9121(6) Å β= 79.312(3)°
	c = 14.0194(5) Å γ = 62.531(5)°
V [Å^3]	1526.27(14) Å^3
Z	2
Density(calc) (Mg/m^3)	1.812 Mg/m^3
Absorption coefficient (mm-1)	9.040 mm^{-1}
Reflections collected	26600
Independent reflections	6098 [R(int) = 0.0362]
Goodness of fit on F^2	1.037
Final R indices [I>2σ(I)]	R1 = 0.0207, wR2 = 0.0452
R indices (all data)	R1 = 0.0246, wR2 = 0.0463

1.9 Rh(COD)(ibiq)]Cl$_2$ (**9**)
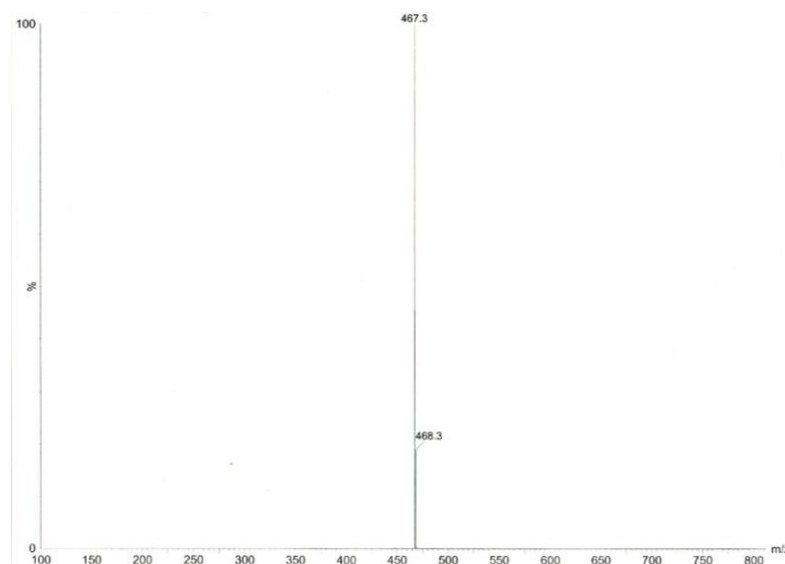
ESI Mass spectrum.

1.10 4-Bromophenyl 2-chloroethyl ketone (**A**)
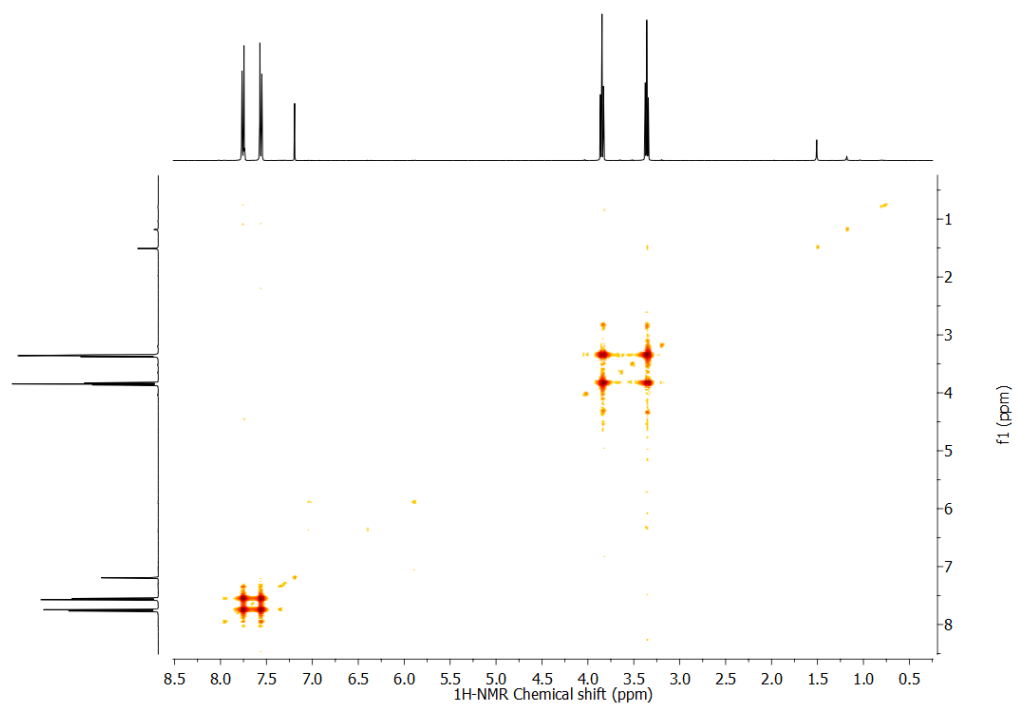
COSY NMR (400 MHz, CDCl$_3$, 298 K).
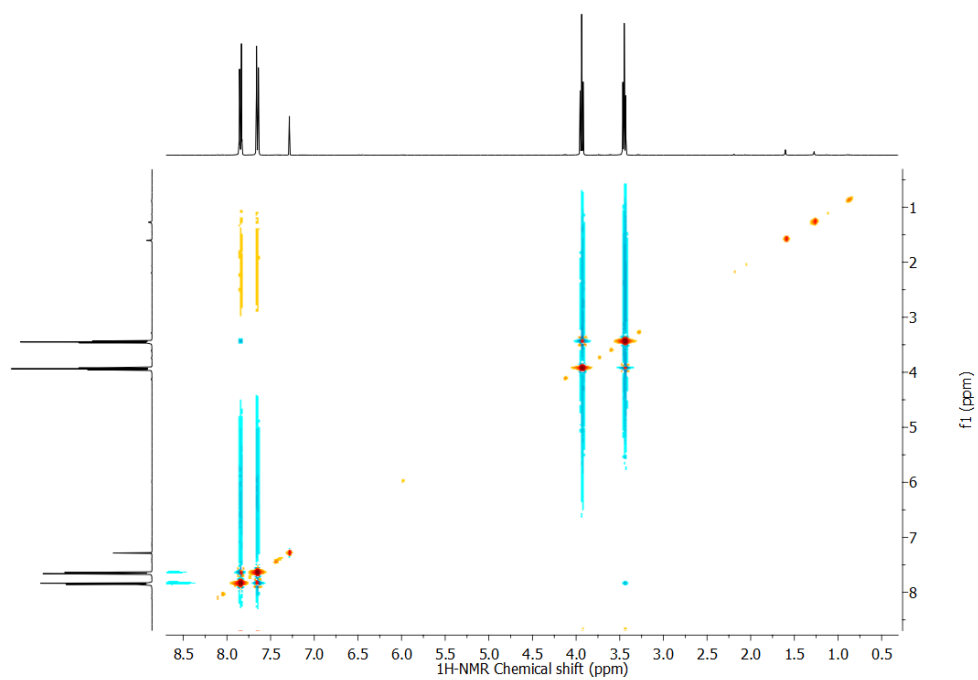
NOESY NMR (400 MHz, CDCl$_3$, 298 K).
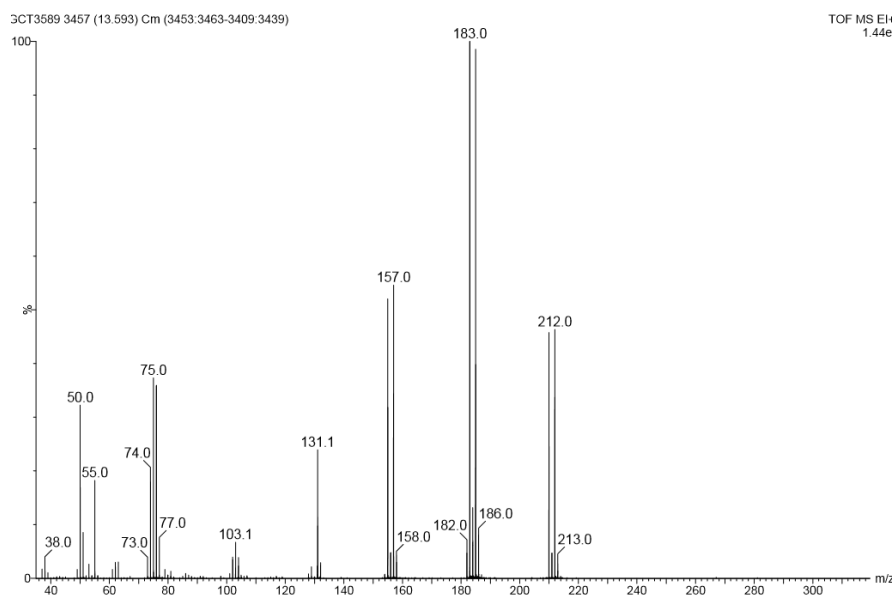
EI Mass spectrum.

1.11 5-Bromoindan-1-one (**B**)
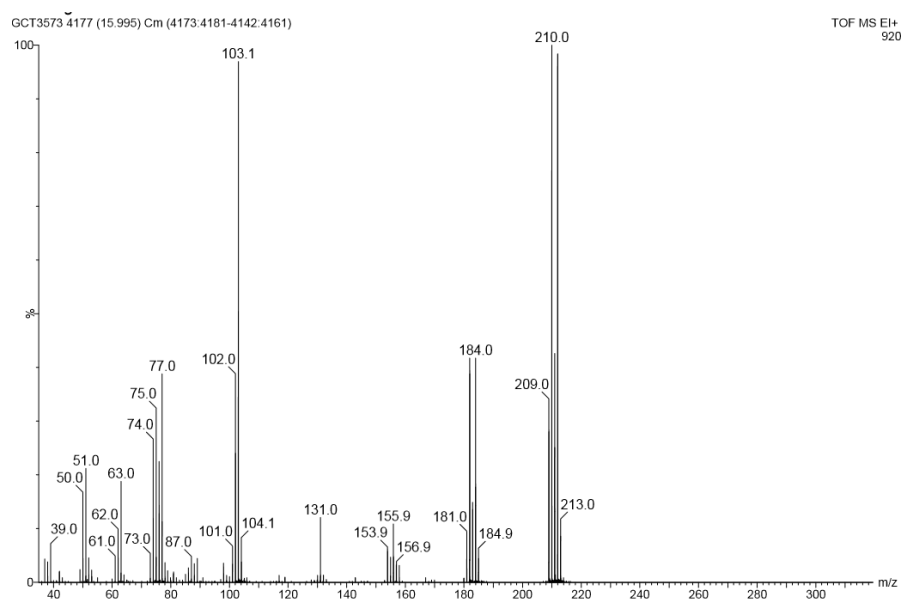
EI Mass spectrum.

1.12 6-Bromo-indan-1,2-dione-1-oxime (**C**)
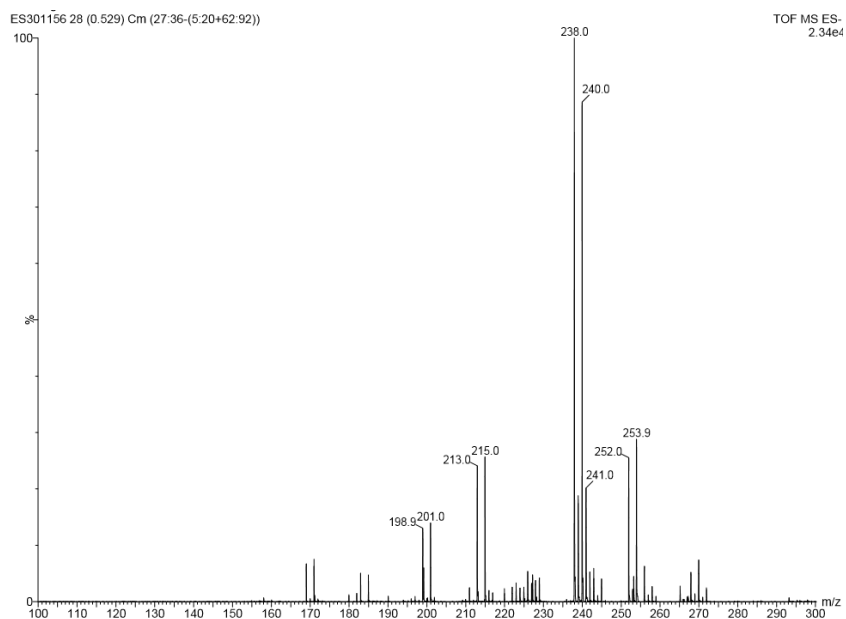
ESI Mass spectrum.

1.13   6-Bromo-1,3-dichloro-isoquinoline (**D**)
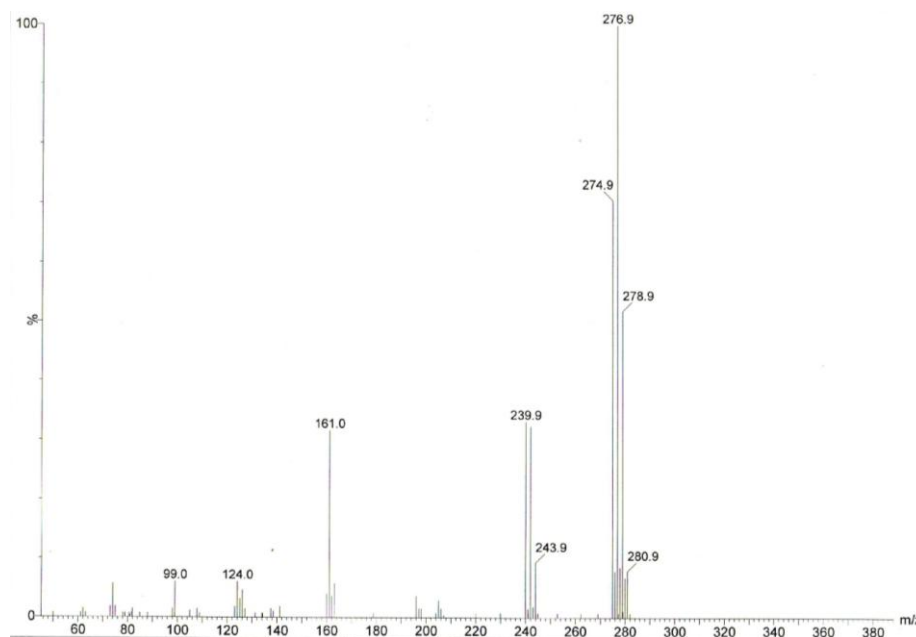
ESI Mass spectrum.

1.14   6-Bromo-3-chloro-isoquinoline (**E**)
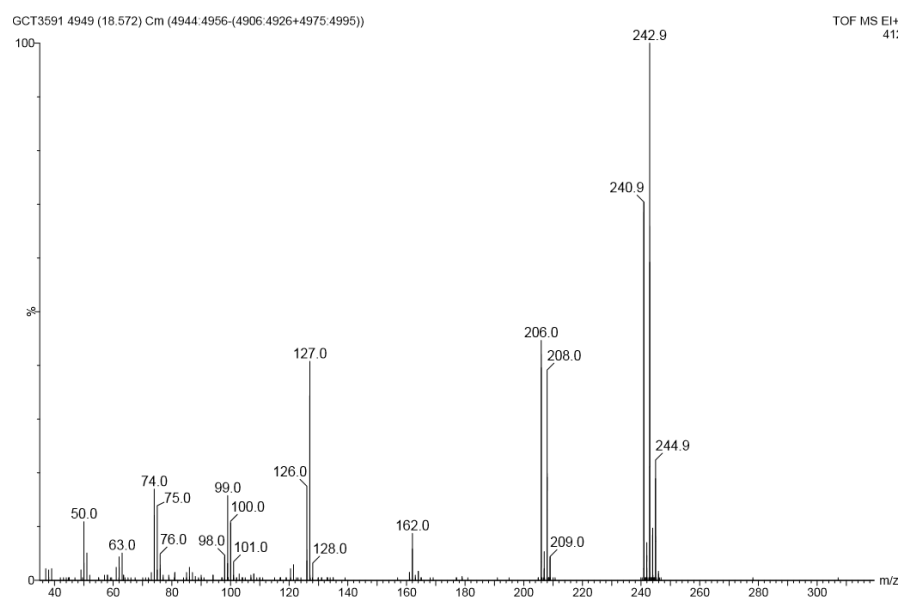
EI Mass spectrum.

1.15 6-(2-Trimethylsilyl)ethynyl-3-chloro isoquinoline (**F**)
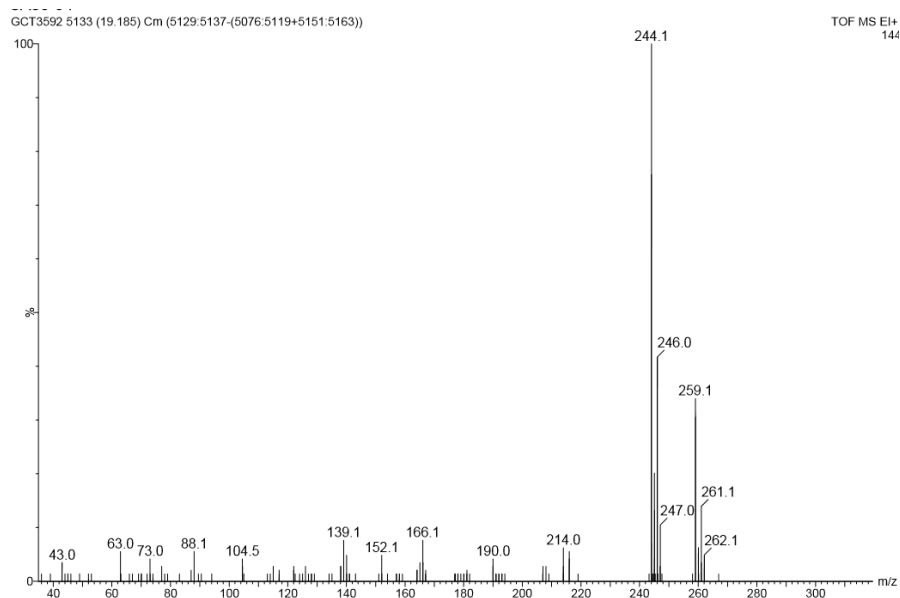
EI Mass spectrum.

1.16 6-Ethynyl-3,3-biisoquinoline (**G**)
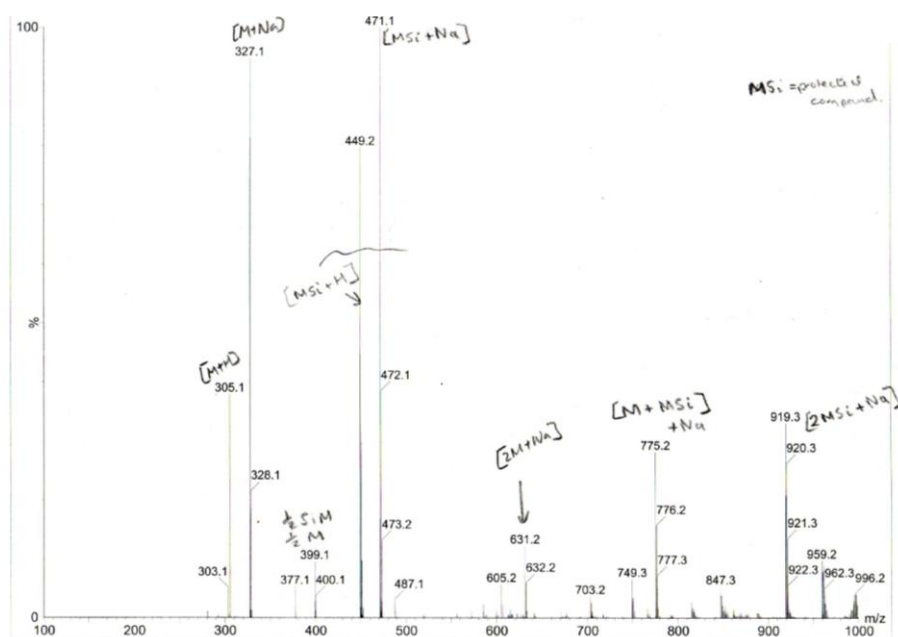
ESI Mass spectrum.

2. Reaction Mechanisms

2.1
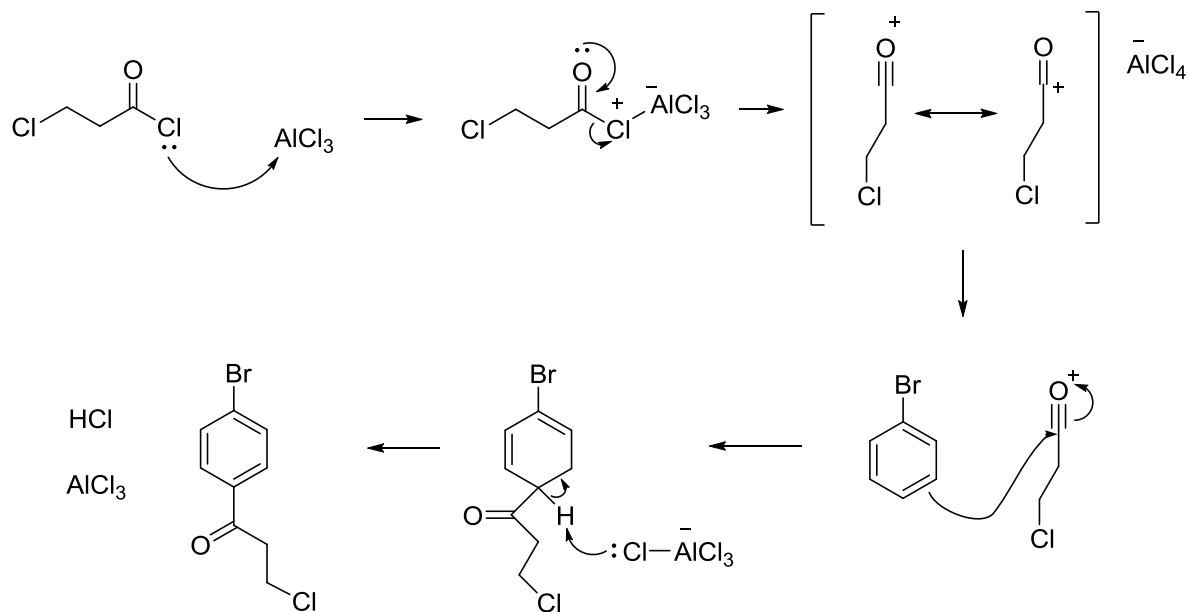
2.2
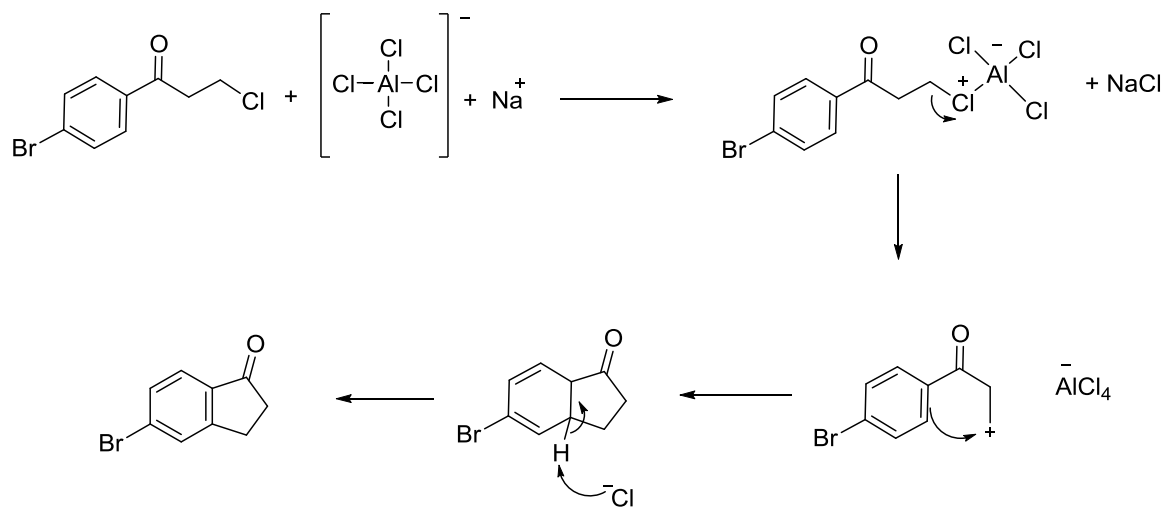
2.3
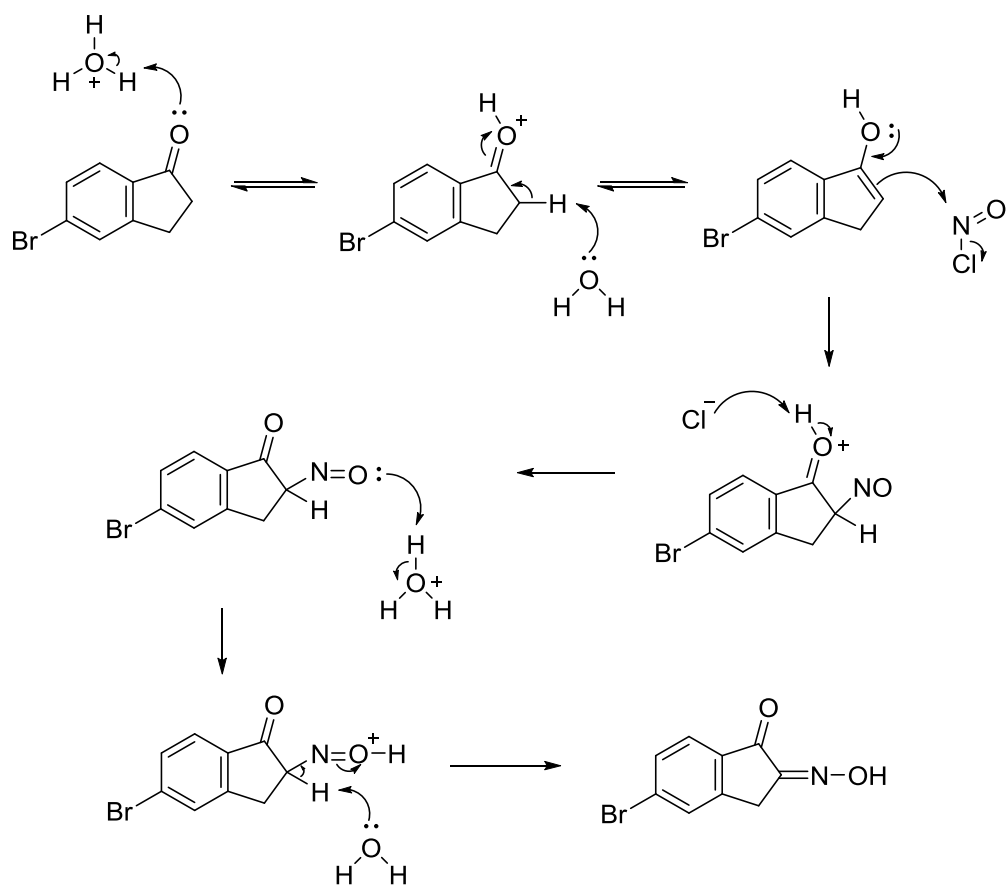
2.4
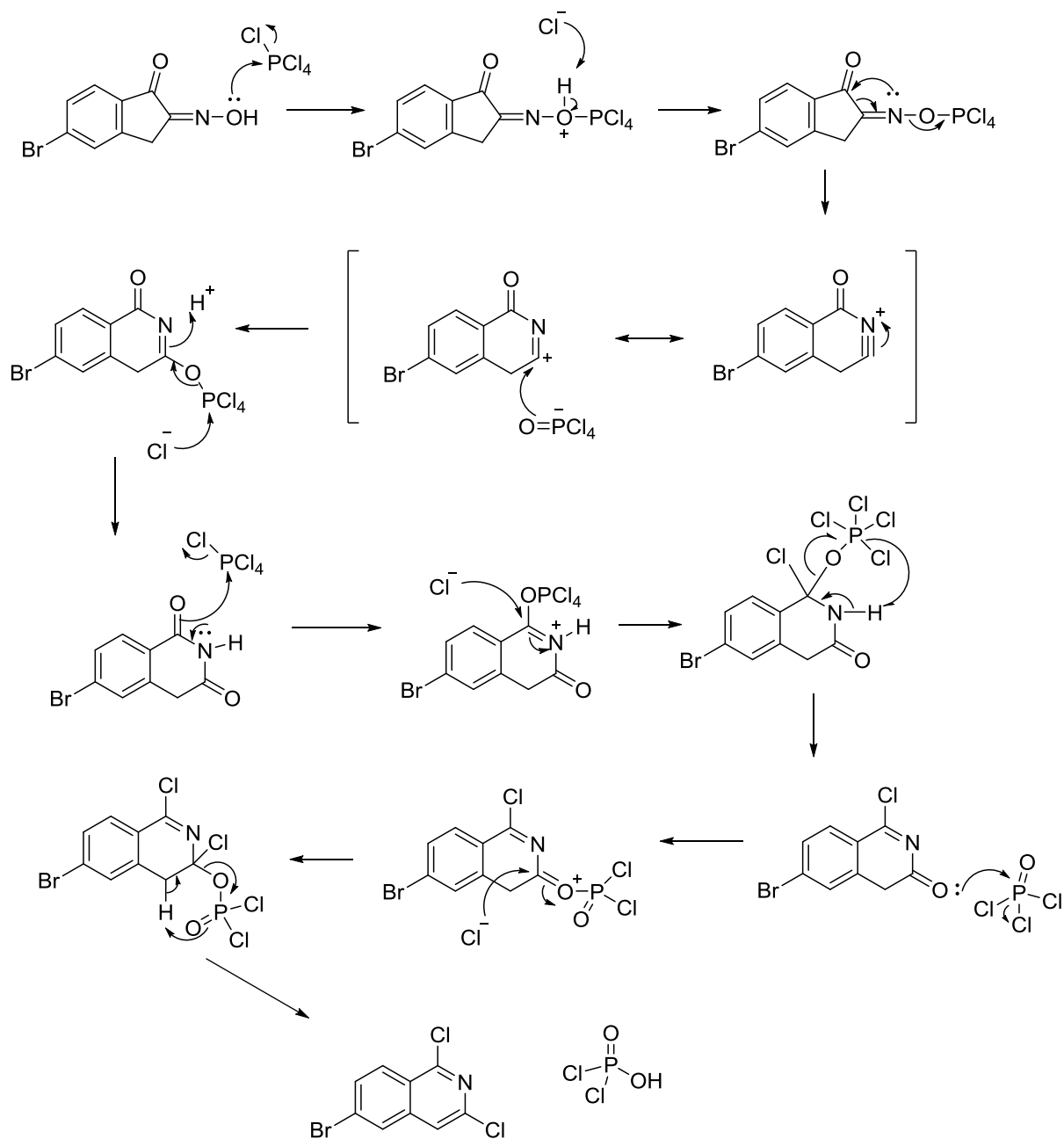
3. PAGE Quantification

Lane 6
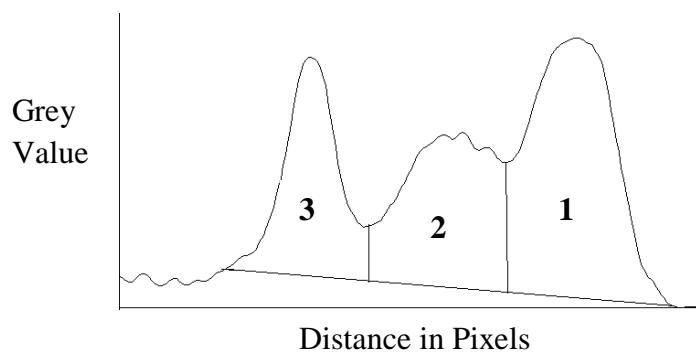
Section	Area
1	31768.62
2	20292.92
3	16804.07

Distance in Pixels

Lane 8
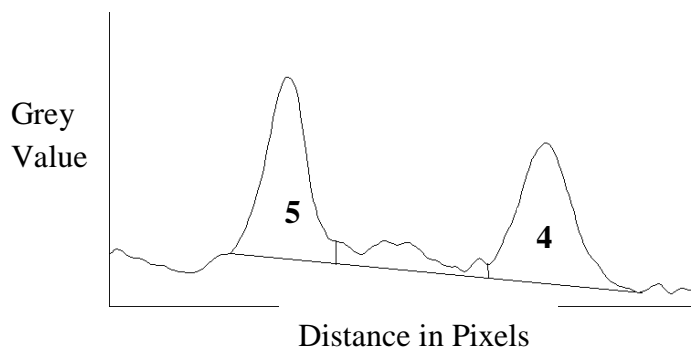
Section	Area
4	10776.43
5	10773.85

Distance in Pixels

4. Examples of Cytotoxicity Data

$[Pd(ibiq)_2][BF_4]$ and cell line A2780
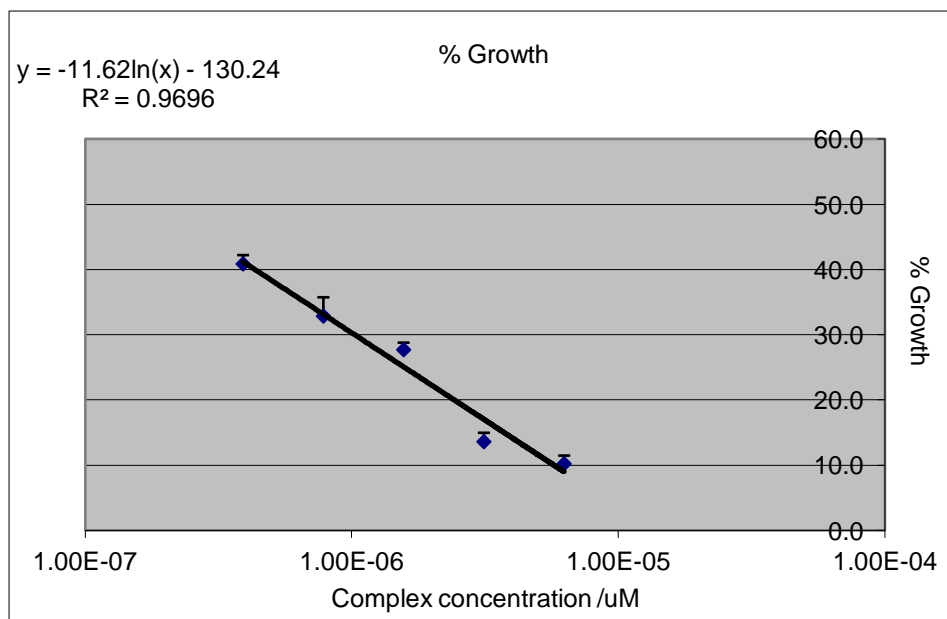
$[Pd(ibiq)_2][BF_4]$ and cell line T47D
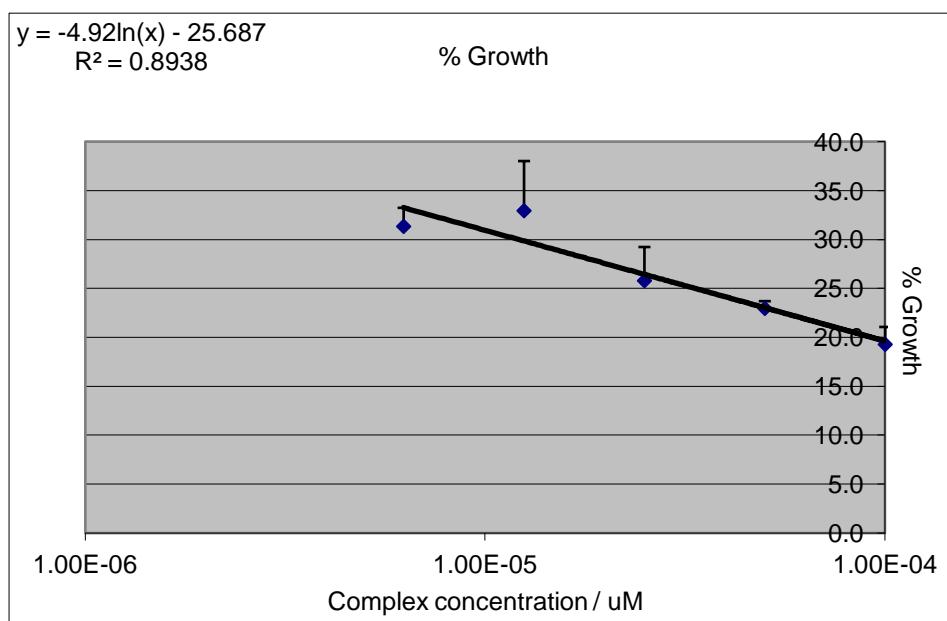
$[Pt(ibiq)_2][PF_6]$ and cell line A2780
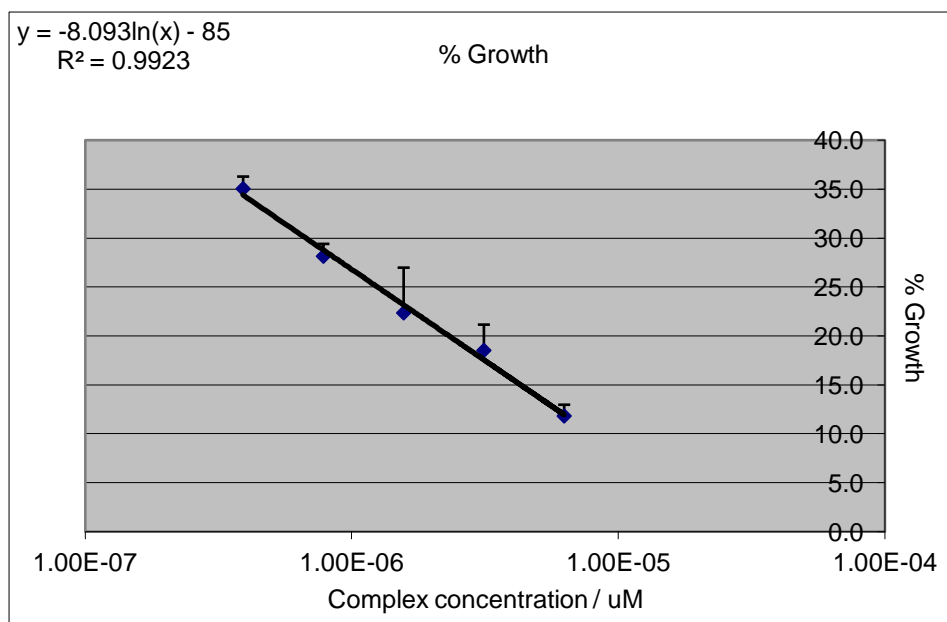
y = -8.093ln(x) - 85
R² = 0.9923

% Growth

$[Pt(ibiq)_2][PF_6]$ and cell line T47D

y = -5.377ln(x) - 28.942
R² = 0.7904

% Growth

Cisplatin and cell line A2780

$y = -24.2\ln(x) - 264.91$
$R^2 = 0.9708$

% Growth
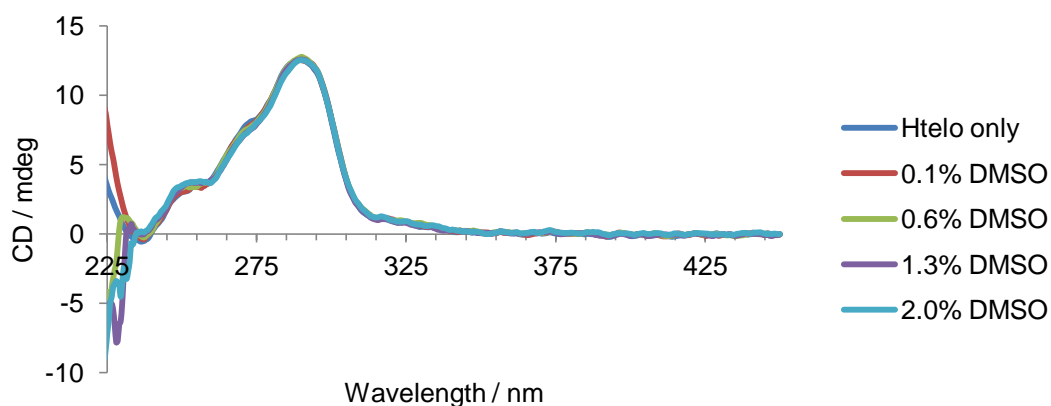
Cisplatin and cell line T47D

$y = -28\ln(x) - 248.67$
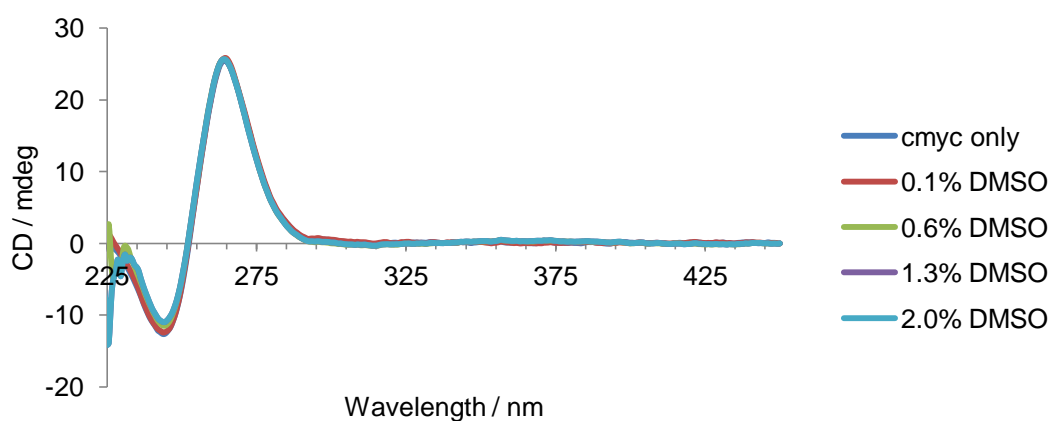$R^2 = 0.9652$

% Growth
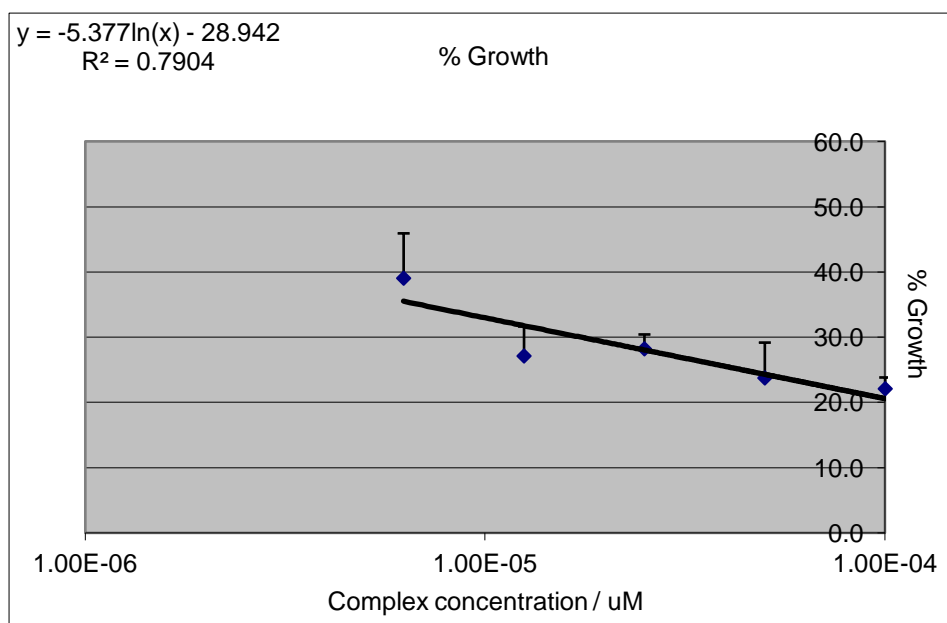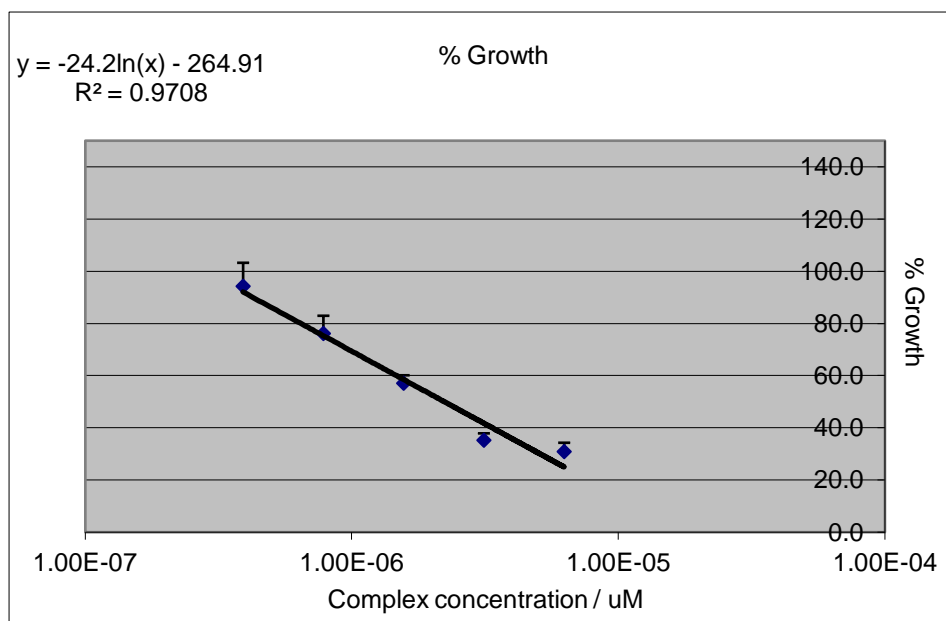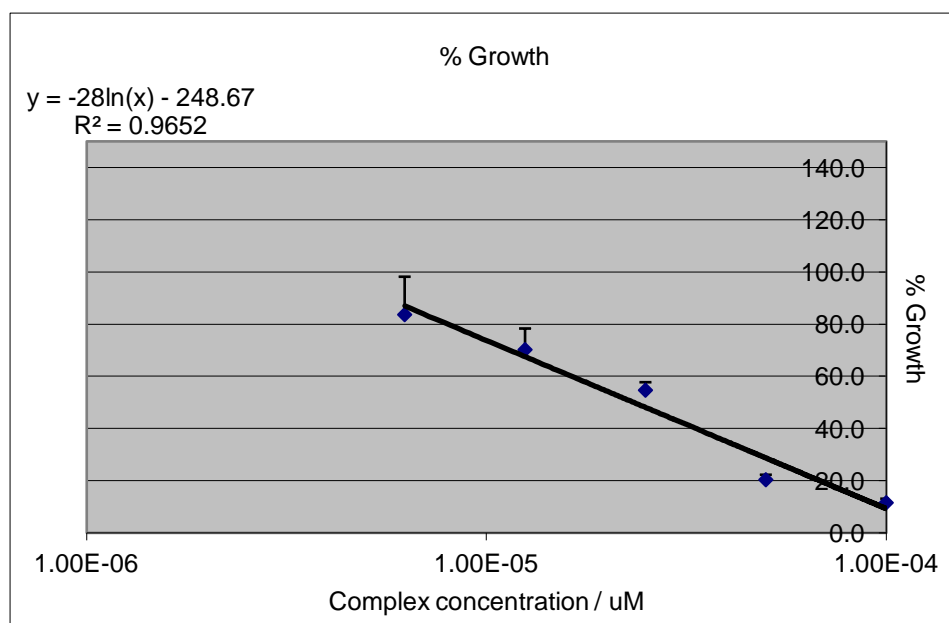
5. CD DMSO control titrations for htelo, cmyc and ct-DNA

2.0% DMSO corresponds to a complex:DNA ratio of 9:1 for htelo and cmyc DNA, and 0.3:1 for ct-DNA

Htelo DNA (3 μM)

cmyc DNA (3 μM)

ct-DNA (300 μM)